Developing an Integrated Building Design Tool by Coupling Building Energy Simulation and Computational Fluid Dynamics Programs

by

Zhiqiang Zhai

M. Eng., Fluid Mechanics
Tsinghua University

Submitted to the Department of Architecture
in partial fulfillment of the
requirements for the Degree of Doctor of Philosophy
in the field of Building Technology

at the

Massachusetts Institute of Technology

September 2003

Signature of Author_____
Department of Architecture
August 1, 2003

Certified by_____
Qingyan Chen
Professor of Mechanical Engineering, Purdue University
Thesis supervisor

Certified by_____
Leon Glicksman
Professor of Building Technology and Mechanical Engineering
Thesis supervisor

Accepted by_____
Stanford Anderson
Chairman, Departmental Committee on Graduate Students
Head, Department of Architecture

Thesis Committee:

Leslie K. Norford, Associate Professor of Building Technology
Ain A. Sonin, Professor of Mechanical Engineering

Developing an Integrated Building Design Tool by Coupling Building Energy Simulation and Computational Fluid Dynamics Programs

by
Zhiqiang Zhai

Submitted to the Department of Architecture
on August 1, 2003 in partial fulfillment of the
requirements for the Degree of Doctor of Philosophy
in the field of Architecture: Building Technology

ABSTRACT

Building energy simulation (ES) and computational fluid dynamics (CFD) can play important roles in building design by providing essential information to help design energy-efficient, thermally comfortable and healthy buildings. However, separate applications of ES and CFD usually cannot give an accurate prediction of building thermal and airflow behaviors due to the partial modeling of the problem. An integration of ES and CFD can eliminate many of the assumptions used in ES and CFD because of the complementary nature of ES and CFD results. This thesis studies the fundamentals, implementation and application of ES and CFD coupling, significantly advancing the knowledge and experience in this area. The study has been focused on the iterative coupling of individual ES and CFD programs, which shows good potential of providing reasonable results with acceptable computing costs.

The research first analyzes the principles and challenges of ES and CFD program coupling. To bridge three major discontinuities in time-scale, spatial resolution and computing speed between ES and CFD programs, special coupling strategies have been developed. Particularly, the staged coupling strategies proposed can effectively reduce computing time while preserving the accuracy and details of the computed results.

The study discusses the solution characteristics of iterative coupling simulation. Through theoretical analysis and numerical experiments, the research verifies the solution existence and uniqueness of a coupled simulation. The investigation concludes that a converged and stable simulation can be achieved with four different data coupling methods. The study has further developed an improved iteration and control algorithm for the coupled simulation.

An integrated program, E+MIT-CFD, has been developed by coupling a new-generation ES program (E+) with a newly-developed ready-to-plug-in CFD solver (MIT-CFD). All the coupling methods and strategies proposed have been implemented in this program. The program has been well validated with various experimental facilities. The comparison of numerical solutions with experimental data reveals the advantages of the integrated simulation over the separate ES and CFD applications. The study further demonstrates the performance and capabilities of the coupled program through practical design projects. Finally, sensitivity analysis of the coupling simulation to building characteristics and coupling strategies has been performed, based on which general guidelines are established for appropriate usage of the coupling simulation.

Thesis Supervisor: Qingyan Chen
Title: Professor of Mechanical Engineering, Purdue University
Thesis Supervisor: Leon R. Glicksman
Title: Professor of Building Technology and Mechanical Engineering, MIT

ACKNOWLEDGEMENTS

I would like to express my sincere thanks to Professor Qingyan Chen, my thesis advisor, for his continuous support and guidance throughout my entire Ph.D. study at MIT. His valuable suggestions and encouragement are important to the completion of this thesis.

I would also like to thank Professor Leon Glicksman, my thesis official advisor and thesis committee chair, for his support and advisement on this thesis work.

I would also express my cordial gratitude to my other thesis committee members, Professor Les Norford and Professor Ain A. Sonin, whose valuable comments helped to improve the thesis.

My sincere thanks also extend to all my colleagues in the Building Technology Program at MIT for their collaboration and friendship.

Finally, I would like to express my special gratitude to my parents, brother, and my wife for their support, understanding and love. My special thanks will go to my lovely daughter, Sophia, who was born at MIT, for the love, hope and encouragement she brings to me.

DEDICATION

To my parents, my wife, and my lovely daughter

Table of Contents

CHAPTER 1

INTRODUCTION

1.1 General Statement of the Problem

Buildings, as one of the largest industries in the world, account for a major part of the total energy consumption. In the United States, building services use more than one third of the primary energy consumption and two thirds of all the electricity (U.S. Energy Information Administration 1995). The energy used by buildings drives diverse mechanical and electronic systems to achieve a convenient, efficient and comfortable environment for all kinds of human activities. Among these systems, the heating, ventilating, and air-conditioning (HVAC) system is the largest energy consumer, as illustrated by Figure 1.1. The usage of HVAC systems allows the creation of an ideal indoor environment with appropriate air speed, temperature, humidity, and contaminant concentrations, where people usually spend 80% to 90% of their time.

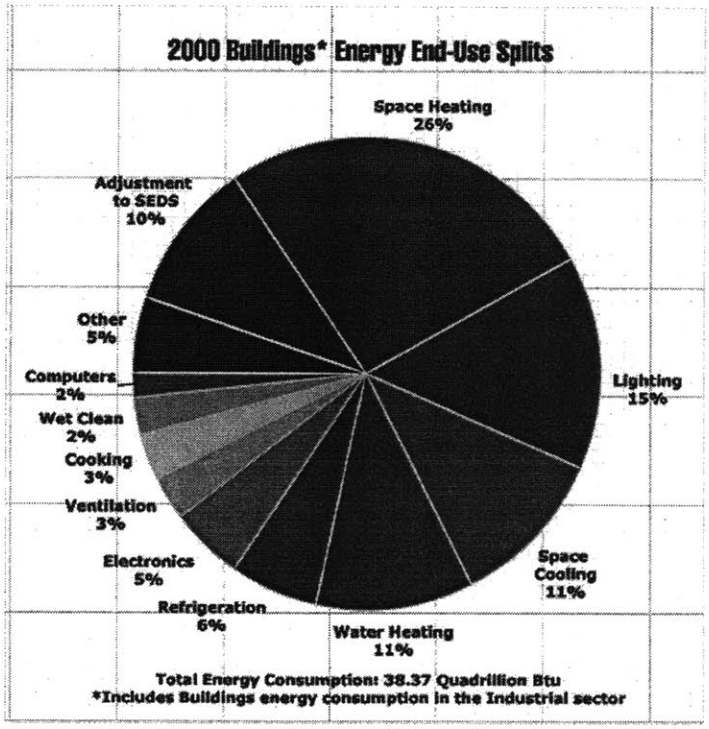

Figure 1.1 Building energy end-use splits (US Department of Energy 2002)

However, with rising concern about the energy conservation, many efforts have been made to lessen the energy consumption of HVAC systems, for example, by using heavy insulation and a tight envelope to reduce the heating load and using a shading

system to reduce the cooling load. The development of new energy-efficient HVAC systems and technologies, such as the displacement ventilation system, can also effectively decrease the system energy consumption. The US National Renewable Energy Laboratory (NREL 1998) estimated that current building energy consumption could be reduced by 30% to 70% with all kinds of energy-efficient designs. This is very attractive because the US spends over $200 billion per year to operate residential and commercial buildings.

On the other hand, the improper design and use of building HVAC systems not only wastes energy but causes thermal discomfort and indoor air quality (IAQ) problems. For example, an inappropriate installation location of supply air diffuser may cause the circulation of the "old" air in a occupied zone. Reports of sick building syndrome and other health complaints related to indoor environments have been increasing recently. Evidence from the literature (NIOSH 1999) shows that poor indoor environments significantly increase the rate of respiratory illness, allergy and asthma symptoms, and sick building symptoms; as a consequence, worker performance is adversely affected. A majority of studies indicate an average productivity loss of 10% due to poor indoor environment, although a conservative value of 6% is widely accepted (Dorgan et al. 1998). The overall economic losses due to the poor indoor environment in US commercial buildings is estimated to be about $40 to $160 billion per year (Fisk 2000) in lost wages and productivity, administrative expenses, and health care costs.

Therefore, it is important to assess comprehensively building performance during all the stages of building design in order to design an energy-efficient, comfortable and healthy building. Most of the building systems, especially newly-promoted systems such as double-skin façade system, usually relate to multiple building components and involve complex interactions between indoor and outdoor environments. It is almost impossible to accurately evaluate the performance of buildings that use diverse building technologies and systems without using the help of sophisticated building design tools.

1.2 Building Energy and Airflow Simulation

Building energy simulation (ES) tools are essential for energy-efficient building design to accurately estimate building energy consumption and thermal performance. By solving the heat (and mass) transfer in the building envelopes, indoor spaces and building systems, a typical building energy simulation tool can provide:

- dynamic building envelope thermal behaviors,
- unsteady indoor environment state (temperature and humidity),
- space heating/cooling load,
- capacity of the HVAC systems selected,
- energy consumption of the HVAC systems.

Numerous building energy simulation programs have been developed in the last three decades and have been widely used in the design practice as more powerful personal computers have become available. Currently, a typical hour-by-hour energy

analysis for a building in a whole year can be completed within a few seconds with a PC. Applications of ES greatly facilitate the development of energy-efficient buildings by providing a rapid prediction and better understanding of the consequences of various design decisions.

However, most ES programs assume the indoor air is completely mixed and with uniform properties. This may not be true for most buildings. The mean indoor air temperature and humidity provided by ES tools are not satisfactory for advanced indoor environment designs. Additionally, ES programs do not solve the air movement and contaminant transportation in the space. All these information are crucial to evaluate the indoor air quality and thermal comfort level of a building as well as the performance of HVAC systems.

Hence, accurate prediction of indoor environment is highly desired for the design of an energy efficient, comfortable and healthy building. Among various airflow modeling tools, computational fluid dynamics (CFD) is undoubtedly the most sophisticated airflow simulation tool. By numerically solving the governing conservation equations of fluid flows, CFD can predict the detailed time-dependent and spatial distributions of

- air velocity in three directions (air speed),
- air pressure,
- air temperature,
- relative humidity,
- turbulent intensity,
- contaminant concentrations.

These results can be directly or indirectly used to quantitatively analyze the indoor environment quality and judge the system performance. For example, the air velocity, temperature, relative humidity, and the surface temperatures of building enclosures are the four most important parameters influencing indoor thermal comfort. For the evaluation of indoor air quality, the concentration level of different pollutants is the most important criterion.

Recently, CFD has played an important role in studying building thermal comfort and indoor air quality problems. Encouraging results have been achieved by using the CFD techniques for diverse indoor environmental and HVAC studies (Ladeinde and Nearon 1997, Spengler and Chen 2000). Generally, a CFD calculation for a typical room with reasonable solution resolution may take a few hours with a modern PC (Srebric 2000).

The usage of both ES and CFD programs provides the most important parameters for the essential evaluation of building performance. Consequently, the evaluation will substantially facilitate the effort of designing an energy-efficient, thermally comfortable and environmentally friendly building with an optimal HVAC system.

1.3 Integration of Building Energy and Airflow Simulation

In the past, energy simulation has tended to be separated from detailed air movement simulation due to their different mathematical models, numerical methods, program characteristics, and modeling emphases. However, ES and CFD programs are, in fact, not independent. The information provided by these two programs is complementary. The integration of ES and CFD programs can eliminate many assumptions employed in the separate applications and result in more accurate predictions of building performance.

On one hand, air movement that ES programs do not handle has a significant influence on the load and energy estimation of a building through convective heat transfer. Most ES models use empirical formulae to generate convective heat transfer coefficients for heat convection calculation on a surface. The values may be far different from the real ones because of the dissimilarity between the case studied and the case used to produce the empirical formulae. With the development of passive cooling techniques, natural ventilation and hybrid ventilation have become more and more important in the energy-efficient building design. However, most ES programs cannot determine the accurate airflow entering/leaving a building where the room air temperature and heating/cooling load heavily depend on the airflow. In addition, the uniform indoor air temperature assumption in most ES models may not be true for some indoor spaces, such as those with displacement ventilation systems, which will also affect the accurate prediction of building energy consumption. CFD, however, can provide the detailed and accurate indoor air velocity and temperature distributions, based on which the precise convective heat transfer coefficients and convective heat flux can be calculated. The indoor air temperature gradient and convective heat transfer can then be used in an ES model for more accurate energy calculation. In addition, CFD can accurately simulate natural ventilation driven by wind effect and stack effect. The information can also be used in an ES model.

On the other hand, the accurate prediction of airflow in CFD requires accurate flow and thermal boundary conditions. In practice, most boundary conditions specified in CFD are based on measurements, empirical data or even personal experience, which may have significant adverse influence on the simulation and solutions (Awbi 1998, Emmerich 1997, Xu and Chen 1998). However, the ES results, such as heating/cooling load and wall surface temperatures, allow the possibility of providing CFD accurate and time-varying boundary conditions.

Therefore, it is attractive and beneficial to couple these two programs for the development of an integrated building design tool with best performance. One may argue that there is no need to integrate an energy simulation program with a CFD program since a CFD program can be extended to solve heat transfer in solid materials, such as building walls. With an appropriate radiation model, HVAC system model, and plant model, the extended CFD program can have the functions of both ES and CFD programs. This type of CFD program solves convective, radiative, and conductive heat transfer simultaneously. Several recent investigations (Off et al. 1996, Fisher and Rosler 1996,

Schild 1997, and Charvat et al. 2001) have attempted to use the CFD programs to analyze the dynamic performance of buildings. The approach employs CFD for the heat conduction in solid materials by the conjugate heat transfer model and uses a radiation model to consider surface-to-surface heat transfer. This allows room airflow to be calculated by prescribing boundary conditions external to the building or in adjoining spaces, rather than within the room. The method sounds powerful but it is very computationally expensive (Chen et al. 1995). The reason for the expensive computing cost is threefold:

- First, when the CFD considers the heat transfer in solid materials, the calculation becomes stiffer than the convection-only CFD. The computing time goes up dramatically in order to reach a converged and stable solution (Thompson 1988).
- Secondly, since room air has a characteristic thermal response time of a few seconds while building envelope has a few hours, the CFD simulation must be performed over a long period for the thermal performance of the building envelope but with a small time step to account for the room air characteristics. It results in the necessity for repeating the computationally demanding calculation a large number of times, providing tremendous intermediate information with which people may not even be concern.
- Thirdly, the CFD computing time grows exponentially with building size. In small indoor spaces with mixing ventilation of a building, the room air temperature is rather uniform and heat transfer coefficient is close to a constant. The CFD simulation is not necessary for these spaces but is still performed within the extended program.

Hence, the extended CFD (the conjugate heat transfer) method is not practical for immediate use in a design context with current computer capabilities and speed.

An alternative to reduce the computing costs in solving convective, radiative, and conductive heat transfer in both solid materials and air by CFD is to couple a CFD program with an energy simulation program. CFD handles the indoor air movement and ES solves the heat radiation between surfaces and the heat conduction in solid materials. Most ES programs deal with the heat conduction in building envelopes with various simplified methods, such as the simplification of one-dimensional heat conduction. As a consequence, the computing time of ES can be reduced to be negligibly small (seconds), compared with the computing cost of CFD that is normally a few hours for a steady calculation. Additionally, in this coupling approach, the simulation time interval of ES can be considerably large (a few minutes to an hour) because the thermal response time of solid materials in building envelopes is relatively long. CFD in this coupling approach, rather than predicting the transient airflow patterns, only simulates the indoor airflows at specific time moments with the corresponding boundary conditions obtained from ES, acting as the "snap-shots" of the airflows. Such a coupling procedure certainly saves computing time because it avoids solving the flow field during the transition from one time step to another. Furthermore, this coupling approach allows performance of CFD simulation for particularly selected indoor spaces rather than the whole building, which further reduces the computing cost.

In principle, a well-iterated ES and CFD coupling program can provide a solution

that is equivalent to the conjugate heat transfer method, provided that the ES program subdivides surfaces reasonably small to model any significant temperature variations. Therefore, it is most interesting and attractive to directly couple ES and CFD programs, which forms the subject of this thesis work.

1.4 Research Objectives and Thesis Outline

With the long-term aim to develop an integrated building design tool in which CAD, ES, CFD and other building models are linked using standard methods, this thesis focuses on the identification of the possible roles and linkage for ES and CFD in such a tool. The thesis will discuss the potential challenges in coupling ES and CFD programs, study the possible coupling methods to the integration of ES and CFD, describe how these methods could be implemented with using a general ES and CFD program, and demonstrate the performance and capabilities of the coupled program developed.

The detailed objectives for this investigation can be summarized as:

- To develop fast and practical coupling strategies;
- To study efficient and reliable iterative coupling algorithms;
- To analyze solution characteristics of coupled simulations;
- To construct a compatible, flexible and easy-to-use coupling platform;
- To demonstrate the applications and benefits of coupled simulations.

This thesis records the major achievements in the research and is organized as follows:

- Chapter 2 reviews the evolution of building energy simulation and airflow simulation, indicating that heat balance based ES and Reynolds-averaged CFD should be used for this coupling study. The chapter suggests the usage of a state-of-the-art ES program – EnergyPlus (E+) developed by Lawrence Berkeley National Laboratory (LBNL) and the development of a new ready-to-plug-in CFD solver – MIT-CFD – for this thesis work. The chapter further reviews the current state of the ES and CFD coupling research, which enlightens the directions of this research.

- Chapter 3 introduces the fundamentals of EnergyPlus with the focus on the thermal performance of building envelope and indoor air. The chapter also discusses the development and principles of MIT-CFD, demonstrating its good program structure and features feasible for the coupling study.

- Chapter 4 validates the MIT-CFD program via the measured data obtained from a number of classic building experiment facilities. Good agreements between the simulations and measurements verify the creditability of the CFD solver developed. The chapter also briefly introduces the validation efforts on EnergyPlus in the literature.

- Chapter 5 presents the primary principles and challenges to ES and CFD program coupling. To bridge the discontinuities between ES and CFD programs due to the different physical models and numerical methods employed, special coupling strategies are developed, in which the staged coupling strategies proposed can effectively reduce the computing costs but preserve the accuracy and details of the computed results. This chapter further introduces the general techniques employed to develop a reliable and flexible ES and CFD coupling platform.

- Chapter 6 discusses the proper calculation method of convective heat transfer at enclosures, which is the key linkage between ES and CFD. The study analytically and numerically investigates the effect of the size of the first CFD grid and turbulence model on surface convective heat transfer.

- Chapter 7 discusses the solution characteristics of iterative coupling simulation of ES and CFD programs. Through theoretical analysis and numerical experiments, the chapter addresses the concerns about the solution existence, uniqueness and correctness of the coupled ES and CFD simulation and the convergence and stability performance of the iterative coupling. The chapter also investigates the influences of some primary simulation parameters on the coupling performance.

- Chapter 8 reports the validations of the coupled program with experimental data from four full-scale building experiment facilities. The comparison of numerical solutions with the experimental data reveals the advantages of the integrated building simulation over the separate ES and CFD applications. The chapter further demonstrates the capabilities of the coupled program through two practical design projects.

- Chapter 9 discusses the building characteristics that may affect the necessity and effectiveness of the ES-CFD coupling simulation. These building characteristics along with the solution resolution requirement determine whether a coupled simulation is essential for a particular type of building and which coupling strategy can provide the best solution with the compromise of accuracy and efficiency. The chapter studies the sensitivity of coupling simulation to the building characteristics. Based on the study, the chapter provides the general suggestions for the appropriate usage of the coupling simulation.

- Chapter 10 summarizes the studies presented in this thesis and provides recommendations for future work.

CHAPTER 2

LITERATURE REVIEW

This chapter reviews the evolution of building energy simulation and airflow simulation, indicating the heat balance based ES and Reynolds-averaged CFD are most suitable for the coupling study. The review suggests the use of the newly developed ES program – EnergyPlus (E+) by Lawrence Berkeley National Laboratory (LBNL) and the development of a new ready-to-plug-in CFD solver for this research. The chapter also reviews the current state of the ES and CFD coupling research, which enlightens the directions of this thesis work.

2.1 Building Energy Simulation (ES)

Designing an energy-efficient building requires an estimate of the energy consumption in buildings. Building energy calculation methods can generally be divided into two categories: manual calculation methods and computer simulation methods. Manual calculation methods, such as the degree-day and bin methods (ASHARE 1997), are widely used in practical design due to their simplicity and efficiency, although they are not precise. Degree-day methods are the simplest methods for energy estimation and are appropriate if the building occupying and operating conditions are constant. If the conditions of the building and systems vary with outdoor temperature, the building energy consumption needs to be calculated for different values of the outdoor temperature and multiplied by the corresponding number of hours; this is the basic idea of various bin methods. More sophisticated models must be used when the situation becomes more complicated, such as varying indoor air temperature and interior heat gains. The manual methods provide a simple estimate of building annual loads, but they cannot, for example, be used for:

- evaluation of air conditioning plant.
- evaluation of most control issues.
- medium or heavy weight buildings with significant diurnal fluctuations in internal temperature.

As more powerful computers have become available, computer modeling has been more and more important for the prediction of the energy and environmental performance of buildings and systems that serve them. Computer simulation is credited with speeding up the design process, enabling the comparison a broader range of design variants and leading to optimal designs. With reasonable physical assumptions and mathematical models, the computer simulations provide more accurate and informative results than the manual calculations. As a result, it provides a better understanding of the consequences of design decisions. The underlying mathematical models and numerical schemes of simulation tools distinguish them from each other, satisfying the different requirements of complexity and accuracy.

The development of computer energy simulation programs can be traced back to the 60's and 70's, when the groundwork of energy simulation methods was laid (e.g. GATC 1967). After Mitalas and Stephenson (1967) published their milestone work on the response factor method to model the transient heat transfer through building envelopes and the heat transfer between internal surfaces and room air, ASHRAE published procedures for determining heating and cooling loads. The load calculation can then be used to size the system and compute the total energy cost.

Most energy simulation programs adopt the Load, System and Plant (LSP) modeling strategy (Sowell and Hittle 1995), which subdivides the building energy simulation into three sequential steps. The building's heating and cooling loads are first calculated for the entire analysis period (often a year) for an assumed set of indoor environmental conditions. These loads are then imposed as inputs to the second step of the simulation, which models the air handling and energy distribution systems (fans, heating coils, cooling coils, air diffusers, etc.). This second simulation step (also conducted for the entire analysis period) predicts the demands placed on the plant's energy conversion systems (boilers, chillers) and related equipment (cooling towers and circulation pumps). The third step is to calculate the source energy requirements in the central plant. Finally, one would estimate the costs of the source energy, sometimes introducing capital and other investment costs for a complete life-cycle economic analysis.

The interest of this thesis has been focused on the accuracy of the load calculation, which forms the base of the next two steps. The weighting factor method and heat balance method (ASHRAE 1997) are the two principal methods used for building load calculation in the past few decades. It is well known that heat gain is not the same as cooling load for a building. For example, the lighting energy in a room does not convert to 100% convective heat immediately. In fact, a part of the heat is radiated and then will be absorbed by the building enclosures and furniture. This part of radiative heat may be released back to the room air at a later time, because of the room thermal capacity.

The weighting factor method estimates the ratio of convective heat to the total energy release in a time sequence. The weighting factors heavily depend on building material properties, and may be pre-calculated and presented in tables for certain types of buildings. These tables can be directly used by an energy simulation program, or even manual calculation, for the load estimate if the actual building is close to the one used to produce the weighting factors. The weighting factor method was popular in the 1970s because of the limited computing capacity at that time. Earlier building energy simulation programs using weighting factors are the Post Office Program (GATC 1967), NESCAP (NASA 1975) and DOE-1 (Diamond et al. 1977).

The heat balance method was introduced in the 1970s (e.g. Kusuda 1976) to enable a more rigorous treatment of building loads. Rather than using pre-calculated weighting factors to characterize the thermal response of the room air to outdoor air temperature changes, solar radiation, and internal gains, this approach solves heat

balances for the room air and enclosure surfaces to determine the loads. The enclosure surface temperatures calculated can be used to determine the radiant temperature. The heat balance method eliminates some significant linearity assumptions and allows building dynamic conditions to be modeled appropriately. For example, the convection coefficients that characterize heat transfer from interior surfaces to the room air could respond to thermal states within the room, rather than being treated as constant. NBSLD (Kusuda 1976) is probably the earliest program of this type. Other current programs that use the heat balance method include popular ones, such as BLAST (Hittle 1979), ESP-r (Clarke 1985) and EnergyPlus (Crawley 2000).

Most weighting factor and heat balance programs use response factors (Mitalas and Stephenson 1967) and transfer functions (Stephenson and Mitalas 1971) to calculate transient conduction through walls, roofs and floors, with the assumption that the heat conduction is one dimensional. The response factors or transfer functions are based on control theory. The mathematical background is rather complicated. However, they determine heat conduction much faster than the finite-difference method. The finite-difference method does not have to assume the one-dimensional heat conduction. It would yield much more accurate results for corner walls and would provide temperature distribution in a wall that is useful for analyzing condensation (Chen et al. 1995). However, the computing time of the finite-difference method is still considerable. Hence, most current energy simulation programs still use the response factor and transfer function methods with the fairly reasonable one-dimension assumption.

Building energy simulation has encountered incredible development since the 1970s. Recent years have especially witnessed the proliferation of building energy simulation software for a broadening range of building performance assessment. Besides the continuous improvement on the well-noticed energy software such as BLAST, DOE-2, TRNSYS, ASHRAE Loads Toolkit, ESP-r, and CODYBA (Noel et al 2001), many new energy programs are developed for research, education and design purposes, such as, ColSim (Wittwer 1999), SIMEDIF(Larsen and Lesino 2001), DOMUS (Mendes et al. 2001). To date, ASHRAE bibliography of computer simulations of building has listed more than 200 programs.

Many of these building energy simulation programs are reaching maturity – using simulation methods and even codes that originated in the 1960s. BLAST and DOE-2 are two of the most popular energy simulation programs and widely used in the building design practices throughout the world. DOE–2 (Winkelmann et al. 1993), sponsored by the U.S. Department of Energy (DOE), was developed from the Post Office program written in the late 1960s for the U.S. Post Office. BLAST (Building System Laboratory 1999), sponsored by the US Department of Defense (DOD), has its origins in the NBSLD program developed at the US National Bureau of Standards (now NIST) in the early 1970s. The main difference between the two programs is the load calculation method – DOE–2 uses a room weighting factor approach while BLAST uses a heat balance approach. These two programs each have pros and cons and have wide utilities in various environments, but both of them have begun to show their ages in a variety of ways (Crawley 2001). The simulation methodologies in both programs are often difficult

to trace due to the decades of development (and multiple authors). To maintain, support and enhance either program, a developer must have many years of experience working with the codes, and knowledge of code unrelated to the task (due to a significant amount of "spaghetti" code). Without substantial redesign and recoding, expanding their capabilities has become difficult, time-consuming, and expensive (Crawley 2001). As a result, DOE eventually decided to start developing a new energy simulation program named EnergyPlus (E+) in 1996. EnergyPlus, developed by Lawrence Berkeley National Laboratory (LBNL), is an all-new heat balance based program with the best efforts to combine the most popular features and capabilities of BLAST and DOE-2. Compared to the legacy programs, the highlights of EnergyPlus are:

(1) simulation management structure that eliminates the interconnections between various program sections. As a result, it eliminates the need to understand all parts of the code in order to make an addition to a very limited part of the program.

(2) modularity that allows other developers to quickly add other component simulation modules with only a limited knowledge of the entire program structure.

(3) integration of loads, systems and plants that overcomes the most serious deficiency of DOE-2 and BLAST: inaccurate space temperature prediction due to lack of feedback from the HVAC module. The integration solution also allows users to evaluate a number of processes that neither DOE-2 nor BLAST can simulate well, for instance, realistic system control and interzone airflow.

Table 2.1 Comparison of major features and capabilities of three ES programs (Crawley 2001)

Features and Capabilities	DOE-2	BLAST	EnergyPlus
Integrated loads/systems/plant solution	×	×	√
Heat balance calculation	×	√	√
Multiple time step for interaction between environment, zones, and systems	×	×	√
Moisture absorption/desorption in building envelope	×	×	√
Interior surface convection dependent on temperature and airflow	×	√	√
Anisotropic sky model	√	×	√
Advanced fenestration calculations	√	×	√
Daylighting illumination and controls	√	×	√
Thermal comfort model	×	√	√
User-configurable HVAC systems	×	×	√
Air and fluid loop in HVAC systems	×	×	√
Links to SPARK, TRNSYS	×	×	√

Table 2.1 compares the major features and capabilities of EnergyPlus with those of BLAST and DOE–2. It is obvious that EnergyPlus is superior to its ancestors. This thesis, therefore, will use this newly developed EnergyPlus program for the coupling study. Chapter 3 will further introduce the fundamentals of the EnergyPlus program.

2.2 Building Air Movement Simulation

Activity in the building simulation field is not limited to thermal and energy considerations. Parallel work is underway on airflow modeling. Airflow models were first developed to estimate wind and buoyancy driven infiltration effects on buildings. After that, different types of airflow models were developed to address all kinds of airflow-related problems, such as outdoor wind pressure on buildings, indoor air pollutant distributions, zone-to-zone air exchanges, natural ventilation, envelope interior surface convection, efficiency of air handling and distribution systems, etc. This study has focused on the airflow modeling of building indoor space, which is important to the building thermal comfort and indoor air quality analysis and to the building energy estimation.

Figure 2.1 shows a general classification of room airflow models. The mixing model is the simplest airflow model, which assumes the air in each single space is completely mixed and has uniform properties. It is a special case of the nodal model, and is thus also called single-nodal model in some literatures.

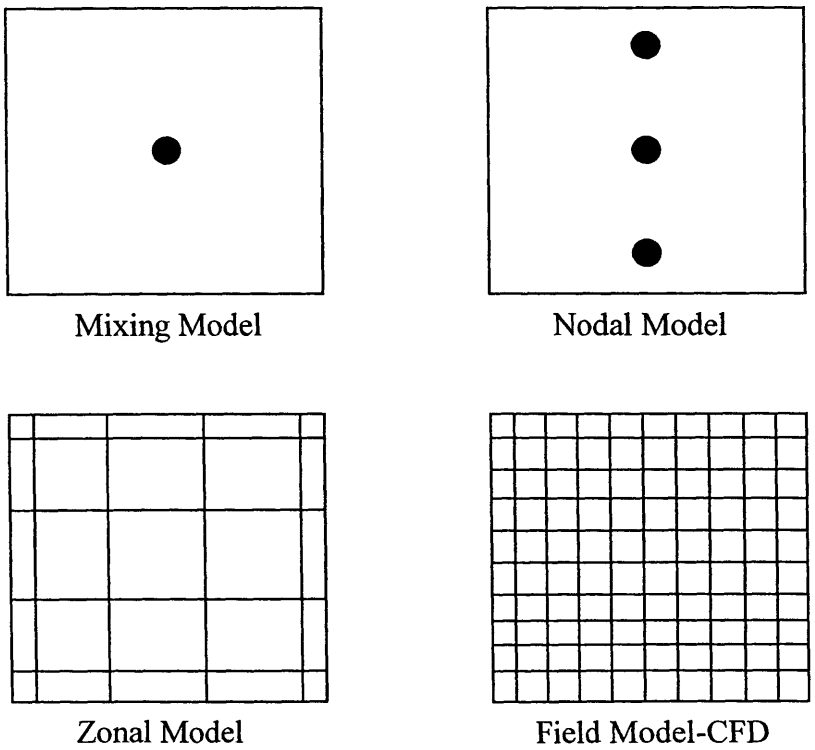

Figure 2.1 Classification of room airflow models

Nodal airflow models were developed in the 1970s for simulating both infiltration and internal airflow between spaces. Nodal models treat the building and room air as an idealized network of nodes connected with flow paths. In a nodal model, a specific airflow configuration is assumed, and the mass and energy balances are written for each node of the nodal network. Lebrun (1970) was apparently the first to propose a nodal model for providing a rough estimate of thermal stratification in the context of building energy use. The work focused on modeling how heat is convected around a room by a baseboard heater under a cold window. Lebrun's pioneering work has led to the development of nodal models. Allard and Inard (1992) reviewed various levels of nodal models used in the prediction of the thermally coupled behavior of a room and its heating system. Some recent nodal models (e.g. Mundt 1996, Yuan et al. 1999, Rees and Haves 2001) can predict the vertical temperature gradient in rooms with displacement ventilation. Harrington (2001) developed a nodal model for natural ventilation where the model selects among five different airflow patterns based on the Archimedes number. The primary drawback of nodal models is that prior knowledge of the airflow patterns is required to specify mass flow in the thermal network, which makes the models difficult to use for most designers.

Zonal models introduce more flow dynamics into the prediction of mean airflows compared to nodal models. Depending on the physically valid hypotheses and experimental experience, zonal models divide the space of a room into several sub-spaces (zones). These sub-zones are combined together with the conservation of mass and energy equations. In a zonal model, air flow rates are usually solved based on temperature differences, length scales and initial momentum. Bouia and Dalicieux (1991) were apparently the first to publish what is termed a pressure-zonal model that uses pressure as a state variable and solves energy and mass balance equations in the context of building room air modeling. Inard et al. (1996) demonstrated a functional three-dimensional pressure zonal model with special cells (handlings) for walls, jets, and plumes. A difficulty in applying pressure-zonal models to most building simulations is the requirement of using special laws to describe flows in certain regions. Togari et al. (1993) presented a temperature-zonal model that was intended for use in HVAC applications for large vertical spaces such as atriums. The temperature-zonal models use empirical correlations based on temperature differences in combination with special laws for flows like jets and plumes. The main problem with temperature-zonal models is that it is difficult to obtain general-purpose convective heat transport terms that are usually developed from a small set of experiments. The recent zonal airflow models include those developed by Wurtz et al. (1998), Feustel (1998, 1999), Lin (1999), Warren (2000), Groleau and Marenne (2001), Musy et al. (2001), and Haghighat et al. (2001), as examples.

Zonal models provide increased generality compared to nodal models. Most zonal models can also be used in a personal computer and require relatively small computing power (Griffith 2002). The most attractive reason for design engineers is that limited investment and training are needed to apply these models. However, zonal models are highly experiment-dependent. The existing zonal models are limited to the predictions of mean temperature and mass flow rate in each zone. More specifically,

zonal models employ two main assumptions: (1) the primary driving flows (boundary layer, jet or thermal plume) can be pre-predicted, and (2) users have a good knowledge of the entire flow structures so that the whole flow field can be divided into zones with distinct features. These two assumptions largely limit the application of these methods in a prediction process. It is not always possible to make a clear decision about the main flow pattern. Much more work is needed to get a better knowledge of the heat and mass transfer in buoyancy-driven flows in a non-isothermal and non-adiabatic environment. Further limitations of using these models include:

- the need to quantify the driving forces and to account accurately for all openings in the room;
- the assumption of uniformly mixed air and pollutant in each zone; and
- uncertainty in the results obtained with zonal models.

Beyond these, Griffith (2002) found that many zonal models are not numerically stable. Hence, it is necessary to develop and utilize more general, accurate, detailed, and stable air movement models.

With the development of fluid mechanics and numerical methodologies, the computational fluid dynamics (CFD) technique has been a popular tool for predicting engineering flows since the early 1970's. CFD is receiving greater acceptance as a technique for building airflow analysis. It offers the potential of much richer details, a higher degree of flexibility, and lower cost than the traditional laboratory study. As the most sophisticated airflow model, CFD provides the detailed spatial (field) distributions of air pressure, velocity, temperature, humidity, contaminants, and turbulence intensity by solving the conservation equations of mass, momentum, energy, and species concentrations. The air velocity, temperature, relative humidity, and the surface temperatures of building enclosures are the four most important parameters influencing thermal comfort of indoor space. The concentration level of different pollutants can be directly used to evaluate building indoor air quality. In addition, Fanger et al. (1989) pointed out that turbulence intensity has a significant impact on draft. Hence, CFD results assist the quantitative analysis of the thermal comfort and indoor air quality status of a building in great detail.

Nielsen (1974) was probably the first one who applied CFD techniques to room air motion. Applications of CFD for room airflow were mushrooming in the 1980s. The International Energy Agency Annex 20 was particularly devoted to room airflow prediction with participants from 13 countries (Moser 1994). In the past two decades, numerous encouraging results have been achieved by using the CFD technique for studies of building thermal comfort and indoor air quality, as reviewed by Whittle (1986), Liddament (1991), Jones and Whittle (1992), Chen and Jiang (1992), Moser (1992), Lemaire et al. (1993), Emmerich (1997), Nielsen (1989, 1998), and Spengler and Chen (2000). Ladeinde and Nearon (1997) reviewed CFD applications in the HVAC industry. These reviews concluded that CFD is powerful in predicting building air movement, although users' knowledge, experience and skills with CFD are essential to the accuracy of CFD results.

The airflows that CFD predicts can be laminar, turbulent, or transitional between laminar and turbulent flows. Turbulence is characterized as chaotic state of fluid motion, which most real flows are. As yet no complete theory on turbulence exists, because its nonlinear dynamics is not well understood. Due to the sophisticated characteristic properties of turbulence, such as irregularity, nonlinearity, diffusivity, large Reynolds numbers, three-dimensional vorticity fluctuations, dissipation and continuum (Tennekes and Lumley 1972), it is difficult to identify whether airflow in a room is a locally artificially induced, transitional, or fully developed turbulence. However, very few room airflows are laminar. All non-laminar room airflows could be defined as turbulence. CFD prediction on turbulent flows currently is by three approaches: direct numerical simulation (DNS), large-eddy simulation (LES), and Reynolds-averaged equations simulation with turbulence models.

DNS computes a turbulent flow by solving the highly reliable Navier-Stokes equation without approximations. DNS requires a very fine grid resolution to capture the smallest eddies in the turbulent flow. According to turbulence theory (Nieuwstadt 1990), the number of grid points required to describe turbulent motions should be at least $N \sim Re^{9/4}$. The computer systems must become rather large (memory at least 10^{10} words and peak performances at least 10^{12} flops) in order to do computations for the flow (Nieuwstadt et al. 1994). In other words, since the smallest eddy size in a room is about 0.01 m to 0.001 m, at least 1000 x 1000 x 1000 grids are needed to solve the airflow. Neither existing parallel computers nor computers of the near future can even approximately supply the storage space or the necessary CPU performance demanded by such a simulation. In addition, the DNS method requires very small time steps, which makes the calculation extremely time consuming. It is clear that in the near future the applications of the direct numerical simulations for indoor flows are not realistic.

Deardorff (1970) developed a method named "large-eddy simulation" with the hypothesis that the turbulent motion could be separated into large-eddies and small-eddies such that the separation between the two does not have a significant effect on the evolution of large-eddies. The large-eddies corresponding to the three-dimensional time-dependent equations can be directly simulated on existing computers. Turbulent transport approximations are then made for small-eddies independently from the flow geometry, which eliminates the need for a very fine spatial grid and short time steps. The philosophy behind this approach is that the macroscopic structure is characteristic for a turbulent flow. Moreover, the large scales of motion are primarily responsible for all transport processes, such as the exchange of momentum and heat. The success of the method stems from the fact that the main contribution to turbulent transport comes from the large-eddy motion. Thus the large-eddy simulation is clearly superior to turbulent transport closure wherein the transport terms (e.g. Reynolds stresses, turbulent heat fluxes, etc...) are treated with full empiricism. LES has been successfully applied to several building indoor and outdoor airflow studies. Some examples of such applications are the flow around a building (Murakami et al. 1996), forced convection flow in a room (Davidson and Nielsen 1996, Emmerich and McGrattan 1998), natural ventilation flow in buildings (Jiang and Chen 2001), and particle dispersion in buildings (Jiang and Chen 2002). Murakami (1998) concluded that LES can produce accurate results both at the

mean and turbulent levels for airflows in and around buildings. However, LES needs large computer power and memory because of the required fine grid and unsteady calculation. Jiang (2002) indicated that LES even with an empirical model, such as a wall model, to reduce the grid number in the near-wall regions, requires 4-5 days of computing time with a fast workstation for a wind-driven airflow. For the simulation of buoyancy-driven airflows, more computing time is needed. This is not acceptable for most building design purposes. With the development in computer capacity and speed, LES may be used as the main tool to building airflows in the future.

Since the details of turbulent flow are difficult to model and engineers are mainly interested in the mean values, one then turns to solving the Reynolds-Averaged Navier-Stokes (RANS) equations with turbulence models. In the RANS approach, CFD treats flow dynamic quantities as some sort of statistically averaged (Reynolds-averaged) turbulent field and simulates merely the gross features of the turbulent flow. The turbulence fluctuation effect on the mean airflow can be represented by different turbulence models. Turbulence models are simplified mathematical descriptions of turbulent flows. They are based on good physical insight, and are applicable to complicated flows encountered in reality. With a turbulence model, it is possible to predict the flows found in practice with the capacity of present computers. Many turbulence models have been developed in the last century, which can be generally divided into two categories: eddy-viscosity models and Reynolds stress models.

The eddy-viscosity models adopt Boussinesq approximation (1877) that relates Reynolds stress to the rate of mean stream through an "eddy" viscosity. Classic eddy-viscosity models include mixing-length model (zero-equation eddy-viscosity model) (e.g. Prandtl 1926), one-equation eddy-viscosity model (e.g. Kolmogorov 1942), and two-equation eddy-viscosity model (e.g. Launder and Spalding 1974).

The zero-equation eddy-viscosity models are the simplest turbulence models. The model has one algebra equation for turbulent viscosity, and no (zero) additional partial differential equations beyond the Reynolds-averaged equations for mass, momentum, energy, and species conservation. Hence, it has the best computing efficiency. Although zero-equation models have fatal physical deficiency, for instance, without considering non-local and flow-history effects in the eddy-viscosity, and although more sophisticated turbulence models are developed, zero-equation models still gain certain attentions in today's industrial practices because they are simple, cost-effective, and once calibrated, can predict mean-flow quantities fairly well. In fact, some simple zero-equation models may provide surprisingly good results. For example, a constant viscosity model (an empirical constant ν_t) can give much better results for swirling flow than the standard k-ε model. Also, Nielsen's study (1998) showed that the constant eddy-viscosity model provides results closer to the measured data than the standard k-ε model for the prediction of smoke movement in a tunnel. Xu (1998) developed a zero-equation model, which was demonstrated to have the high feasibility in predicting room airflows by many validations such as Chen and Xu (1998), Srebric et al (1999), and Beausoleil-Morrison (2000).

The k-ε two-equation eddy-viscosity model developed by Launder and Spalding

(1974), so-called "standard" k-ε model, has been widely used in practice, where k is turbulence kinetic energy and ε is the dissipation rate of turbulence energy. Numerous other two-equation models have been suggested afterwards. Chen (1995) has tested five different k-ε models for natural convection, forced convection, mixed convection and impinging jet in a room, but it is very difficult to identify any other models superior to the standard k-ε model.

The Boussinesq approximation is sometimes inadequate to represent the local state of turbulence for complex flow situations, such as recirculating flows in a room. This deficiency can be overcome in Reynolds stress models (RSMs) that explicitly employ transport equations for the individual Reynolds stresses. Although the study of RSMs has been started in the 1970s, the applications of RSMs toward three-dimensional flows began to appear in the 1990s. Direct applications in room airflow computation include those by Murakami et al. (1990) and Renz and Terhaag (1990). They computed airflow patterns in a room with jets. The results show that the RSM is superior to the standard *k*-ε model, because anisotropic effects of turbulence are taken into account. Chen (1996) compared three RSMs with the standard k-ε model for natural convection, forced convection, mixed convection, and impinging jet in a room. He concluded that the RSMs are only slightly better than the k-ε model but have a severe penalty in computing time. Based on a large number of applications for engineering flows, Leschziner (1990) concluded that RSMs are appropriate and beneficial when the flow is dominated by a recirculation zone driven by a shear layer. Thakur and Shyy (1999) reviewed the latest status of Reynolds stress models and the various associated modeling issues. The review confirmed the importance of RSMs for the flows involving strong streamline curvature due to the geometry complexity or a high degree of swirl. However, the implementation and application of RSMs are not a trivial task – it brings with it a number of issues associated with the stability of the overall algorithm and boundary conditions. The simulations with RSMs requires (three to ten times) more computing time than those with eddy-viscosity models because of greater algebraic complexity. Additionally, although with the continuous development (e.g. Craft 1998, Hanjalic and Jakirlic 2002), the RSMs still have various defects and weaknesses, especially for low-Reynolds and buoyancy-driven airflows. Hence, the models need further study, improvement and validation before they can be widely used for room airflow prediction.

Most of today's CFD programs used in practice solve the Reynolds-Averaged Navier-Stokes (RANS) equations with different kinds of eddy-viscosity turbulence models, which provides reasonably accurate results with acceptable computing costs. To satisfy the building design purpose that mostly focuses on the macro-level characteristics of flow and heat transfer and requires fast simulation responses, the present study should adopt the RANS simulation approach using several simple and classical turbulence models for room airflows, i.e. constant viscosity model, zero-equation model (Xu 1998), and standard k-ε model (Launder and Spalding 1974).

Many commercial CFD software have been developed in the last two decades. Some of them are even specially developed for building industry applications, such as AirPak (Fluent 2001). However, most commercial CFD programs are usually difficult to

integrate into the whole building simulation program because of its huge code size and complicated program features for versatile simulation purposes. Existing research CFD programs also require major modifications, sometime even re-organization of the entire program structure, before they can be plugged into a building simulation program. Therefore, the present investigation will develop a new CFD solver, MIT-CFD, for the coupling with the EnergyPlus program. The program will use the standard CFD techniques and can predict building room airflows with a reasonable accuracy and computing speed. The highlights of the program will be the well designed and implemented data and program structures that allows the easy plug-in of the program to an arbitrary building energy simulation program. Chapter 3 will present the fundamentals, development and features of this CFD program.

2.3 Integration of Energy Simulation and CFD Programs

Building energy simulation and CFD programs provide important and complementary information for the evaluation of building performance. Due to their different modeling emphases and methodologies, these two programs are usually applied separately. However, in the past ten years, efforts have been made to combine these two aspects. This is because the integration of ES and CFD allows the elimination of many assumptions used in separate ES and CFD and results in more accurate and detailed predictions of building performance. On one side, the energy simulation of a building, a complicated system, requires the concurrency of many physical phenomena. Particularly, the air movement has the most significant influence on the convective heat transfer, and therefore the energy estimate of a building. On the other hand, the airflow simulation by CFD requires the enclosure surface temperatures and supply heating or cooling energy as inputs, which can be obtained from the energy simulation.

Chen (1988) was probably the first one to try to couple an energy simulation program with a CFD program. In his approach, the CFD program solves the convective heat transfer and airflow in a room. An energy simulation program simulates radiative and conductive heat transfer in buildings. The outputs of the energy simulation program, such as wall surface temperatures and loads, are the inputs of the CFD program. On the other hand, the results of the CFD program, such as room air temperature distribution and convective heat transfer coefficients, are the inputs of the energy simulation program. With this coupling approach, the computing costs are much cheaper than that with a conjugated CFD program, while reasonable solutions are still achieved. Limited by the computer capacity available at that time, manual/static coupling was conducted in his study. Chen also proposed some other measures to further reduce the computing costs, such as using a few fixed airflow patterns to calculate hour-by-hour air temperature distribution.

Srebric et al. (2000) improved Chen's study (1988) by automatically/dynamically coupling a CFD program with an ES program for building heating/cooling load calculation. The simulations show the explicit benefits from the coupling, as Nielsen and Tryggvason (1998) confirmed that an interconnection between a CFD program and a

building energy performance simulation program would improve both the energy consumption data and the prediction of thermal comfort and air quality in a selected area of a building. However, as a preliminary investigation, Srebric did not conduct substantial performance analyses and validation studies on the coupled simulation. Moreover, Srebric's coupling is still not a full dynamic process that implies a sufficient iteration between two programs at each time step to reach a mutually consistent solution before moving on to the next time step.

Clarke (1995a, 1995b) and Negrao (1995) integrated a CFD code into the ESP-r building simulation program (ESRU 1999). The two modeling programs operate in tandem, "handshaking" on a time step basis. The thermal/energy simulation program can supply CFD with realistic and time-varying boundary conditions. CFD then can be used to predict the details of flow and temperature fields within particular zones, thus enabling flow visualization, studies on pollutant dispersion, thermal comfort assessments, and accurate modeling of convection heat transfer at building internal surfaces.

Negrao (1995) devised several integration approaches to address different degrees of complexity and sophistication. The first one corresponds to a simple approach where the ES and CFD systems exchange information without any direct interaction. The second approach consists of three dynamic schemes to handle the thermal coupling at the zone internal surfaces. The first scheme makes use of nominal convection coefficient to combine ES and CFD models. Nominal convection coefficients which link the air node and surface temperatures of ES are calculated by CFD. The second scheme, called sequential approach, is an improvement of the first scheme, where the convection heat transfer computed by CFD, rather than the convection coefficients, is directly inserted in the zone interior surface heat balance. The third scheme, the simultaneous approach, iteratively solves all energy equations describing the heat fluxes within a zone within one time-step; with the surface and intra-constructional energy balances computed by ES and the inside zone energy balances calculated by CFD.

The investigations by Clarke and Negrao indicate that the integration of the two modeling programs can be satisfactorily achieved by maintaining each program's separate solution algorithm. The connection between the two modeling programs is then made within regions that each model considers as its boundary condition. The overall system balance is then achieved through an iterative procedure. Their studies show that, although substantially different in approach, the dynamic thermal coupling methods devised produce very similar results when time-steps are sufficiently small.

Beausoleil-Morrison (2000, 2001) continued Negrao's work by creating adaptive convection algorithm and adaptive conflation controller to the ESP-r program. The conflation controller can monitor the evolving thermal and air flow conditions in the room and dynamically select an appropriate combination of modeling programs for the prevailing conditions based on a two-stage CFD simulation.

Although the coupling approaches of the ESP-r program have behaved qualitatively well, Negrao (1995) and Beausoleil-Morrison (2000) found the convergence

of the combined simulation is usually difficult to obtain, even for a simple case, and indicated the refined knowledge necessary to improve the combined approach. Negrao (1995) also pointed out that further development of coupling strategies is necessary in order to reduce the total computing time of a coupled simulation and make it practical for design purposes.

Clovis (2001) summarized the issues on the integration of CFD and building simulation tools and indicated four major problems: (1) CFD time cost; (2) stability and convergence of numerical methods; (3) user expertise; and (4) physical modeling of flows. He concluded that CFD seems to be the most complex package to be integrated with the whole building simulation package and a careful approach must be exercised when coupling CFD tools with other systemic simulation tools.

The available coupling studies in the literature have clearly verified that the ES and CFD program coupling can improve the solutions with acceptable computing efforts although many problems are still unsolved. The review notices that most of the current ES and CFD coupling efforts have been focused on the development of specific ES and CFD coupling programs. Few studies can be found that address the fundamental issues in the coupling of ES and CFD programs, such as:

(1) How many methods are available to connect these two programs? Do they have identical performance?
(2) Does the coupled solution necessarily exist? Is the solution unique?
(3) Is it necessary to iterate ES and CFD calculation at each time step? Can an iterative coupling always reach a converged and stable solution?

The answers to these problems are extremely important, forming the foundation to the further development, improvement and application of such an integrated building design tool. The study conducted by this thesis attempts to address these questions through theoretical analysis and numerical experimentation. Chapter 5 discusses the principles and challenges of the coupling and develops special coupling strategies to bridge the disparities between ES and CFD. Chapter 7 intensively analyzes the solution characteristics, including the solution existence, uniqueness, convergence, and stability. The chapter also discusses the feasibility and compares the performance of various potential coupling methods. Chapter 9 suggests the appropriate usages of the iterative coupling based on the sensitivity analysis of coupling simulation.

CHAPTER 3

FUNDAMENTALS OF ENERGYPLUS AND MIT-CFD

This chapter introduces the fundamentals of the building energy simulation program (EnergyPlus) and the CFD program (MIT-CFD), which are two basic components of the integrated building design tool to be developed. EnergyPlus is a building energy simulation program recently developed by Lawrence Berkeley National Laboratory. MIT-CFD is a new ready-to-plug-in CFD solver developed by this study, with special program structure and features that are feasible for the coupling investigation.

3.1 Fundamentals of EnergyPlus (E+)

3.1.1 General Descriptions of EnergyPlus

EnergyPlus (Crawley 2000) is a new-generation building energy analysis and thermal load simulation program, having its root in both the BLAST (Hittle 1979) and DOE-2 (Winkelmann et al. 1993) programs. Based on a user's description of a building from the perspective of the building's physical makeup, associated mechanical systems, etc..., EnergyPlus can calculate the heating and cooling loads necessary to maintain thermal control setpoints, the conditions throughout an secondary HVAC system and coil loads, and the energy consumption of primary plant equipment. The program has inherited many simulation characteristics from the legacy programs of BLAST and DOE-2, as well as created many particular features to overcome the shortcomings of its parent programs. In particular, the special simulation management philosophy and modular nature of the program eliminate the interconnections between various program sections and the need to understand all parts of the code in order to make an addition to a very limited part of the program. As a consequence, the program allows the easy expansion of functions and linkages to other programs, as illustrated in Figure 3.1.

Figure 3.1 shows the overall structure of the EnergyPlus program. It has three basic components – surface heat balance manager, air heat balance manager, and building systems simulation manager – all under the control of the integrated solution manager. The surface and air heat balance managers calculate the outside and inside surface and room air heat balance and act as an interface between the heat balance and the building systems simulation manager. The building systems simulation manager handles communication between the heat balance managers and various HVAC modules and loops, such as coils, boilers, chillers, pumps, fans, and other equipment/components. With this program structure, more independent model modules, such as daylighing module, can be easily plugged into the individual manager component without cross-influencing the others. Therefore, it can maximize the number of developers who can quickly integrate their work into EnergyPlus for the minimum investment of resources.

This feature of EnergyPlus particularly highlights its feasibility for the present coupling study.

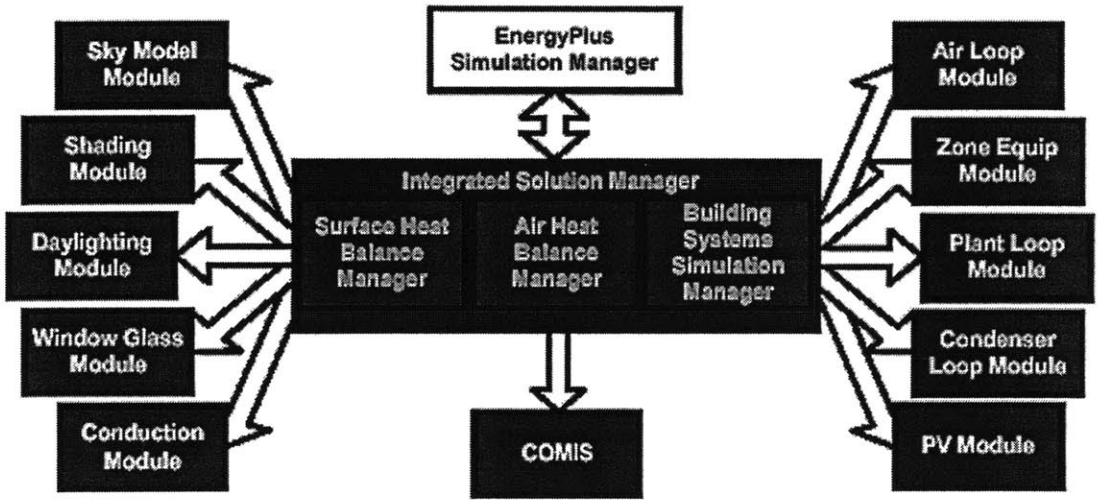

Figure 3.1 Overall EnergyPlus structure (LBNL 2001)

3.1.2 Heat Balance Method of EnergyPlus

As shown in Figure 3.1, EnergyPlus is a heat-balance-method-based building energy simulation program. Chapter 2 has clarified that the heat balance method provides more flexibility and generality with less physical and numerical assumptions, compared to the conventional weighting factor method.

The heat balance equations for room air and surface heat transfer are two essential equations solved by EnergyPlus to determine the building heating/cooling load.

The heat balance equation for room air is

$$\sum_{i=1}^{N} q_{i,c} A_i + Q_{lights} + Q_{people} + Q_{appliances} + Q_{inf\,iltration} - Q_{heat\_extraction} = \frac{\rho V_{room} C_p \Delta T}{\Delta t} \quad (3.1)$$

where

$\sum_{i=1}^{N} q_{i,c} A_i$ = convective heat transfer from enclosure surfaces to room air
$q_{i,c}$ = convective flux from surface i
i, N = index and number of enclosure surfaces
A_i = area of surface i
Q_{lights} = heat gains from lights
Q_{people} = heat gains from people

$Q_{appliances}$ = heat gains from appliances
$Q_{infiltration}$ = heat gains from infiltration
$Q_{heat\_extraction}$ = heat extraction rate of the room
$\frac{\rho V_{room} C_p \Delta T}{\Delta t}$ = internal energy change rate of room air
ρ = air density
V_{room} = room volume
C_p = specific heat of air
ΔT = temperature change of room air
Δt = sampling time interval, normally one hour

The heat extraction rate is the same as the cooling/heating load when the room air temperature is maintained as constant ($\Delta T = 0$). The convective heat flux from a wall is determined from the heat balance equation for the wall surface, as shown in Figure 3.2. A similar heat balance can be obtained for each window. The heat balance equation for a surface (wall/window) can be written as:

$$q_i + q_{ir} = \sum_{k=1}^{N} q_{ik} + q_{i,c} \tag{3.2}$$

where
q_i = conductive heat flux on surface i
q_{ir} = radiative heat flux from internal heat sources and solar radiation
q_{ik} = radiative heat flux from surface i to surface k

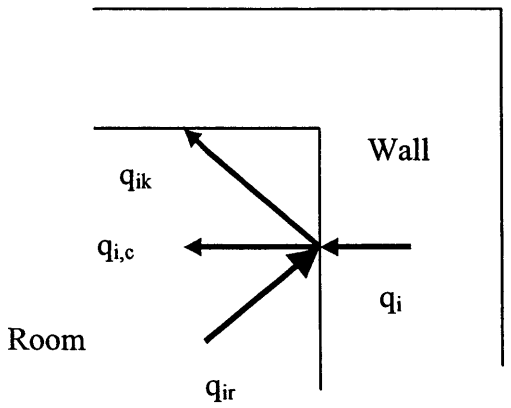

Figure 3.2 Energy balance on the interior surface of a wall, ceiling, floor, roof or slab

EnergyPlus uses the conduction transfer functions (CTF) method (Meyers 1980, Seem 1987) to compute surface conductive heat fluxes q_i through the building enclosures. The radiative heat flux is determined by

$$q_{ik} = h_{ik,r}(T_i - T_k) \tag{3.3}$$

where

$h_{ik,r}$ = linearized radiative heat transfer coefficient between surfaces i and k
T_i = temperature of interior surface i
T_k = temperature of interior surface k

And the convective heat flux is

$$q_{i,c} = h_c (T_i - T_{room}) \tag{3.4}$$

where

h_c = convective heat transfer coefficient
T_{room} = room air temperature

The convective heat transfer coefficient, h_c, is unknown, usually determined by empirical correlations in ES programs. EnergyPlus allows choosing one of the following models (LBNL 2001) to calculate the convective heat transfer coefficients (unit: $W/m^2 \cdot K$):

(1) Detailed natural convection model

Based on flat plate experiments, the detailed natural convection model correlates the convective heat transfer coefficient to the surface orientation and the temperature difference between the surface and zone air (where ΔT = Surface Temperature - Air Temperature).

- If $\Delta T = 0.0$ or a vertical surface, then

$$h = 1.31|\Delta T|^{1/3} \tag{3.5}$$

- If $\Delta T < 0.0$ with an upward facing surface or $\Delta T > 0.0$ with an downward facing surface (enhanced convection), then

$$h = \frac{9.482|\Delta T|^{1/3}}{7.283 - |\cos \Sigma|} \tag{3.6}$$

where Σ is the surface tilt angle.

- If $\Delta T > 0.0$ with an upward facing surface or $\Delta T < 0.0$ with an downward facing surface (reduced convection), then

$$h = \frac{1.810|\Delta T|^{1/3}}{1.382 + |\cos \Sigma|} \tag{3.7}$$

where Σ is the surface tilt angle.

(2) Simple natural convection model

The simple convection model uses constant coefficients for each of three heat transfer configurations as follows.

- For a horizontal surface with reduced convection,

$$h=0.948 \tag{3.8}$$

- For a horizontal surface with enhanced convection,

$$h=4.040 \tag{3.9}$$

- For a vertical surface,

$$h=3.076 \tag{3.10}$$

- For a tilted surface with reduced convection,

$$h=2.281 \tag{3.11}$$

- For a tilted surface with enhanced convection,

$$h=3.870 \tag{3.12}$$

(3) Ceiling diffuser model

The ceiling diffuser model correlates the convective heat transfer coefficient to the supply mass flow rate (ACH).

- For floors,

$$h=3.873+0.082\times ACH^{0.98} \tag{3.13}$$

- For ceilings,

$$h=2.234+4.099\times ACH^{0.503} \tag{3.14}$$

- For walls,

$$h=1.208+1.012\times ACH^{0.604} \tag{3.15}$$

After obtaining the expressions of the convective, radiative and conductive heat fluxes on each envelope surface, the interior surface temperatures, T_i, can be determined by simultaneously solving Eq. (3.2), if the room air temperature, T_{room}, is assumed to be uniform and known. Space cooling/heating load can then be determined from Eq. (3.1) with the calculated convection heat from the enclosures. Thereafter, the coil load is determined from the heat extraction rate and the corresponding air handling processes and HVAC equipment selected. With a plant model and hour-by-hour calculation of the coil load, the energy consumption of the whole HVAC system for a building can be determined.

On the other hand, if there is no HVAC system running in the space, iteratively solving Eqs. (3.1) and (3.2) then predicts the change of uniform indoor air temperature and enclosure surface temperatures during a day, season, or year concerned. It is obvious, in both air-conditioned and non-air-conditioned scenarios, that the interior

convective heat transfer from the building enclosures to the indoor air is the explicit linkage between the room air and surface heat balance equations. Its accuracy will directly affect the energy calculated.

Figure 3.3 demonstrates the executive streamline of the EnergyPlus program. Given the building materials and geometry information, the ES program first calculates the conduction transfer factors. Under the weather condition at each time step, the ES program then simulates the heat balance of building envelope surfaces and room air to obtain the building heating/cooling load and thermal behaviors of the building. Based on this information, the second system and plant models can be operated for the system energy consumption and the total building operating cost.

However, unlike the conventional ES programs, EnergyPlus allows the system and plant output to directly impact the building thermal response at the current time step, rather than calculating all loads first, then simulating systems and plants. This integrated simulation approach can help to more accurately investigate the effect of undersizing fans and equipment on the thermal comfort of occupants within the build. By using the integrated solution technique, EnergyPlus can solve the most serious deficiency of the BLAST and DOE–2 sequential simulations – inaccurate space temperature predication due to no feedback from the HVAC module to the loads calculations. Accurate prediction of space temperatures is crucial to energy efficient system engineering – heating/cooling load, system size, plant size, occupant comfort and health. Integrated simulation also allows users to evaluate a number of processes that neither BLAST nor DOE–2 can simulate well, including realistic system controls, moisture adsorption and desorption in building elements, radiant heating and cooling systems, and interzone air flow (Crawley 2001).

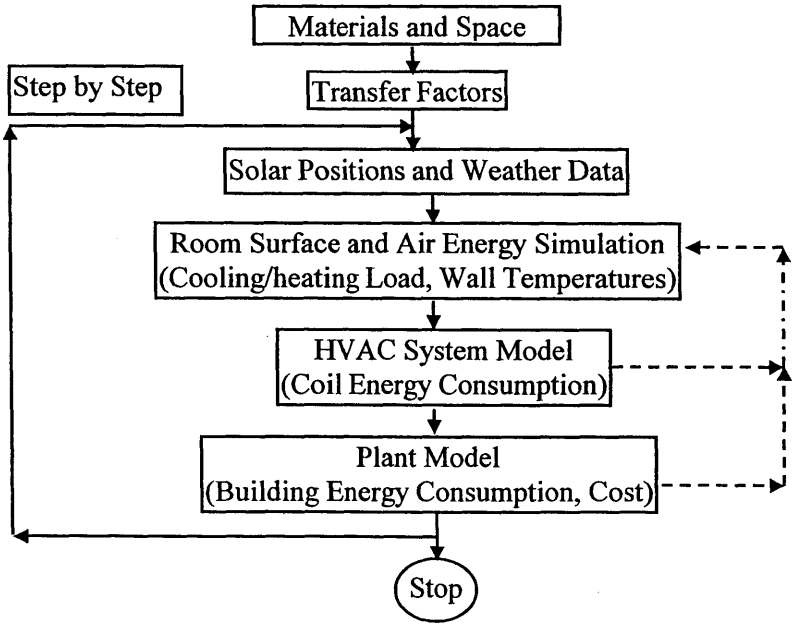

Figure 3.3 Executive streamline of the EnergyPlus program

3.2 Fundamentals of MIT-CFD

3.2.1 General Descriptions of MIT-CFD

To develop an integrated building simulation tool that consists of energy and airflow simulation models, the present investigation has developed a new CFD solver, MIT-CFD, for the coupling with the EnergyPlus program. The CFD program can predict the steady/unsteady three-dimensional incompressible turbulence/laminar airflows in and around buildings with reasonable accuracy and computing cost. The well designed and implemented data and code structures allow the program to be easily integrated into a commercial building energy simulation program.

MIT-CFD was developed using Standard Fortran Language (Fortran 90) to be consistent with the EnergyPlus program. The program can be either used separately as a regular CFD solver or an embeddable module for EnergyPlus to form the integrated program. In either case, the CFD program is rather independent, which makes it easy to maintain as a stand alone CFD code or to couple with other building simulation programs. MIT-CFD uses the modular method to organize the program structure. The modularity allows the expansion of the program capacity and the connection to other simulation models. Figure 3.4 sketches the major structure of MIT-CFD. The problem-independent part of the program handles the core of the CFD calculation, which does not need to change when solving different problems or when coupled with different programs. The problem-dependent part deals with all the operations before and after the CFD core calculation, including the input of case descriptions, the output of simulation results, and the effort to couple with other programs.

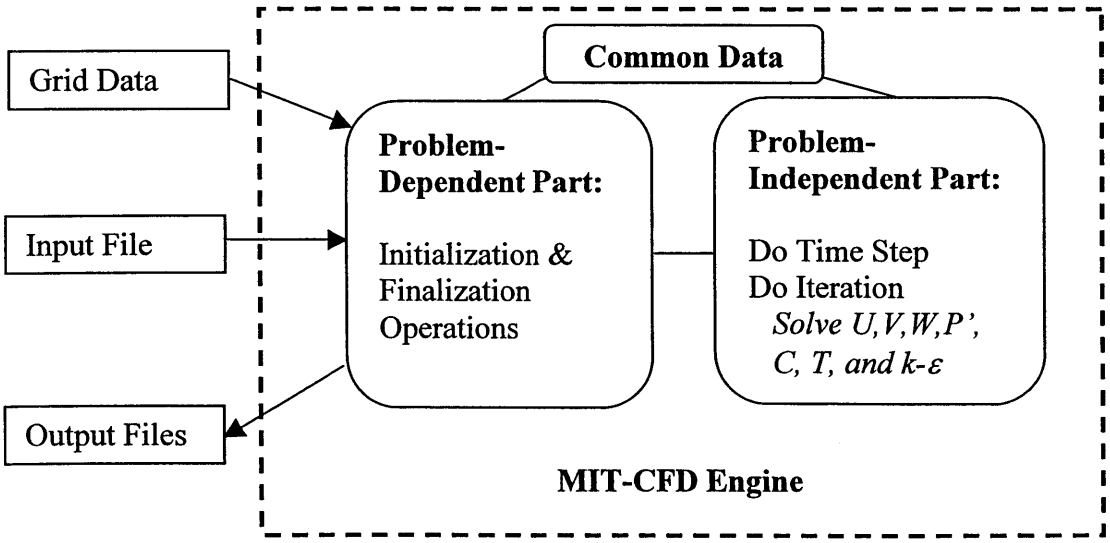

Figure 3.4 Sketch of MIT-CFD program

The present MIT-CFD program has been developed to allow AutoCAD files of the STL form to be imported into the simulation. This function provides convenience to building designers who are most familiar with AutoCAD programs, and facilitates the effort to generate a complex object for CFD simulation, such as a complex site-plan. This feature will become more attractive when the EnergyPlus program will be developed to also have the capability of importing AutoCAD files.

3.2.2 Mathematical Models and Numerical Methods of MIT-CFD

3.2.2.1 Reynolds-Averaged Governing Equations of Incompressible Fluid Flows

MIT-CFD calculates the spatial and temporal distributions of air pressure, velocity, temperature, humidity ratio, contaminant concentration, and turbulence (if turbulent flows) by solving the conservative governing equations of fluid flows.

The Reynolds-averaged governing equations of incompressible fluid flows, which the real airflows in and around buildings are, can be expressed in a Cartesian coordinate system as:

- Continuity equation

$$\frac{\partial U_i}{\partial x_i} = \frac{\partial u_i'}{\partial x_i} = 0 \tag{3.16}$$

where U_i and u_i' are the Reynolds-averaged and turbulence fluctuant velocity component, respectively, in three perpendicular coordinate directions x_i ($i = 1, 2, 3$).

- Momentum equations

$$\frac{\partial U_i}{\partial t} + U_j \frac{\partial U_i}{\partial x_j} = -\frac{\partial P}{\partial x_i} + \frac{\partial}{\partial x_j}\left(\nu \frac{\partial U_i}{\partial x_j} - \overline{u_i' u_j'}\right) - g_i \beta (T - T_\infty) \tag{3.17}$$

where U_i and U_j are the Reynolds-averaged velocity components in x_i and x_j directions, t is the time, P is the Reynolds-averaged pressure, $\nu = \frac{\mu}{\rho}$ is the air molecular kinematic viscosity, μ is the air molecular dynamic viscosity, ρ is the air density, g_i is the gravity acceleration in i-direction, β is the thermal expansion coefficient of air, T_∞ is the temperature of a reference point, and T is the Reynolds-averaged air temperature. $\overline{u_i' u_j'}$, called Reynolds stresses, represents the turbulence influence on the mean airflow.

- Energy equation

$$\frac{\partial T}{\partial t} + U_j \frac{\partial T}{\partial x_j} = \frac{\partial}{\partial x_k}\left(\Gamma \frac{\partial T}{\partial x_k} - \overline{u_k' T'} \right) + q_{source} \tag{3.18}$$

where T is the Reynolds-averaged air temperature, $\Gamma = \frac{\kappa}{\rho c_p} = \frac{\nu}{Pr}$ is the temperature viscous diffusion coefficient, κ is the thermal conductivity of air, ρ is the air density, c_p is the specific heat of air at constant pressure, Pr is the Prandtl number, q_{source} is the energy source in the fluid. $\overline{u_k' T'}$, called turbulent heat flux, represents the turbulence influence on the mean air temperature development.

- Concentration equation

$$\frac{\partial C}{\partial t} + U_j \frac{\partial C}{\partial x_j} = \frac{\partial}{\partial x_k}\left(\alpha \frac{\partial C}{\partial x_k} - \overline{u_k' c'} \right) + q_{source} \tag{3.19}$$

where C is the Reynolds-averaged species concentration, $\alpha = \frac{\nu}{Sc}$ is the concentration viscous diffusion coefficient, Sc is the Schmidt number, q_{source} is the species source. $\overline{u_k' c'}$, called turbulent concentration flux, represents the turbulence influence on the mean concentration development. $\overline{u_i' u_j'}$, $\overline{u_k' T'}$, and $\overline{u_k' c'}$ are unknown and need to be solved or modeled approximately.

3.2.2.2 Turbulence Models

In the last hundred years, numerous turbulence models have been developed to represent the unknown $\overline{u_i' u_j'}$, $\overline{u_k' T'}$, $\overline{u_k' c'}$ and close Eqs. (3.16)-(3.19). The current MIT-CFD program employs the traditional eddy-viscosity turbulence models that adopt the Boussinesq approximation (1877) to relate Reynolds stress to the rate of mean stream through an "eddy" viscosity ν_t.

$$\overline{u_i' u_j'} = \frac{2}{3}\delta_{ij} k - \nu_t \left(\frac{\partial U_i}{\partial x_j} + \frac{\partial U_j}{\partial x_i} \right) \tag{3.20}$$

Similarly, the turbulent scalar fluxes, such as turbulent heat and concentration fluxes, can be approximated as additional diffusion caused by turbulence (eddy-diffusivity)

$$\overline{u_k' T'} = -\frac{\nu_t}{Pr_t} \frac{\partial T}{\partial x_k} \tag{3.21}$$

$$\overline{u_k' c'} = -\frac{\nu_t}{Sc_t}\frac{\partial C}{\partial x_k} \tag{3.22}$$

where δ_{ij} is the Kronecker delta (when $i \neq j$, $\delta_{ij}=0$; and when $i=j$, $\delta_{ij}=1$), and k is the turbulence kinetic energy ($k = \frac{\overline{u_i' u_i'}}{2}$). Pr_t is the turbulent Prandtl number, and Sc_t is the turbulent Schmidt number.

How to obtain this "eddy" viscosity ν_t then becomes the main subject of the different eddy-viscosity models. The MIT-CFD program has implemented three classical eddy-viscosity turbulence models for user's choice.

(1) Constant eddy-viscosity model:

$$\nu_t = 100\nu \tag{3.23}$$

(2) Zero-equation eddy-viscosity model (Xu 1998):

$$\nu_t = 0.03874|U_D|L \tag{3.24}$$

where U_D is the local mean airflow speed and L is the normal distance to the nearest wall.

(3) Standard k-ε two-equation eddy-viscosity model (Launder and Spalding 1974)

$$\nu_t = C_\mu \frac{k^2}{\varepsilon} \tag{3.25}$$

where $C_\mu = 0.09$ is the empirical constant. k and ε can be determined by solving the transport equations of k and ε:

$$U_j \frac{\partial k}{\partial x_j} = \frac{\partial}{\partial x_j}\left[\left(\nu + \frac{\nu_t}{\sigma_k}\right)\frac{\partial k}{\partial x_j}\right] + P + G - \varepsilon \tag{3.26}$$

$$U_j \frac{\partial \varepsilon}{\partial x_j} = \frac{\partial}{\partial x_j}\left[\left(\nu + \frac{\nu_t}{\sigma_\varepsilon}\right)\frac{\partial \varepsilon}{\partial x_j}\right] + \left[C_{\varepsilon 1}(P+G) - C_{\varepsilon 2}\varepsilon\right]\frac{\varepsilon}{k} \tag{3.27}$$

where,

$$P = \nu_t \frac{1}{2}\left(\frac{\partial U_i}{\partial x_j} + \frac{\partial U_j}{\partial x_i}\right)^2, \quad G = -g_k \beta \frac{\nu_t}{\sigma_t}\frac{\partial T}{\partial x_k} \tag{3.28}$$

and $\sigma_t = 1.0$, $\sigma_k = 1.0$, $\sigma_\varepsilon = 1.3$, $C_{\varepsilon 1} = 1.44$, and $C_{\varepsilon 2} = 1.92$ are the empirical constants.

3.2.2.3 Boundary Conditions

Turbulence models enclose the governing equations of (3.16)-(3.19). However, a closed system of flow transport equations that can be solved mathematically has not been formed until the boundary conditions are specified at all the boundaries around the flow field. MIT-CFD implemented most of the conventional flow boundary conditions that include: inflow, outflow, symmetry surface, rigid surface, and internal object. Standard treatments of these boundary conditions were applied to MIT-CFD (Patankar 1980). In particular, for the turbulent flow around the rigid surfaces, besides the common no-slip condition for viscous flows, special near-wall handling techniques need to be used to describe the low-Reynolds turbulent flow and heat transfer at this region. The standard wall function approach (Launder and Spalding 1974) has been employed in the current MIT-CFD program to work with the standard k-ε eddy-viscosity model for the simulation of the flows with rigid boundaries.

3.2.2.4 Numerical Simulation Methods

The flow governing equations (3.16)-(3.19) with turbulence models, such as the zero-equation model (3.24) or the standard k-ε model (3.25)-(3.27), as well as appropriate boundary conditions, establish a complete system of flow equations. However, these equations are highly non-linear and strongly self-coupled. It is impossible to obtain analytical solutions for most real airflow problems. Therefore, the partial differential governing equations must be solved numerically. The basic concept of the numerical simulation is to discretize the accurate, spatial and temporal continuous differential equations into approximate, discrete algebraic equations that can be solved by a computer through iteration. As a result, the discrete field-distributed numerical values, instead of the continuous solutions, are obtained in the space concerned (computation domain).

Three major numerical simulation approaches have been broadly used to model fluid flows: finite difference (Roache 1972), finite volume (Patankar 1980), and finite elements (Baker 1983) methods. The finite difference method discretizes the equations by expressing the derivatives with divided difference quotients. The finite volume method integrates the conservation equations on each control-volume and replaces all cell fluxes with difference quotients. The finite element method employs the so-called Galerkin weighted residual method to integrate the equations on each cell (Baker 1983, Patankar 1980).

The finite difference method is simple and easy to analyze the numerical accuracy of the discretization. But, it is generally difficult to interpret the physical meanings of some higher-order terms in the Taylor series. The finite difference method does not guarantee the conservation of the discretized equations. In contrast, the finite volume method retains most physical information, and the conservation of the equations can be strictly achieved on every control-volume. The shortcoming of the finite volume method is that the accuracy of the discretization is difficult to analyze. The finite element method is powerful for handling complex geometry but it is difficult to use due to its

mathematical complexity and is thus less popular. Therefore, the finite volume method, which possesses both mathematical simplicity and physical conservation, has been used in the development of the MIT-CFD program.

(1) Discretization of Computation Domain and Governing Equations

The first step of the numerical procedure in the finite-volume-method-based CFD is to discretize the computation domain by dividing the whole flow field into a finite number of cells (control volume) by a grid system, as illustrated by a two-dimensional example in Fig 3.5.

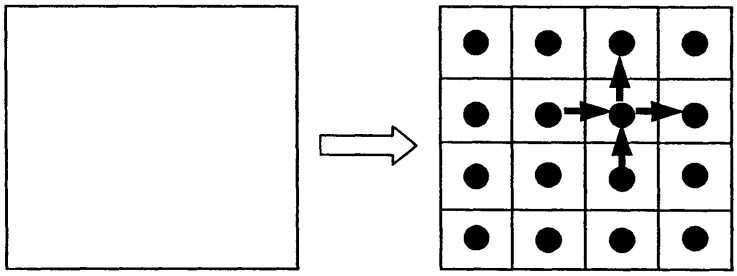

Fig 3.5 Two-dimensional illustration of computation domain discretization

The transport/conservation equations of mass, momentum and energy on this whole computation domain are then applied to each of the control volumes. The flow properties in each cell are assumed uniform. Note that the size of cells can be different (non-uniform grid) and the geometry of cells can be nonorthogonal (body-fitted grid).

The second step of the numerical procedure is to spatially and temporally discretize the flow governing equations. The governing equations of incompressible turbulent flow (3.16)-(3.19) and the k-ε turbulence model equations (3.26)-(3.27) can be expressed in the following general form:

$$\frac{\partial \rho\phi}{\partial t}+\frac{\partial \rho U_j\phi}{\partial x_j}=\frac{\partial}{\partial x_j}\left(\Gamma_{\phi,\text{eff}}\frac{\partial \phi}{\partial x_j}\right)+S_\phi \tag{3.29}$$

where ϕ represents the physical variable in question, as shown in Table 3.1. The equation has time, convection, diffusion and source terms.

Integrating Eq. (3.29) over a typical control volume centered at P (Figure 3.6 shows a two-dimensional projection of this cell on x-y plane, for clear demonstration) leads to a flux balance equation

$$\int_{\Delta V}\frac{\partial(\rho\phi)}{\partial t}dV+I_e-I_w+I_n-I_s+I_t-I_b=\int_{\Delta V}S_\phi dV \tag{3.30}$$

where I_f represents the total flux of ϕ across the cell-face f (=e, w, n, s, t, or b). Each of the surface fluxes I_f contains a convective contribution I_f^C and a diffusive contribution I_f^D, that is

$$I_f = I_f^C + I_f^D \tag{3.31}$$

Table 3.1 Formula for the general form equation (3.29)

Equation	ϕ	$\Gamma_{\phi,eff}$	S_ϕ
Continuity	1	0	0
Momentum	U_i	$\mu+\mu_t$	$-\frac{\partial p}{\partial x_i}-\rho\beta(T-T_\infty)g_i$
Turbulent kinetic energy	k	$\mu+\frac{\mu_t}{\sigma_k}$	$\rho P+\rho G-\rho\varepsilon$
Dissipation rate of k	ε	$\mu+\frac{\mu_t}{\sigma_\varepsilon}$	$(C_{\varepsilon 1}\rho P+C_{\varepsilon 1}\rho G-C_{\varepsilon 2}\rho\varepsilon)\frac{\varepsilon}{k}$
Temperature	T	$\frac{\mu}{Pr}+\frac{\mu_t}{Pr_t}$	S_T
Concentration	C	$\frac{\mu}{Sc}+\frac{\mu_t}{Sc_t}$	S_C

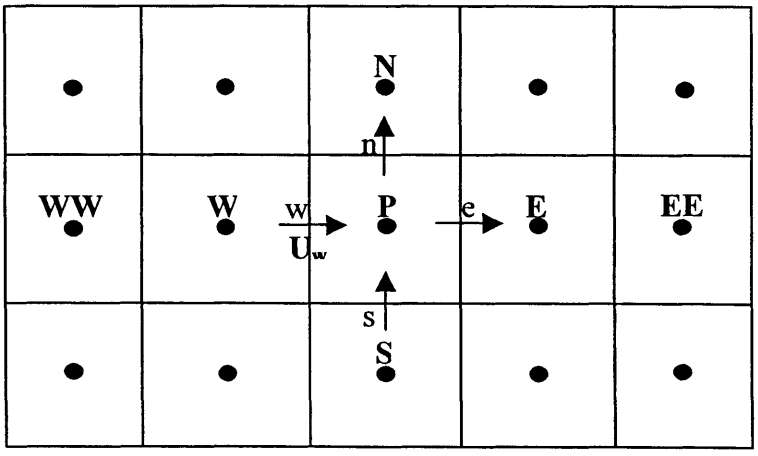

Fig 3.6 Two-dimensional illustration of control volume

- *Approximation of convection term*

The convective contribution I_f^C in Eq. (3.31) can be approximated as:

$$I_f^C = C_f \phi_f \tag{3.32}$$

where C_f is the mass flux across the cell face f and can be calculated, for w-, s- and b-faces, as:

$$C_w=(\rho AU)_w,\ C_s=(\rho AU)_s,\ C_b=(\rho AU)_b \tag{3.33}$$

The determination of ϕ_f is a key element for both accuracy and stability of numerical solutions. Various numerical schemes with different orders of numerical accuracy are available to approximate ϕ_f at faces of each cell by using the adjacent cell center values. Generally, the more accurate schemes tend to be less stable, and vice versa. This study has incorporated the first-order-accurate upwind differencing scheme, the first-order-accurate hybrid differencing scheme (Spalding 1972), the second-order-accurate HLPA differencing scheme (Zhu 1991), and the third-order-accurate QUICK differencing scheme (Leonard 1979) into the MIT-CFD program, leaving a choice to the user. Taking the w-face of the control volume P as an example, if using QUICK scheme, the face value ϕ_w can be calculated through three adjacent nodal values ϕ_P, ϕ_W and ϕ_{WW}:

$$\phi_w = \frac{3}{8}\phi_P + \frac{3}{4}\phi_W - \frac{1}{8}\phi_{WW} \tag{3.34}$$

- *Approximation of diffusion term*

A second-order-accurate central differencing scheme (Patankar 1980) is usually good for the approximation of second-derivative terms. By applying a central differencing scheme to the diffusion term in Eq. (3.29), I_f^D can be written, for the w-face as an example, as:

$$I_w^D = D_w(\varphi_P - \varphi_W) \tag{3.35}$$

where

$$D_w = \left(A^2 \Gamma_\phi / \Delta V\right)_w \tag{3.36}$$

is the diffusive coefficient; A is w-face surface area and ΔV is cell volume.

- *Approximation of time derivative*

The time derivative term in Eq. (3.30) can be approximated by different time discretization schemes. A simple time scheme – Full Implicit (FI) scheme of first-order accuracy has been used in MIT-CFD, which gives

$$\frac{\partial(\rho\phi)}{\partial t} = \frac{(\rho\phi)^n - (\rho\phi)^{n-1}}{\Delta t} \tag{3.37}$$

where n refers to the current time step, and Δt is the time step increase. The volume integral of the time term can therefore be approximated as

$$\int_{\Delta V} \frac{\partial(\rho\phi)}{\partial t} dV = \frac{(\rho\phi)^n - (\rho\phi)^{n-1}}{\Delta t} \Delta V = \frac{\rho \Delta V}{\Delta t}\left(\phi_P^n - \phi_P^{n-1}\right) = S_P^T \phi_P^n - S_U^T \tag{3.38}$$

where $S_P^T = \frac{\rho \Delta V}{\Delta t}$, $S_U^T = \frac{\rho \Delta V}{\Delta t} \phi_P^{n-1}$

- *Approximation of source derivative*

The source term S_ϕ is usually linearized as

$$S_\phi = S_\phi^U + S_\phi^P \phi_P \tag{3.39}$$

where the coefficient S_ϕ^P is defined so that it is always less than zero for all the conservation equations. This operation enhances the stability of the numerical process (Patankar 1980). The volume integral of the source term can therefore be approximated as

$$\int_{\Delta V} S_\phi dV = S_\phi^U \Delta V + S_\phi^P \phi_P \Delta V = S'_U + S'_P \phi_P \tag{3.40}$$

- *Final form of discretized governing equations*

After replacing all the terms in Eq. (3.30) by their discretized analogues, the final form of the discretized governing equations results:

$$A_P \phi_P = \sum_{nb} A_{nb} \phi_{nb} + S_U \quad , \text{nb=w,e,s,n,b,t} \tag{3.41}$$

where

$$A_P = \sum_{nb} A_{nb} - S_P \tag{3.42}$$

$$S_U = S'_U + S_U^T \tag{3.43}$$

$$S_P = S'_P - S_P^T \tag{3.44}$$

The main coefficients A_{nb} that relate the principal unknown ϕ_P to its neighbors ϕ_{nb} contain the combined contribution from convection and diffusion. Eq. (3.41) represents a set of algebraic equations describing the conservative features of the flow on each discrete cell.

In order to stabilize the solution process, it is often necessary to under-relax the current solution by retaining part of the old solution:

$$\phi_P = (1-\alpha_\phi)\phi_P^{old} + \alpha_\phi \phi_P \tag{3.45}$$

where $\alpha_\phi \in [0,1]$ is an under-relaxation factor. Introducing Eq. (3.45) into Eq. (3.41) leads to an under-relaxed difference equation which has the same form as Eq. (3.41) except that the coefficients A_P and S_U are replaced by:

$$S_U = S_U + \frac{1-\alpha_\phi}{\alpha_\phi} A_P \phi_P^{old} \tag{3.46}$$

$$A_P = \frac{A_P}{\alpha_\phi} \tag{3.47}$$

(2) Treatment of Pressure-Velocity Coupling

The above numerical processes produce a set of algebraic equations describing the airflows. However, the pressure gradient term $-\partial P/\partial x_i$ in the momentum equations has not been discussed and included. Pressure gradient is an important term in the momentum equations, which is usually included in the source term of Eq. (3.30). Integrating $-\partial P/\partial x_i$ over a control volume gives

$$\int -\frac{\partial P}{\partial x_1} dV = (PA)_w - (PA)_e \quad \text{(for U momentum)} \tag{3.48a}$$

$$\int -\frac{\partial P}{\partial x_2} dV = (PA)_s - (PA)_n \quad \text{(for V momentum)} \tag{3.48b}$$

$$\int -\frac{\partial P}{\partial x_3} dV = (PA)_b - (PA)_t \quad \text{(for W momentum)} \tag{3.48c}$$

where A is surface area of cell faces.

In incompressible flows, the momentum equations link the velocities to the respective pressure gradients whereas the continuity equation, apparently having no link to the pressure, is just an additional constraint on the velocity field. Owing to such weak linkage, the convergence and stability of a numerical solution of the momentum and continuity equations largely depend on how the pressure gradients and velocities are evaluated in these equations.

The MIT-CFD program adopts the SIMPLE (Semi-Implicit Method for Pressure-Linked Equations) algorithm (Patankar and Spalding 1972) to convert the continuity equation into the pressure correction equation and therefore establish a coupling between the pressure and velocity fields. In the computation, MIT-CFD uses the collocated (non-

staggered) grid system, rather than the traditional staggered grid system that introduces extra complexity to the calculation. In the non-staggered grid, all the variables in question are stored at the central node of each control volume. In order to avoid the non-physical oscillation associated with the non-staggered grid, the special momentum interpolation technique (Rhie and Chow 1983) has been applied to evaluate cell face variables from the cell centered quantities.

(3) Solution Procedure

With the establishment of the whole set of algebraic equations for flows, the following iterative calculation sequence can be carried out to obtain the solution:

1. Initialize all field values by guess.
2. Solve the momentum equations based on the guessed pressure field. To calculate the solution of the system of Eqs. (3.41) for each variable over the entire computation domain, different algebraic algorithms can be used and the SIP (Strongly Implicit Procedure) of Stone (1968) has been used by MIT-CFD.
3. Solve the pressure-correction equation to obtain the pressure-correction at the cell-center; correct the convective fluxes at the cell-faces, the velocity and pressure at the cell-centers.
4. Solve the k and ε equations, if turbulence and using k-ε model.
5. Update eddy viscosity if turbulence.
6. Solve the scalar (temperature and concentration) transport equations, if required.
7. Return to step 2 with updated field values.

The procedure will be repeated until the convergent solution is reached. This SIMPLE algorithm has been widely and successfully used in many CFD practices.

3.3 Summary

The above two sections briefly introduce the main features and underlying principles of the EnergyPlus and MIT-CFD programs that will be used later on to develop the integrated building modeling tool. The investigation shows the good qualities of these two programs that are feasible for the further coupling study. The substantial knowledge of the two programs that has been presented in this chapter will help to identify the potential coupling approaches between them, as will be shown in the later chapters.

CHAPTER 4

VALIDATIONS OF ENERGYPLUS AND MIT-CFD

Before the EnergyPlus and MIT-CFD program can be used to develop an integrated simulation tool, this chapter reports the validation efforts on the individual programs. The validations in literatures demonstrate the validity of EnergyPlus as well as indicate its deficiency in handling some complex situations. The chapter extensively validates the newly-developed MIT-CFD program by using five building experiment facilities. Good agreement between the simulations and measurements verifies the creditability of the CFD solver developed.

4.1 Validations of EnergyPlus in Literatures

The verification of EnergyPlus has received good attention during the entire development process of the program. A number of efforts have been performed to assure the quality of the program. First, the heat transfer code of EnergyPlus has been reengineered from its original parent programs – BLAST and DOE-2 – by using what has been termed an "evolutionary reengineering" (ER) process. In the ER process, the code is significantly restructured, modularized, and modified stepwise with the goal of bringing it up to current programming standards without starting over with new code. But, at each step along the way, the program is exercised over a variety of input files and parameters to insure that what were intended to be algorithm-neutral-changes have not resulted in changes to the output. According to the developer (LBNL 2001), this process was very successful and bolstered confidence in the program. Secondly, numerous comparisons have been made back to the legacy programs during the program development, which verify that the new program is at a minimum as accurate as its predecessors. Thirdly, before the official release of EnergyPlus v1.0 in June 2001, five beta versions of EnergyPlus were released and subjected to lengthy and rigorous testing by an independent test agency and numerous beta testers. This level of effort and collaboration is unprecedented in the history of energy analysis and thermal load calculation programs and has resulted in a much higher level of confidence in the results produced by EnergyPlus (Crawley et al 2001).

In various validations of EnergyPlus, the most notable work was done by Witte et al. in 2001 (Witte et al 2001), the formal independent testers of EnergyPlus. They performed a variety of analytical, inter-model comparative and empirical tests, which include:

- Analytical – BEPAC/Bland Conduction Tests (BEPAC 1993, Bland 1992),
- Analytical – ASHRAE 1052-RP Building Fabric (ASHRAE 2000),
- Comparative – BESTEST/ASHRAE Standard 140P (ASHRAE 2000),
- Comparative/Analytical – HVAC-BESTEST (IEA 2000), and
- Empirical – IEA Validation Suite (IEA 1994).

Their investigations showed that EnergyPlus provides results in good agreement with other published results on simple cases. EnergyPlus results generally are similar to those from well-established simulation tools such as DOE-2, BLAST, TRNSYS and ESP-r.

Olsen (2002) performed an additional set of validation tests, which further demonstrated the validity of EnergyPlus as well as indicated the deficiency of EnergyPlus in handling some complex situations, such as the buildings with displacement ventilation, night cooling and natural ventilation, which are becoming more and more popular in today's building designs with sustainability concepts. This finding further exhibits the necessity of the integration of building energy simulation programs with other building models, especially the airflow models. The current research repeated some validations in order to demonstrate good skills in using this program and compare uncoupled and coupled solutions. The investigations and results will be presented in Chapter 8 Case Studies: Validations and Applications, to be compared with the coupled simulations.

4.2 Validations of MIT-CFD

Before the new MIT-CFD solver can be integrated with EnergyPlus, it is important to validate the program to ensure its accuracy. This study has selected a number of two-dimensional and three-dimensional airflows in buildings with experimental data for the validation:

- Two-dimensional natural convection case (Cheesewright et al1986)
- Two-dimensional forced convection case (Nielsen et al 1978)
- Two-dimensional mixed convection case (Schwenke 1975)
- Three-dimensional mixing ventilation case (Fisher 1995)
- Three-dimensional displacement ventilation case (Chen et al. 1998)

The two-dimensional cases, although simple and ideal, reflects most substantial airflow characteristics that exist in real buildings, such as recirculation and separation. Besides, because of the simplicity, the quality of the experimental data is much better than those obtained from real building measurements. Hence, these two-dimensional cases have been widely used for the validation of airflow models. The three-dimensional cases provide the more realistic building indoor environments. The entire validation has followed the procedure recommended by Chen and Srebric (2002).

4.2.1 Natural Convection in an Enclosure with an Aspect Ratio of 5

Building airflows can be generally cataloged as forced convection, natural convection or mixed convection, according to the driving force of the air. A flow is considered as forced convection if the driving force is pressure, or natural convection if the driving force is buoyancy, or mixed convection if the driving force contains both.

Natural convection occurs in many practical situations, such as a room heated by a radiator, or a room with a cold window. Most natural convections are weakly turbulent, which challenges the turbulence models and CFD simulation.

This study tests the MIT-CFD's capability of handling room natural convection by a natural convection in a tall cavity of 0.5m width and 2.5m height. Cheesewright et al. (1986) conducted the experimental studies on this case. The experiment maintained isothermal conditions (64.8°C and 20°C) on the two vertical walls and insulated the two horizontal walls, although, they were not ideally insulated. The Rayleigh number (Ra) based on cavity height (h) was

$$\mathrm{Ra} = \frac{g\beta\Delta T h^3}{\nu\kappa} = 5\times10^{10} \tag{4.1}$$

where g is the gravity, β is the thermal expansion coefficient of air, ν is the air kinematic viscosity, and κ is the thermal diffusivity of air.

Figure 4.1 shows the geometry and boundary conditions used in the CFD simulation. Two isothermal boundary conditions were given at the two vertical walls and the adiabatic conditions at the horizontal walls. The study employed both the zero-equation model and standard k-ε model for the turbulence simulation. The grid number of the computation is 30×30, which was indicated sufficient for obtaining a grid-independent solution by Xu (1998).

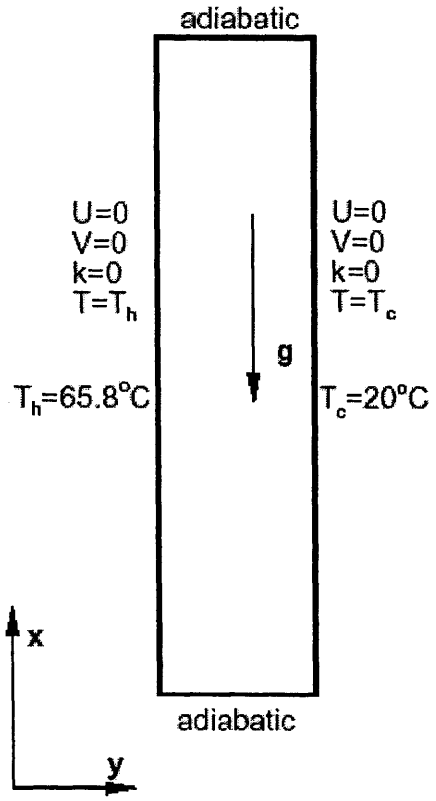

Figure 4.1 Geometry and boundary conditions for 2-D natural convection in an enclosure with an aspect ratio of 5:1

Figure 4.2a compares the computed and measured mean velocity at the mid-height of the enclosure, which shows good agreement except at the near-wall regions. The standard k-ε model with the wall function appears better than the zero-equation model to capture the airflows near the surfaces. The predicted core air temperatures with the k-ε model, as shown in Figure 4.2b, also agree well with Cheesewright's measurements. The results with the zero-equation model are higher than the measurements, although the computed and measured temperature gradients in the core region are similar. This may imply that larger convective heat transfer coefficients at surfaces are obtained when using the zero-equation model due to the overestimated air velocity near the surfaces.

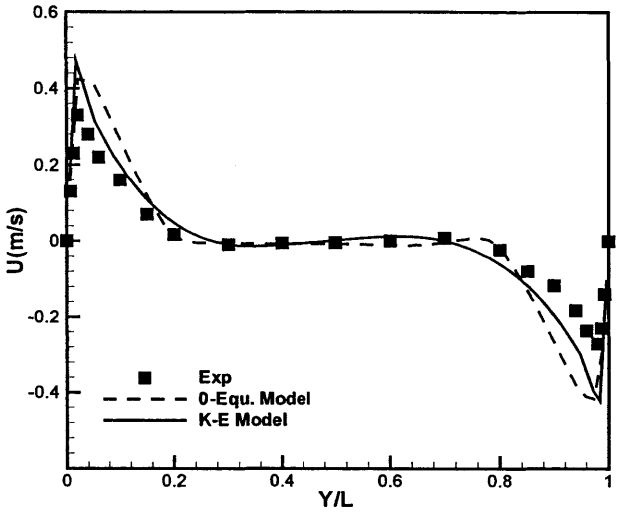

(a)

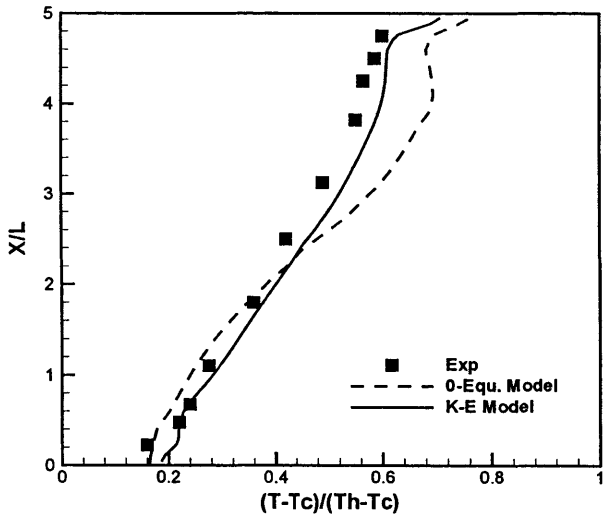

(b)

Figure 4.2 (a) U velocity profile at mid-height and (b) temperature profile in the core for 2-D natural convection in an enclosure with an aspect ratio of 5:1

4.2.2 Forced Airflow in a Ventilated Room with an Aspect Ratio of 3

Forced convection flows are often encountered in rooms where buoyancy effect is negligibly small. This section tests the performance of the MIT-CFD program in the forced convection flow scenario. The case used for the validation is shown in Figure 4.3. The isothermally ventilated room has the length (L) to height (H) ratio of 3. The Reynolds number is 5000 based on the air supply inlet height and supply air velocity. The air supply inlet h=0.056H and the exhaust outlet t=0.16H. Nielsen et al. (1978) conducted an experiment in this configuration and measured the mean velocity and velocity fluctuation in the room by a Laser Doppler Velocimetry (LDV) system. The experimental data have been extensively used by many researchers for program and method validations (e.g. Chen 1995 and 1996, Emvin 1997).

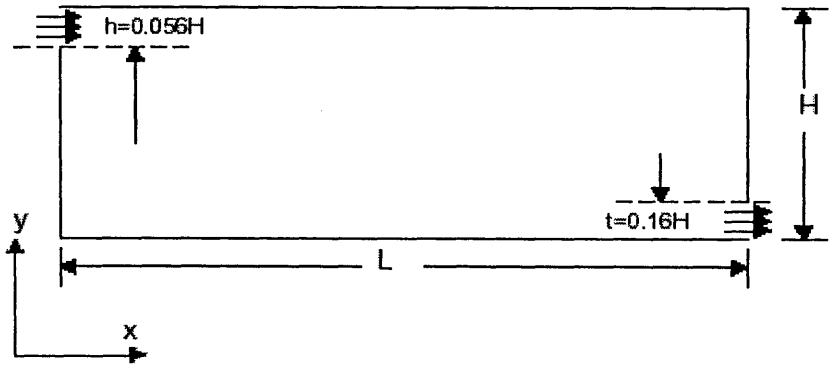

Figure 4.3 Sketch of the room with forced convection

The study used both the zero-equation model and the standard k-ε model to simulate the turbulent flow in the room with a coarse grid of 20×18. Figure 4.4 shows the airflow patterns obtained with two different turbulence models. The flow patterns mostly agree with those obtained by other researchers, e.g. Chen (1996). The result with the k-ε model basically shows a large re-circulation in the room with a very small secondary re-circulation at the lower-left corner, but fails to predict the secondary re-circulation at the upper-right corner. The zero-equation model can predict this secondary re-circulation, however, it over-predicts the secondary re-circulation at the lower-left corner.

Figure 4.5 presents the velocity profiles at two vertical (x/H=1.0 and 2.0) and two horizontal (y/H=0.028 and 0.972) locations. The predicted mean velocity profile at x/H = 1.0 and x/H = 2.0 agree with the experimental data very well, as shown in Figs.4.5a and 4.5b. The k-ε model with the wall function appears a little more satisfactory for the near-wall flows than the zero-equation model. Figs. 4.5c and 4.5d show the velocity profiles in the region close to the ceiling and the floor, respectively, with one profile through the air supply inlet and another through the air exhaust outlet. The trend and magnitude of the predicted velocities agree with the measured data except at the room's upper-right and lower-left corners, where two small secondary re-circulations exist. The small secondary re-circulation usually cannot be predicted by a one- or two- equation

turbulence model. To capture these small eddies, an an-isotropic turbulence model such as a Reynolds stress model (RSM) may have to be used (Chen 1996). However, the zero equation model developed by Xu (1998) demonstrates the capability in this case to predict the secondary re-circulations, although the scales of the re-circulations may be somehow over-estimated.

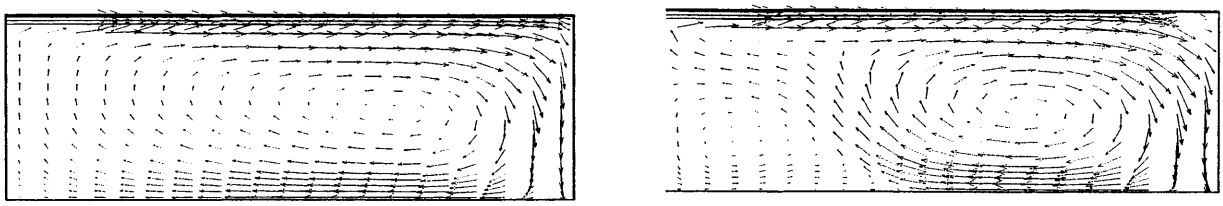

Figure 4.4 Predicted airflow patterns for the forced convection
(left: standard k-ε model; right: zero-equation model)

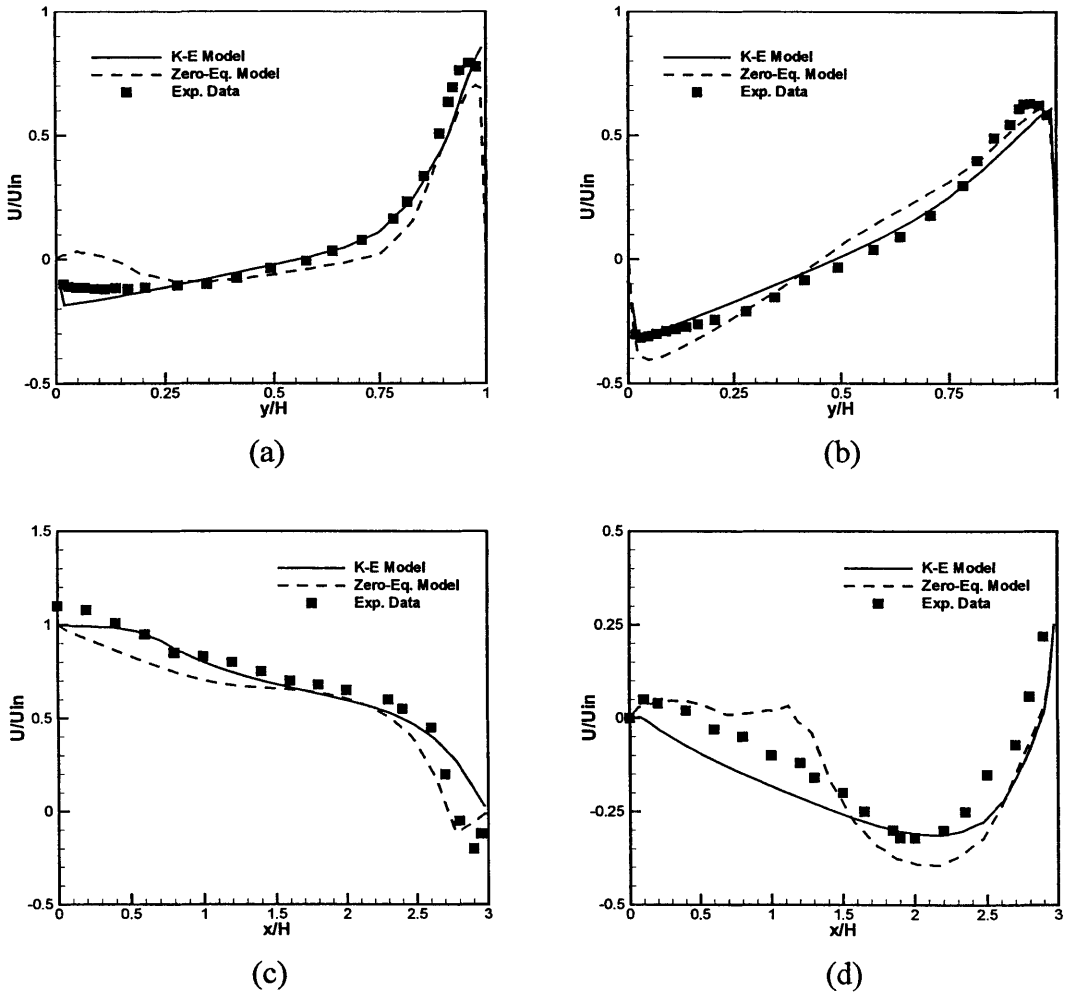

Figure 4.5 Predicted velocity profiles for the forced convection
(a) at x/H=1, (b) at x/H=2, (c) at y/H=0.972, and (d) at y/H=0.028

4.2.3 Mixed Airflow in a Ventilated Room with an Aspect Ratio of 4.7

Mixed convection is the most common flow encountered indoors, which combines both effects of forced convection and natural convection. A ventilated room with non-isothermal surfaces is a typical example of mixed airflow. This section uses a ventilated room with a heated wall to examine the capability of the MIT-CFD program of handling mixed indoor airflows. The configuration of the mixed airflow is similar to the forced convection case (Figure 4.3) except that the room length (L) to height (H) ratio is 4.7 and the air supply inlet h is 0.025H. The right wall is heated with prescribed heat fluxes, while the other surfaces (left wall, ceiling, floor) are adiabatic. Schwenke (1975) conducted a series of experiments and measured the penetration length, x_e, under various Archimedes numbers. x_e is the horizontal distance of supply air movement along the ceiling before it falls to the floor. The Archimedes number is the ratio of gravitational force to viscous force and is defined as:

$$\mathrm{Ar} = \frac{g\beta(T_{out} - T_{in})h}{U_{in}^2} \tag{4.2}$$

where h is the inlet size and U_{in} is the supply inlet velocity.

A grid of 25×18 was used in CFD to simulate the airflow. Figure 4.6 presents the velocity and temperature distributions in the room with this mixed convection. The result by the standard k-ε model is quite similar to that by the zero-equation model. The buoyancy-driven natural convection, due to the right-hand heated wall, travels along the ceiling and meets the forced convection from the supply inlet. The collapsed stream then goes down to the floor, splitting into two opposite directions and forming two large eddies in the room. The length between the inlet and the location where two jets meet is called the penetration length, x_e. The penetration length is important for an engineer to design a ventilation system that can prevent draft or over-throw conditions.

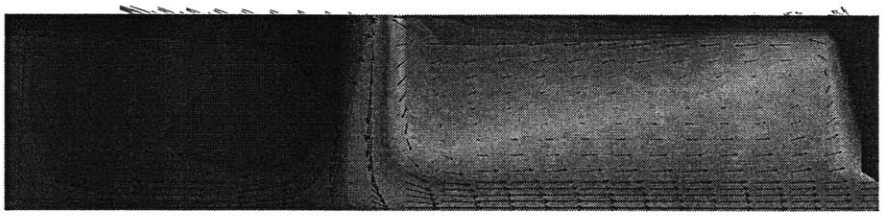

Figure 4.6 Predicted velocity and temperature patterns for the mixed convection (standard k-ε model)

The penetration length is highly sensitive to the Ar number. Figure 4.7 compares the calculated and measured penetration lengths under various Ar conditions. As seen in Figure 4.7, the agreement between the calculated and measured values is fairly good.

The zero-equation turbulence model provides satisfactory results for this mixed convection case, while using much less computing time (about 50%) than the k-ε model because of no need to solve the k and ε transport equations.

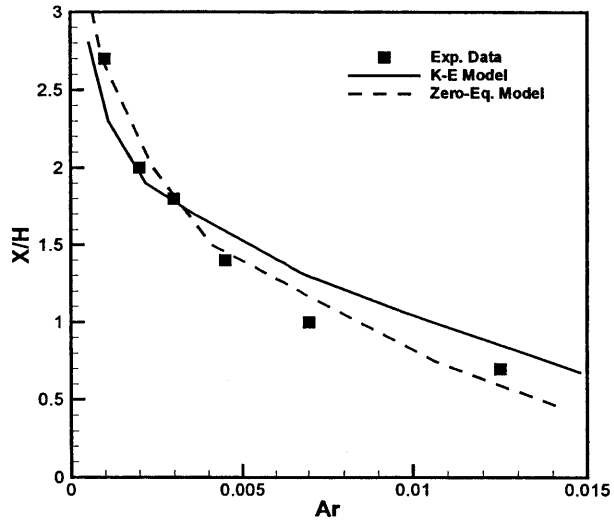

Figure 4.7 Comparison of the computed and measured penetration lengths for the mixed convection

So far, the cases studied have demonstrated good performance of MIT-CFD on some typical but simple indoor airflows with natural convection, forced convection, or mixed convection. The practical indoor airflows are more complicated, due to the room geometry, partition, internal objects, and HVAC systems. The program, therefore, needs to be further validated through more complex and realistic indoor airflow cases.

4.2.4 Three-Dimensional Airflow in a Room with Mixing Ventilation

Mixing ventilation is the most popular ventilation approach, often occurring with use of conventional jet-diffusers. In a room with mixing ventilation, the mechanically driven jet flows and the buoyancy driven flows interact with each other and produce complicated indoor airflow and heat transfer patterns. Usually, due to the strong indoor airflows, the convective heat transfer from building enclosures has a considerable impact on the airflow and thermal distributions as well as the space heating/cooling load calculation. Hence, how to precisely model the convective heat from enclosures has received particular attention of building researchers in the recent decades. In CFD, the convective heat transfer from enclosures significantly challenges the turbulence models because of the near-wall airflow and thermal effect. This section, therefore, uses the Fisher's experiment facility (1995) to verify if the MIT-CFD program can simulate such a mixing ventilation case using simple turbulence models.

Fisher (1995) conducted a detailed experimental investigation on the mixed convection and heat transfer phenomena in a full-size experimental chamber (Figure 4.8) with mixing ventilation. He studied different mixing ventilation scenarios by using different ceiling jets and free horizontal jets in an isothermal or non-isothermal room. The study provided plentiful measurements of the surface and air temperatures, based on which convective heat fluxes through enclosures were calculated. Fisher then developed the corresponding correlations of convective heat transfer coefficients for different room conditions and different surfaces, which can be used to estimate the total building energy consumption.

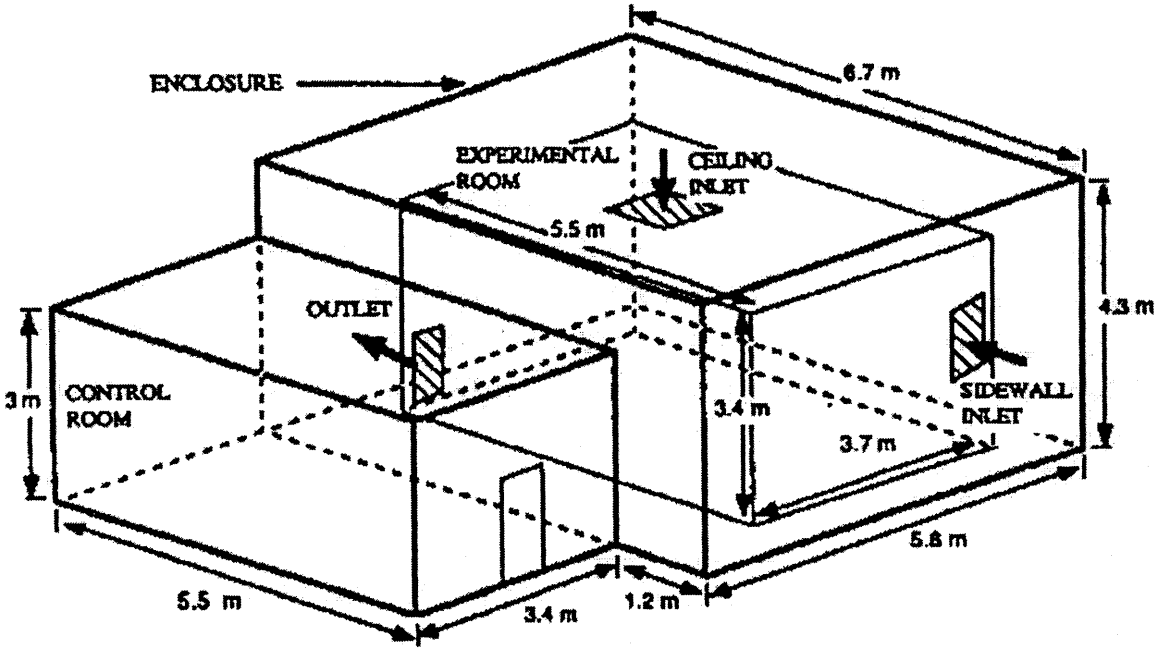

Figure 4.8 Schematic of experimental facility (Fisher 1995)

The present study simulated the mixed airflows in an isothermal room in which the interior surface temperatures of all the enclosures were 30°C. Both the case with sidewall jet and with ceiling jet were investigated, with the 6ACH supply air mass flow rate at two different supply air temperatures – 10°C and 20°C. The research investigated the influences of turbulence models on the convective heat transfer and the airflow and temperature distributions. All three turbulence models of MIT-CFD have been tested. In the CFD simulation, the local convective heat flux from a surface can be calculated through:

$$Q_{local} = h_{local} A_{local} (T_{surface} - T_{air-local}) \tag{4.3}$$

$$h_{local} = C_p \frac{\rho(\nu_t + \nu)}{Pr} \frac{1}{\Delta x} \tag{4.4}$$

where h_{local} is the local convective heat transfer coefficient, A_{local} is the local surface area, $T_{air\text{-}local}$ is the local air temperature at the distance Δx to the surface, C_p is the air specific heat, Pr is the Prandtl number, Δx is the normal distance from a point near a surface to the surface. The present study employed an optimal distance Δx=0.05m for simple zero-equation turbulence models, which was recommended by Chen (1988) and confirmed by the numerical investigation of this thesis, as will be further presented in Chapter 6.

Based on the local heat fluxes, the total convective heat flux from the surface can be obtained by summing Q_{local} over the whole surface area:

$$Q_{all} = \sum Q_{local} \tag{4.5}$$

The averaged convective heat transfer coefficient at this surface can then be defined, as Fisher's suggestion:

$$h_{average} = \frac{Q_{all}}{(T_{surface} - T_{supply}) \times \sum A_{local}} \tag{4.6}$$

Since $T_{surface}$ and T_{supply} are constant and given in an isothermal case, $h_{average}$ is linearly proportional to Q_{all}. This investigation compared the simulated and measured convective heat fluxes, rather than $h_{average}$, due to the accuracy consideration of the available measurement data.

(1) The Sidewall Jet Case

The study first simulated the airflow in the ventilated room with a sidewall jet-diffuser. The "side wall" inlet configuration, as shown in Figure 4.8, results in a horizontal wall or free jet flow in the space, in which the buoyancy and momentum work together to determine the path of the jet. In the experimental and numerical investigation, the inlet was configured as a vertical slot (24.5 mm x 904 mm) located midway up the east wall. The jet entered the room near the corner and traversed the room diagonally toward the room outlet.

For the comparative purpose, the CFD used four sets of grid system to simulate the indoor airflow: a course grid (22×17×15 = 5,610 cells), a moderate grid (44×34×30 = 44,880 cells), a fine grid (66×51×45 = 151,470 cells), and a locally refined course grid (27×19×17 = 8,721 cells) that has the same resolution in the near-wall regions as the fine grid.

Figure 4.9 presents the measured and calculated air speed contour, which shows the similarity of the primary airflow structures between the measurement and simulation. The study indicates that both the low temperature and high temperature jets will drop down to the floor of the room after traveling forward for a certain distance due to the negative buoyancy effect, the same as observed.

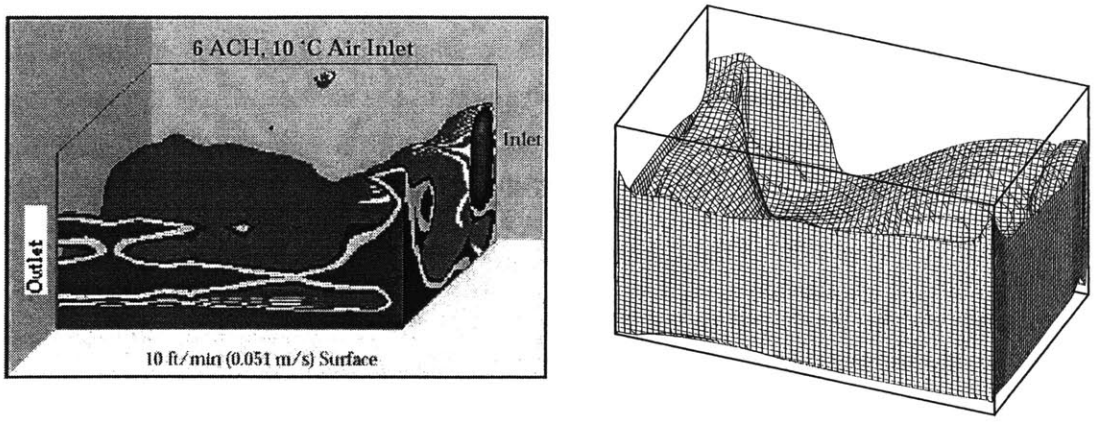

(a) (b)

Figure 4.9 Air speed contour in the room with sidewall jet ventilation
(a) measurement; (b) simulation with zero-equation model and fine grid

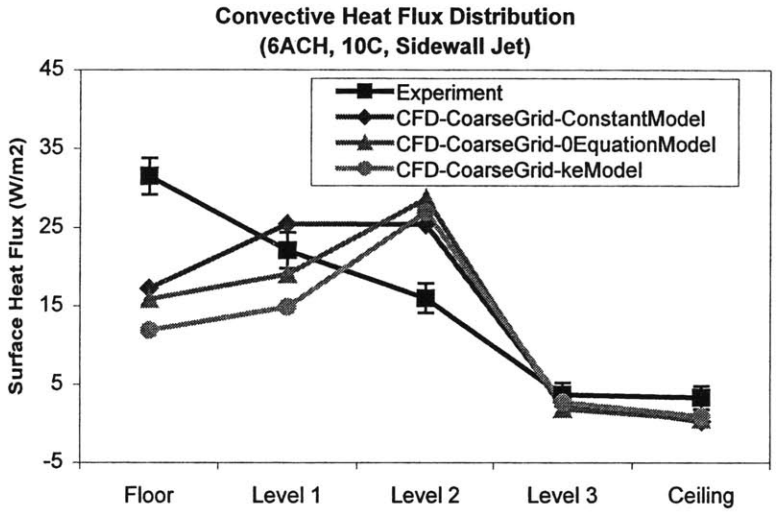

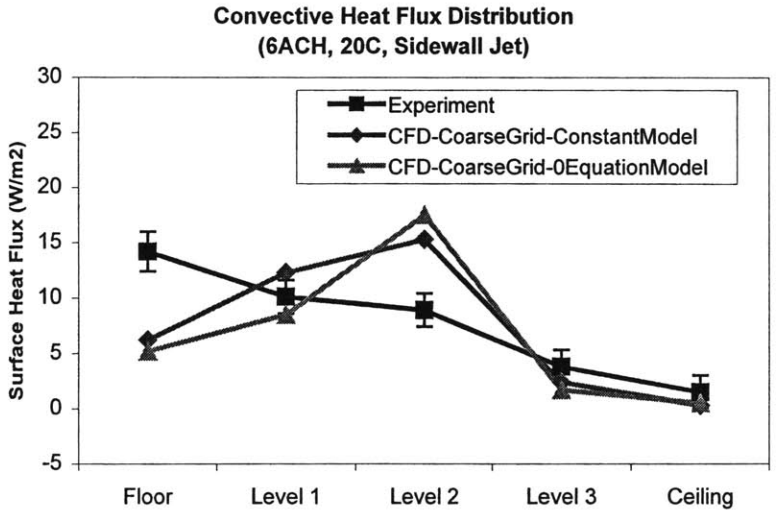

Figure 4.10 Comparison of convective heat fluxes from enclosures

Figure 4.10 compares the calculated (with the coarse grid) and measured convective heat fluxes from floor, ceiling, and three different levels of walls (Level 1, 2 and 3 each represent 1/3 of the vertical wall area in the room, with "Level 3" being the one third of the wall area nearest the ceiling). The results show that different turbulence models predict the heat transfer with the same trend. The simulated results show the significant difference from the measurement at the floor and wall Level 2.

The simulation error at the floor is mainly because the coarse grid at the near-floor region cannot precisely capture the temperature gradient between the floor and the air close to the floor. Figure 4.11 presents the predicted temperature gradient along the vertical central line of the room with the different grid resolutions. The simulation with the coarse grid predicts a smaller temperature gradient at the floor and therefore produces a lower convective heat flux from the floor. However, since the room air temperature gradient, except at the floor region, is almost linearly increasing, the coarse grid can provide acceptable results for other surface areas. This prediction error at the floor can be corrected by using the moderate grid, fine grid or locally refined coarse grid, as shown in Figure 4.12.

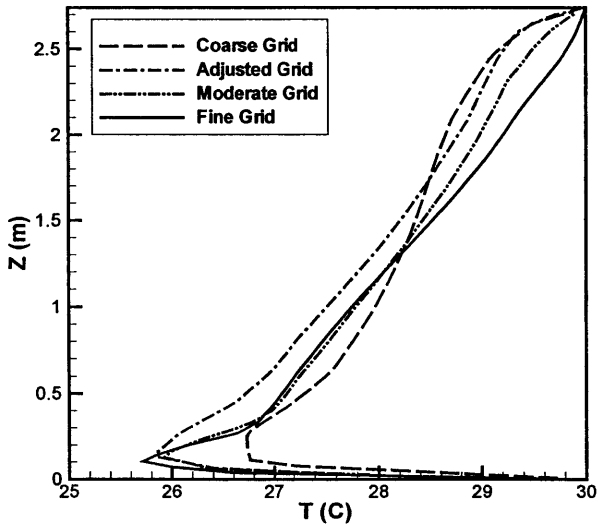

Figure 4.11 Predicted temperature gradient along the vertical central line of the room

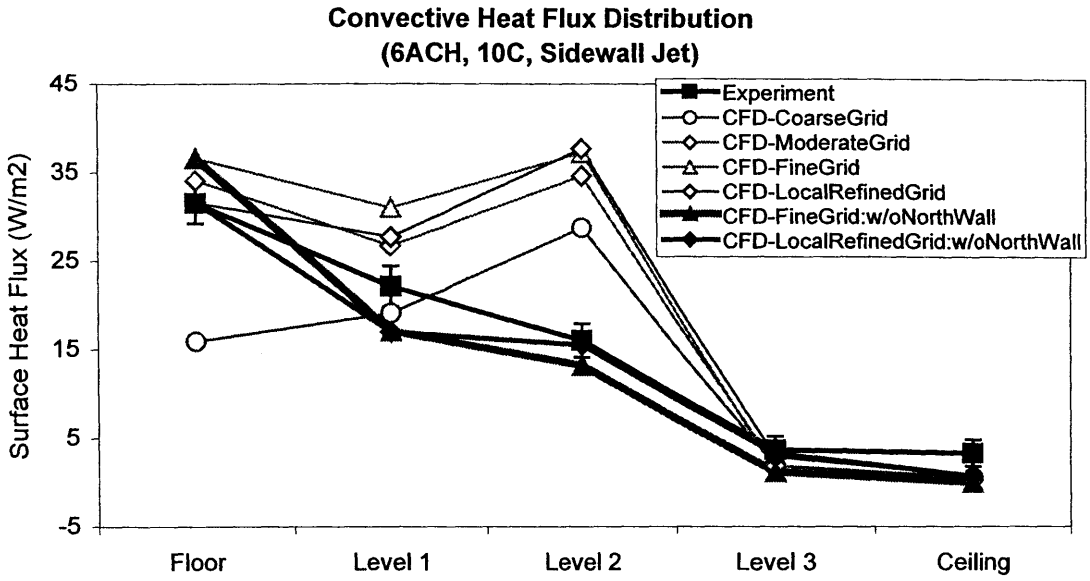

Figure 4.12 Comparison of convective heat fluxes from enclosures with zero-equation turbulence model and various grid systems

Figure 4.12 presents the predicted convective heat fluxes from enclosures with different grid systems. The convective heat fluxes from the floor predicted with the refined grid systems are much closer to the measurement than that with the coarse grid. However, the difference between the measured and simulated results at wall Level 2 is still distinct, even with the fine grid. The analysis indicates that the impact of the high speed jet flow on Level 2 of the north wall is the main reason for the large heat flux at the entire wall Level 2. Since the vertical jet slot is very close to the north wall, the cold airflow from the jet inlet causes the strong shear flow at the north wall, introducing the extra heat transfer at this particular area, as demonstrated by Figure 4.13. The experiment did not measure this heat transfer zone within the inner jet flow. If the north wall is removed from the analysis of the wall convective heat fluxes, encouraging results are found, as revealed in Figure 4.12.

Figure 4.12 also indicates that instead of using a global refined grid that may need long computing time, a locally refined coarse grid can effectively predict the airflow and heat transfer for such an indoor case. Good resolution for the near-wall regions is much more important than for the inner space because the indoor air temperature in the core of a space is generally more uniform than the perimeter of a space.

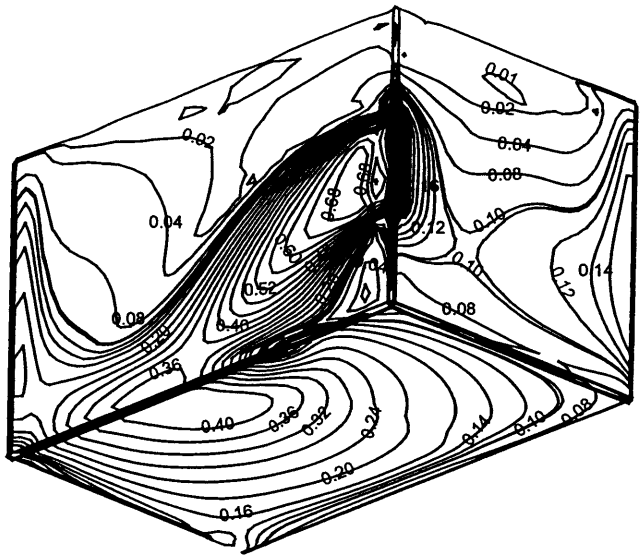

(a) air speed contours close to the surfaces (m/s)

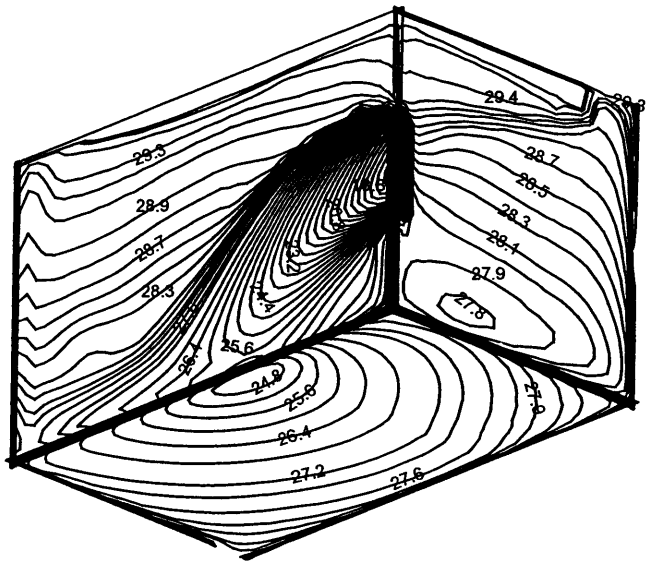

(b) air temperature contours close to the surfaces (°C)

Figure 4.13 Predicted distributions of (a)air speed and (b)indoor air temperature close to the surfaces

(2) The Ceiling Jet Case

The study further simulated the airflow in the room with a ceiling-center-mounted jet-diffuser. The investigation used the same air supply conditions (6ACH and 10/20°C) as those for the sidewall jet case. A locally refined coarse grid (28×22×21=12,936 cells) was generated to simulate the indoor airflow, which has the dense grids in the enclosure vicinities. Both the constant viscosity and zero-equation turbulence model were tested in the simulation.

Figure 4.14 shows the airflow and temperature distributions in the two crossing middle sections of the room that is supplied with the 10°C fresh air. The room air temperature predicted appears to be relatively "well-stirred", the same as observed in the experiment. As seen in the short middle section (south-north direction) of Figure 4.14, the dense and cold jet does not fall down toward the floor immediately after it leaves the supply diffuser even at such small supply flow rate and low supply air temperature. The viscous effect of airflow seems to compete with the negative buoyancy of the jet and tenaciously attach the jet air to the south and north walls.

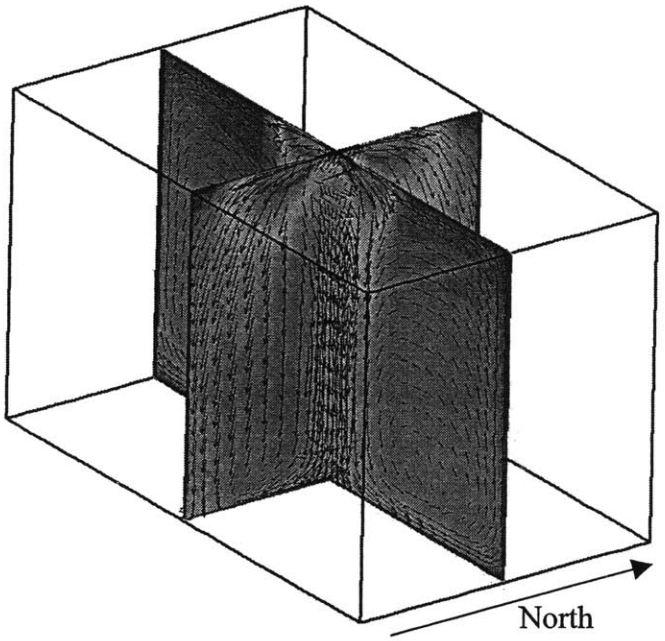

Figure 4.14 Velocity and temperature distributions in two crossing middle sections of the room supplied with the 10°C fresh air
(simulated with zero-equation turbulence model)

However, in the long middle section (west-east direction) of Figure 4.14, the cold supply air falls down after it leaves the supply inlet and forms a strong downward airflow toward the floor due to the low supply air temperature and velocity as well as the long distance to the west and east walls. As a result, large circulations are generated in the room, which well stirs the room air. In the experiment, the cold air appears to travel a certain distance before it drops in the west-east direction, although it was not explicitly mentioned. The predicted negative buoyancy effect of the cold air might be stronger than the experiment observation. This is probably because the simplification and approximation of the complicated ceiling diffuser and the coarse grid used there may reduce the momentum of the supply air. Meanwhile, the simple zero-equation turbulence models, developed for indoor airflow, may not be able to accurately simulate the flow in the inner region of a jet flow. On the other hand, in the experiment, the uni-strut trolley rails mounted in the upper right and left corners of the room tend to exaggerate the effect of the upper corners, as indicated by Fisher (1995).

The study shows that the different turbulence models provide similar flow and temperature patterns. Figure 4.15 compares the calculated and measured convective heat transfer from floor, ceiling, and three different levels of walls. The CFD results reasonably agree with the measure ones, with the largest difference located at the upper level of the walls (Level 3). This is because the cold jet flow in the experiment may reach more area of the upper wall due to the viscous effect while the simulation overestimates the buoyancy effect. Despite this difference of flow mechanics, the simulation still achieves acceptable heat fluxes from the floor and the lower walls. It is interesting to notice that the constant viscosity model in this case provides more realistic heat flux from the ceiling than the zero-equation model. It may be because the CFD simulation predicts less area of high air velocity and cold air temperature near the ceiling than the measurement, as illustrated in Figure 4.16, due to the overestimated buoyancy effect. It results in the obvious reduction of heat flux through the ceiling using the zero-equation model that is explicitly related to local air velocity.

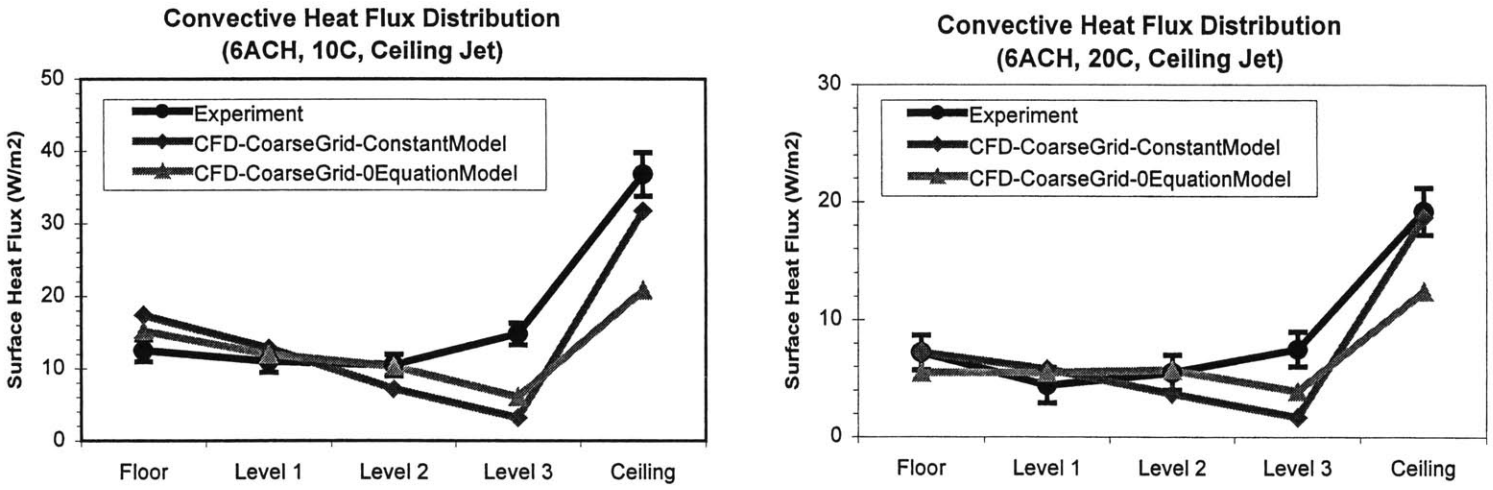

Figure 4.15 Comparison of convective heat fluxes from enclosures

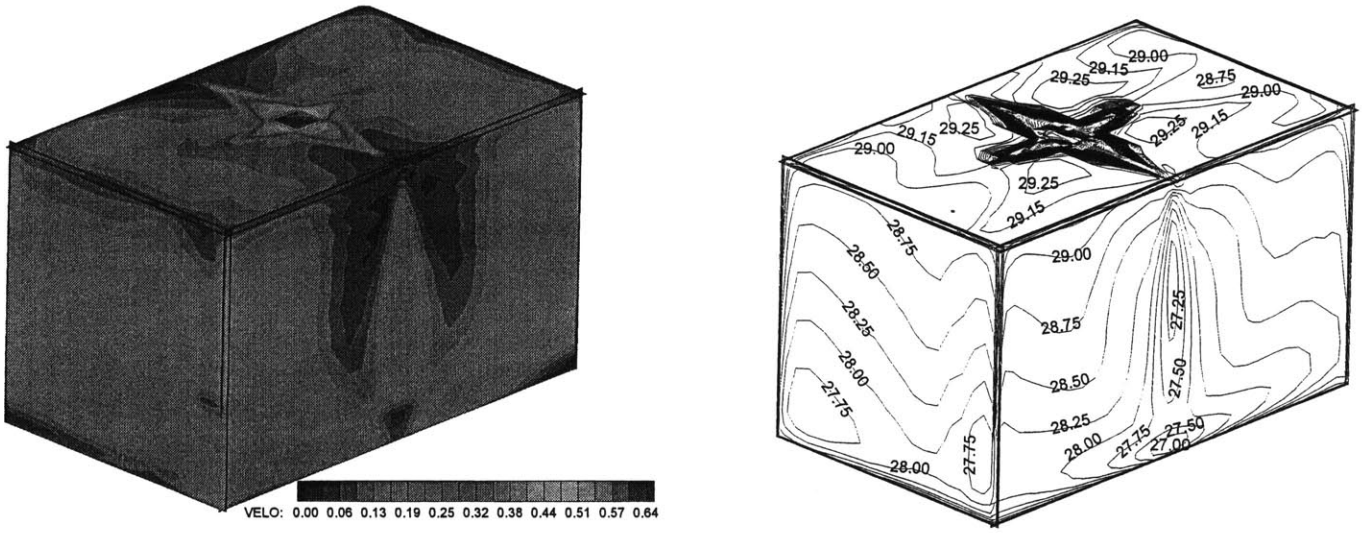

Figure 4.16 Predicted distributions of air speed and indoor air temperature close to three surfaces

4.2.5 Three-Dimensional Airflow in a Room with Displacement Ventilation

Displacement ventilation is an advanced indoor ventilation approach. Unlike the conventional mixing ventilation, displacement ventilation provides a cleaner indoor environment with less energy consumption. A typical displacement ventilation system supplies fresh air at or near floor level at a very low velocity and a temperature slightly below room temperature. Exhausts are located at or near the ceiling. The supply air spreads across the floor and rises as it is heated by sources such as people and equipment (Figure 4.17), removing indoor heat and contaminants directly from the occupied zone to the upper zone without mixing. Since only the occupied zone must be maintained at the room setpoint temperature while the upper zone may be warmer, the supply air flow rate can be significantly reduced due to the vertical temperature gradient, resulting in reduced fan energy.

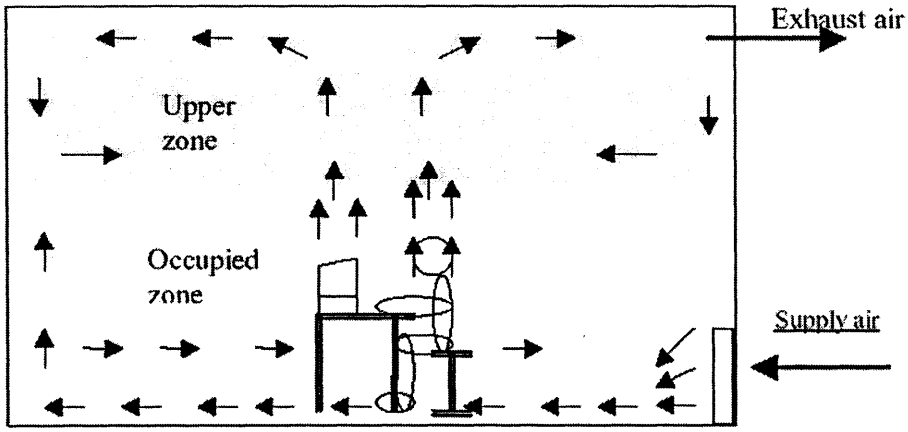

Figure 4.17 Schematic of conventional displacement ventilation

However, the complexity added by this non-uniform air temperature distribution makes displacement ventilation systems more difficult to model and design than mixing ventilation systems. Yuan et al. (1998) provides a review of many issues and models associated with displacement ventilation.

The displacement ventilation case used here to validate the MIT-CFD program is one of the experiments conducted by the ASHRAE displacement ventilation project (Chen et al. 1998). Figure 4.18, Table 4.1 and Table 4.2 provide detailed information about the geometrical, thermal and flow conditions of the case.

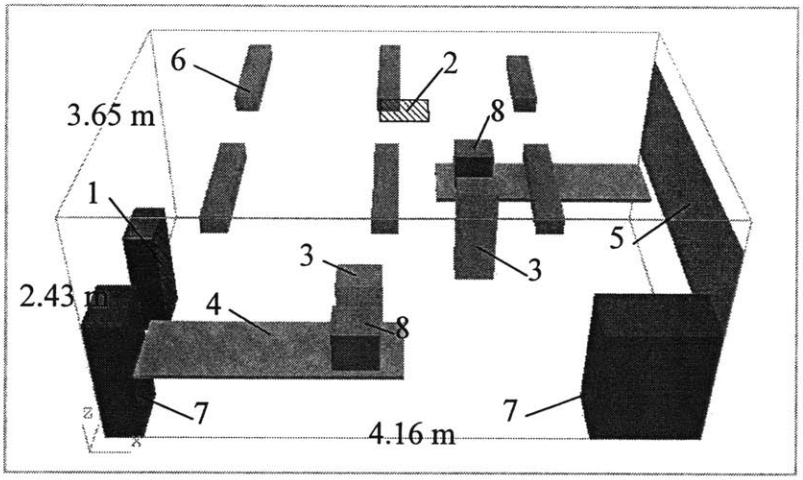

Figure 4.18 The layout of the displacement ventilation case (inlet-1, outlet-2, person-3, table-4, window-5, fluorescent lamps-6, cabinet-7, computer-8)

Table 4.1 The geometrical, thermal and flow conditions for the diffuser and window

Displacement ventilation case			
Inlet diffuser	Size: 0.53 m x 1.1 m (1.7 ft x 3.6 ft)	Temperature: 17.0°C (62.6°F)	Velocity: 0.086 m/s (17.5 fpm)
Window	Size: 3.65 m x 1.16 m (12 ft x 3.8 ft)	Temperature: 27.7°C (81.9°F)	Closed

Table 4.2 The size and capacity of the heat sources

Heat source	**Size**	**Power**
Person	0.4 x 0.35 x 1.1m^3 (1.3 x 1.15 x 3.6 ft^3)	75 W (256 Btu/h)
Computer 1	0.4 x 0.4 x 0.4m^3 (1.3 x 1.3 x 1.3 ft^3)	108 W (368 Btu/h)
Computer 2	0.4 x 0.4 x 0.4m^3 (1.3 x 1.3 x 1.3 ft^3)	173 W (590 Btu/h)
Overhead lighting	0.2 x 1.2 x 0.15 (0.7 x 3.9 x 0.5 ft^3)	34 W (116 Btu/h)

The MIT-CFD program with both the zero-equation turbulence model and the standard k-ε model was used to simulate the airflow in this experiment facility. The computational grid is 55×37×29, which is sufficient for obtaining the grid-independent solution according to Srebric's investigation (2000). Figure 4.19(a) shows the calculated air velocity and temperature distributions in the middle section of the room with the zero-

equation model. The solutions with the standard k-ε model are fairly similar. The computed results are in very good agreement with the flow pattern observed by smoke visualization, as illustrated in Figure 4.19(b). The large re-circulation in the lower part of the room, which is known as a typical flow characteristic of displacement ventilation, is well captured by the CFD simulation. The airflow and temperature patterns in the respective sections across a person and a computer, as shown in Figure 4.19(c) and 4.19(d), clearly exhibit the upward thermal plumes due to the positive buoyancy from the heat sources.

The study further compared the measured and calculated velocity and air temperature profiles at nine pole locations where detailed measurements were carried out. The pole locations are illustrated in the lower-right pictures of Figure 4.20 and 4.21. Figure 4.20 shows the comparison of measured and calculated air velocities along the nine vertical poles and Figure 4.21 shows the comparison of air temperatures. Both of the figures have a very good agreement between the computed and measured results, indicating that the program and the turbulence models have good capability to predict this kind of indoor airflow.

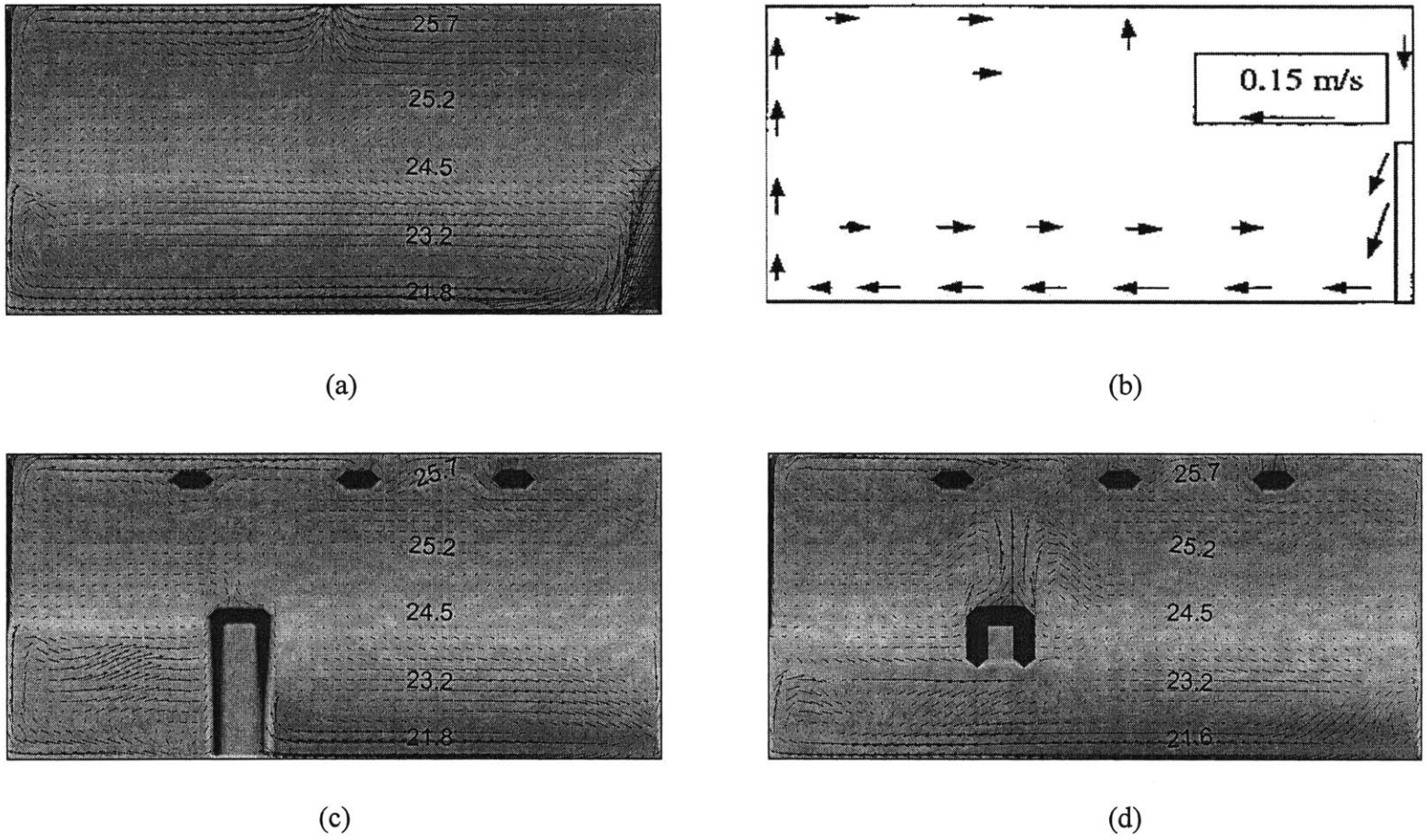

Figure 4.19 Velocity and temperature distributions for the displacement ventilation case (a) calculated results in the middle section, (b) observed airflow pattern with smoke visualization in the middle section, (c) calculated results in the section across a computer, (c) calculated results in the section across an occupant

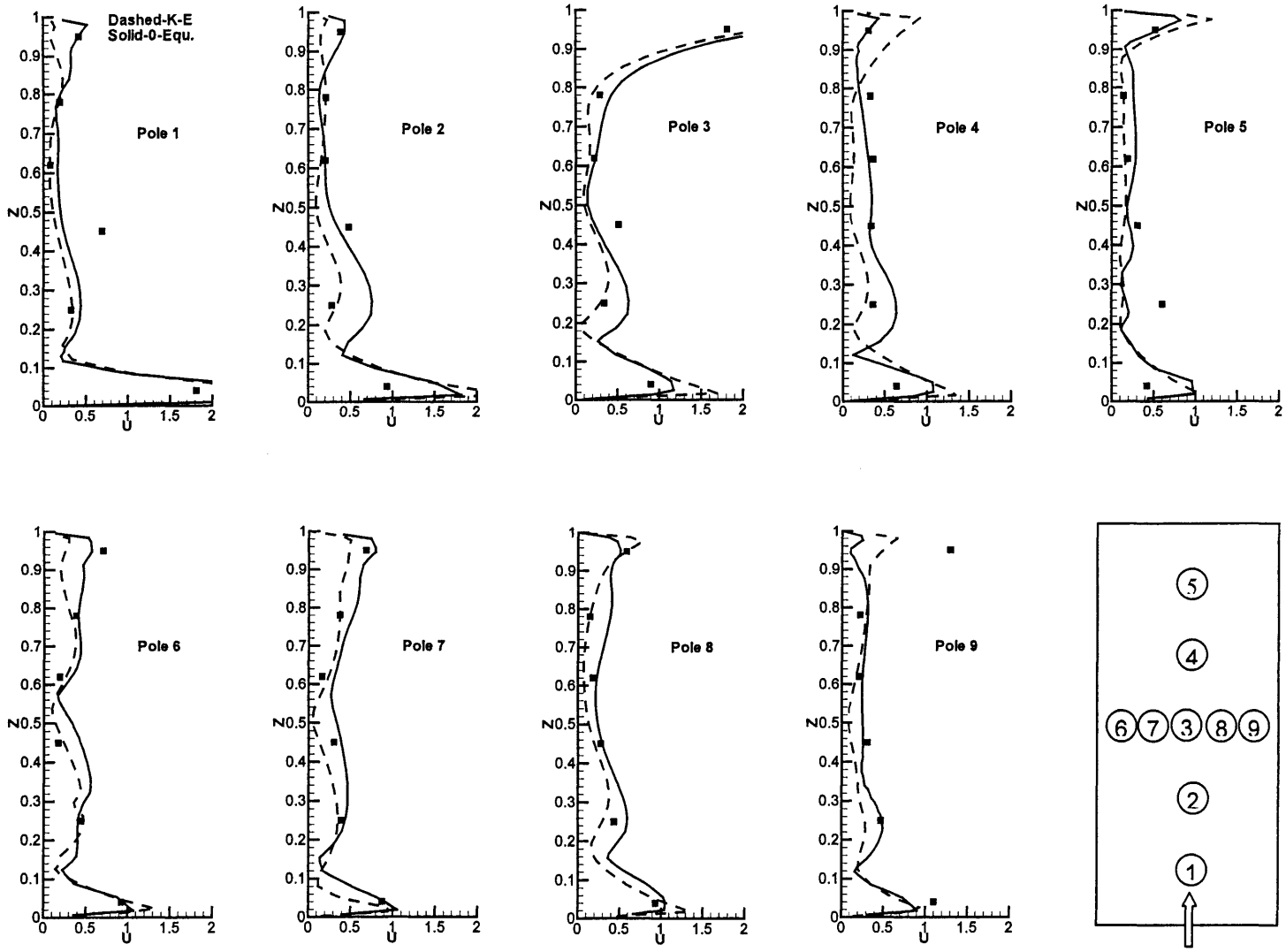

Figure 4.20 The comparison of the velocity profiles at nine positions in the room between the calculated and measured data for the displacement ventilation case. Z=height/total room height (H), V=velocity/inlet velocity (V_{in}), H=2.43m, V_{in}=0.086m/s

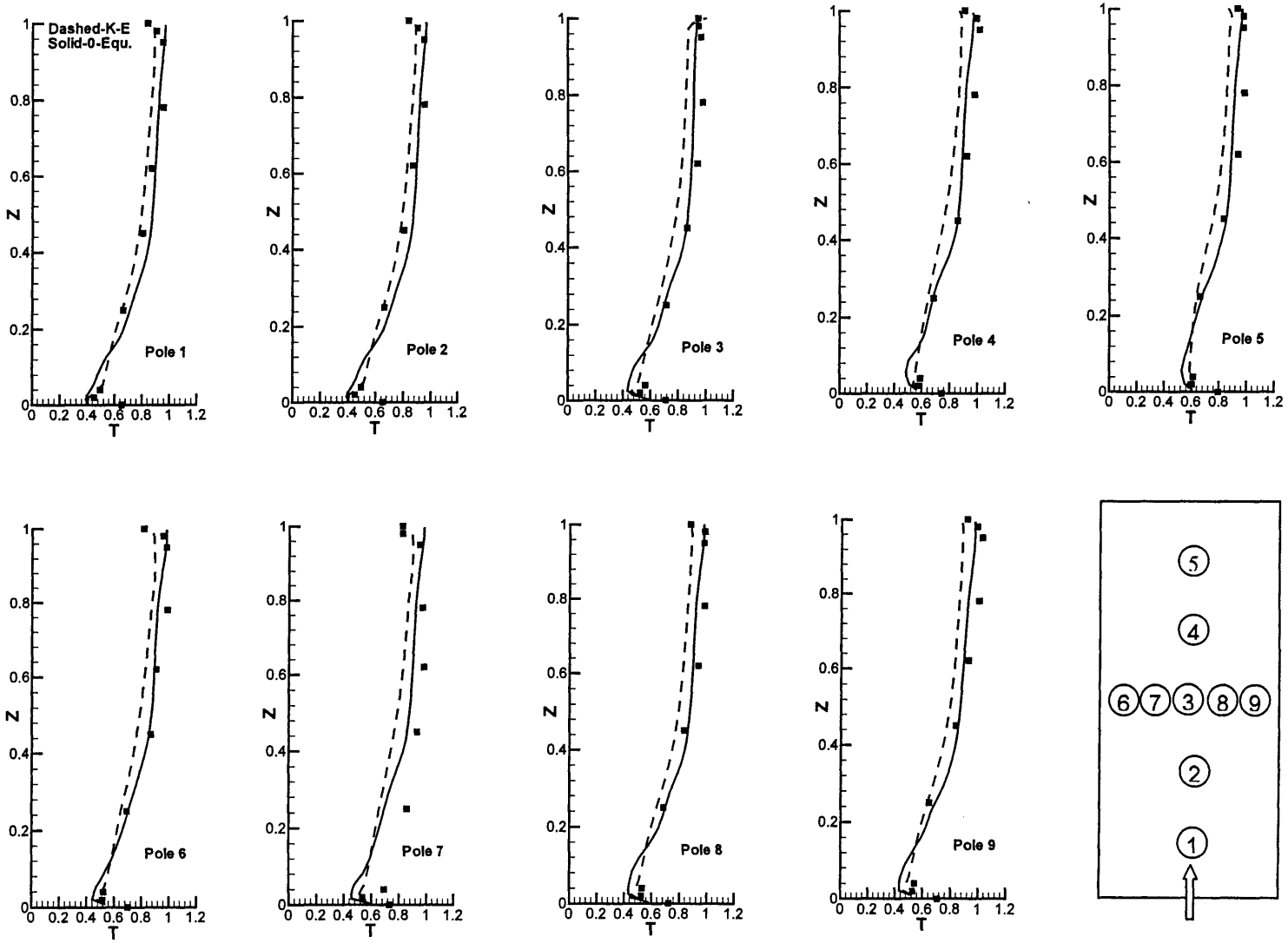

Figure 4.21 The comparison of the temperature profiles at nine positions in the room between the calculated and measured data for the displacement ventilation case. Z=height/total room height (H), $T=(T_{air}-T_{in}/T_{out}-T_{in})$, H=2.43m, T_{in}=17.0°C, T_{out}=26.7°C

4.3 Summary

This chapter reports the validations of the EnergyPlus and MIT-CFD programs. The good performance shown for both programs enhances the confidence of using them to develop an integrated building simulation tool. The investigation shows that EnergyPlus is at least as capable and accurate as other well-known energy simulation programs. But its superb program structure makes the integration to other simulation models, such as CFD models, more convenient.

The validations verify that MIT-CFD is capable of simulating most building indoor airflows. The program employs many standard CFD methods and adopts a number of newly-developed CFD techniques, allowing the program to provide correct, accurate, robust, and fast prediction of various airflows. The modularity of the code makes the program ready for the integration with other simulation programs. The program has been used by Gao (2002) to couple with a multi-zone airflow simulation program – CONTAM – for indoor environmental analysis. In her study, the program has been further validated through a set of validation cases to demonstrate its applicability for indoor airflow analysis. These validation cases include three typical building indoor airflow cases involving natural, forced and mixed convections, and two duct cases – a three-duct-in-series and a 90-degree planar branch. The results were verified having a good agreement with analytical solutions, experiment data or other CFD solutions. The coupling practice between MIT-CFD and CONTAM shows that MIT-CFD can be effectively integrated into other simulation programs and the integrated program can provide reliable and informative results.

CHAPTER 5

PRINCIPLES, STRATEGIES AND IMPLEMENTATIONS OF ENERGYPLUS AND MIT-CFD THERMAL COUPLING

This chapter presents the main coupling efforts to the EnergyPlus and MIT-CFD programs. The primary coupling principles, routings and challenges are discussed. To bridge the discontinuities between these two different programs, special coupling strategies have been developed. Particularly, the staged coupling strategies proposed can greatly reduce the computing costs while preserving the accuracy and details of the computed results. This chapter also introduces the principal techniques used to develop a reliable and flexible coupling program.

5.1 Coupling Principles of Energy Simulation and CFD Programs

Energy simulation (ES) and CFD programs are two important building design tools. The information provided by them is essential for the evaluation of the most important building performance, including thermal comfort, indoor air quality, system efficiency, and energy consumption. Based on these information, a building designer is able to modify his/her design toward an optimal solution.

The information provided by ES and CFD programs is complementary, as partially demonstrated by Table 5.1. The integration of these two tools can eliminate many assumptions employed in the separate simulations and results in more accurate predictions of building performance. For example, the ES program can provide heating/cooling load and interior surface temperatures of building envelopes to CFD as boundary conditions while CFD can determine surface convective heat fluxes for ES.

Table 5.1 Some functions of ES and CFD programs

	ES	CFD
Weather and solar impact	Yes	No
Enclosure thermal behaviors	Yes	No
HVAC system capacity	Yes	No
Energy consumption	Yes	No
Thermal comfort (T, V, Humidity, Turbulence)	No	Yes
Indoor air quality (C)	No	Yes
HVAC system distribution	No	Yes
Natural ventilation	No	Yes

Therefore, this study attempts to develop an integrated building design tool by incorporating a CFD program (MIT-CFD) into an ES program (EnergyPlus). The

investigation has been focused on the thermal coupling of these two programs, without considering their connections at system and plant levels that may heavily depend on specific system and plant model used. In such a thermal coupling, ES provides heating/cooling energy requirement and building envelope thermal information, such as surface temperature and heat flux, to CFD as boundary conditions; CFD predicts detailed room air temperature distribution and accurate convective heat transfer that help ES achieve more precise estimation of building energy consumption.

The principles of the ES program, as introduced in Chapter 3, indicate that ES essentially solve the heat balance equations (Eqs. (3.1) and (3.2)) for room air and building envelopes. The solution of Eq. (3.2) provides the enclosure interior surface temperatures and convective heat transfers. With the convective heats, the solution of Eq. (3.1) determines the mean room air temperature and heating/cooling energy demand.

In a coupled simulation, CFD replaces the integral heat balance equation (3.1) of ES to handle the air movement and heat transfer in the space. ES still handles the heat transfer through building envelopes. The substantial connection of ES and CFD is thus between CFD and Eq. (3.2) of ES, as illustrated by Figure 5.1. The unknown convective heat transfer $Q_{i,conv}$ on the interior surfaces links ES and CFD. This appears a "separate" conjugate heat transfer method. In principle, if the conduction and radiation models used in this method are the same as those used in the conjugate heat transfer method, the only two differences between these two methods are:

(1) the conjugate method divides each envelope surface into many grid cells, while ES in the coupled simulation generally assumes uniform surfaces.
(2) the conjugate heat transfer method solves the equation matrix that contains all the heat balance equations for both enclosures and indoor air at one time, whereas the coupling method solves two separate equation matrices (one for the heat balance in enclosures and another for indoor air) in tandem.

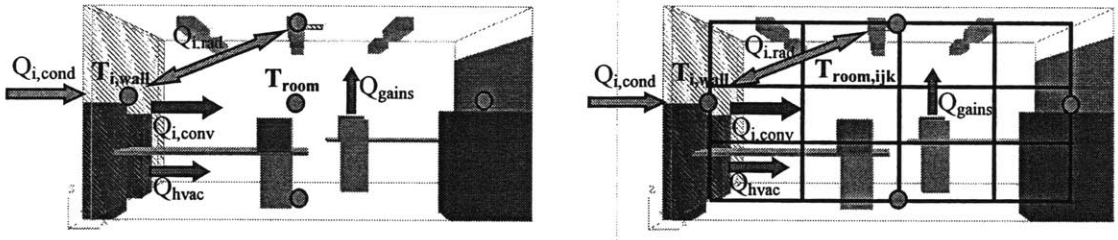

(a) (b)

Figure 5.1 Illustration of thermal connection between envelope and indoor air: (a) pure ES with nodal model; (b) ES and CFD coupling (ES nodal model for envelope and CFD field model for indoor air)

As discussed in Chapter 1, the conjugate heat transfer method with an appropriate radiation model, system and plant models, can predict the whole building performance; however, it is too computationally expensive to be practical with the current computer capacity. In contrast, the coupling of ES and CFD programs can dramatically reduce the computing costs by focusing on the airflows in spaces of particular interest in a building at significant time steps. This time-saving advantage is very attractive to building designers who are more interested in obtaining an acceptable solution with a relatively short modeling time.

In the ES and CFD program coupling, the convective heat transfer from interior surfaces of a space is the major linkage between the enclosure heat balance of ES and the indoor air heat balance of CFD. The accuracy of the convective heat transfer directly influences the predictions of the enclosure thermal behaviors in ES and the indoor airflow patterns in CFD. Surface temperature, air temperature close to the surface and convective heat transfer coefficient are three key elements to the determination of the convective heat transfer.

ES can directly determine the interior surface temperature. In a separate ES, the mean room air temperature is usually used to represent the air temperature close to a surface because of the complete mixing assumption for room air. This is not true for most real situations. In a coupled simulation, the air temperature near surfaces can be explicitly obtained since CFD produces the detailed air temperature distribution. Moreover, CFD can numerically determine the convective heat transfer coefficients as defined in Eq.(4.4). With the convective heat transfer coefficient and the air temperature close to the surface, the convective heat transfer from surface i can be calculated via:

$$q_{i,conv} = h_{i,conv} (T_i - T_{i,air}) \tag{5.1}$$

where T_i is the surface temperature, $T_{i,air}$ is the air temperature close to the surface, and $h_{i,conc}$ is the convective heat transfer coefficient. To be consistent with the expression in ES, expression (5.1) can be further written as

$$q_{i,conv} = h_{i,conv} (T_i - T_{i,air}) = h_{i,conv} (T_i - T_{room}) - h_{i,conv} \Delta T_{i,air} \tag{5.2}$$

where T_{room} is the mean room air temperature and $\Delta T_{i,air} = T_{i,air} - T_{room}$.

With this convective heat in which some of the variables are obtained from ES and others from CFD, both ES and CFD can improve the accuracy of their solutions. A straightforward method to exchange the information between ES and CFD is to pass the air temperature, $T_{i,air}$, and the corresponding convective heat transfer coefficient, $h_{i,conv}$, obtained in CFD at a particular time step to ES. ES uses this $T_{i,air}$ and $h_{i,conv}$ to update the convective heat transfer, $q_{i,conv}$, with Eq.(5.2). Then, by solving the heat balance Eqs. (3.2) and (3.1) with the new convective heat transfer, the surface temperatures and heat extraction rate can be determined to provide the boundary conditions for the next CFD run. In each CFD calculation, the use of the surface temperatures obtained from ES is direct. The heat extraction rate from ES, which is the same as the convective heat

transfer when the room air temperature is constant, can be used to determine the system supply inlet boundary conditions in CFD. For a constant-air-volume (CAV) HVAC system with a known air supply flow rate V, the supply air temperature, T_{supply}, is

$$T_{supply} = Q_{heat\_extraction}/(\rho C_p A V) + T_{outlet} \quad (5.3)$$

where A is the diffuser air-supply area and T_{outlet} is the return air temperature. For a variable-air-volume (VAV) system, T_{supply} is constant, and the V becomes

$$V = Q_{heat\_extraction}/(\rho C_p A)\,(T_{supply}-T_{outlet}) \quad (5.4)$$

The coupling method presented above is fairly straightforward. However, it only represents one of the possible approaches to exchange the convective heat transfer information between ES and CFD programs. It is interesting and helpful to line up all the possible coupling methods and analyze the performance of each method with the aim to find a most efficient and robust coupling method.

In general, CFD has three different kinds of thermal boundary conditions – given surface temperature T_i (Dirichlet condition), given surface heat flux $Q_{i,conv}$ (Newmann condition), and given $Q_{i,conv}$-T_i relationship (Robbins condition). The third boundary condition describes a relationship between the conduction in solid materials and the convection in neighboring air. It is not suitable for the CFD calculation that does not solve the conductive heat in solid materials.

On the other hand, the convective heat transfer from enclosure interior surfaces can be expressed as

$$\begin{aligned} Q_{i,conv} &= h_{i,conv}A(T_i - T_{i,air}) = h_{i,conv}A[T_i - T_{room} - (T_{i,air} - T_{room})] \\ &= h_{i,conv}A(T_i - T_{room} - \Delta T_{i,air}) \\ &= h_{i,conv\text{-}nominal}A(T_i - T_{room}) \end{aligned} \quad (5.5)$$

where $h_{i,conv\text{-}nominal}$ is the nominal convective heat transfer coefficient based on the temperature difference of surface and mean room air. As a result, ES has three approaches to acquire the accurate thermal information (convection heat from envelopes) from CFD: (1) by $Q_{i,conv}$ directly; (2) by $h_{i,conv}$ and $T_{i,air}$ (or indoor air temperature gradient $\Delta T_{i,air}$); (3) by $h_{i,conv\text{-}nominal}$ only.

Hence, the potential exchanging methods of the inter-coupled convection conditions between ES and CFD can be:

- coupling method-1: ES to CFD by T_i; CFD to ES by $h_{i,conv}$ and $\Delta T_{i,air}$;
- coupling method-2: ES to CFD by T_i; CFD to ES by $h_{i,conv\text{-}nominal}$;
- coupling method-3: ES to CFD by T_i; CFD to ES by $Q_{i,conv}$;
- coupling method-4: ES to CFD by $Q_{i,conv}$; CFD to ES by $h_{i,conv}$ and $\Delta T_{i,air}$;
- coupling method-5: ES to CFD by $Q_{i,conv}$; CFD to ES by $h_{i,conv\text{-}nominal}$;
- coupling method-6: ES to CFD by $Q_{i,conv}$; CFD to ES by $Q_{i,conv}$.

where coupling method-1 is exactly the one described above in detail.

Not all the coupling methods listed are feasible. For example, the $Q_{i,conv}$ obtained in ES will never be updated in the CFD simulation with method-6 due to the fixed heat flux boundary condition in CFD. CFD can not provide a new $Q_{i,conv}$ to ES with this data coupling method. Chapter 7 will intensively discuss the feasibility and the performance of the other coupling methods through theoretical analysis and numerical experimentation.

Since the heat flows and surface temperatures vary with time in buildings, the coupling of ES and CFD, theoretically, needs to be performed at each time step of the whole building simulation. Even at each time step, iteration between ES and CFD models may be required in order to reach a mutually consistent solution between ES and CFD.

In order to automate the iterative coupling of the simulations and produce one integrated design tool, the individual ES and CFD programs should be assembled into one body. Since ES programs simulate the whole building performance for a long period of time while CFD programs focus on the flow and heat transfer in some particular spaces, a reasonable assembling strategy is to embed a CFD program into an ES program. The structure of such a coupled simulation program has been illustrated in Figure 5.2, as a modification to the structure of a separate ES shown in Figure 3.3.

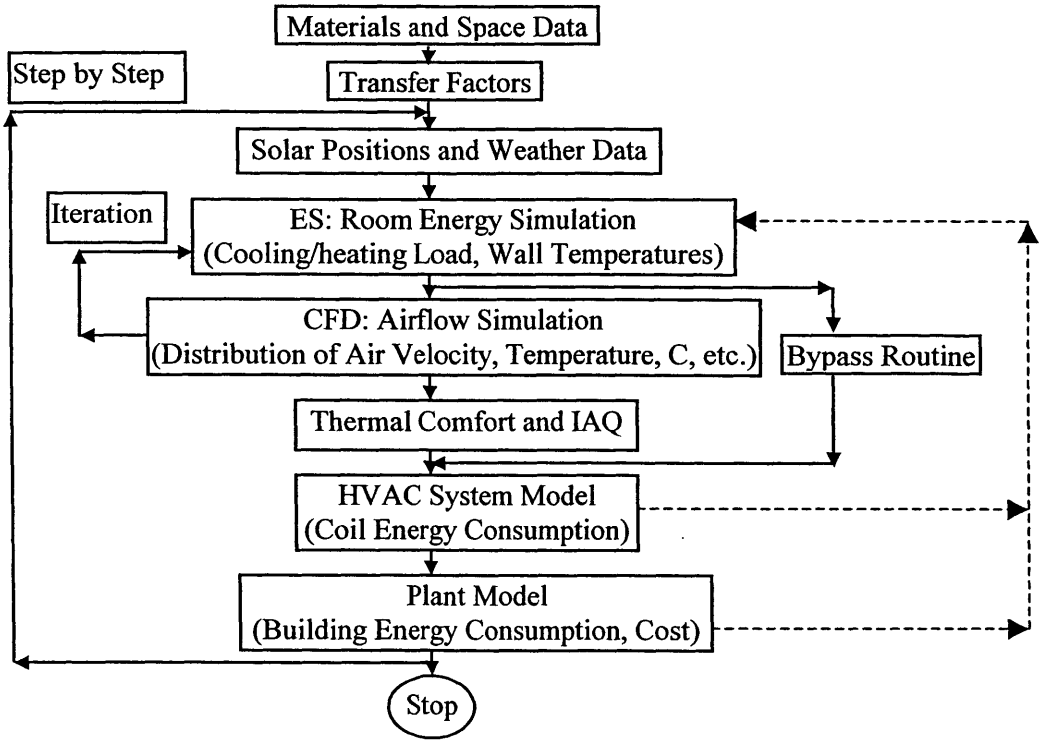

Figure 5.2 Structure of the coupled simulation program

5.2 Coupling Strategies of Energy Simulation and CFD Programs

5.2.1 Challenges for Program Coupling

The coupling principles presented above look straightforward. However, the coupling is not very practical due to the considerable disparities of the physical models and numerical schemes between ES and CFD programs. Basically, three major discontinuities exist between these two different programs.

(1) Time-scale discontinuity

ES and CFD have very different characteristic time-scales for heat transfer in building envelope and room air. The scale analysis (Bejan 1995) gave the order of magnitude for the penetration of the heat flux in the wall as

$$t \sim L^2/\alpha \tag{5.6}$$

For instance, for a wall with thermal diffusivity $\alpha \sim 10^{-5}\,m^2/s$ and thickness $L \sim 10^{-1}\,m$, the time for the heat flux through the wall is of the order of 10^3 seconds, or is of the order of hours.

However, for the transient flow inside a room, Bejan (1995) found the order of the magnitude of the time required for reaching the steady state natural convection flow as

$$t \sim (\nu H/g\beta\Delta T\alpha)^{0.5} \tag{5.7}$$

Considering a typical room with a typical indoor temperature, the time for reaching the steady state is of the order of 10^1 seconds. The time scale ratio of the two transfer phenomena is of the order of 10^2.

(2) Spatial model discontinuity

ES adopts the nodal model, which implies that the indoor environmental conditions predicted for each space are spatially averaged. For example, the surface temperature obtained in ES is uniform. In contrast, CFD divides the space and surfaces into many cells in which the mass, momentum and energy conservation equations are solved. CFD, therefore, presents the field distributions (field model) of the velocity, temperature, humidity, and contaminant concentrations. The connection between ES and CFD thus confronts the significant model switch between the nodal model and the field model.

(3) Computing speed discontinuity

The computing time for ES is very fast due to the nodal model. Usually, ES requires a few seconds/minutes per zone for an annual energy analysis and requires little computer memory. However, a CFD calculation for a typical room may take a few hours

and require a large amount of memory (Srebric 2000), despite the tremendous growth in the capacity and speed of modern computers. When the building size increases, the computing time of CFD may dramatically increase, even with a modest grid resolution.

5.2.2 Time and Spatial Coupling Strategies

This investigation proposes several special coupling strategies to bridge these discontinuities between ES and CFD and make the coupling feasible for design applications.

For the time-scale discontinuity, the present study partitions the whole simulation into a long-time process for ES and a short-time scale (strictly speaking, a quasi-static process at a given time-step) process for CFD. As illustrated in Figure 5.3, ES handles a long-term simulation, such as a design day, while CFD runs only at some specific time steps, such as 8:00 am, with the boundary conditions provided by ES at that time step. ES then uses the updated information from CFD for the next two hours till the next CFD call at 10:00 am. For most room airflows, the quasi-static simulation of CFD is reasonably accurate since the thermal responding time of indoor air is of the order of 10^1 seconds (or at most minutes). It implies that the current indoor airflow pattern is dominantly determined by the current boundary conditions that may involve the thermal history of thermal mass (e.g. building envelopes) predicted by ES. The history of the airflows in the last seconds or minutes has very limited influence on the current airflow since the change of airflow patterns in the seconds or even minutes is very small in most normal building scenarios.

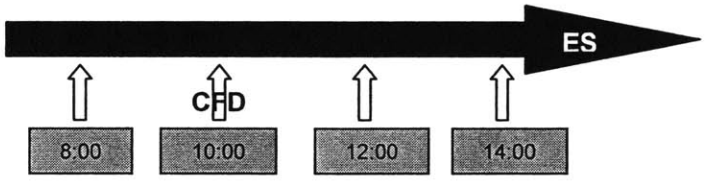

Figure 5.3 Illustration of time-scale coupling (ES handles a long-term simulation, such as a design day, while CFD runs only at some specific times, such as 8:00 am)

The spatial model discontinuity can also be effectively bridged by appropriate numerical approximation. Although different numerical approximation algorithms may have different impacts on the coupling performance depending on the problems studied, sufficiently fine subdivisions of enclosure surfaces in ES can always diminish this effect. For example, if a wall has a small temperature gradient, the whole wall surface can then be treated as a single node in ES and an area-weighted algebraic average method can be used to connect the nodal value from ES and the distributed field values from CFD. Otherwise, ES can model the wall with more nodes and connect them individually to the corresponding field values from CFD by proper average calculations, as Figure 5.4 illustrates.

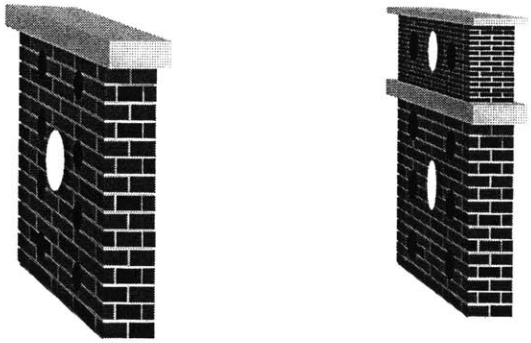

Figure 5.4 Illustration of spatial model coupling with numerical approximation (white: nodes in ES; black: points in CFD)

5.2.3 Staged Coupling Strategies

As to the computing speed discontinuity, the demand of CFD in computing time makes the coupling almost unfeasible for most design practices. Although the quasi-static CFD simulation has enormously reduced the computing costs by avoiding solving the transitional flows between two coupling steps, the iterative coupling simulation at those discrete coupling steps still imposes a heavy load on the computer. Besides using more numerical approximations, such as simpler turbulence models, to directly reduce the computing time of CFD, it is necessary to develop simplified coupling strategies to minimize the number of CFD calls during a coupled simulation due to the limitation of the available hardware.

The present study proposes staged coupling strategies that consist of *static coupling process*, *dynamic coupling process* and *bin coupling process*, as illustrated in Figure 5.5. The static coupling process has occasional (static) information exchange between ES and CFD while the dynamic coupling process performs continuous (dynamic) information exchange for a simulation. The bin coupling process provides ES the information that are pre-computed by CFD and saved in the bins for continuous energy calculation.

The static coupling process involves one-step or two-step information exchange between ES and CFD programs, depending on the sensitivity of building thermal performance and user's solution accuracy requirement. With only a few coupling steps, the static coupling can be performed manually, which does not require arduous modifications of individual ES and CFD programs. Generally, the one-step static coupling is good for cases where ES or CFD or both are not very sensitive to the exchanged variables. For example, ES is rather insensitive to $\Delta T_{i,air}$ and $h_{i,conv,}$ in an air-conditioned room with low velocity mixing ventilation. To provide CFD inlet conditions and wall temperatures as inputs, one-step static coupling from ES to CFD is a good choice.

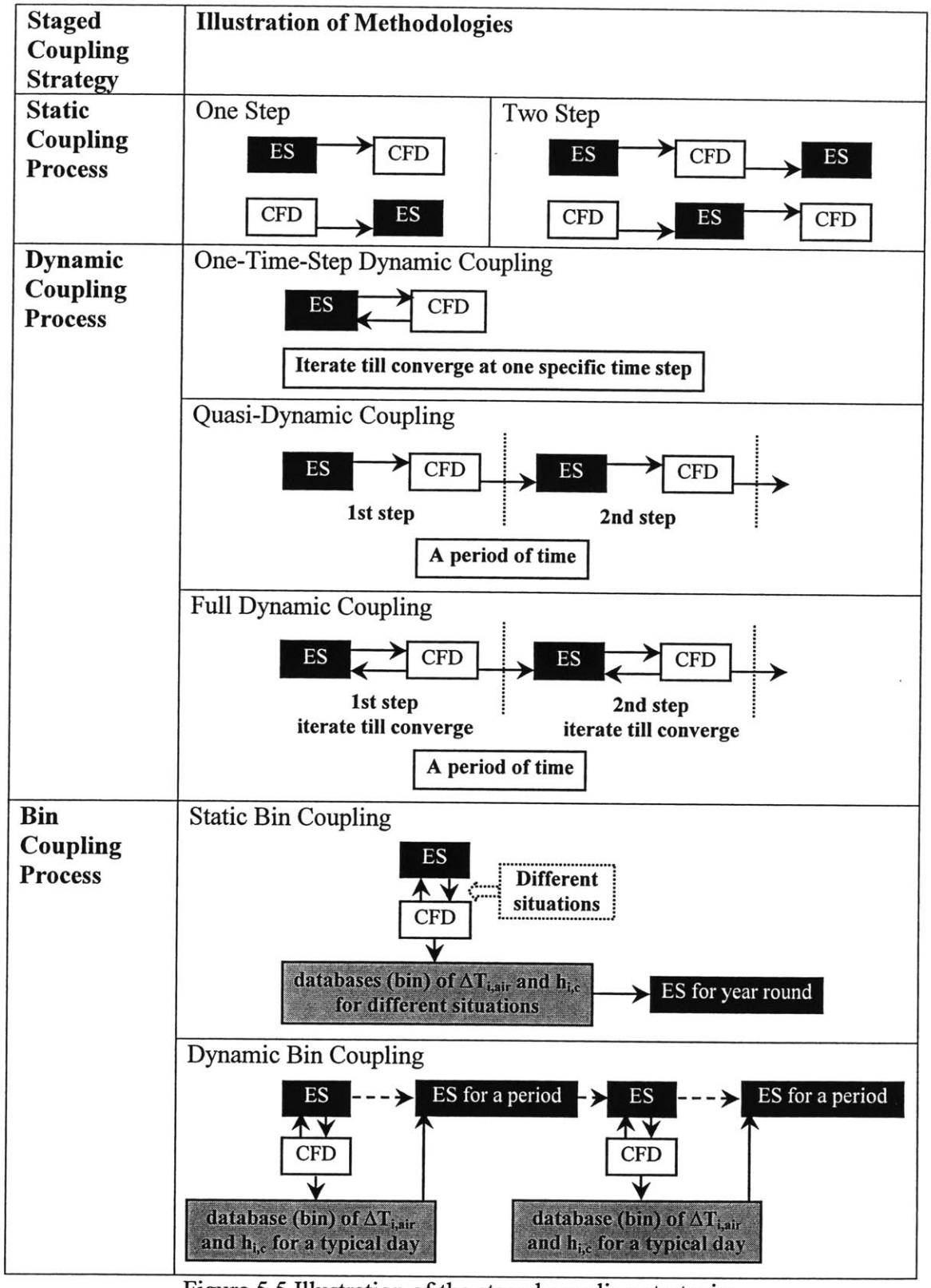

Figure 5.5 Illustration of the staged coupling strategies
(The arrows from CFD to ES indicate the transfer of $\Delta T_{i,air}$ and $h_{i,conv}$ while the arrows from ES to CFD indicate the transfer of T_i and $Q_{heat\text{-}extraction}$)

If the information from CFD, such as $h_{i,conv}$, differs significantly from that used in the ES calculation, ES may use that from CFD as inputs for the next ES run. This is the ES-CFD-ES two-step static coupling. The coupling is good for buildings with little changes in the exchanged information, and the results of ES do not strongly depend on the exchanged data. Such an example is the building without an HVAC system in the mild seasons.

The dynamic coupling process, which involves coupling between the two programs at every time step, is required when both ES and CFD solutions are sensitive to the transient boundary conditions. This study further proposes three kinds of dynamic coupling processes. The first one is *one-time-step dynamic coupling process*, which focuses on the ES-CFD coupling at one specific time step of interest. At that time step, the iteration between ES and CFD is performed to reach a converged solution. This coupling is for cases where a designer is interested in only a few typical scenarios (design conditions) and both ES and CFD are very sensitive to the exchanged information. For example, one-time-step dynamic coupling process is good for the study of residential buildings under winter design conditions. In that case, the indoor load and outdoor weather have small variation during a day while the continuously operating HVAC system may tightly link the energy consumption with the indoor airflow.

Many building designs require flow and energy information over a period of time with dynamic conditions, such as startup and shutdown periods. The ES-CFD coupling may be conducted at every time step over this period. When the time-step is small (for instance, a few minutes), it may not be necessary to couple the two programs at every time-step because the changes of the required information may not be significant. Further, the coupling may require no iteration between ES and CFD in order to reduce the computing time. This is *quasi-dynamic coupling*. In quasi-dynamic coupling, the CFD receives the boundary conditions from the previous ES calculation at the current n^{th} time step and returns the thermal information of indoor air to the next ES at the next $(n+1)^{th}$ time step. A regular residential building under a mild weather condition is a good example to have this coupling strategy applied because of the small fluctuation of building performance.

If ES and CFD iterate a number of times at each time step to reach a converged solution, the coupling is *full dynamic coupling*. Full dynamic coupling is undoubtedly the most accurate, but also most computationally intensive. Full dynamic coupling may be necessary for poorly insulated buildings with dynamical loads. Note that the iteration of ES and CFD at each coupling time step may result in convergence and stability problems due to the physical and numerical differences between ES and CFD programs. Different data coupling methods in iteration may produce differences in convergence and stability behaviors. More analysis of this topic will be presented in Chapter 7.

As mentioned above, in theory, the quasi-dynamic coupling and full dynamic coupling should be conducted at each time step of energy simulation, which may be of the order of minutes. Since the change of building performance may not be significant during this small period of time, the coupling can be performed with a larger time

interval. The coupling frequency thus can be: (1) every day; (2) every couple hours; (3) every hour; or (4) every time step that ES uses. The choice of coupling frequency is determined by building conditions and solution accuracy requirements. For example, the startup and shutdown periods of a commercial building in each day may need more couplings than the rest of the day because of the significant condition changes. But if the energy consumption during these time periods is small compared to the total energy consumption of the day, the same low coupling frequency may be used for the whole day modeling. This may significantly reduce the computing time without noticeably decreasing the accuracy.

One way to further reduce the computational costs is to use *bin coupling process,* as first proposed by Chen and Kooi (1988). Two bin coupling processes – *static bin coupling process* and *dynamic bin coupling process* – are developed in this study. In a static bin coupling (also called virtual coupling), the room air temperatures and the convective heat transfer coefficients required by ES are pre-calculated by CFD as the functions of cooling/heating loads (for conditioned periods) or indoor-outdoor air temperature difference (for unconditioned periods). ES determines $\Delta T_{i,air}$ and $h_{i,conv}$ by directly interpolating the CFD results from the static function bins at each time step of the calculation. Static bin coupling is suitable for buildings without dramatic changes of heat/cooling load and outdoor air temperature because the dramatic changes make the curve-fitted functions less accurate. Dynamic bin coupling, rather than generating curve-fitted functions and constructing a comprehensive bin system in advance, predicts the airflow details in some typical days by either quasi-dynamic or full dynamic coupling process. These results are then used in ES for days with similar conditions (e.g. weather, internal load, system operating conditions, etc...). Figure 5.6 shows the year-round outdoor dry bulb temperature of Boston. It may be a good example where the dynamic bin coupling process can be used, if other building conditions are the same during the time. The bin coupling process dramatically reduces the computational cost because of the significant cut of CFD calling times.

In general, the building characteristics and the purpose of the simulation determine which coupling process is most suitable for a particular case. Several coupling processes may be used together to achieve the best solution for a specific case. For example, static bin coupling may be good for a whole year energy analysis, while one-time-step dynamic coupling may be adequate for equipment sizing. Through the sensitivity study of coupling strategy performance, Chapter 9 will further demonstrate how to select an appropriate coupling strategy for a particular building according to the building characteristics.

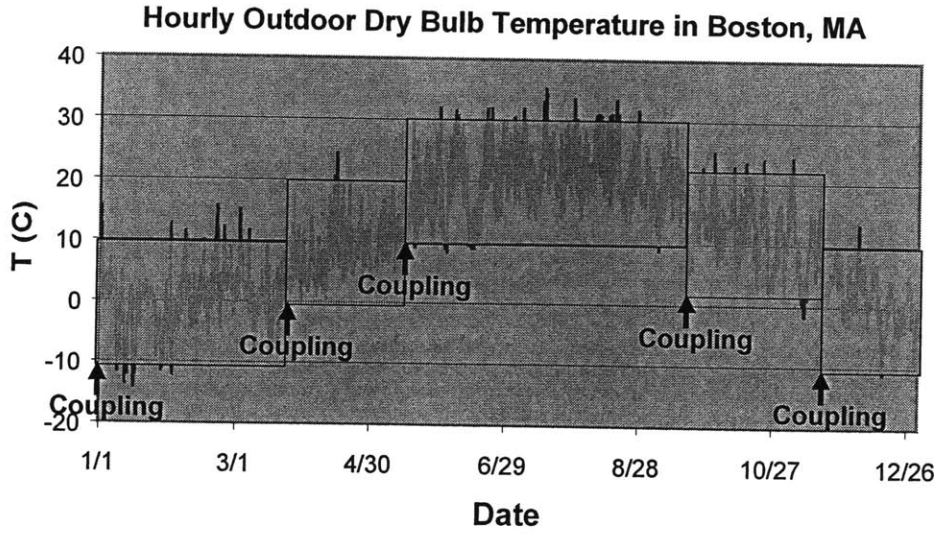

Figure 5.6 Dynamic bin coupling process (five typical days coupling) for year-round energy simulation of buildings in Boston according to the hourly outdoor dry bulb temperature distribution

5.3 Coupling Implementation of Energy Simulation and CFD Programs

All the coupling strategies and coupling methods proposed in this chapter have been implemented by using the EnergyPlus and MIT-CFD programs. A coupling program named E+MIT-CFD has been developed and ready for building design usage. This section will briefly introduce the development of such a coupling program. More detailed descriptions of the E+MIT-CFD program and its operation can be found in the Appendix.

5.3.1 General Rules for Developing the Coupling Program

The EnergyPlus and MIT-CFD programs are under continuous and independent development and maintenance. To avoid significant changes of the coupling program each time the individual ES and CFD models get updated, the three-module code structure as illustrated in Figure 5.7 has been used to develop the coupling program. Within this structure, the ES and CFD programs plug into the interface module rather than contact each other directly. The interface module works as a bridge between the ES and CFD modules, containing all the essential coupling data and performing all the necessary data exchanging and handling operations. As a consequence, any updates in EnergyPlus and/or MIT-CFD will not explicitly affect the other part. This structure also allows the easy replacement of the ES and/or CFD solver with other programs. The appendix will demonstrate, in practice, how to replace the MIT-CFD program in the coupling program with other CFD solvers.

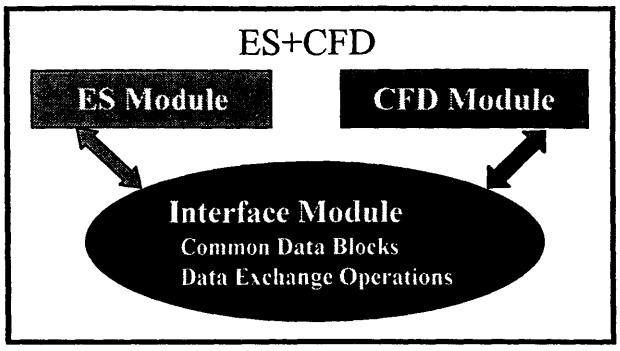

Figure 5.7 Illustration of three-module structure in the coupling program

To be consistent with the EnergyPlus and MIT-CFD programs, the entire coupling program was also developed with Standard Fortran Language (Fortran 90). The programming practice of the coupling program follows the general coding rules, such as:

- standardization: e.g. standard and clear data and file names, standard program structure, and standard input and output;
- modularization: each module can perform certain similar functions without cross-calling other modules;
- expandability: more functions and models can be plugged into the program without significant changes of the initial codes

5.3.2 Executive Streamline of the Coupling Program

Figure 5.8 shows the executive streamline of the coupling program developed. Generally, four input files are required to run a coupled simulation.

- Two of them are for the ES calculation: one is the weather file that may be needed for a simulation over a period of weather time; the other is the input file describing the building and simulation conditions.
- The other two are for CFD simulation: one is the grid file containing the coordinates of discrete mesh points; the other is the input file including the problem descriptions and simulation parameters.

These input files can be generated by using particular graphical user interfaces (GUI) developed for ES and CFD programs, such as the IDFEditor for EnergyPlus and SCI (Simplified CFD Interface) (Broderick and Chen 2001) for MIT-CFD. In the future, users may even consider developing a uniform GUI for both EnergyPlus and CFD.

With these input files, the pre-compiled executable file of the coupling program, i.e. E+MIT-CFD.exe, can be called to launch a coupled simulation. At the start of each simulation, a user is offered a number of coupling choices, such as coupling strategy and coupling method. After selecting a particular coupling approach according to the building characteristics and solution requirements, the simulation will be automatically performed along this prescribed coupling routing. The pre-selected output results will be

exported and can be further handled by various post-processing tools, such as MS Excel, TechPlot, etc...

Note that it is also possible to perform the sole ES calculation within this system by selecting "no coupling" option in the coupling choices. That is, users can ignore the CFD section and run E+MIT-CFD.exe with only two input files for ES, which produces the non-coupled ES results.

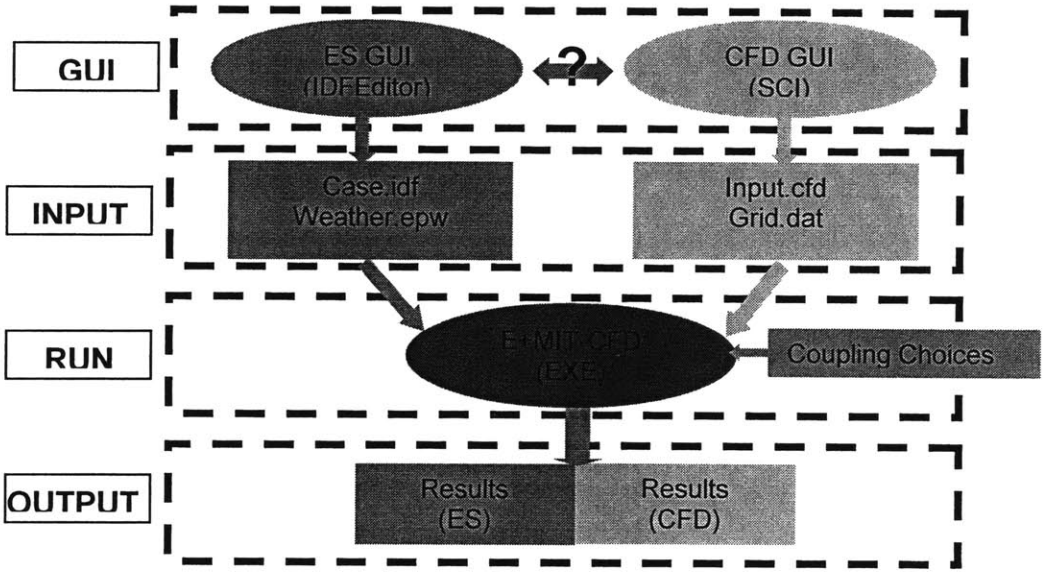

Figure 5.8 Executive streamlines of the coupling program

5.3.3 Core Structure of the Coupling Program

In order to have one single executable program (E+MIT-CFD.exe) and automate the coupling process, the individual ES and CFD programs should be assembled into one body to form an integrated program. Because ES simulates the whole building performance for a long period of time while CFD focuses on the "snap-shot" of the airflow and heat transfer in a single space, the MIT-CFD program has been embedded into the EnergyPlus program. Figure 5.9 shows the core structure of such a coupling program developed by using the three-module strategy.

As seen in Figure 5.9, the ES and CFD modules are connected to each other by exchanging the inter-coupled information through the interface modules. The essential change in both individual ES and CFD programs for the construction of the integrated program is to create two additional functions:

(1) passing newly updated information to the partner;
(2) receiving information from the partner and using them in the current calculation.

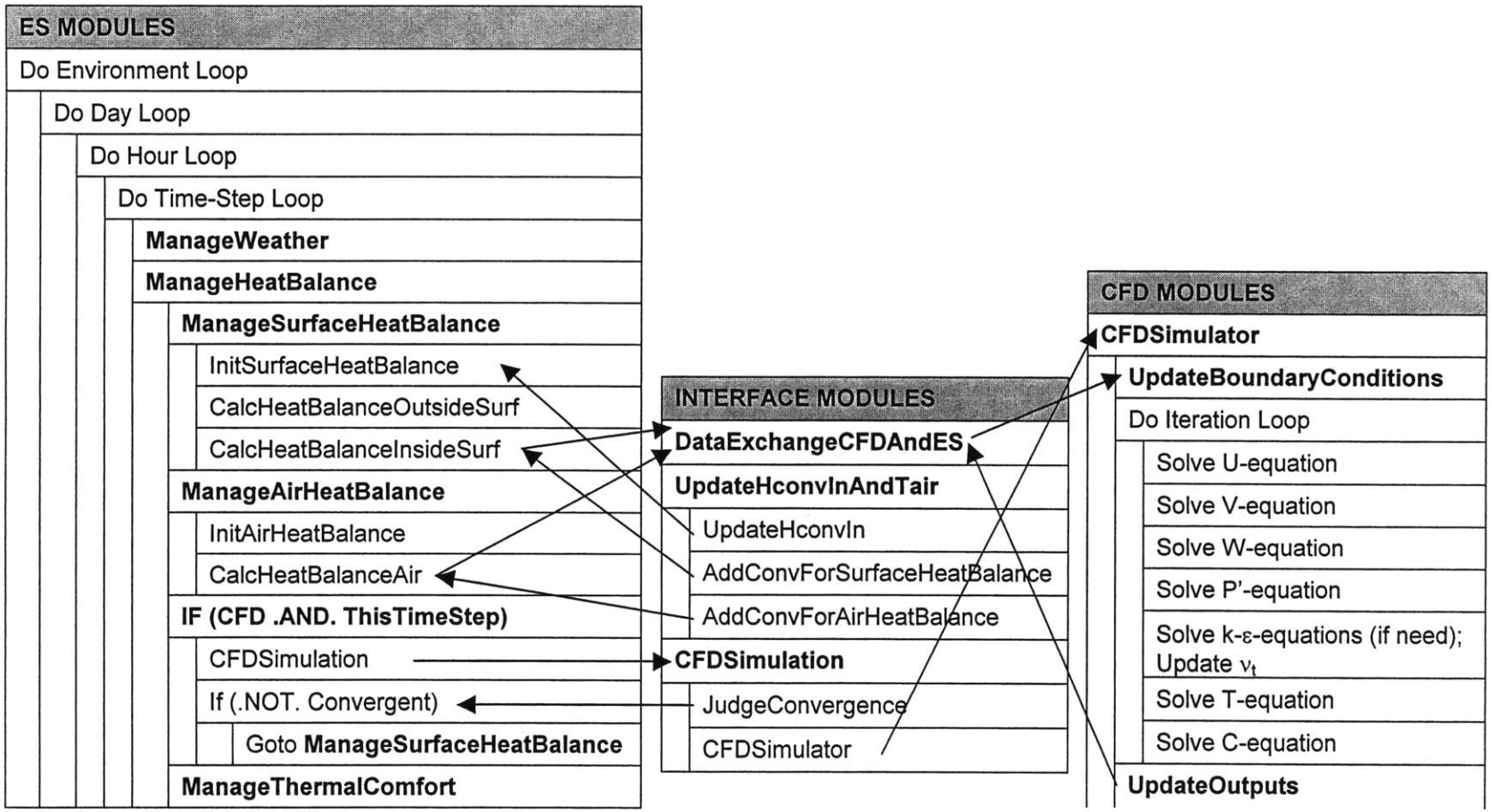

Figure 5.9 Core structure of EnergyPlus embedded with MIT-CFD (E+MIT-CFD)

The following paragraphs describe the major coupling-related modifications and developments in the ES and CFD and interface modules, respectively.

(1) Modifications in ES Modules

To accommodate the different data coupling methods, the corresponding modules in the ES program are modified to insert the new terms, update the variables, and output the inter-coupled data. Without considering the connection of ES and CFD at system and plant levels, the primary modifications may include, as shown in Figure 5.9,

a. **ManagerSurfaceHeatBalance** – InitSurfaceHeatBalance: call the update of the interior surface heat transfer coefficients from CFD solutions.

b. **ManagerSurfaceHeatBalance** – CalcHeatBalanceInsideSurf: introduce the updated value and additional term related to interior surface convection into the interior surface heat balance equation:

$$q_i + q_{ir} = \sum_{k=1}^{N} q_{ik} + q_{i,conv} \tag{5.8}$$

where,

$$\begin{aligned} q_{i,conv} &= h_{i,conv}(T_i - T_{i,air}) = h_{i,conv}(T_i - T_{room}) - h_{i,conv}(T_{i,air} - T_{room}) \\ &= h_{i,conv}(T_i - T_{room}) - h_{i,conv}\Delta T_{i,air} \end{aligned} \tag{5.9}$$

If data coupling method-1, 2 or 4 is used, the additional convective heat transfer $Q_{additional\text{-}conv}=h_{i,conv}\Delta T_{i,air}$ as well as the updated $h_{i,conv}$ from CFD are introduced into the interior surface heat balance equation. If data coupling method-3 is used, $q_{i,conv}$ obtained from CFD is directly introduced into the interior surface heat balance equation.

c. **ManagerSurfaceHeatBalance** – CalcHeatBalanceInsideSurf: export the new interior surface temperatures produced by the current ES calculation for the next CFD simulation.

d. **ManagerAirHeatBalance** – CalcHeatBalanceAir: introduce the additional interior surface convection term and natural ventilation energy (if any) and actual exhaust air temperature from CFD into the indoor air energy balance equation:

$$\begin{aligned} \frac{\rho V_{room} C_p \Delta T_{room}}{\Delta t} = & \sum_{i=1}^{N_{surfaces}} h_i A_i \left(T_{si} - T_{room} - \Delta T_{i,air}\right) + \dot{m}_{sys} C_p \left(T_{sup} - T_{exhaust-CFD}\right) \\ & + Q_{natural-ventilation} + Q_{lights} + Q_{people} + Q_{appliances} + Q_{inf\,iltration} \end{aligned} \tag{5.10}$$

e. **ManagerAirHeatBalance** – CalcHeatBalanceAir: export the system supply heating/ cooling energy requirement (if any) for the zone concerned, and the mean room air temperature newly computed by ES, for the next CFD simulation.

f. **ManagerHeatBalance** – IF(CFD.AND.ThisTimeStep): determine whether to run CFD simulation at the current time step of ES according to the selected coupling strategy and coupling frequency; if positive, call the CFD solver; determine whether to conduct one more ES-CFD iteration at the current coupling step based on the convergence status of the simulation.

Note that most of these modifications are only to call the corresponding operations in the interface modules, or to insert the new terms that are generated in the interface modules. This facilitates the implementation of diverse coupling methods and strategies as well as further improvement of the ES and/or CFD programs.

(2) Modifications in CFD Modules

As shown in Figure 5.9, ES calls CFD, whenever needed, through one of the interface modules – CFDSimulation. After checking the convergence of the whole coupling simulation, the CFDSimulation module will determine whether to call the main program of the CFD solver – CFDSimulator – in another module. A user can easily convert an independent CFD program into the CFDSimulator module, as will be explained in the Appendix.

Similarly, CFD should also have two new function modules. One is the UpdateBoundaryConditions module at the beginning of each CFD calculation to update the relevant boundary conditions based on the last ES calculation. The other is the UpdateOutputs module at the end of each CFD calculation to update the information to be transferred back to ES. The following paragraphs detail the information that is updated in the UpdateBoundaryConditions and UpdateOutputs modules.

a. **UpdateBoundaryConditions:** the updated CFD boundary conditions during a coupled simulation include:
   - envelope interior surface temperature or surface heat flux, according to the data coupling methods selected;
   - supply air inlet conditions;
     - For a constant-air-volume system, air supply airflow rate V is specified and the supply air temperature T_{supply} is determined by

$$T_{supply} = Q_{heat\_extraction}/(\rho C_p A V) + T_{outlet} \quad (5.11)$$

     - For a variable-air-volume system, T_{supply} is fixed and the V is determined by

$$V = Q_{heat\_extraction}/(\rho C_p A)\,(T_{supply}-T_{outlet}) \quad (5.12)$$

- heat flux for dynamic internal thermal objects, such as radiator;
- pressure and temperature conditions for natural ventilation.

b. **UpdateOutputs:** the information obtained in CFD, which may be used for ES calculation, include:
   - convective heat transfer coefficients at each surface;
   - air temperature close to the surfaces or air temperature gradient $\Delta T_{i,air}=T_{i,air}-T_{room}$;
   - surface temperature or surface heat flux, depending on the data coupling methods selected;
   - exhaust air temperature;
   - volume-weighted mean air temperature;
   - cooling capacity of natural ventilation.

(3) Interface Modules

The ES and CFD modules call the relevant data-exchange operations to invoke the data transfer processes. The interface modules implement the substantial exchange of the information, as illustrated in Figure 5.9. The interface modules consist of the common data module (DataExchangeCFDAndES) and the data-exchange operation modules (UpdateHconvInAndTair and CFDSimulation). The common data module contains all the interface variables connecting ES and CFD. By incorporating these new interface variables, the original ES and CFD programs do not need to change their own data structures and variable names. The data-exchange operation modules work as the bridge between ES and CFD and perform most of the data transfer functions in a coupled simulation. Consequently, the ES and CFD programs merely need limited modifications to plug into the interface modules, rather than directly connecting with each other by sophisticated code changes. It allows easy update and maintenance of individual ES and CFD programs. It is also convenient to create new functions in the interface modules to study different data coupling methods and strategies. The following paragraphs briefly introduce what the UpdateHconvInAndTair and CFDSimulation do to bridge the ES and CFD programs and transfer information between them.

a. **UpdateHconvInAndTair** module consists of several sub-modules. Each of them has a particular purpose of transferring certain information between CFD and ES, such as:
   - **UpdateHconvIn** provides ES the proper convective heat transfer coefficients by importing the results from the last CFD calculation or extracting them from appropriate static or dynamic bins, depending on the coupling strategy used.
   - **AddConvForSurfaceHeatBalance** imports the indoor air temperature gradients from static or dynamic bins or the last CFD run, and calculates the additional convection term $Q_{additional\text{-}conv}=h_{i,conv}\Delta T_{i,air}$ for the inside surface heat balance equations of ES.
   - **AddConvForAirHeatBalance** imports the indoor air temperature gradients from static or dynamic bins or last CFD run, and calculates the additional convection

terms, such as $-\sum_{i=1}^{N_{surfaces}} h_i A_i \Delta T_{i,air}$ and $Q_{natural\text{-}ventilation}$ (if any), for the indoor air heat balance equation of ES.

UpdateHconvInAndTair module also includes some typical static function databases for static bin coupling process, such as those developed by Chen (1988). Based on these, the convective heat transfer coefficients and the indoor air temperature gradients can be dynamically determined and used for the ES calculation.

b. **CFDSimulation** module is the gate to the main program of the CFD solver. When ES needs a CFD simulation, it calls the CFDSimulation module. The module will first evaluate the convergence status of the whole coupling simulation by comparing the temperature difference of each surface between this ES run and the last ES run. If the largest temperature difference is smaller than the prescribed criteria, the coupling simulation at this coupling step is converged and no more CFD is needed. Otherwise, the CFD solver will be called one more time. For the quasi-dynamic coupling, the convergence status is always set as "True" because of no requirement for iteration at each coupling step. In order to avoid the infinite (dead) iteration between ES and CFD, the module sets ten as the maximum iteration step and provides a warning if the iteration does not converge at a coupling step. In the current version of E+MIT-CFD, the CFDSimulation module also produces the dynamic bins of the convective heat transfer coefficients and indoor air temperature gradients according to the CFD results on the typical days simulated.

5.4 Summary

This chapter presents the fundamentals of ES and CFD coupling and discusses the potential coupling methods between ES and CFD programs. The study develops the special coupling strategies to bridge the discontinuities of time-scale, spatial-model and computing-speed between ES and CFD models. The staged coupling strategies proposed, which consist of the static, dynamic and bin coupling processes, can effectively reduce the computing cost of a coupled simulation by reasonably controlling the CFD calling times.

The coupling strategies and methods proposed have been implemented by coupling the EnergyPlus and MIT-CFD programs. The chapter introduces the principal technical routes used in the implementation. The coupling program developed, named E+MIT-CFD, provides users a few of simulation options, as illustrated in Figure 5.10. Based on the building characteristics and solution accuracy requirement for a particular building, a user can choose:

- whether to couple ES with CFD;
- which indoor space to perform CFD;
- which coupling strategy to use;
- which coupling frequency to use;
- which coupling method to use;

- which bin and function to use if static bin coupling.

The next chapters will discuss the solution characteristics of a coupled simulation through theoretical analysis and numerical experiments by using this coupling program.

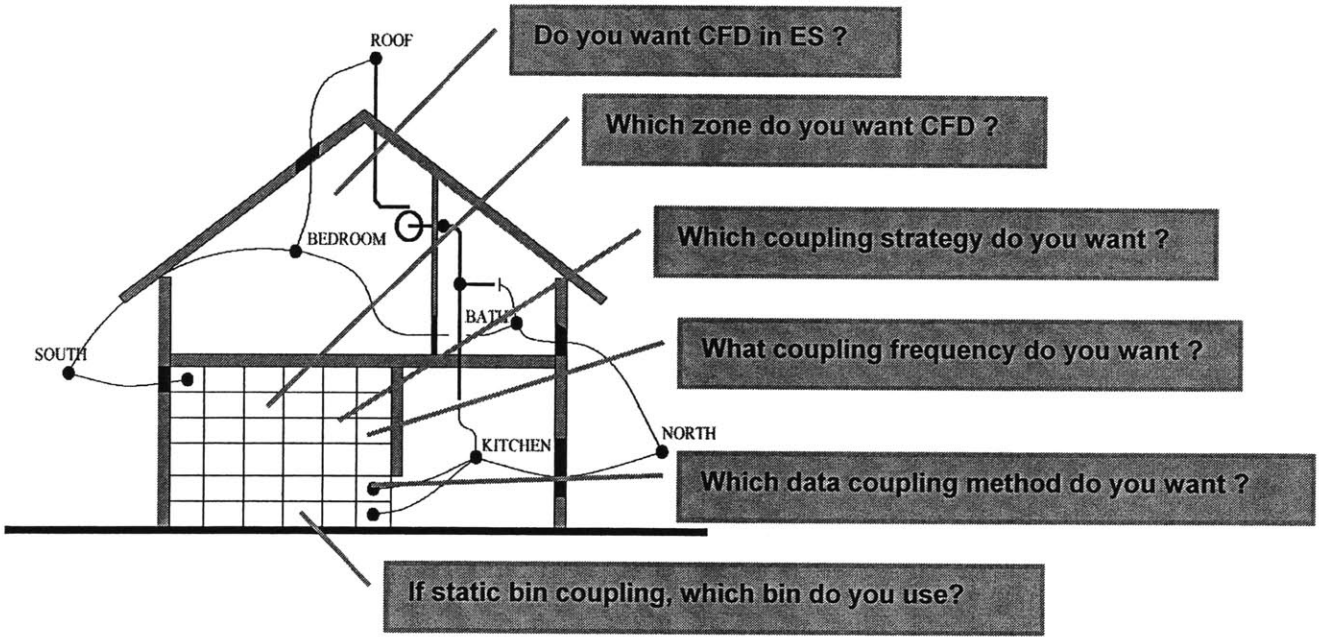

Figure 5.10 Illustration of the coupling options E+MIT-CFD offers

CHAPTER 6

DETERMINATION OF CONVECTIVE HEAT TRANSFER IN COUPLED SIMULATION

The convective heat transfer at building envelope plays an important role in the coupling of ES and CFD programs. In a coupled simulation, CFD is responsible for providing ES accurate convective heat transfer on each enclosure surface. However, the convective heat calculated by CFD is highly sensitive to the numerical methods and turbulence models employed in CFD. This chapter investigates the effect of the size of the first CFD grid to a wall on the heat transfer and examines how zero-equation turbulence models determine the convective heat transfer.

6.1 Factors to Numerical Solution of Convective Heat Transfer

As introduced in Chapter 3, CFD discretizes the continuous computational domain into many grid cells and solves the governing conservation equations of flow on these grid cells. CFD calculates convective heat transfer from a rigid surface through

$$Q = hA\left(T_{surface} - T_1\right) \tag{6.1}$$

$$h = C_p \frac{\rho\left(\nu_t + \nu\right)}{Pr} \frac{1}{D} \tag{6.2}$$

where h is the convective heat transfer coefficient, A is the surface area, $T_{surface}$ is the surface temperature, T_1 is the air temperature at the first grid node that is at a normal distance of D to the surface as shown in Figure 6.1(a), C_p is the specific heat of air, Pr is the Prandtl number, ρ is the air density, ν_t is the turbulence viscosity determined by turbulence models at the first grid node, and ν is the molecular viscosity of air. According to Eqs.(6.1) and (6.2), the convective heat is determined by the convective heat transfer coefficient and temperature difference between the surface and air at the first grid node, and the convective heat transfer coefficient is determined by effective viscosity of air (turbulence viscosity plus molecular viscosity) at the first grid node. To obtain accurate surface convective heat transfer, it is important to find its relationship with the D and turbulence model.

Since the size of the first grids in CFD can be adjusted according to the resolution requirement, the convective heat calculated in this manner could be grid-dependent. Another method is to use a prescribed distance, D_2, to a wall surface and calculate convective heat transfer based on the air temperature and effective viscosity there, as illustrated in Figure 6.1(b). Because the D_2 is a prescribed value, this method would eliminate the grid dependence problem.

However, the convective heat transfer calculated with the second method could be different from that calculated based on the information at the first grid node. For example, if assuming laminar flow and $D_2 = 2D$, the same heat transfer would require $T_{surface}-T_2 = 2(T_{surface}-T_1)$. This implies a linear air temperature profile in the region, which is true only at the very close vicinity of the surface for laminar flow. Such a condition is difficult to meet for most indoor airflows.

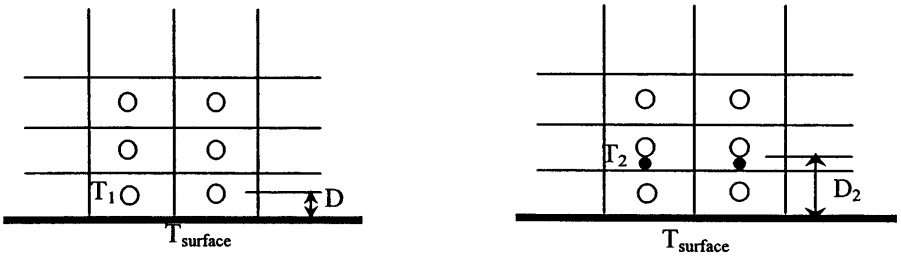

(a) (b)

Figure 6.1 Illustration of the grid, cell, node, and distance to the surface in CFD

Therefore, the calculation of convective heat transfer should use the first method. The question now is how to avoid the grid dependence problem or what the size of first grids should be for the correct prediction of convective heat transfer. CFD theory indicates that finer grids provide more accurate results (Patankar 1980). This may not be true when using simple turbulence models. The following sections will first analytically discuss the grid dependence problem by using laminar and turbulent flows over a flat plate as examples. Numerical investigations are then used to verify the theoretical finds.

6.2 Theoretical Analysis

6.2.1 Convective Heat transfer in Laminar Flows

This study first considers a laminar flow of forced convection along a horizontal plate and that of natural convection along a vertical plate, as illustrated in Figure 6.2. The convective heat transfer computed by CFD is compared with the analytical and empirical solutions to identify the impact of the size of first grid on the heat transfer.

The convective heat transfer through the thermal boundary layer of the plate is

$$q_{surface} = -k\frac{\partial T}{\partial y}\bigg|_{y=0} = h(T_{surface} - T_{\infty}) \tag{6.3}$$

where k is the fluid conductivity, $T_{surface}$ is the plate surface temperature, T_{∞} is the temperature of the free stream outside of the thermal boundary layer. Equation (6.3) shows that the heat conduction at y=0 is the same as the convective heat transfer, because there is no fluid motion in the direction of heat transfer.

(1) Forced Convection

The exact solution of the laminar plate flow of forced convection provides (Lienhard 1999)

$$\frac{U}{U_\infty} = \frac{T_{surface} - T}{T_{surface} - T_\infty} = 1 - \frac{T - T_\infty}{T_{surface} - T_\infty} \tag{6.4}$$

$$q_{surface} = -k\frac{\partial T}{\partial y} = -\rho C_p \frac{\nu}{Pr}\frac{\partial T}{\partial y} = \frac{3}{2}k\frac{T_{surface} - T_\infty}{\delta_t} \tag{6.5}$$

where δ_t is the thickness of thermal boundary layer and $k = \rho C_p \nu/Pr$.

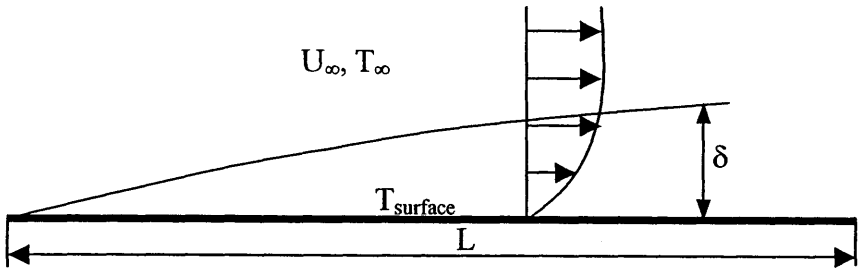

(a) forced convection

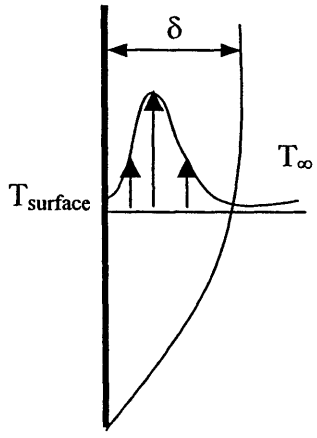

(b) natural convection

Figure 6.2 Illustration of forced and natural plate flow

The analytical solution of the boundary layer equations shows $\delta = \delta_t$ when $Pr = 1$, where δ is the thickness of velocity boundary layer. The exact solution of the boundary layer equations produces (Lienhard 1999)

$$\delta = 4.92x/\sqrt{Re_x} \tag{6.6}$$

where $Re_x = \frac{U_\infty x}{\nu}$ is the Reynolds number of plate flow. For example, if the velocity is 0.1m/s over a 5m long plate,

$$Re_{L/2} = \frac{UL/2}{\nu} = \frac{0.1 \times 2.5}{1.5 \times 10^{-5}} = 1.7 \times 10^4 \tag{6.7}$$

the δ_t at the middle length of the plate is $\delta_t = \delta \approx 0.09m$.

A CFD program would calculate the convective heat transfer from the plate as

$$q_{CFD} = -\rho C_p \frac{\nu}{Pr} \frac{T_D - T_{surface}}{D} = k \frac{T_{surface} - T_D}{D} \tag{6.8}$$

where D is the normal distance from the center of the first grid cell to the surface (half of the cell size) and T_D is the air temperature at cell center. In order to analyze possible errors associated with grid size, this study considers two different first grid sizes: D is smaller than δ_t and D is larger than δ_t.

- $D < \delta_t$

When D is smaller than δ_t, the possible numerical error is

$$\Delta q = q_{CFD} - q_{surface} = -\rho C_p \frac{\nu}{Pr} \frac{T_D - T_{surface}}{D} - q_{surfae} = k \frac{T_{surface} - T_D}{D} - k \frac{T_{surface} - T_\infty}{\frac{2}{3}\delta_t} \tag{6.9}$$

Because the temperature profile in the thermal boundary can be approximated as (Lienhard 1999)

$$\frac{T_D - T_{surface}}{T_\infty - T_{surface}} = \frac{3}{2}\frac{D}{\delta_t} - \frac{1}{2}\left(\frac{D}{\delta_t}\right)^3 \tag{6.10}$$

the relative error of convective heat transfer due to D then becomes

$$\frac{\Delta q}{k(T_{surface} - T_\infty)} = \frac{T_{surface} - T_D}{(T_{surface} - T_\infty)D} - \frac{T_{surface} - T_\infty}{(T_{surface} - T_\infty)\frac{2}{3}\delta_t} = \left(\frac{3}{2}\frac{D}{\delta_t} - \frac{1}{2}\left(\frac{D}{\delta_t}\right)^3\right)\frac{1}{D} - \frac{1}{\frac{2}{3}\delta_t} = -\frac{1}{2}\frac{D^2}{\delta_t^3} \tag{6.11}$$

Equation (6.11) verifies that the smaller the D the more accurate the calculated convective heat transfer. The error of convective heat transfer due to D is on the order of $O(D^2)$ for this case.

- $D \geq \delta_t$

The same analysis can be conducted when D is equal to or larger than δ_t, where $T_D = T_\infty$. Then,

$$\frac{\Delta q}{k(T_{surface} - T_\infty)} = \frac{1}{D} - \frac{1}{\frac{2}{3}\delta_t} = \frac{1}{D} - \frac{3}{2\delta_t} \tag{6.12}$$

Equation (6.12) shows that the minimum error of the calculated heat flux is one-third of the analytical solution in Equation (6.5) as D equals δ_t. The convective heat transfer calculated will deviate significantly from the actual solution if the size of first grids is unreasonably large.

(2) Natural Convection

For the natural convection case, the analytical solution shows (Lienhard 1999)

$$\delta_t^4 = \frac{240(\frac{20}{21} + Pr)}{Pr^2 \frac{g\beta|T_{surface} - T_\infty|}{\nu^2}} x \tag{6.13}$$

With this equation, one can roughly estimate the scale of δ_t due to natural convection in the middle of a 3m vertical wall at 40°C and room air temperature at 25°C to be 0.024m.

The analytical solution of the convective heat transfer for natural convection is (Lienhard 1999)

$$q_{surface} = 2\frac{k(T_{surface} - T_\infty)}{\delta_t} \tag{6.14}$$

while the CFD equation for natural convection is the same as Equation (6.8) for forced convection. Therefore,

$$\frac{\Delta q}{k(T_{surface} - T_\infty)} = \frac{T_{surface} - T_D}{(T_{surface} - T_\infty)D} - \frac{2}{\delta_t} \tag{6.15}$$

- $D < \delta_t$

When D is smaller than δ_t,

$$\frac{T_{surface}-T_D}{T_{surface}-T_\infty}=1-\frac{T_D-T_\infty}{T_{surface}-T_\infty}=1-\left(1-\frac{D}{\delta_t}\right)^2 \tag{6.16}$$

$$\begin{aligned}\frac{\Delta q}{k(T_{surface}-T_\infty)}&=\frac{T_{surface}-T_D}{(T_{surface}-T_\infty)D}-\frac{2}{\delta_t}=\frac{1}{D}\left(1-\left(1-\frac{D}{\delta_t}\right)^2\right)-\frac{2}{\delta_t}\\&=\frac{1}{D}\left(\frac{2D}{\delta_t}-\frac{D^2}{\delta_t^2}\right)-\frac{2}{\delta_t}=-\frac{D}{\delta_t^2}\end{aligned} \tag{6.17}$$

Hence, the smaller the size of first grids, the better the accuracy. The error of the convective heat transfer due to the size of first grids (2D) is on the order of O(D) for natural convection.

- $D \geq \delta_t$

  Since $T_D = T_\infty$ when $D \geq \delta_t$, Equation (6.15) becomes

$$\frac{\Delta q}{k(T_{surface}-T_\infty)}=\frac{1}{D}-\frac{2}{\delta_t} \tag{6.18}$$

The equation is very similar to Equation (6.12) for forced convection, except that the analytical heat flux is different.

6.2.2 Convective Heat Transfer in Turbulent Flows

The study on laminar flows verifies that finer grid distribution provides more accurate solutions. However, most indoor airflows are turbulent. The analysis for turbulent flows is more complicated than that for laminar flow, because the accuracy of convective heat transfer predicted in turbulent flows depends on both the size of first grids and turbulence model used. This study examines the simulation accuracy by using three zero-equation turbulence models and different grid resolutions for a forced convection flow along a plate. The zero-equation turbulence models are frequently used in the CFD simulation for building design due to their simplicity and efficiency. The three zero-equation turbulence models analyzed here are:

- Constant viscosity model:

$$\nu_t = 100\nu \tag{6.19}$$

- Xu's zero-equation model (Xu 1998):

$$\nu_t = 0.03874|U_D|l \tag{6.20}$$

where l is the normal distance to the surface and U_D is the airflow speed at this location.

- Prandtl's zero-equation model (Prandtl 1926):

$$\nu_t = 2\kappa^2 y^2 \left|\frac{\partial U}{\partial y}\right| \tag{6.21}$$

where $\kappa = 0.41$ and y is the distance to the surface.

The convective heat transfer in turbulent flows is related to turbulence as defined by

$$q = -\rho C_p \left(\frac{\nu}{Pr} + \frac{\nu_t}{Pr_t}\right)\frac{\partial T}{\partial y}\bigg|_{y=0} = h(T_{surface} - T_\infty) \tag{6.22}$$

where ν_t is the turbulence eddy viscosity and T represents the Reynolds-averaged temperature. In Equation (6.22), $\nu_t >> \nu$ for the flow region away from walls, and $\nu_t << \nu$ for the near wall region, which is called viscous sub-layer. It is obvious that if the first grid is located in the viscous sub-layer, the relationship between the convective heat transfer predicted and the size of first grids is similar to that for laminar flow. The heat transfer computed does not directly depend on the turbulence model, although the turbulence model does influence the velocity and temperature profiles. According to the empirical equation (Lienhard 1999),

$$\delta_{turbulence} = 0.057[(n+1)(n+2)/n]^{0.8} Re_x^{-0.2} x \tag{6.23}$$

where n=7 for a common velocity profile in the boundary layer, $\delta_{turbulence}$ for a forced convection with a velocity 0.1m/s over a 5m long plate is

$$\delta_{turbulence} = 0.13 \text{ m} \tag{6.24}$$

and $\delta_{sub\text{-}layer} \approx 0.15\sim0.2\delta_{turbulence} = 0.02\sim0.03$m. When the velocity is increased to 1m/s, $\delta_{turbulence}$ and $\delta_{sub\text{-}layer}$ are reduced to 0.08m and 0.01~0.02m, respectively.

The empirical solution for the turbulent plate flow and heat transfer gives (Lienhard 1999)

$$Nu_x = 0.0296 Re_x^{0.8} Pr^{1/3} = h x/k \tag{6.25}$$

Considering the heat transfer in the middle of the plate with a velocity of 0.1m/s,

$$Nu_{L/2} = 0.0296 Re_{L/2}^{0.8} Pr^{1/3} = 0.0296 \times \left(\frac{0.1 \times 2.5}{1.5 \times 10^{-5}} \right)^{0.8} \times 1^{1/3} = 70.6 = hL/2k \quad (6.26)$$

As a result,

$$q_{surfce} = h(T_{surface} - T_\infty) = 28.2k(T_{surface} - T_\infty) \quad (6.27)$$

On the other hand, with the assumption of $Pr_t = Pr$, a CFD program would calculate the heat transfer as,

$$q_{CFD} = -\rho C_p \left(\frac{\nu}{Pr} + \frac{\nu_t}{Pr_t} \right) \left. \frac{\partial T}{\partial y} \right|_{y=0} = -\rho C_p \frac{\nu + \nu_t}{Pr} \frac{T_D - T_{surface}}{D} = -k \frac{\nu + \nu_t}{\nu} \frac{T_D - T_{surface}}{D} \quad (6.28)$$

- $D \geq \delta_t$

  Since $T_D = T_\infty$ when $D \geq \delta_t$,

$$\frac{\Delta q}{k(T_{surface} - T_\infty)} = \frac{q_{CFD} - q_{surface}}{k(T_{surface} - T_\infty)} = \frac{\nu + \nu_t}{\nu} \frac{1}{D} - 28.2 \quad (6.29)$$

  With constant viscosity model:

$$\frac{\Delta q}{k(T_{surface} - T_\infty)} = \frac{\nu + \nu_t}{\nu} \frac{1}{D} - 28.2 = \frac{101}{D} - 28.2 \quad (6.30)$$

  With Xu's zero-equation model:

$$\frac{\Delta q}{k(T_{surface} - T_\infty)} = \frac{\nu + \nu_t}{\nu} \frac{1}{D} - 28.2 \approx \frac{\nu_t}{\nu} \frac{1}{D} - 28.2 = 230 \quad (6.31)$$

  With Prandtl's zero-equation model:

$$\frac{\Delta q}{k(T_{surface} - T_\infty)} = \frac{\nu + \nu_t}{\nu} \frac{1}{D} - 28.2 \approx \frac{\nu_t}{\nu} \frac{1}{D} - 28.2 = 2213 \quad (6.32)$$

- $D < \delta_t$

  The temperature and velocity profiles in the boundary layer are approximated as (Lienhard 1999)

$$\frac{T - T_{surface}}{T_\infty - T_{surface}} = \frac{U}{U_\infty} = \left(\frac{y}{\delta} \right)^{1/n} \quad (6.33)$$

Hence,

$$\frac{T_D - T_{surface}}{T_\infty - T_{surface}} = \frac{U_D}{U_\infty} = \left(\frac{D}{\delta}\right)^{1/n} \tag{6.34}$$

and

$$q_{CFD} = -k\frac{\nu+\nu_t}{\nu}\frac{T_D - T_{surface}}{D} = -k\frac{\nu+\nu_t}{\nu}\frac{T_\infty - T_{surface}}{D}\left(\frac{D}{\delta}\right)^{1/n} \tag{6.35}$$

With constant viscosity model:

$$\frac{\Delta q}{k(T_{surface} - T_\infty)} = \frac{\nu+\nu_t}{\nu}\left(\frac{D}{\delta}\right)^{1/n}\frac{1}{D} - 28.2 = \frac{101}{D^{1-1/n}\delta^{1/n}} - 28.2 \tag{6.36}$$

With Xu's zero-equation model:

$$\frac{\Delta q}{k(T_{surface} - T_\infty)} = \frac{\nu+\nu_t}{\nu}\left(\frac{D}{\delta}\right)^{1/n}\frac{1}{D} - 28.2 \approx \frac{0.03874U_\infty}{\nu}\left(\frac{D}{\delta}\right)^{2/n} - 28.2 = 258\left(\frac{D}{\delta}\right)^{2/n} - 28.2 \tag{6.37}$$

With Prandtl's zero-equation model:

$$\frac{\Delta q}{k(T_{surface} - T_\infty)} = \frac{\nu+\nu_t}{\nu}\left(\frac{D}{\delta}\right)^{1/n}\frac{1}{D} - 28.2 \approx \frac{2\kappa^2 U_\infty}{\nu}\left(\frac{D}{\delta}\right)^{2/n} - 28.2 = 2241\left(\frac{D}{\delta}\right)^{2/n} - 28.2 \tag{6.38}$$

Equations (6.30)-(6.32) and (6.36)-(6.38) can be illustrated as Figure 6.3 by using the common velocity profile of n=7 and δ=0.13m. Figure 6.3 indicates that:

(1) The use of small first grid with the constant viscosity turbulence model would increase the error in predicting the heat flux. A large first grid seems better than a small one.

(2) The error in predicting the heat flux increases as the grid resolution decreases when the other two zero-equation models are used. A finer grid solution is preferred with the two zero-equation models.

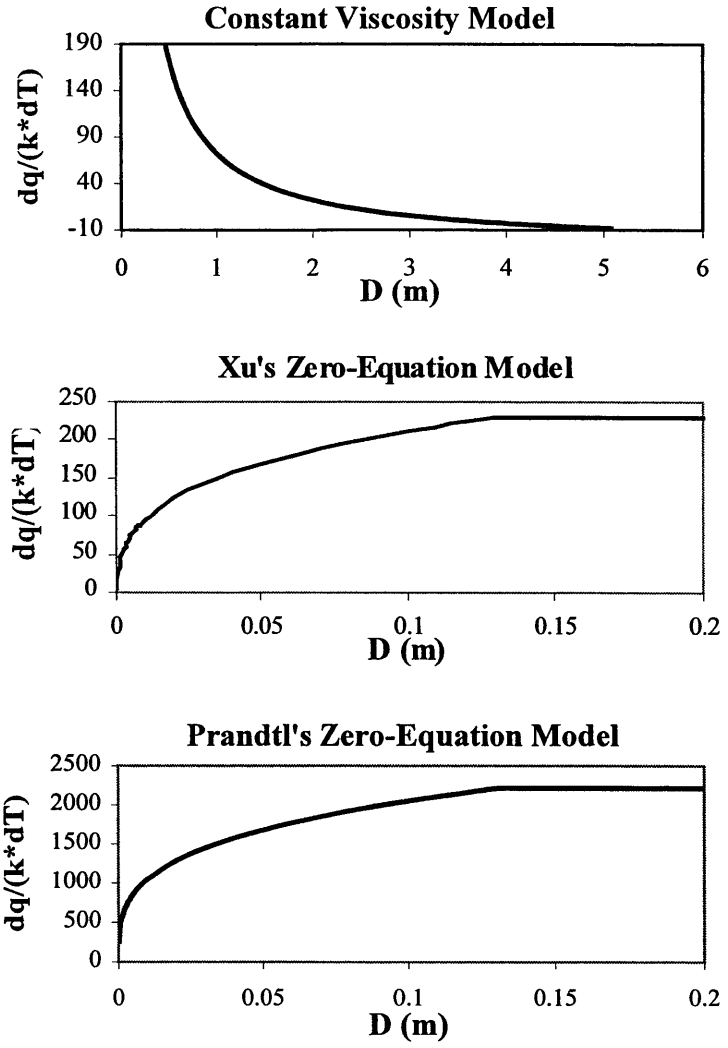

Figure 6.3 Impact of turbulence model and first grid size on the error of convective heat transfer predicted by CFD

Further analysis of Equation (6.37) indicates that $q_{CFD} = q_{surface}$ only when $D/\delta = 0.0004$. In fact, under this condition, the first grid falls into the viscous sub-layer ($\delta_{sub\text{-}layer}/\delta = 0.15\sim0.2$). In other words, the first grid should be placed in the sub-layer so as to obtain the correct heat flux. Since $\nu_t << \nu$ in the sub-layer, Equation (6.35) can be re-arranged

$$q_{CFD} = -k\frac{\nu+\nu_t}{\nu}\frac{T_\infty - T_{surface}}{D}\left(\frac{D}{\delta}\right)^{1/n} \approx -k\frac{T_\infty - T_{surface}}{D}\left(\frac{D}{\delta}\right)^{1/n} \qquad (6.39)$$

$$\frac{\Delta q}{k(T_{surface}-T_{\infty})}=\left(\frac{D}{\delta}\right)^{1/n}\frac{1}{D}-28.2 \qquad (6.40)$$

To achieve $\Delta q = 0$, D should be 0.03m if n=7 and δ=0.13m. The value is obtained based on the simple plate flow. Practical indoor airflows are more complicated. Usually, the momentum and thermal boundary layer in a room airflow are thicker than those in the plate flow. In order to verify the theoretical conclusions and identify reasonable grid sizes for room airflows, this study further investigates, numerically, the convective heat transfer in vertical and horizontal plate flows and two typical room airflows with Xu's 0-equation turbulence model.

6.3 Numerical Investigation

6.3.1 Natural Convection along a Heated, Vertical, Flat Plate

The study first simulates the natural convection along a heated vertical plate, as illustrated in Figure 6.2(b). In the simulation, the plate has a limited length of 2.5m (the same magnitude of a typical vertical wall height). The plate is maintained at constant 40°C. The investigation changes the surrounding air temperature to achieve different Rayleigh numbers. Churchill and Chu (1975) correlated the average Nusselt number for such a turbulent natural convection on a vertical wall as

$$\overline{Nu_L}=0.68+0.670(Ra_L\Psi)^{1/4}(1+1.6\times10^{-8}Ra_L\Psi)^{1/12};\ 10^9\le Ra_L\le10^{12} \qquad (6.41)$$

where $\Psi=\left[1+(0.492/Pr)^{9/16}\right]^{-16/9}$.

Figure 6.4 shows the convective heat transfer coefficients obtained by CFD using different grid systems, compared to the results from the empirical correlation. The figure exhibits that CFD can predict an acceptable solution by choosing a reasonably fine grid. The study indicates that both the coarse grid (e.g. 0.0125m) and the too-fine grid (e.g. 0.001m) will destroy the accuracy of the solution, as further demonstrated by Figure 6.5. The figure shows that the first CFD grid size around 0.005m is ideal for such a natural convection case, which is independent on the Rayleigh number. Even with the Rayleight number as high as $2.55\text{x}10^{11}$ (which is analogical to the airflow at $Re=5.05\text{x}10^5$), the first grid of 0.005m still has good performance.

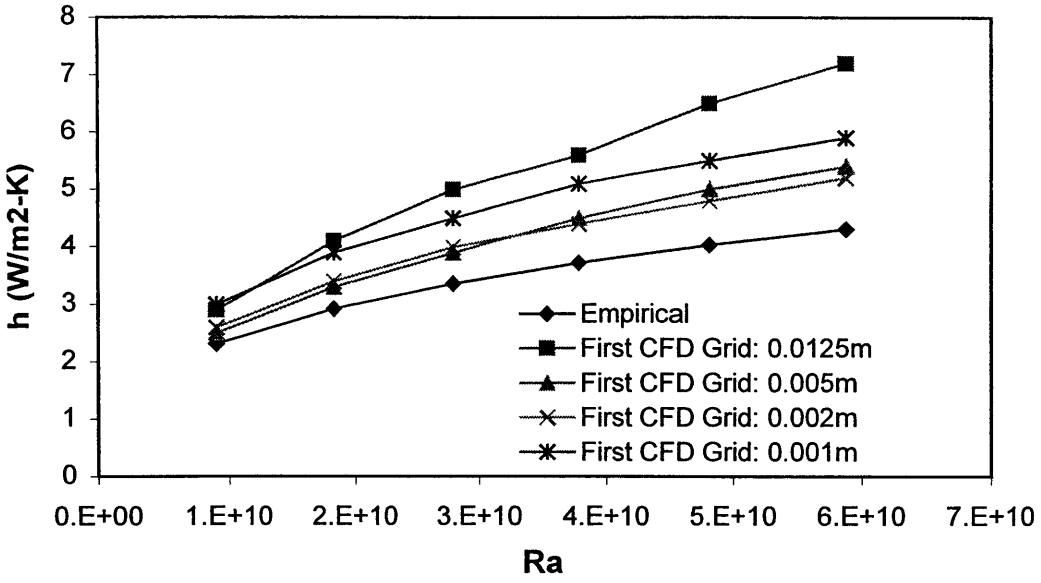

Figure 6.4 Comparison of calculated h values with different CFD grids for natural convection along a heated vertical plate

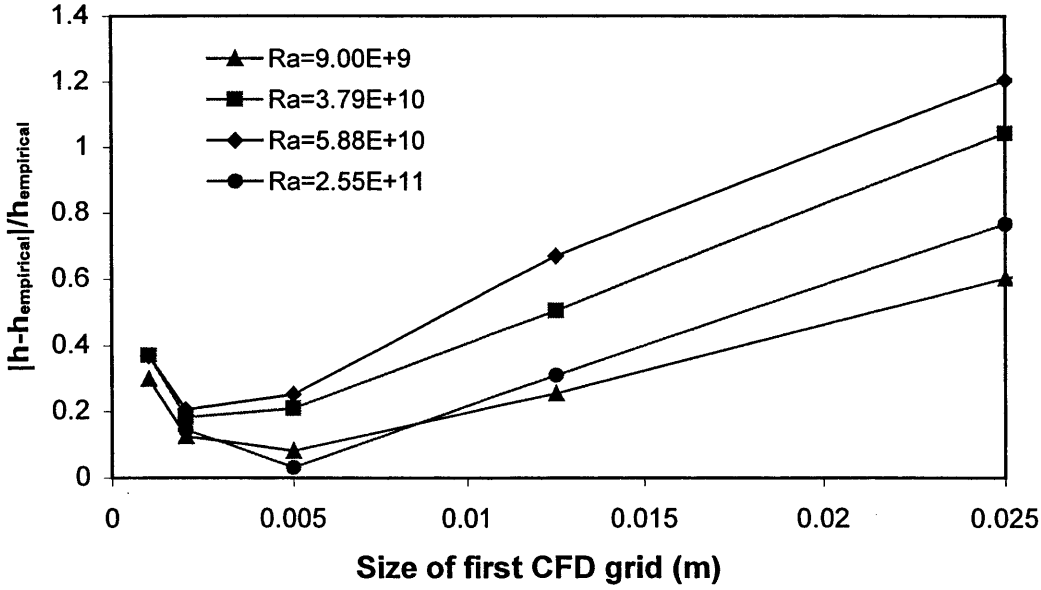

Figure 6.5 Influence of first CFD grid size on the calculation error of h value

6.3.2 Forced Convection along a Heated, Horizontal, Flat Plate

The second case this study simulates is the forced convection on a heated horizontal plate, as shown in Figure 6.2(a), which has different flow and heat transfer mechanics from the natural convection. The forced convection investigated is on a 5m long plate at the constant surface temperature of 40°C. The free airflow above the plate

has the fixed temperature of 20°C, while the flow velocity is adjustable to reach different Reynolds number. The local Nusselt number can be determined according to the classical empirical correlation (6.25).

Figure 6.6 compares the predicted h values at X=4m in CFD with those calculated based on the correlation. The CFD results agree very well with the empirical solutions as using the first grid size of 0.05m. A coarser or finer grid results in a large prediction error. The conclusion from the numerical study matches the theoretical finding that indicates that the first grid size should be around 0.06m (D=0.03m) in order to achieve a good solution. Figure 6.7 further demonstrates that the 0.05m first grid is good for such a kind of forced convection regardless of the Reynolds number (at least between $5x10^5$~$3x10^6$). In other words, a reasonable grid size is mostly determined by the form of airflow (natural or forced convection), rather that by the Rayleigh or Reynolds number.

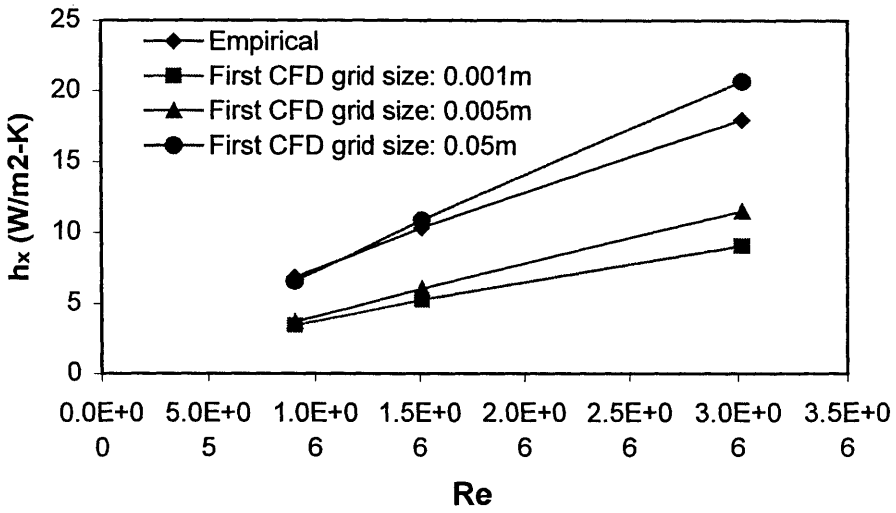

Figure 6.6 Comparison of calculated h values with different CFD grids for forced convection along a heated horizontal plate

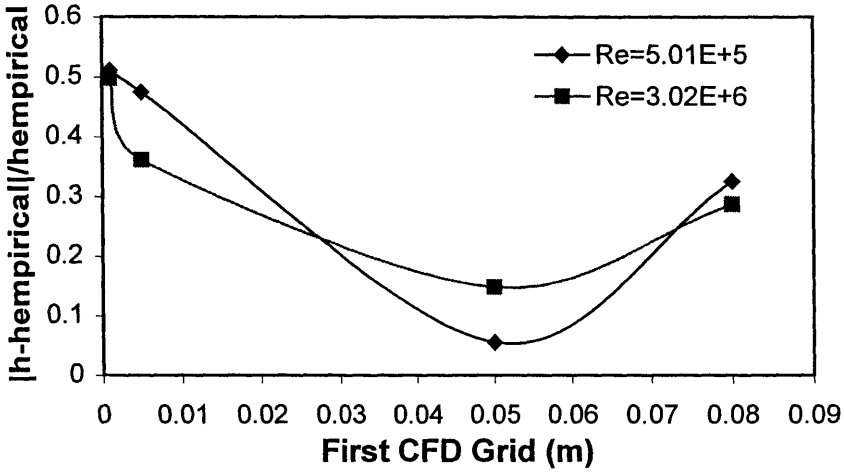

Figure 6.7 Influence of first CFD grid size on the calculation error of h_x value

6.3.3 Natural Convection in a Room with an Aspect Ratio of 2.5:7.9

In order to define a reasonable CFD grid for a real room airflow, the study further simulates the natural convection and forced convection in a more realistic room space. The natural convection case tested is the experiment conducted by Olson et al (1990). Olson experimentally studied the natural convection in both a full-scale room and a 1:5.5 small-scale physical model containing R114 gas. Figure 6.8 shows the configuration of the full-scale room with the opposing hot and cold side walls. The small-scale model was geometrically similar, had the same Reyleigh number, and had the same dimensionless side wall temperature as the full-scale room. The experiment found good agreement between the full-scale room and the scale model in flow patterns, velocity levels, temperature distributions, and heat transfer. This study is particularly interested in the convective heat transfer at the hot and cold walls and compares both experimental results with the simulated results.

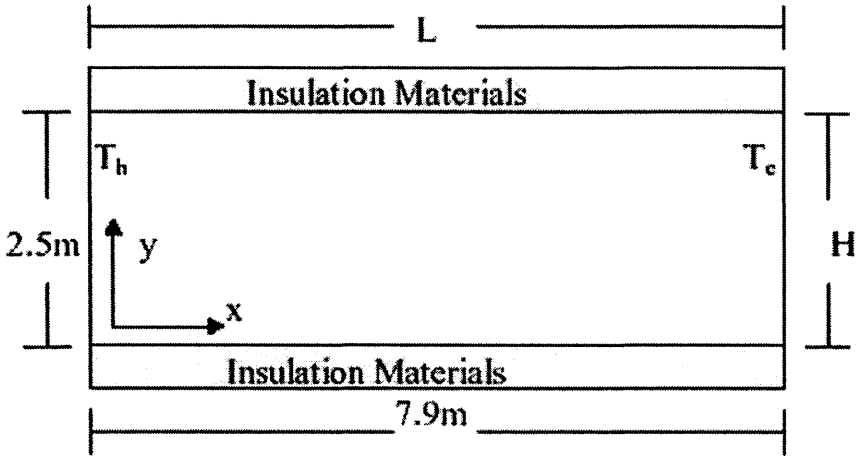

Figure 6.8 Configuration of the experiment (Olson et al., 1990)

Figure 6.9 presents the convective heat transfer at the hot and cold walls for both the measurement and simulation as Nusselt number as a function of Reyleigh number. Also included is the correlation from Bohn et al. (1984), $Nu=0.31Ra^{1/4}$, for enclosure flows. The Nu and Ra number are based on the temperature difference between the hot and cold walls. The experimental uncertainty is approximately 10 percent for the scale model and 30 percent for the full scale. The results show that the simulations with the first grid size of 0.002-0.005m agree very well with the measurement, exhibiting the expected trend of the increasing Nu with increasing Ra. Figure 6.10 further demonstrates the effect of the first grid size on the heat transfer calculation. It appears that a first grid size at 0.005m is good for the indoor natural convection cases, which is the same as the conclusion from the plate natural convection study.

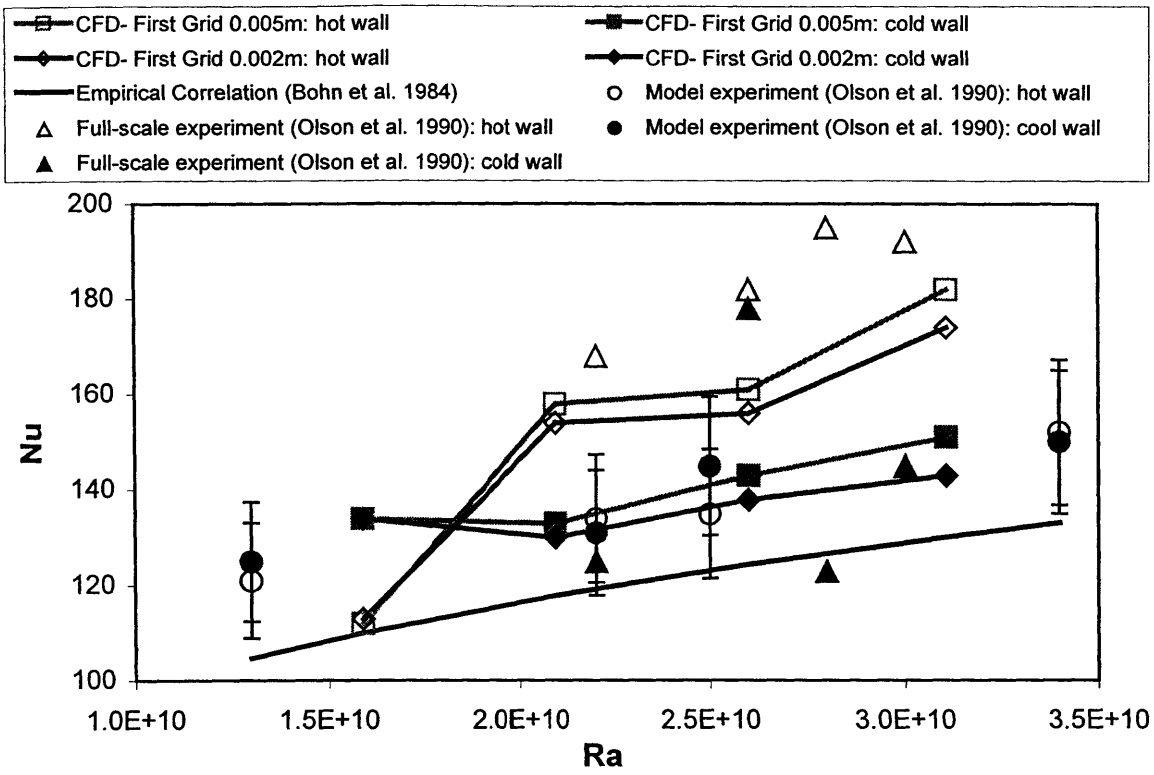

Figure 6.9 Comparison of simulated heat transfer at enclosures with the measurement

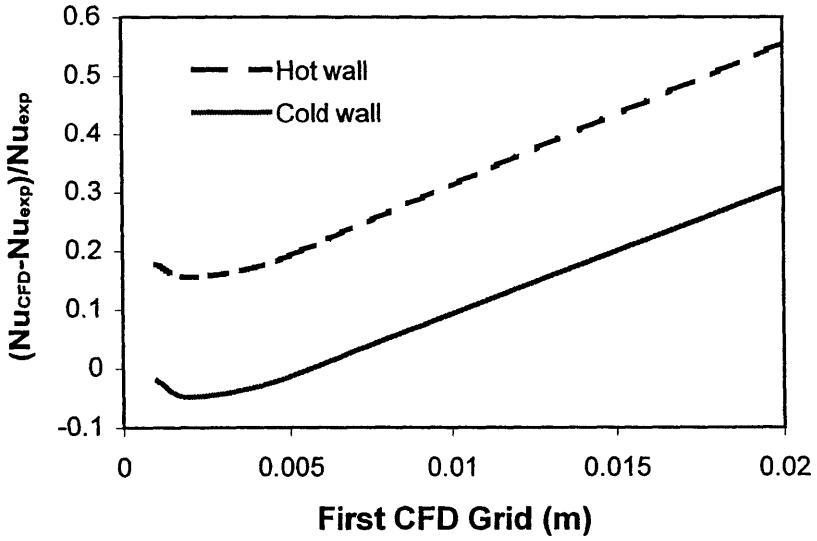

Figure 6.10 Influence of first CFD grid size on the calculation of Nu at $Ra=2.6\times10^{10}$

6.3.4 Three-Dimensional Airflow in a Room with Mixing Ventilation

The study further investigates the forced convection in the Fisher's experimental chamber (1995) with the side-wall jet, with the focus on the influence of first grid size on the heat flux calculation at enclosures. The configuration of the experimental facility was shown in Figure 4.8. The simulation uses three different grid densities: the fine grid has the first grid size at 0.05m; the moderate grid has the first grid at 0.1m; and the coarse grid has the first grid at 0.2m. The area-averaged heat fluxes at enclosures are then calculated and compared with the measurement, as shown in Figure 6.11.

The results show that the simulation with the first grid size at 0.05-0.1m can provide reasonable solutions for such a forced convection room airflow. The same conclusion was found in the simulation experience from the literatures (e.g. Chen 1988) that indicates the first grid size at 0.1m is a good value for most indoor airflows.

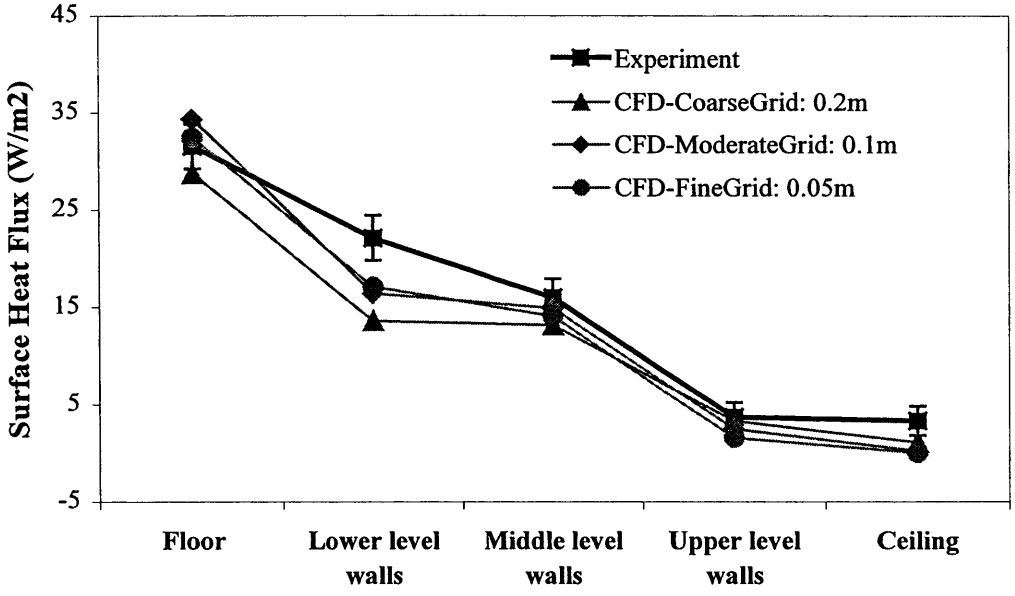

Figure 6.11 Comparison of simulated heat flux at enclosures with the measurement

6.4 Summary

The chapter discusses the proper calculation method of convective heat transfer at enclosures, which is the key linkage between ES and CFD. The investigation indicates that the heat transfer through the first CFD grid cell near a surface should be used in a coupled simulation. This convective heat, although grid-dependent, represents the actual heat input into the indoor air domain of CFD. The study analyzes the effect of the size of the first CFD grid and turbulence model on surface convective heat transfer. The analysis indicates that a finer grid in CFD does not always lead to a more accurate solution when using zero-equation turbulence models. Based on the theoretical analysis and numerical

experimentation, this study recommends a universal first grid size of 0.005m for natural convection airflows and 0.1m for forced convection indoor airflows.

CHAPTER 7

SOLUTION CHARACTERISTICS OF ITERATIVE COUPLING OF ENERGY SIMULATION AND CFD PROGRAMS

This chapter discusses the solution characteristics of iterative coupling between energy simulation (ES) and CFD programs. Through theoretical analysis and numerical experimentation, the chapter addresses the concerns about the solution existence and uniqueness of the coupled simulation and the convergence and stability performance of different iterative coupling methods. The chapter also investigates the influences of primary simulation parameters, such as simulation convergence criteria, on the coupling. Finally, an improved iteration and control algorithm for the coupled simulation has been developed.

7.1 Problem Statement

In a coupled simulation, the ES and CFD programs couple to each other by providing complementary boundary information. Iteration may be required during each coupling step to exchange the inter-related boundary conditions and reach mutually consistent results between ES and CFD. However, due to the different mathematical models and numerical methods employed in ES and CFD, solution existence and uniqueness as well as convergence and stability of the iterative procedure are always major concerns.

As presented in Chapter 5, the program coupling of ES and CFD is equivalent to a "separate" conjugate heat transfer method, where ES handles the heat transfer in building envelope while CFD simulates the indoor airflow. The conjugate heat transfer method simultaneously solves the assembled equation group that includes all the energy balance equations for enclosures and indoor air. The program coupling method iteratively solves two separate energy equation groups (one for enclosures in ES and another for indoor air in CFD). It is well known that the conjugate heat transfer method generally has a converged and stable solution although it is computationally demanding. The question is whether the iterative solution of separate equation groups can provide the same results as that of the assembled equation group from the conjugate heat transfer approach. Furthermore, since different data coupling methods between ES and CFD are available, it is unknown whether each of the methods has the same performance or one method is superior to the others. This chapter will discuss these problems through theoretical analysis and numerical experimentation.

7.2 Theoretical Analysis

7.2.1 Solution Existence and Uniqueness of ES-CFD Program Coupling

(1) Clarke's verification

Clarke et al. (1995 a, b) investigated the integration of the network nodal airflow model and CFD model. The study indicated that the coupling of network flow model and CFD can be satisfactorily achieved by maintaining separate solution algorithm of each method. The connection between the two approaches is made within regions that each approach considers as its boundary condition. The overall system balance is then achieved through an iterative procedure. These conclusions are applicable to the ES and CFD coupling since ES also uses nodal model.

The following gives a brief explanation of how the assembled equation group for both ES and CFD calculations can be separated into two sub-matrix equations, using Clarke's analysis method. Figure 7.1 shows an empty, two-dimensional room. A, B, C, D are the four enclosures surrounding the indoor space, with "e" representing exterior surfaces and "i" representing interior surfaces. The indoor space is divided into four cells in CFD.

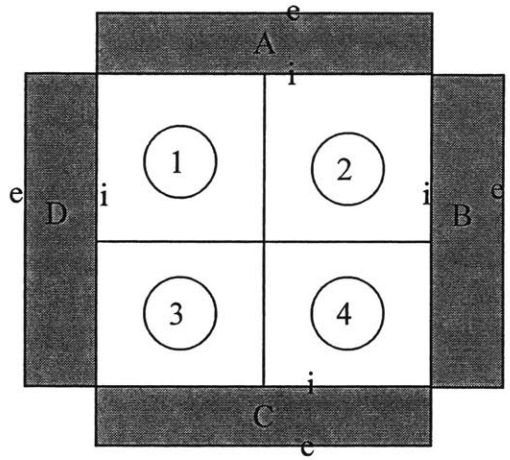

Figure 7.1 Illustration of an empty, two-dimensional room for ES-CFD coupling

Considering the energy balance on each component in Figure 7.1, one can obtain the super energy balance equation group (7.1), which includes all ES and CFD energy equations. Equation (7.1) can be written as **AT=B**, where **A**, **T**, and **B** are tensor/vector matrices.

Due to the sparse character of matrix **A**, the numerical techniques developed by Clarke and Tang (1990) and Duff et al. (1986) can be used to "condense" matrix **A** into the form in Eq. (7.2) (the detailed process can be found in the references). Here, the upper left part of **A** represents the energy balances in ES and the lower right part

represents the energy balances in CFD. The connection between ES and CFD has been transferred into the coefficients of the new matrix **A** and **B** in Eq. (7.2). Therefore, the independent solutions of sub-matrix equations in computational tandem are identical to the simultaneous solution of super-matrix equation including all ES and CFD equations. In other words, the "separate" conjugate heat transfer method can produce the same solution as the conjugate heat transfer method.

$$\begin{bmatrix}
a_{1,1} & a_{1,2} & & & & & & & & & & & \\
a_{2,1} & a_{2,2} & & a_{2,4} & & a_{2,6} & & a_{2,8} & a_{2,9} & a_{2,10} & & & \\
 & & a_{3,3} & a_{3,4} & & & & & & & & & \\
 & a_{4,2} & a_{4,3} & a_{4,4} & & a_{4,6} & & a_{4,8} & & a_{4,10} & & a_{4,12} & \\
 & & & & a_{5,5} & a_{5,6} & & & & & & & \\
 & a_{6,2} & & a_{6,4} & a_{6,5} & a_{6,6} & & a_{6,8} & & & a_{6,11} & a_{6,12} & \\
 & & & & & & a_{7,7} & a_{7,8} & & & & & \\
 & a_{8,2} & & a_{8,4} & & a_{8,6} & a_{8,7} & a_{8,8} & a_{8,9} & & a_{8,11} & & \\
 & a_{9,2} & & & & & & a_{9,8} & a_{9,9} & a_{9,10} & a_{9,11} & & \\
 & a_{10,2} & & a_{10,4} & & & & & a_{10,9} & a_{10,10} & & a_{10,12} & \\
 & & & & & a_{11,6} & & a_{11,8} & a_{11,9} & & a_{11,11} & a_{11,12} & \\
 & & & a_{12,4} & & a_{12,6} & & & & a_{12,10} & a_{12,11} & a_{12,12} &
\end{bmatrix}
\begin{bmatrix} T_{e,A} \\ T_{i,A} \\ T_{e,B} \\ T_{i,B} \\ T_{e,C} \\ T_{i,C} \\ T_{e,D} \\ T_{i,D} \\ T_{(1)} \\ T_{(2)} \\ T_{(3)} \\ T_{(4)} \end{bmatrix}
=
\begin{bmatrix} b_{e,A} \\ b_{i,A} \\ b_{e,B} \\ b_{i,B} \\ b_{e,C} \\ b_{i,C} \\ b_{e,D} \\ b_{i,D} \\ b_{(1)} \\ b_{(2)} \\ b_{(3)} \\ b_{(4)} \end{bmatrix}
\tag{7.1}$$

$$\begin{bmatrix}
a_{1,1} & a_{1,2} & a_{1,3} & a_{1,4} & a_{1,5} & a_{1,6} & a_{1,7} & a_{1,8} & & & & \\
a_{2,1} & a_{2,2} & a_{2,3} & a_{2,4} & a_{2,5} & a_{2,6} & a_{2,7} & a_{2,8} & & & & \\
a_{3,1} & a_{3,2} & a_{3,3} & a_{3,4} & a_{3,5} & a_{3,6} & a_{3,7} & a_{3,8} & & & & \\
a_{4,1} & a_{4,2} & a_{4,3} & a_{4,4} & a_{4,5} & a_{4,6} & a_{4,7} & a_{4,8} & & & & \\
a_{5,1} & a_{5,2} & a_{5,3} & a_{5,4} & a_{5,5} & a_{5,6} & a_{5,7} & a_{5,8} & & & & \\
a_{6,1} & a_{6,2} & a_{6,3} & a_{6,4} & a_{6,5} & a_{6,6} & a_{6,7} & a_{6,8} & & & & \\
a_{7,1} & a_{7,2} & a_{7,3} & a_{7,4} & a_{7,5} & a_{7,6} & a_{7,7} & a_{7,8} & & & & \\
a_{8,1} & a_{8,2} & a_{8,3} & a_{8,4} & a_{8,5} & a_{8,6} & a_{8,7} & a_{8,8} & & & & \\
 & & & & & & & & a_{9,9} & a_{9,10} & a_{9,11} & a_{9,12} \\
 & & & & & & & & a_{10,9} & a_{10,10} & a_{10,11} & a_{10,12} \\
 & & & & & & & & a_{11,9} & a_{11,10} & a_{11,11} & a_{11,12} \\
 & & & & & & & & a_{12,9} & a_{12,10} & a_{12,11} & a_{12,12}
\end{bmatrix}
\begin{bmatrix} T_{e,A} \\ T_{i,A} \\ T_{e,B} \\ T_{i,B} \\ T_{e,C} \\ T_{i,C} \\ T_{e,D} \\ T_{i,D} \\ T_{(1)} \\ T_{(2)} \\ T_{(3)} \\ T_{(4)} \end{bmatrix}
=
\begin{bmatrix} b'_{e,A} \\ b'_{i,A} \\ b'_{e,B} \\ b'_{i,B} \\ b'_{e,C} \\ b'_{i,C} \\ b'_{e,D} \\ b'_{i,D} \\ b'_{(1)} \\ b'_{(2)} \\ b'_{(3)} \\ b'_{(4)} \end{bmatrix}
\tag{7.2}$$

(2) Klems's verification

Klems (1999) studied the solutions of ES-CFD coupling simulation in a more mathematical manner. As explained previously, the substantial coupling of ES and CFD is between the envelope energy balance of ES and the indoor air energy balance of CFD. Both the energy balances are represented by non-linear equations. The intersection of the hyperplanes represented by these two sets of equations is the solution of coupled calculation. To verify whether there is an "intersection" between ES and CFD and to show how different iteration routes may influence the convergence, it is important to

identify the $Q_{convection}$ and $T_{surface}$ relationship in the ES and CFD energy equations. $Q_{convection}$ and $T_{surface}$ are the interior surface convective heat flux and surface temperature, which explicitly link ES and CFD.

Klems mathematically studied the ES and CFD equations, both of which can be written as $Q_{convection}=f(T_{surface})$. Klems analyzed the slopes of $Q_{convection}=f(T_{surface})$ for both ES and CFD, and then determined the possibility of the intersection of these two equations. With elaborate assumptions and mathematical deductions to handle the highly non-linear equation systems, Klems verified that the $Q_{convection}$-$T_{surface}$ curve for CFD probably has a positive slope and may be either concave upward or downward, while the curve for ES has a negative slope if all of the phenomenological convective coefficients are positive. Otherwise, the curve for ES may have positive slope depending on the dynamics of the particular situation. The shapes of the $Q_{convection}$-$T_{surface}$ curves imply that the intersection of CFD and ES curves is possible, which intimates the existence of a coupled solution between ES and CFD programs.

(3) Verification by this study

This study attempts to address and demonstrate the possibility of "intersection" between ES and CFD, in another manner.

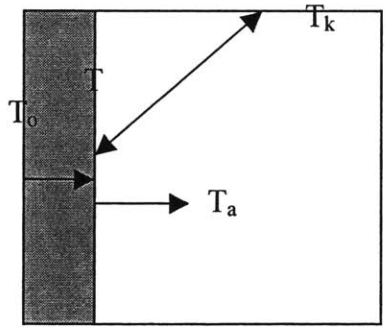

Figure 7.2 Illustration of a typical room and wall

Considering the heat transfer on one interior surface in terms of conduction, convection and radiation, and ignoring the radiative heat flux from internal heat sources and solar radiation, as shown in Figure 7.2, one has in ES:

$$\sum h_{k,r}(T-T_k)+h_c(T-T_a)=\frac{K}{L}(T_o-T) \tag{7.3}$$

$$(\sum h_{k,r}+h_c+\frac{K}{L})T=\sum h_{k,r}T_k+h_cT_a+\frac{K}{L}T_o \tag{7.4}$$

$$T = \frac{\sum h_{k,r} T_k + h_c T_a + \frac{K}{L} T_o}{\sum h_{k,r} + h_c + \frac{K}{L}} = \frac{h_c}{\sum h_{k,r} + h_c + \frac{K}{L}} T_a + \frac{\sum h_{k,r} T_k + \frac{K}{L} T_o}{\sum h_{k,r} + h_c + \frac{K}{L}} \quad (7.5)$$

where,

T	interior surface temperature of the surface concerned
T_k	other interior surface temperature
T_a	indoor air temperature close to the surface concerned
T_o	exterior surface temperature of the surface concerned
h_c	interior convective heat transfer coefficient of the surface concerned
$h_{k,r}$	radiative heat transfer coefficient between surface k and the surface
K	conductivity of the enclosure concerned
L	thickness of the enclosure concerned

For simplicity, the analysis assumes: (1) all the coefficients are constant; (2) $h_{k,r}$ and K are greater than zero; and (3) T_k and T_o are independent variables. Then it comes

$$\frac{\partial T}{\partial T_a} = \frac{h_c}{\sum h_{k,r} + h_c + \frac{K}{L}} = \begin{Bmatrix} (0,1) & h_c > 0 \\ 0 & h_c = 0 \\ \text{else} & h_c < 0 \end{Bmatrix} \quad (7.6)$$

or

$$\frac{\partial T_a}{\partial T} = \frac{\sum h_{k,r} + h_c + \frac{K}{L}}{h_c} = \begin{Bmatrix} >1 & h_c > 0 \\ \infty & h_c = 0 \\ <1 & h_c < 0 \end{Bmatrix} \quad (7.7)$$

Therefore

$$\frac{\partial q_c}{\partial T} = \frac{\partial [h_c (T - T_a)]}{\partial T} = \frac{\partial h_c}{\partial T}(T - T_a) + h_c \frac{\partial (T - T_a)}{\partial T} = h_c \left(1 - \frac{\partial T_a}{\partial T}\right) = \begin{Bmatrix} <0 & h_c > 0 \\ 0 & h_c = 0 \\ <0 & h_c < 0 \end{Bmatrix} \quad (7.8)$$

The situation with $h_c<0$ in this analysis is possible although rare, because $h_c=q_c/(T-T_a)$ and the value of T_a may change with location. A typical example is a space with displacement ventilation, where the near-floor air temperature may be lower than the floor temperature while the upper air temperature may be higher.

Equation (7.8) can be understood in physics. Table 7.1 shows the phenomenal changes of conductive, convective and radiative heat with the interior surface temperature T, if all other conditions are fixed as assumed in the analysis above. For example, in the

summer, assuming the exterior surface temperature T_o is larger than the interior surface temperature T and other interior surface temperatures T_k are smaller than T, when T increases, the temperature gradient over the wall is decreased. Therefore, the conductive heat through the wall is reduced. On the other hand, the radiative heat is increased because of the larger gradient between this surface temperature and others. As a result, the convective heat from the surface $q_{conv} = q_{cond} - q_{rad}$ is decreased, which fits the expression of Eq. (7.8). The same results can be obtained by assuming $T_o<T$ or $T_k>T$.

Table 7.1 Changes of $Q_{conduction}$, $Q_{radiation}$ and $Q_{convection}$ with interior surface temperature T

	T	Q_{cond}	Q_{rad}	Q_{conv} ($=Q_{cond}- Q_{rad}$)		T	$-Q_{cond}$	$-Q_{rad}$	$-Q_{conv}$ ($=-Q_{cond}+ Q_{rad}$)
Summer	↑	↓	↑	↓	Winter	↑	↑	↓	↑
	↓	↑	↓	↑		↓	↓	↑	↓

CFD, on the other hand, focuses on the energy balance of indoor air, with the interior surfaces as the boundaries of the space. If the thermal behaviors of other enclosures are fixed, one could physically find that:

- For cooling situation, the increase of the interior surface temperature T of the surface questioned will increase the convective heat gain q_c (positive) and the air temperature T_a close to the surface.
- For the heating situation, the decrease of T will increase the convective heat loss q_c (negative) and decrease the air temperature T_a close to the wall.

This means, $\frac{\partial q_c}{\partial T} > 0$ and $\frac{\partial T_a}{\partial T} > 0$. Therefore, with a constant h_c,

$$\frac{\partial q_c}{\partial T} = \frac{\partial [h_c (T - T_a)]}{\partial T} = \frac{\partial h_c}{\partial T}(T - T_a) + h_c \frac{\partial (T - T_a)}{\partial T} = h_c (1 - \frac{\partial T_a}{\partial T}) > 0 \qquad (7.9)$$

It can be further expressed as

$$1 > \frac{\partial T_a}{\partial T} > 0 \quad \text{when} \quad h_c > 0 \qquad (7.10a)$$

$$\frac{\partial T_a}{\partial T} > 1 \quad \text{when} \quad h_c < 0 \qquad (7.10b)$$

Klems (1999) defines the condition $\frac{\partial T_a}{\partial T} > 1$ as a super-linear response of the CFD calculation. That is, the change in air temperature caused by the change in surface temperature is larger than the original surface temperature change. Such a response cannot be excluded, although it is uncommon. The q_c-T curve slopes from this analysis

(Eqs. (7.8) and (7.9)) are partly coincident with those from the verification by Klems. With these slopes of the T_a-T and q_c-T curves, the positive intersection between ES and CFD models becomes possible, as shown in Figures 7.3 and 7.4, although the curves are not necessarily straight.

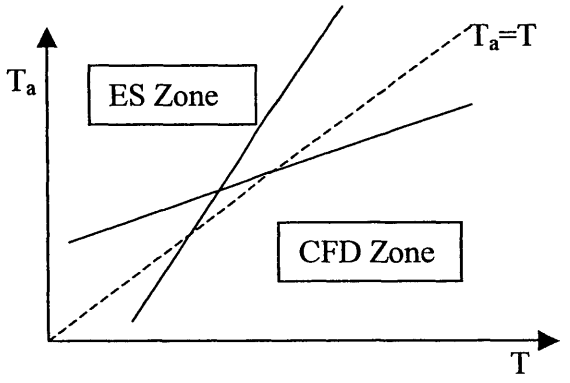

(a) h>0

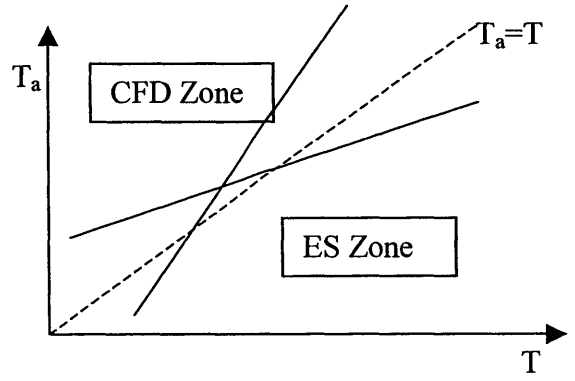

(a) h<0

Figure 7.3 T_a-T curve of ES and CFD

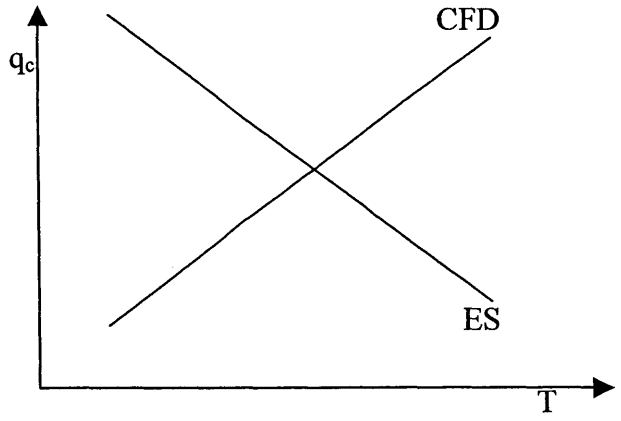

Figure 7.4 q_c-T curve of ES and CFD

The next question is whether there are multiple intersections (solutions) for the ES and CFD coupling. If there were multiple intersections, Figure 7.5 illustrates two possible scenarios with positive h values (similar analysis can be offered for the scenarios with negative h values). Since the T_a-T slope for CFD at $h_c>0$ is between 0 and 1 while that for ES is larger than 1, the scenario shown in Figure 7.5(a) is impossible because the slope around point 2 does not satisfy the slope requirement. The scenario shown in Figure 7.5(b) is also impossible because one specific surface temperature T in CFD can have only one corresponding T_a for a given situation (including given numerical models and techniques). The same applies to ES. Therefore, there is one and only one solution for ES and CFD coupling.

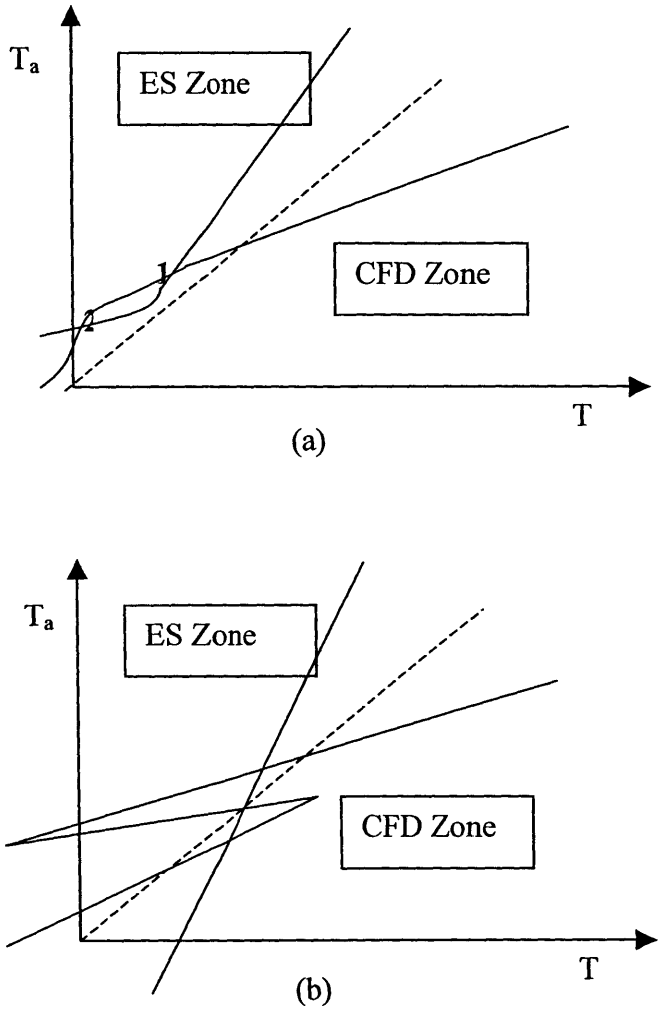

Figure 7.5 Assumed multiple intersections between T_a-T curves of ES and CFD (h>0)

In reality, the convective heat transfer coefficients and other thermal conditions may change over time, and the system is non-linear in nature. The theoretical analysis for this non-linear system is almost impossible. Although the above analysis assumed constant coefficients and fixed other conditions, the study is rather valuable because:

(1) the analysis provides essential understanding of the ES-CFD coupling and the potential solutions;
(2) the coefficients in most real cases usually do not change dramatically with time and environmental conditions;
(3) the assumption of constant coefficients is used in a number of simulation tools.

7.2.2 Convergence and Stability of Iterative ES-CFD Coupling

7.2.2.1 Inherent Relationships of Various Coupling Methods

The previous section demonstrates that the solution of a coupled simulation does exist and is unique. The prime connection between ES and CFD is the convective heat transfer on building envelope. The implementation method of this connection can be multiple, as first introduced in Chapter 5:

- coupling method-1: ES to CFD by T_i; CFD to ES by $h_{i,conv}$ and $\Delta T_{i,air}$;
- coupling method-2: ES to CFD by T_i; CFD to ES by $h_{i,conv\text{-}nominal}$;
- coupling method-3: ES to CFD by T_i; CFD to ES by $Q_{i,conv}$;
- coupling method-4: ES to CFD by $Q_{i,conv}$; CFD to ES by $h_{i,conv}$ and $\Delta T_{i,air}$;
- coupling method-5: ES to CFD by $Q_{i,conv}$; CFD to ES by $h_{i,conv\text{-}nominal}$;
- coupling method-6: ES to CFD by $Q_{i,conv}$; CFD to ES by $Q_{i,conv}$.

Chapter 5 indicates that not all the coupling methods are feasible; for example, coupling method-6 is obviously not workable. This section will discuss the feasibility of the other potential coupling methods and their inherent relationships. Since coupling method-2 and -5 are substantially equivalent to coupling method-1 and -4, respectively, this study focuses on the investigation of the inherent relationships among coupling methods-1, -3 and -4. The following discussion still assumes constant convective heat transfer coefficient h for simplicity.

In a coupled simulation, CFD replaces the ES zone air energy balance equation to connect with the ES envelope energy balance equation. Iteratively solving these two sets of equations provides the envelope thermal conditions (heat flux and temperature) and indoor air temperature distribution. The envelope energy balance equation of ES can be expressed in tensor form:

$$\mathbf{AT=B+Q} \tag{7.11}$$

where **T** is the unknown interior surface temperature vector, **A** and **B** are coefficient matrices. **Q** is the unknown interior surface heat convection vector, which can be obtained in CFD with the non-linear energy equations for indoor air

$$\mathbf{Q}=f(\mathbf{T}) \tag{7.12}$$

Iteratively solving Eqs. (7.11) and (7.12) provides the surface temperature **T** and heat flux **Q**, as promised by the above solution existence analysis. This is the basic route of coupling method-3.

Since $\mathbf{Q} = h(\mathbf{T}-\mathbf{T_a})$, where $\mathbf{T_a}$ is the air temperature close to the surface, substitute it to (7.11)

$$\mathbf{AT}=\mathbf{B}+h\mathbf{T}-h\mathbf{T_a} \tag{7.13}$$

Rearrange it to be

$$(\mathbf{A}-h)\mathbf{T}=\mathbf{B}-h\mathbf{T_a} \tag{7.14}$$

In CFD

$$\mathbf{Q}=f(\mathbf{T})=h(\mathbf{T}-\mathbf{T_a}) \tag{7.15}$$
$$\mathbf{T_a}=\mathbf{T}-f(\mathbf{T})/h=g(\mathbf{T}) \tag{7.16}$$

(7.14) and (7.16) are the equation group about unknown variables **T** and $\mathbf{T_a}$. They are derived from Eqs. (7.11) and (7.12) and therefore exactly the same as (7.11) and (7.12) but in different forms. The solutions of (7.14) and (7.16) are surface temperature and the air temperature close to the surface. This is coupling method-1. Method-1, therefore, is mathematically equivalent to method-3.

In coupling method-4, **Q**, rather than **T**, is transferred from ES to CFD as boundary conditions, therefore in CFD

$$\mathbf{T_a}=f(\mathbf{Q})=g(\mathbf{T}-\mathbf{T_a}) \tag{7.17}$$

And Eq. (7.13) can be rewritten as

$$\mathbf{AT}-\mathbf{AT_a}+\mathbf{AT_a}=\mathbf{B}+h\mathbf{T}-h\mathbf{T_a} \tag{7.18}$$
$$(\mathbf{A}-h)(\mathbf{T}-\mathbf{T_a})=\mathbf{B}-\mathbf{AT_a} \tag{7.19}$$

(7.17) and (7.19) form the equation group for unknown variable $\mathbf{T}-\mathbf{T_a}$ and $\mathbf{T_a}$. They are again identical to Eqs. (7.12) and (7.11) because of the straightforward derivation. Iteration of $\mathbf{T}-\mathbf{T_a}$ and $\mathbf{T_a}$ between (7.17) and (7.19) can thus achieve the same results as method-1.

Therefore, coupling methods-1, -3 and -4, in fact, represent three different expressions of one original equation group. They are identical mathematically, and thus theoretically can produce the same solutions with the same set of boundary conditions (climate, geometry, etc...).

7.2.2.2 Numerical Convergence and Stability of the Coupling

The study so far verifies the solution existence and uniqueness of a coupled simulation using different data coupling methods. However, an improper numerical process may lead to wrong or no solution, even if the solution does exist physically and mathematically. This section thus will discuss the numerical convergence and stability performance of the coupling methods, with the focus on coupling methods-1 and -3 due to their representative nature. The discussion continues to use the constant h assumption.

Rewrite energy equations (7.14) and (7.16) for method-1

$$\mathbf{T}=f(\mathbf{T}_a) \quad \text{(ES)} \tag{7.20}$$
$$\mathbf{T}_a=g(\mathbf{T}) \quad \text{(CFD)} \tag{7.21}$$

The slopes for these two equations are indicated in Eqs. (7.6), (7.7), (7.10) and as illustrated in Figure 7.6. The figure shows that a typical numerical process of method-1 will always lead to a converged point for h>0. However, if h<0, the situation becomes more complicated, as shown in Figure 7.7. Only if

$$\left|\frac{\partial T_a}{\partial T}\right|_{ES} > \left|\frac{\partial T_a}{\partial T}\right|_{CFD} \tag{7.22}$$

the coupling may have a converged solution. In fact, this is also the condition always satisfied by the case with h>0.

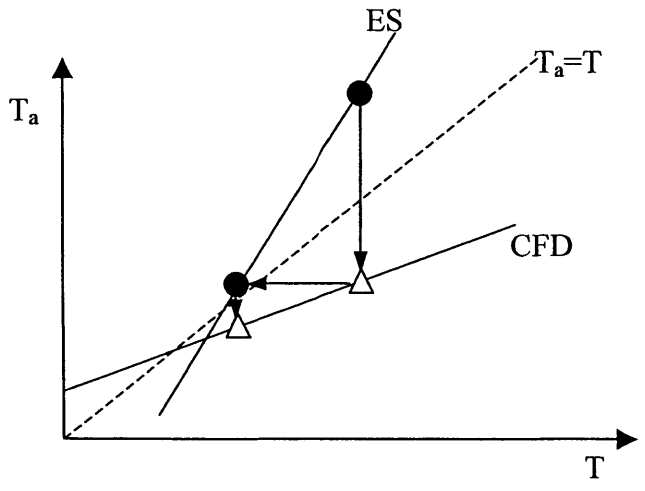

Figure 7.6 Converged iteration process of coupling ES with CFD in T_a-T plot (h>0) (ES provides T to CFD as boundary conditions, and then CFD returns a new T_a to ES. The process repeats and a converged point can be reached finally.)

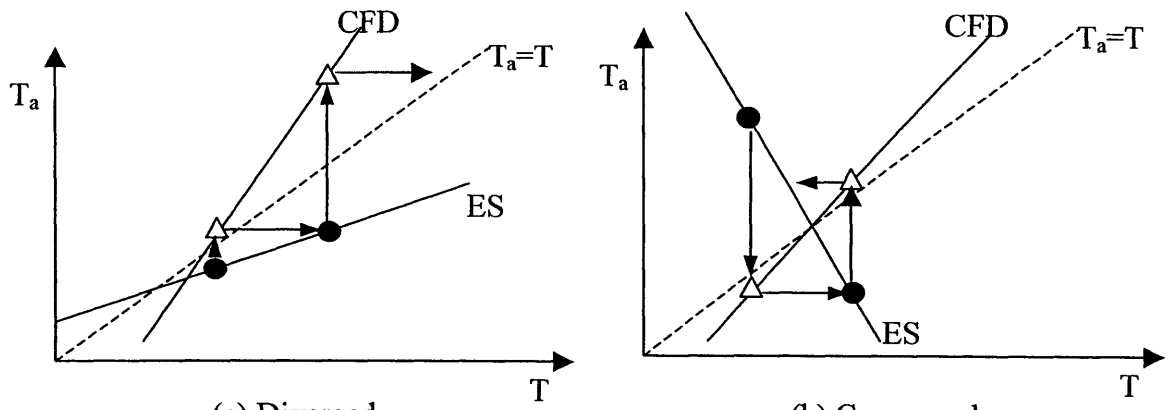

Figure 7.7 Iteration process of coupling ES and CFD in T_a-T plot (h<0)
(ES provides T to CFD as boundary conditions, and then CFD returns a new T_a to ES.)

A similar analysis can be conducted for method-3. The ES and CFD equations for method-3 are

$$\mathbf{T}=f(\mathbf{Q}) \quad \text{(ES)} \tag{7.23}$$
$$\mathbf{Q}=g(\mathbf{T}) \quad \text{(CFD)} \tag{7.24}$$

Equations (7.8) and (7.9) indicate that the slope of Q-T curve in Eq. (7.23) for ES is negative while that of Eq. (7.24) for CFD is positive, regardless of the h value. Figure 7.8 illustrates a typical iteration of Q and T between Eqs. (7.23) and (7.24). A converged solution of the coupling can be obtained if

$$\left|\frac{\partial Q}{\partial T}\right|_{ES} > \left|\frac{\partial Q}{\partial T}\right|_{CFD} \tag{7.25}$$

Otherwise, the iteration may lead to divergence.

Equation (7.25) can be further written as

$$\left.\frac{\partial T_a}{\partial T}\right|_{ES} > 2 - \left.\frac{\partial T_a}{\partial T}\right|_{CFD} > 1, \text{ when } h>0 \tag{7.26}$$

$$\left.\frac{\partial T_a}{\partial T}\right|_{ES} < 2 - \left.\frac{\partial T_a}{\partial T}\right|_{CFD} < 1, \text{ when } h<0 \tag{7.27}$$

If the case simulated satisfies Eqs. (7.26) and (7.27), the iteration with method-3 may converge to a solution. The iteration with method-1, however, will always unconditionally converge when h>0, and it can converge when h<0 and

$$\left|\frac{\partial T_a}{\partial T}\right|_{ES} > \frac{\partial T_a}{\partial T}_{CFD} > 1 \qquad (7.28)$$

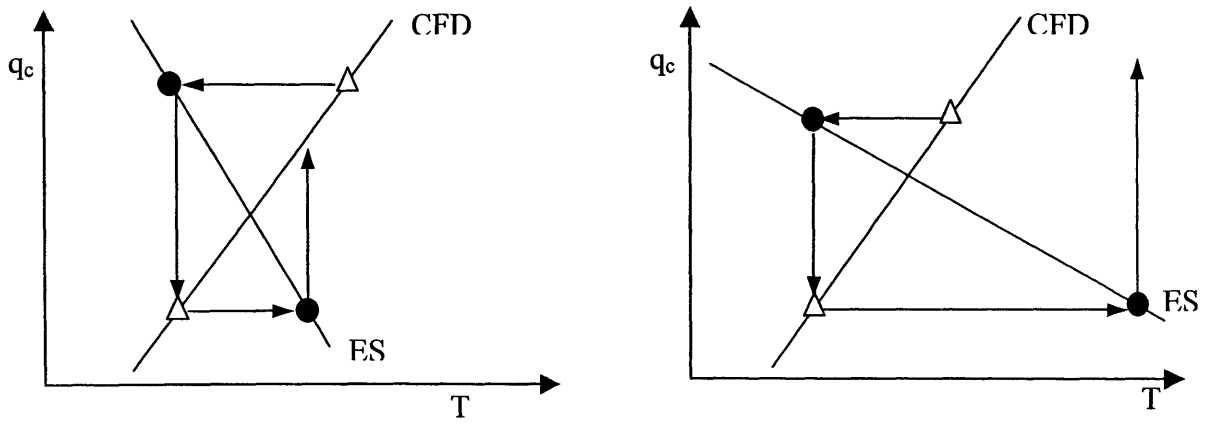

(a) Converged (b) Diverged

Figure 7.8 Iteration process of ES and CFD in q_c-T plot
(a) with $|\partial q_c/\partial T|_{ES} > |\partial q_c/\partial T|_{CFD}$ and (b) with $|\partial q_c/\partial T|_{ES} < |\partial q_c/\partial T|_{CFD}$
(CFD provides q_c to ES, and ES returns a new T for CFD as boundary conditions.)

In addition, coupling method-3, in fact, performs an explicit iteration, while method-1 is an implicit iteration. Method-3 transfers $\mathbf{Q}(=h\mathbf{T}-h\mathbf{T_a})$, instead of h and $\mathbf{T_a}$, from the last CFD (n^{th} iteration step) to the next ES ($n+1^{th}$ iteration step), therefore

$$\mathbf{A}\mathbf{T}^{n+1}=\mathbf{B}+h\mathbf{T}^{n}-h\mathbf{T}^{n}_{a} \qquad \text{(ES)} \qquad (7.29)$$
$$h\mathbf{T}^{n}-h\mathbf{T}^{n}_{a}=f(\mathbf{T}^{n}) \qquad \text{(CFD)} \qquad (7.30)$$

It is an explicit iteration for **T** in Eq. (7.29). As a result, $\mathbf{T}^{n+1}$ gets updated slowly and the entire coupled simulation needs more CFD calls. Consequently, the total computing time is expected to increase.

On the contrary, method-1 performs an implicit iteration for **T** in ES by importing h and $\mathbf{T_a}$ from the last CFD.

$$\mathbf{A}\mathbf{T}^{n+1}=\mathbf{B}+h\mathbf{T}^{n+1}-h\mathbf{T}^{n}_{a} \qquad \text{(ES)} \qquad (7.31)$$
$$h\mathbf{T}^{n}-h\mathbf{T}^{n}_{a}=f(\mathbf{T}^{n}) \qquad \text{(CFD)} \qquad (7.32)$$

Generally, the implicit algorithm is more stable and moves on faster (hence needs less CFD calls) than the explicit algorithm, although it may need more computing effort for

the iteration in ES. However, the computing time for ES is tiny compared with that for CFD. As a result, coupling method-1 would need less computing time than method-3.

From all the analysis above, one may conclude that coupling method-1 seems to be better than method-3. Real problems are more complicated, usually without constant slopes and highly non-linear. A theoretical analysis on those problems is impossible. Stability and convergence of real problem simulations can only be verified through numerical experiments, which will be conducted in the Section 7.3.

The analysis of coupling method-4 indicates the method has difficulty controlling the indoor air temperature although it has the same coupling substance as method-1, which will be further discussed in Section 7.3.3. Coupling methods-2 and -5 have very similar performance as method-1 and -4, but they may introduce the negative h problem. Section 7.2.4 will address this negative h problem.

7.2.3 Spatial Average Methods for ES-CFD Program Coupling

The sections above indicate that the iteration of ES and CFD equations with an appropriate data coupling method can provide the solution of a coupled simulation. However, the variables in the ES and CFD equations, such as **T**, $\mathbf{T_a}$ and **Q**, are solved with different spatial models. ES uses the nodal model to represent surfaces and spaces while CFD provides distributed information. Numerical approximation is obligatory to bridge this disparity at the joint boundaries of ES and CFD. A straightforward method is to use the nodal model (uniform assumption) for the particular regions of CFD that connect with ES.

On one hand, ES provides CFD the uniform boundary conditions, such as uniform surface temperature and/or heat flux. This may influence the airflow and temperature distributions because the real conditions may not be uniform. However, it is always possible to improve the results by subdividing surfaces into even smaller pieces in ES to eliminate any important temperature gradients, as discussed in Chapter 5.

On the other hand, the distributed information provided by CFD, such as air temperature T_a close to surfaces and convective heat transfer coefficient h, should be spatially averaged to serve ES. These averaged values, although losing some details from the original CFD results, should still reflect the macro characteristics of the information from CFD, such as the total convective heat flux from each surface. However, the total heat flux calculated by using the spatially averaged T_s, T_a and h may not equal the actual sum of local heat flux for some data coupling methods. Special treatments to the averaged T_a and h are thus required, as demonstrated below.

For coupling methods-1 and -3, the local heat flux is

$$q = h(T_s - T_{room} - \Delta T_{air}) \tag{7.33}$$

where $\Delta T_{air} = T_a - T_{room}$ and T_{room} is the controlled room air temperature. The mean heat flux is

$$\bar{q} = \sum qA / \sum A = \sum h(T_s - T_{room} - \Delta T_{air})A / \sum A \tag{7.34}$$

which can also be written as

$$\bar{q} = \overline{h(T_s - T_{room} - \Delta T_{air})} \tag{7.35}$$

Since in CFD, T_s is constant from last ES calculation, h is usually not constant, and ΔT_{air} is much smaller than T_s and T_{room},

$$\bar{q} = \overline{h(T_s - T_{room} - \Delta T_{air})} = \bar{h}(T_s - T_{room}) - \overline{h\Delta T_{air}} \approx \bar{h}(T_s - T_{room}) - \overline{h}\,\overline{\Delta T_{air}} \tag{7.36}$$

Hence, spatially-averaged $\bar{h}$ and $\overline{\Delta T_{air}}$ are able to represent reasonably accurate total heat flux in method-1 and -3.

For coupling method-2, local heat flux is

$$q = h(T_s - T_{room}) \tag{7.37}$$

The mean heat flux becomes

$$\bar{q} = \overline{h(T_s - T_{room})} = \bar{h}(T_s - T_{room}) \tag{7.38}$$

Therefore, the average heat flux calculated by the spatially-averaged $\bar{h}$ exactly equals the average of the local heat flux in method-2.

For coupling method-4, at the n^{th} coupling step, ES provides CFD

$$\overline{q_n} = \overline{h_n}(T_{s,ES} - T_{room} - \overline{\Delta T_{air,n}}) \tag{7.39}$$

where $\overline{h_n}$ and $\overline{\Delta T_{air,n}}$ are constant values from last CFD calculation, and $T_{s,ES}$ is the updated surface mean temperature by the current ES. All the local heat fluxes in CFD are then specified to equal this mean heat flux from ES,

$$q_{n+1} = \overline{q_n} = h_{n+1}(T_{s,CFD} - T_{room} - \Delta T_{air,n+1}) \tag{7.40}$$

The mean heat flux can be calculated as

$$\overline{q_{n+1}} = \overline{q_n} = \overline{h_{n+1}(T_{s,CFD} - T_{room} - \Delta T_{air,n+1})} = \overline{h_{n+1}T_{s,CFD}} - \overline{h_{n+1}T_{room}} - \overline{h_{n+1}\Delta T_{air,n+1}} \tag{7.41}$$

Since $T_{s,CFD}$ is the local surface temperature calculated by CFD and is not constant,

$$\overline{q_{n+1}} = \overline{h_{n+1}T_{s,CFD}} - \overline{h_{n+1}T_{room}} - \overline{h_{n+1}\Delta T_{air,n+1}} \neq \overline{h_{n+1}}(\overline{T_{s,CFD}} - T_{room} - \overline{\Delta T_{air,n+1}}) \quad (7.42)$$

As a result, the heat flux calculated with the new spatially averaged $\overline{h_{n+1}}$, $\overline{T_{s,CFD}}$ and $\overline{\Delta T_{air,n+1}}$ is different from the actual $\overline{q_{n+1}}$ used in the CFD simulation. This may cause the inconsistence between CFD and ES. One way to solve this problem is to update the mean h value by using the actual $\overline{q_{n+1}}$:

$$\overline{h_{n+1}} = \overline{q_{n+1}} / (\overline{T_{s,CFD}} - T_{room} - \overline{\Delta T_{air,n+1}}) \quad (7.43)$$

Another method is to implement the heat flux boundary condition in CFD by confining the temperature difference between the surface and the neighboring air, rather than explicitly inserting a heat flux source term into the energy equation. With this method, the n^{th} ES calculation provides CFD with

$$\frac{\overline{q_n}}{\overline{h_n}} = \overline{(T_s - T_i)} \quad (7.44)$$

The temperature difference between the surface and the neighboring air is then fixed in the next CFD calculation. The local heat flux becomes

$$q_{n+1} = h_{n+1}(T_s - T_i) = h_{n+1}\overline{(T_s - T_i)} = h_{n+1}\frac{\overline{q_n}}{\overline{h_n}} \quad (7.45)$$

Therefore, the mean heat flux is

$$\overline{q_{n+1}} = \overline{h_{n+1}(T_s - T_i)} = \overline{h_{n+1}(T_s - T_i)} = \frac{\overline{h_{n+1}}}{\overline{h_n}}\overline{q_n} \quad (7.46)$$

The new $\overline{h_{n+1}}$ carries the exact heat flux information used in the current CFD calculation. The $\overline{q_{n+1}}$ may not be the same as the $\overline{q_n}$ transferred from last ES because $\overline{h_{n+1}}$ does not equal $\overline{h_n}$ in the initial iteration steps. But the $\overline{q}$ value will eventually reach a converged and constant value during an iteration when $\overline{h}$ gradually converges. This analysis, from one particular aspect, shows that coupling method-4 needs more sophisticated treatments than the other coupling methods to obtain a correct and converged solution.

7.2.4 Influence of Negative Convection Coefficient on the Coupling Simulation

The convective heat at enclosures predicted by CFD can be transferred to ES by multiple methods, as explained in Section 7.2.2. The theoretical study indicates that a good method to exchange convective heat between ES and CFD is that ES provides envelope interior surface temperatures to CFD while CFD returns the convective heat transfer coefficients h and the air temperatures T_D near the surfaces to ES. To minimize the modifications in ES programs that use the traditional definition of convection coefficient h based on the temperature difference of an interior surface and room air, a nominal convective heat transfer coefficient, $h_{nominal}$, rather than h and T_D, can be calculated from CFD results and used in ES. This is coupling method-2. The $h_{nominal}$ is calculated in CFD through:

$$h_{nominal} = hA(T_{surface} - T_D)/A(T_{surface} - T_{room}) \tag{7.47}$$

The h, calculated in CFD based on the flow viscosity (Equation (6.2)), is always positive. However, $h_{nominal}$ can be negative in some particular cases.

Figure 7.9 illustrates such an example in a room with displacement ventilation. If assuming h = 4W/m^2°C at the floor surface, the heat gain from the floor Q = h(T_{floor}-T_{air}) = 4W/m^2. If Q is represented by the temperature difference between $T_{control}$ and T_{floor}, then Q = $h_{nominal}$(T_{floor}-$T_{control}$) = $h_{nominal}$(20-24) = 4W/m^2, one would obtain $h_{nominal}$ = -1W/m^2°C. It may even cause the singularity problem if $T_{control}$=20°C.

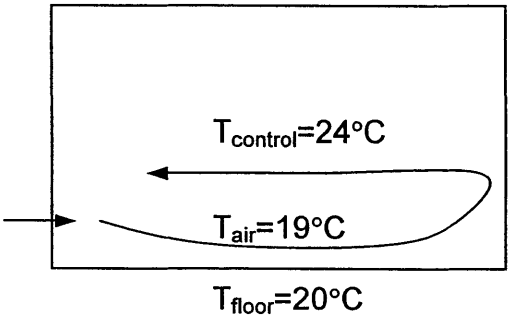

Figure 7.9 Illustration of negative h

Negative h may cause divergence and instability of an ES simulation. ES solves the following matrix equation for surface energy balance

$$\mathbf{H \cdot T = q} \tag{7.48}$$

where,

$$\mathbf{H}=\begin{bmatrix} h_{1,c}+\sum_{k=1}^{N}h_{1k,r} & -h_{12,r} & \cdots & -h_{1N,r} \\ -h_{21,r} & h_{2,c}+\sum_{k=1}^{N}h_{2k,r} & \cdots & -h_{2N,r} \\ \cdots & \cdots & \cdots & \cdots \\ -h_{N1,r} & \cdots & -h_{NN-1,r} & h_{N,c}+\sum_{k=1}^{N}h_{Nk,r} \end{bmatrix} \tag{7.49}$$

$$\mathbf{T}=\begin{bmatrix} T_1 \\ T_2 \\ \cdots \\ T_N \end{bmatrix} \tag{7.50}$$

$$\mathbf{q}=\begin{bmatrix} q_{1,in}+h_{1,c}T_{room} \\ q_{2,in}+h_{2,c}T_{room} \\ \cdots \\ q_{N,in}+h_{N,c}T_{room} \end{bmatrix} \tag{7.51}$$

and T_i is the temperature of interior surface i, $h_{i,c}$ is the convective heat transfer coefficient of surface i, $h_{ij,r}$ is the radiative heat transfer coefficient between surface i and surface j, $q_{i,in}$ is the incoming heat to surface i (e.g. the conductive heat through the envelopes), N is the total surface number.

Therefore,

$$\mathbf{T}=\mathbf{q}/\mathbf{H} \tag{7.52}$$

From matrix theory (Assem 1991), **T** has a unique solution if only if $|\mathbf{H}|\neq 0$, i.e. **H** is nonsingular. **H** is singular if and only if the rank of n×n matrix **H** < n, which means that at least one row in **H** could be represented by the algebraic combination of the others. Due to the randomness of the coefficients in **H**, it is impossible to anticipate the determinant of matrix **H** in general. However, the energy equation for each surface (each row in Equation (7.48)), although connected with other surfaces, cannot be determined by energy balances of the other surfaces. Therefore, matrix **H** is nonsingular, regardless of the sign of h.

When iteratively solving Equation (7.48) in ES, one may still meet the instability and divergence problems. Matrix theory (Assem 1991) proves that the matrix should possess some properties to guarantee a converged solution. Following is a brief discussion on the issue with Jacobi method.

Equation (7.48) can be rewritten in the following manner

$$\begin{bmatrix} 1 & h_{1,2}/h_{1,1} & \cdots & h_{1,N}/h_{1,1} \\ h_{2,1}/h_{2,2} & 1 & \cdots & h_{2,N}/h_{2,2} \\ \cdots & \cdots & \cdots & \cdots \\ h_{N,1}/h_{N,N} & \cdots & h_{N,N-1}/h_{N,N} & 1 \end{bmatrix} \begin{bmatrix} T_1 \\ T_2 \\ \cdots \\ T_N \end{bmatrix} = \begin{bmatrix} q_1/h_{1,1} \\ q_2/h_{2,2} \\ \cdots \\ q_N/h_{N,N} \end{bmatrix} \tag{7.53}$$

$$\begin{bmatrix} T_1 \\ T_2 \\ \cdots \\ T_N \end{bmatrix} = \begin{bmatrix} q_1/h_{1,1} \\ q_2/h_{2,2} \\ \cdots \\ q_N/h_{N,N} \end{bmatrix} - \begin{bmatrix} 0 & h_{1,2}/h_{1,1} & \cdots & h_{1,N}/h_{1,1} \\ h_{2,1}/h_{2,2} & 0 & \cdots & h_{2,N}/h_{2,2} \\ \cdots & \cdots & \cdots & \cdots \\ h_{N,1}/h_{N,N} & \cdots & h_{N,N-1}/h_{N,N} & 0 \end{bmatrix} \begin{bmatrix} T_1 \\ T_2 \\ \cdots \\ T_N \end{bmatrix} \tag{7.54}$$

By iteratively solving (7.54), one can obtain the solution with a prescribed accuracy. Assume after the m^{th} iteration,

$$\mathbf{T}_m=\mathbf{q}'-\mathbf{H}'\mathbf{T}_{m-1} \tag{7.55}$$

And if **T** is the exact solution, i.e.

$$\mathbf{T}=\mathbf{q}'-\mathbf{H}'\mathbf{T} \tag{7.56}$$

It can be easily seen, upon subtraction, that

$$\mathbf{T}_m-\mathbf{T}=-\mathbf{H}'(\mathbf{T}_{m-1}-\mathbf{T})=\mathbf{H}'^2(\mathbf{T}_{m-2}-\mathbf{T})=\ldots=(-1)^m\,\mathbf{H}'^m\,(\mathbf{T}_0-\mathbf{T}) \tag{7.57}$$

Hence

$$\lim_{m\to\infty}(T_m - T)=0 \text{ if } \lim_{m\to\infty}\mathbf{H}'^m=0 \tag{7.58}$$

In other words, a necessary and sufficient condition for the convergence of the Jacobi method is that $\mathbf{H}'^m$ tends to zero as m tends to infinity. Such a limit occurs if the spectral radius of **H** is less than unit. For the moment, a sufficient condition can be

$$|\mathbf{H}|<1 \tag{7.59}$$

since

$$|\mathbf{H}^m|\le|\mathbf{H}|^m \tag{7.60}$$

From matrix theory, a sufficient condition when $|\mathbf{H}|$ is less than unity is to satisfy the following condition

$$\sum_{\substack{j=1 \\ j\neq i}}^{N}\left|\frac{h_{i,j}}{h_{i,i}}\right| < 1, \quad i=1, 2, .., N \tag{7.61}$$

With positive h values, the elements in the matrix **H** of Eq. (7.48) always satisfy

$$\left|h_{i,c} + \sum_{j=1}^{N} h_{ij,r}\right| > \sum_{\substack{j=1 \\ j\neq i}}^{N}\left|-h_{ij,r}\right| \tag{7.62}$$

which makes **H** a diagonal dominant matrix, assuring that there exists a unique solution for the vector **T**.

When $h_{i,c}$ is negative, Equations (7.61) or (7.62) may not be satisfied, which could cause divergence and instability during a calculation. The divergence and instability may not always occur, since satisfying Equation (7.61) is only a sufficient condition. In general, the further the real situation departs from Equation (7.61) (i.e. the larger negative $h_{i,c}$), the higher the probability of divergence and instability.

7.3 Numerical Experimentation

7.3.1 Case Setup

The above theoretical analysis and verification provide the essential confidence and understanding on solutions of iterative ES-CFD coupling. To further verify the performance of coupling methods and numerical algorithms on a practical building problem, it is necessary to conduct numerical experiments on some well-designed cases. The well-designed cases that can minimize the effects from other factors on convergence and stability should have the following features:

- Simple geometry
- Basic heat transfer processes
- Minimum fluctuation of outdoor environment conditions
- Controlled indoor air temperature
- Reasonable ventilation rate

Following these requirements, the study has designed an empty room as shown in Figure 7.10. The cubic room (3×3×3m) is on a middle floor of a building and has only one south-facing exterior wall without windows. Table 7.2 lists the enclosure materials; they are the same as those in an environmental chamber at MIT. The room has no internal heat gains, and the heat load is solely due to the southern exterior wall. The outdoor air temperature was assumed to be constant at –12.8°C (Boston winter design condition). The room air temperature is conditioned to be constant at 23°C. A variable air volume system supplies T_{supply} = 25°C warm air from a diffuser on the north wall close to the ceiling. The exhaust outlet is on the same wall close to the floor.

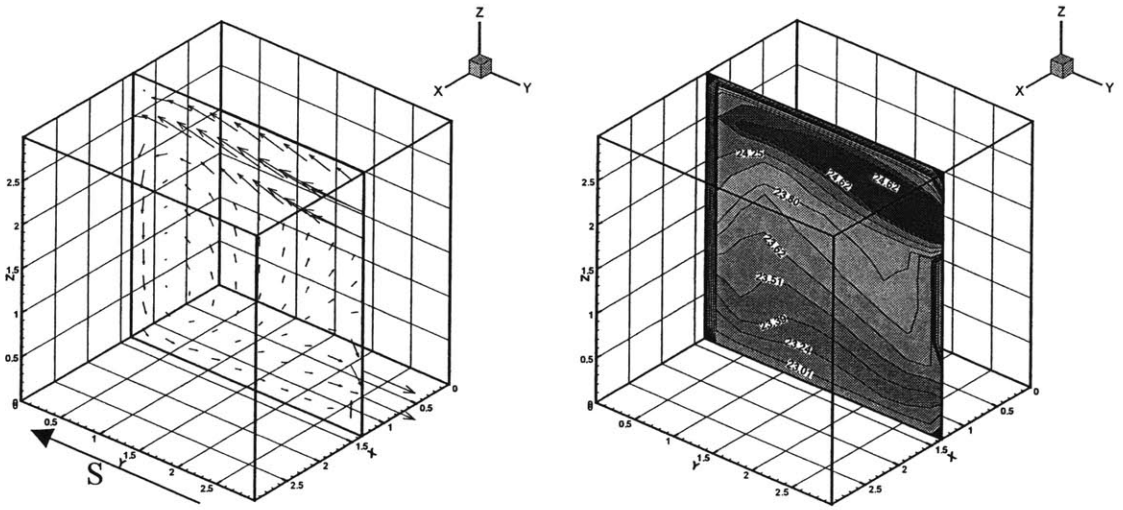

Figure 7.10 The air velocity (a) and temperature (b) distributions at the middle section of the room (V_{supply}=0.78m/s; T_{supply}=25°C)

Table 7.2 Room enclosure materials

Enclosure	Thickness (m)	Density (kg/m^3)	Specific heat (J/kgK)	Thermal conductivity (W/mK)
Ceiling/Floor	0.175	2300	840	1.9
Walls	0.140	700	840	0.23

7.3.2 Solution Performance of Iterative Coupling Methods

The coupling method-1, -2, -3, and -4 discussed above have been implemented into E+MIT-CFD, a coupled program of EnergyPlus (E+) and MIT-CFD, as introduced in Chapter 5. This section reports the numerical experiments on the case shown in Figure 7.10 with the four coupling methods.

Although the case is steady, it is necessary to perform the simulation for a few days to reach a steady state because the assumed initial values, such as wall temperatures, are not the true values. The coupling between ES and CFD is performed once a day during this period. After a call to CFD, ES uses the results from CFD, such as convective heat fluxes, until it calls CFD again the next day. This one-time-step dynamic coupling is quite reasonable for the case with small variation of the influencing parameters, such as the environmental conditions and internal loads. In this simulation, CFD uses a coarse 12x12x14 rectangular grid and both the constant viscosity and zero-equation turbulence model to reduce the computing time. Chen and Xu's study (1998) indicated that such a

coarse grid and simple turbulence model can provide acceptably reasonable results for the building design purpose.

The CFD calculation uses the upwind numerical scheme to discretize the convection term and the central scheme to discretize the diffusion term. The convergence criterion for CFD requires the normalized residuals for all variables solved to be less than 1%, with a maximum iteration limit of 1000 steps per CFD run. Because the convective heat flux Q_{conv} and the interior surface temperature T_s are the linkages of ES and CFD, the difference in Q_{conv} between ES and CFD and the difference in T_s between the current and last ES runs are used to judge the convergence of ES-CFD iterations. In fact, only one of these needs to be specified as the convergence criterion because of the inherent relationship between Q_{conv} and T_s. The present study considers the solution fully converged if the maximum difference in interior surface temperatures between two ES runs is less than 1%.

Figure 7.11 shows that coupling method-1 can lead to a converged solution in four iterations for this case. The experience shows that convergence takes no more than 10 iterations for a more sophisticated case. Figure 7.13 shows the convergence performance for three continuous days (the first two days are used to eliminate the impact of initial values on the final results). The converged solutions are reached on the second and third day in Figure 7.13 (a), but not on the first day. The reason for this is that CFD needs more time steps in the startup period to obtain a converged solution. A stricter CFD criteria can overcome this problem, as demonstrated in Figure 7.13 (b), which, however, requires more computing time.

Coupling method-2 provides very similar results and convergence process as method-1, as shown in Figure 7.12. The order of computing time (75 seconds) is the same as that with method-1 (64 second). It is because $h_{nominal} \cong h$ in this particular case. The numerical experiment with coupling method-3 shows similar performance as method-1 either, but it needs about 30% more computing time due to the explicit iteration procedure. Coupling method-4 can also produce a converged solution, but the solution is quite different from those by method-1 and method-2. The primary reason for this is that the coupling with method-4 cannot properly control the indoor air temperature, which will be discussed in detail in the next section.

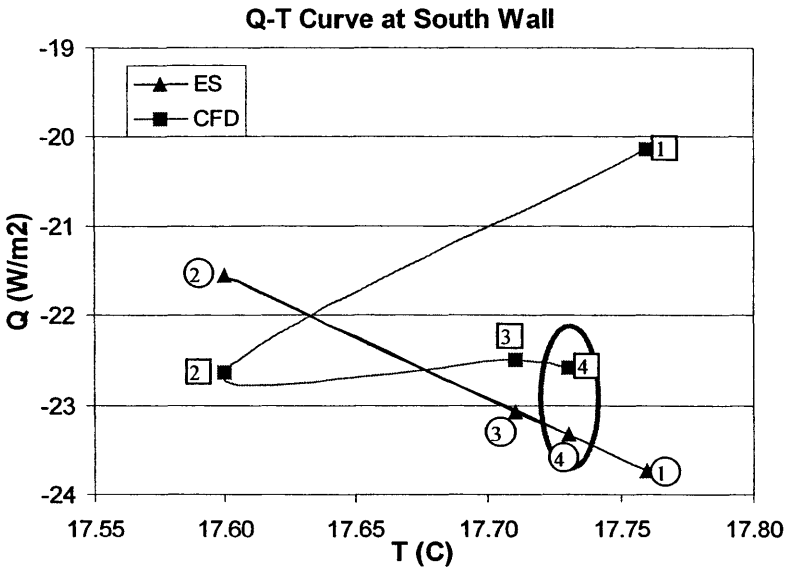

Figure 7.11 A typical convergence process of E+CFD-MIT with coupling method-1 for a particular time step (with zero-equation turbulence model)

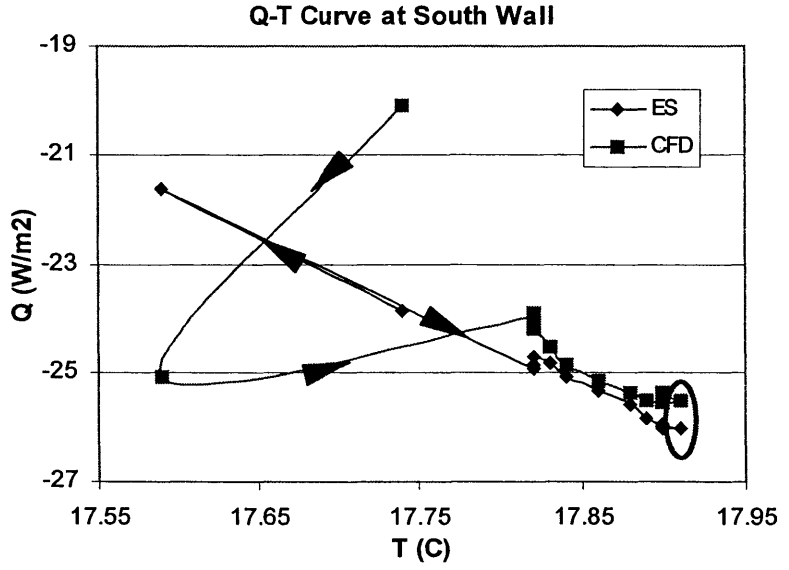

Figure 7.12 A typical convergence process of E+CFD-MIT with coupling method-2 for a particular time step (with zero-equation turbulence model)

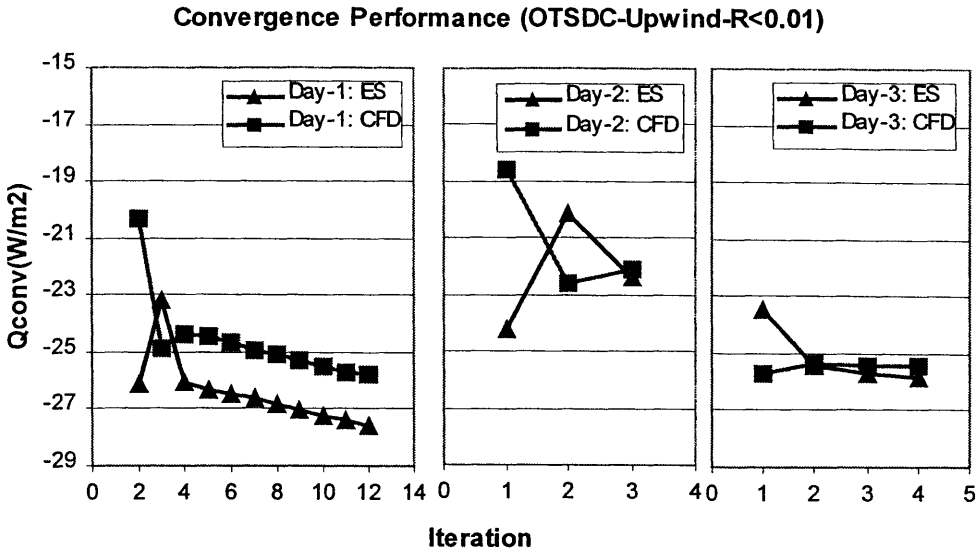

[Computing time = 64 seconds]

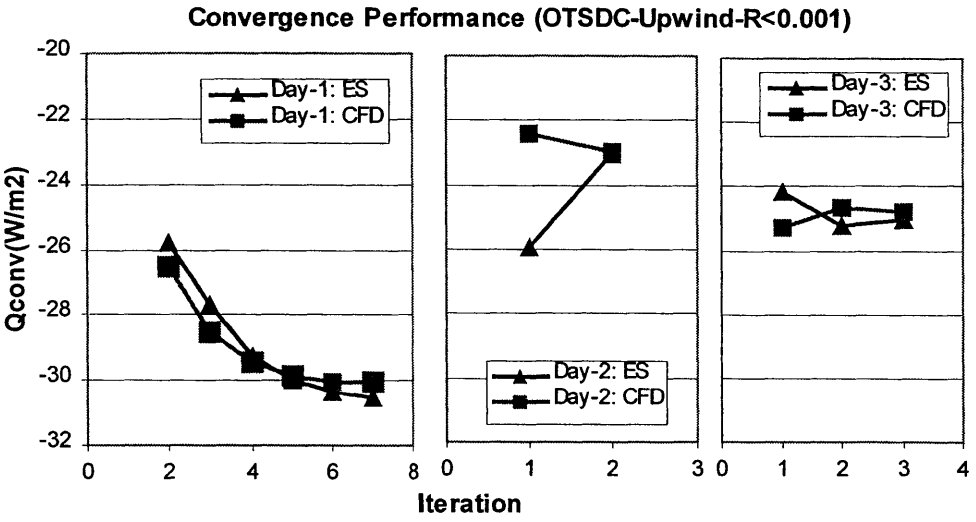

[Computing time = 351 seconds]

Figure 7.13 Convergence of one-time-step dynamic coupling for three continuous days with coupling method-1 and 0-equation turbulence model
(Top (a): CFD residuals<0.01; Bottom (b): CFD residuals<0.001)

7.3.3 Control of Indoor Air Temperature in the Coupling Simulation

In the ES-CFD program coupling, the partial differential energy equation of CFD simulates the room air energy balance and connects with the enclosure energy balance equation of ES. The integral room air energy balance equation of ES is no longer needed. In fact, the ES room air energy balance equation should be used to control the indoor air temperature in a coupled simulation.

Figure 7.14 illustrates the control process in the coupled simulation of the test case by using coupling method-1. With the constant h values provided by the constant viscosity turbulence model, method-1 transfers surface temperature from ES to CFD and returns indoor air temperature gradient from CFD to ES, at one specific coupling time step.

CFD first calculates the indoor air temperature distribution based on the boundary conditions (south wall interior surface temperature T=18°C from the last ES). It predicts a temperature difference 0.2°C (=24°C-23.8°C) between the calculated control point temperature $T_{control\text{-}cal}$ and the air temperature close to the surface T_a, as shown in Figure 7.14. In the steady state CFD, the supply air energy requirement Q_{supply} equals the convective heat transfer Q_{conv} through the envelope, that is, $Q_{supply} = hA(T_a\text{-}T)=hA(23.8\text{-}18)$.

With this temperature gradient ($T_{control\text{-}cal}$ - T_a=0.2°C) from CFD, ES obtains the air temperature close to the surface (T_a=22.8°C) in the controlled room with the prescribed constant room air temperature (23°C). The integral energy equation in ES, therefore, produces a new $Q_{supply}=hA(T_a\text{-}T)=hA(22.8\text{-}18)$ and passes it to the next CFD run. The new Q_{supply} in CFD will drag the indoor air temperature down toward the desired air temperature. Only if $T_{control\text{-}cal}$ in CFD equals the required indoor air temperature $T_{control\text{-}set}$ in ES can the indoor air energy balance be satisfied in both CFD and ES.

Coupling method-4, on the other hand, transfers Q_{conv} from ES to CFD. It results in Q_{conv}, instead of surface temperature T, being unchanged during one specific iteration step. Therefore, $T_{control\text{-}set}$ in ES will adjust T to achieve the same heat flux for both ES and CFD. Consequently, both of the thermal distributions in ES and CFD can satisfy the heat balance $Q_{supply}=Q_{conv}$ and $Q_{convES}= Q_{convCFD}$ but the temperature patterns are different, as illustrated by Figure 7.15. The main reason for this is that $T_{control\text{-}set}$ of ES has no relationship with the temperature field predicted by CFD. Hence, $T_{control\text{-}set}$ in ES cannot properly function as a controller for the entire coupled simulation with method-4.

To acquire proper solutions with method-4, a new control strategy needs to be developed. Since in each iteration the air temperature at the exhaust outlet, T_{outlet}, needs to be transferred from CFD to ES for accurate estimation of supply air mass flow rate, one method to create a connection between $T_{control\text{-}set}$ and the temperature field from CFD is to introduce ES a new $T_{outlet\text{-}new}$

$$T_{outlet\text{-}new}=T_{outlet}-(T_{control\text{-}cal}-T_{control\text{-}set}) \quad (7.63)$$

However, numerical experiments show that the direct implementation of this numerical technique is quite unstable. The present investigation develops an improved control and iteration algorithm, consisting of three basic steps:

(1) In each CFD calculation, CFD runs for up to one hundred iteration steps without the necessity of convergence. This is because the supply air enthalpy (or, mass flow rate with a VAV system) is always updated during the coupling before reaching the final solution. The final CFD solution at each coupling step will be well converged if the boundary conditions approach stable values.

(2) The entire CFD temperature field is modified according to the difference between $T_{control-set}$ and $T_{control-cal}$.

(3) The modified exhaust outlet temperature from CFD is used in ES to generate the new inlet supply air enthalpy for the next CFD run.

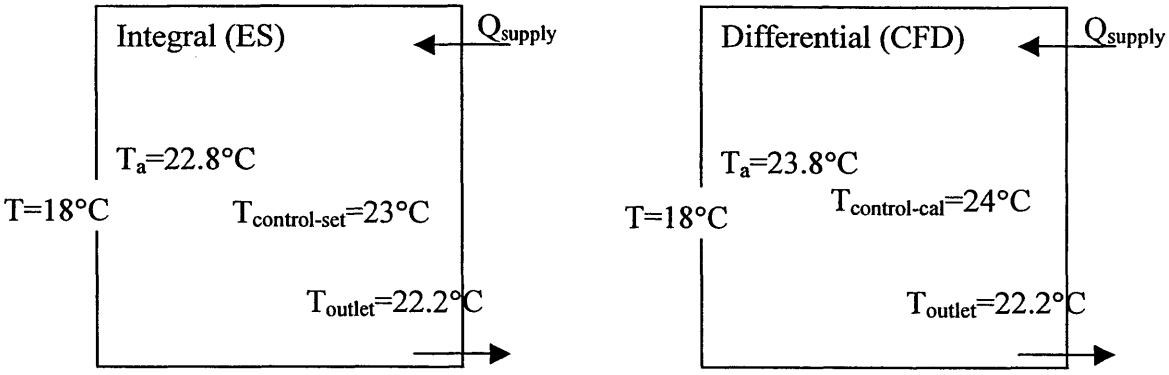

Figure 7.14 Control process of indoor air temperature in the coupled simulation with coupling method-1

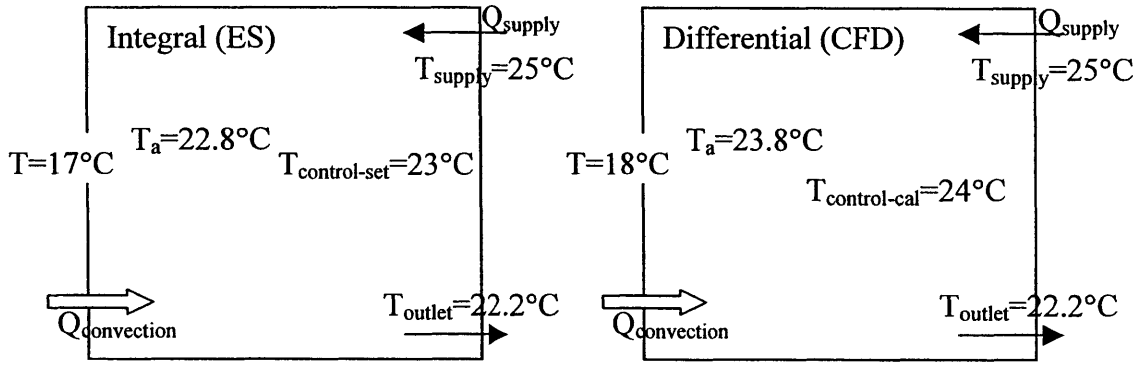

Figure 7.15 Control process of indoor air temperature in the coupled simulation with coupling method-4

Although this new algorithm is specifically developed to solve the control problem of coupling method-4, it is also suitable to be exploited by the other methods. In fact, this algorithm can accelerate the convergence for all the coupling methods, because:

(1) Superfluous iterations and critical convergence criteria within each CFD run is not necessary since the boundary conditions are updated all the time.
(2) The modification of the temperature field forces it to approach the required temperature (the control temperature in ES) faster. The effect is similar to providing a more reasonable initial temperature field for each CFD run.
(3) The modified exhaust outlet temperature, which is closer to the final result than the original one without the artificial modification, helps to capture the correct inlet supply enthalpy more quickly.

The new iteration and control algorithm has been implemented and used to test the four coupling methods. Table 7.3 shows that all the four coupling methods can reach converged solutions. Methods-1, 2, 3, especially methods-1 and 3, provide nearly identical results, as expected. Method-3 needs more computing time than methods-1 and 2. Note that the integral surface convective heat flux with coupling method-2 is exactly the same as the one calculated based on averaged h and T, while it is almost same with methods-1 and 3. This agrees with the theoretical analysis.

Method-4 provides somewhat different solutions when using the zero-equation turbulence model. This is because method-4 directly introduces the convective heat flux into the energy equation of CFD while methods-1, 2 and 3 provide CFD the surface temperature. The surface temperature relies on convection to affect the indoor air and thus heavily depends on the near-wall turbulence model. However, the turbulence model will influence the solution of method-4 when calculating the air temperature close to the surfaces and surface heat transfer coefficients. The explanation of the result differences can be further verified by the simulation with the constant viscosity turbulence model. The results in Table 7.4 show that methods-1, -3 and -4 produce almost the same solutions when using the constant viscosity turbulence model. It is also interesting to notice that the Q-T curves from the simulation with the constant viscosity turbulence model verify the theoretical analysis with constant h assumption, as demonstrated in Figure 7.16.

The numerical experiments with both turbulence models exhibit that the residuals of CFD calculations with the new iteration algorithm are smaller than those with the original algorithm for all the coupling methods, although the iteration within each CFD calculation reduces to 100 steps. The tests with the stricter convergence criteria as in method-1', method-1" and method-4" of Table 7.3 verify that the solutions from method-1 and method-4 are converged and stable. The calculation with method-4' indicates that extra iterations in CFD with intermediate boundary information are not useful and may cause numerical instability. Finally, the coupling exercises demonstrate that methods-1, 2 and 3 are more stable than method-4.

Table 7.3 Results comparison for different coupling methods with new iteration and control algorithm (zero-equation turbulence model, upwind scheme, IterCFD=100 or R_{CFD}<0.1%, R_{ES}<1%)

	Q_{total} (W)	Q_{surfES} (W/m^2)	$Q_{surfMCFD}$ (W/m^2)	$Q_{surfCFD}$ (W/m^2)	ΔQ_{surf} (W/m^2)	$T_{southES}$ (C)	$T_{southCFD}$ (C)	h_{south} (W/m^2K)	R_{CFD} (<)	Time (s)
Method-1	383	23.94	24.01	23.99	0.05	18.04	18.04	4.84	0.23%	85
Method-2	393	24.00	24.11	24.11	0.11	18.08	18.08	4.90	0.17%	91
Method-3	384	24.08	24.06	24.03	0.05	18.04	18.04	4.85	0.11%	109
Method-4	308	19.33	19.33	19.33	0.00	17.54	17.55	3.52	0.55%	108
Method-4'	283	17.94	17.94	17.94	0.00	17.66	17.62	3.31	0.50%	459
Method-4"	308	19.39	19.39	19.39	0.00	17.56	17.56	3.54	0.19%	199
Method-1'	409	25.18	25.28	25.14	0.04	17.97	17.97	5.04	0.10%	144
Method-1"	385	24.09	24.09	24.06	0.03	18.05	18.05	4.87	0.10%	105

Note:

' means the change of IterCFD=100 or R_{CFD}<0.1% to IterCFD=500 or R_{CFD}<0.1%;

" means the change of R_{ES}<1% to R_{ES}<0.1%.

Q_{total} – total energy requirement for space; Q_{surfES} – convective heat flux at south wall from ES; $Q_{surfMCFD}$ – total convective heat flux at south wall from CFD based on mean h and T; $Q_{surfCFD}$ – integral convective heat flux at south wall from CFD; ΔQ_{surf}= Q_{surfES}- $Q_{surfCFD}$; $T_{roomCFD}$ – control room air temperature in CFD; $T_{southES}$ – south wall surface temperature from ES; $T_{southCFD}$ – south wall surface temperature from CFD; h_{south} – convective heat transfer coefficient at south wall; R_{CFD} – final residuals in CFD; Time – computing time.

Table 7.4 Results comparison for different coupling methods with new iteration and control algorithm (constant viscosity turbulence model, upwind scheme, IterCFD=100 or R_{CFD}<0.1%, R_{ES}<1%)

	Q_{total} (W)	Q_{surfES} (W/m^2)	$Q_{surfMCFD}$ (W/m^2)	$Q_{surfCFD}$ (W/m^2)	ΔQ_{surf} (W/m^2)	$T_{southES}$ (C)	$T_{southCFD}$ (C)	h_{south} (W/m^2K)	R_{CFD} (<)	Time (s)
Method-1-C	444	31.57	31.72	31.72	0.15	19.77	19.77	10.73	0.10%	52
Method-3-C	450	31.57	31.61	31.61	0.04	19.78	19.78	10.73	0.10%	199
Method-4-C	425	31.77	31.77	31.78	0.01	19.89	19.89	10.73	0.10%	62

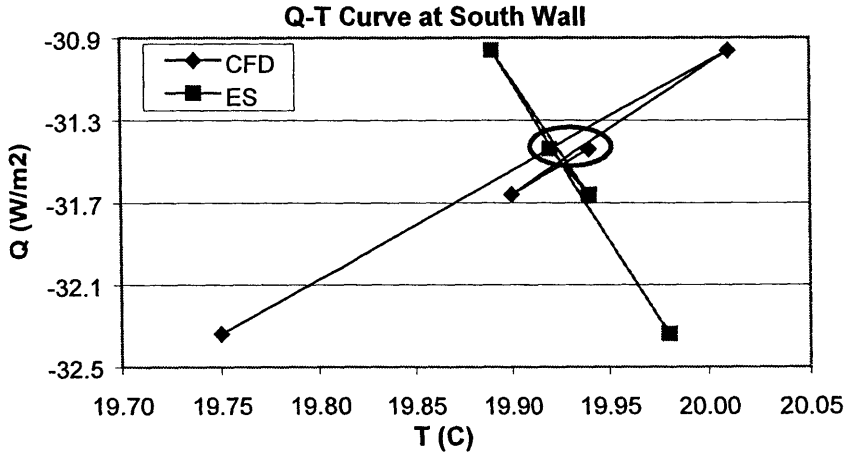

Figure 7.16 Convergence of one-time-step dynamic coupling using method-4 with constant viscosity turbulence model (ending points in red circle)

7.3.4 Effect of Convergence Criteria on the Coupling Simulation

The above simulations reveal that the convergence criteria of ES and CFD calculations are essential to the acquirement of an accurate and fast solution. In a coupled simulation, both the convergence criteria for ES and CFD can be adjusted. The CFD convergence criteria (normalized residuals for all variables solved fall to less than the prescribed criteria) control the iteration procedure during each CFD run, while the ES convergence criteria (maximum of interior surface temperature differences between two ES runs falls to less than the prescribed value) control the entire coupling calculation.

This section investigates the impact of CFD and ES convergence criteria on the computing time and accuracy of a coupled simulation using coupling method-1. Table 7.5 lists the different combinations of CFD and ES convergence criteria and the corresponding computing results. Test 2 and Test 5 have the best, nearly identical, performance of convergence in terms of the difference of convective heat flux on the interior surface of south wall between ES and CFD. Test 2 needs more computing time than Test 5 due to more iterations in CFD. Figure 7.17 and 7.18 show the converging processes of Test 2 and Test 5. The results indicate that frequent exchange of inter-coupled information between ES and CFD is more efficient than more iterations in a single CFD run (the cases with a smaller R_{CFD} in Table 7.5). However, the iteration number for each CFD cannot be too small. For example, Test 3 and Test 6 could not yield good results. Hence, a reasonable combination of ES and CFD convergence criteria is significant to quickly obtain correct results, although this combination may vary with problems studied and numerical techniques employed.

Table 7.5 Comparison for different convergence criteria with coupling method-1 (Zero-equation turbulence model, $Iter_{CFD}<1000$)

	Convergence Criteria	$T_{RoomCFD}$ (C)	$Q_{surfaceES}$ (W/m^2)	$\Delta Q_{surface}$ (W/m^2)	Time (s)
Test 1	$R_{CFD}<0.01$, $R_{ES}<0.01$	22.80	23.4	0.8	68
Test 2	$R_{CFD}<0.001$, $R_{ES}<0.01$	22.95	24.6	0.2	403
Test 3	$R_{CFD}<0.1$, $R_{ES}<0.01$	22.60	15.9	1.1	98
Test 4	$R_{CFD}<0.01$, $R_{ES}<0.001$	22.88	25.0	0.5	81
Test 5	$R_{CFD}<0.01$, $R_{ES}<0.0001$	22.96	24.6	0.2	138
Test 6	$R_{CFD}<0.1$, $R_{ES}<0.0001$	22.88	13.7	0.3	48
Test 7	$R_{CFD}<0.001$, $R_{ES}<0.1$	22.87	25.1	0.1	274

Note: $T_{roomCFD}$ – room air temperature obtained from CFD; $Q_{surfaceES}$ – convective heat flux at south wall obtained from ES; $\Delta Q_{surface}= Q_{surfaceES}- Q_{surfaceCFD}$; $Q_{surfaceCFD}$ – convective heat flux at south wall obtained from CFD; Time: computing time.

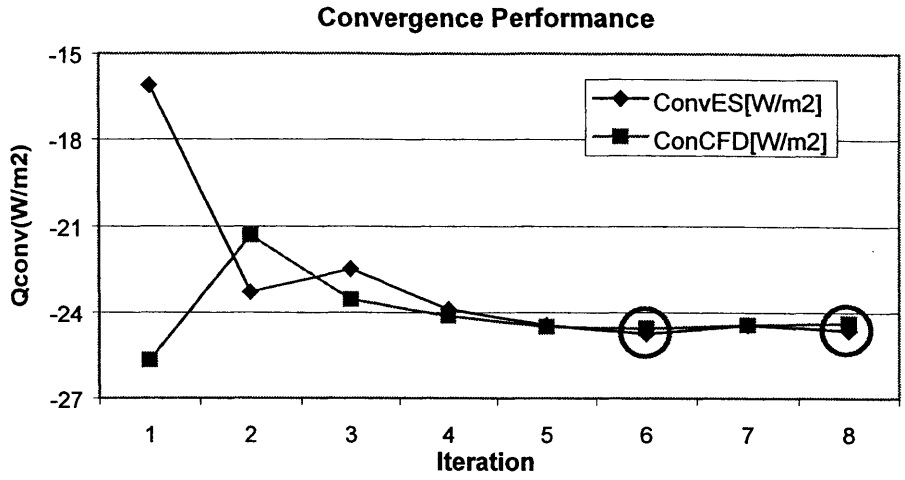

Figure 7.17 Convergence of one-time-step dynamic coupling over two days using method-1 (Case2) (ending points in circles)

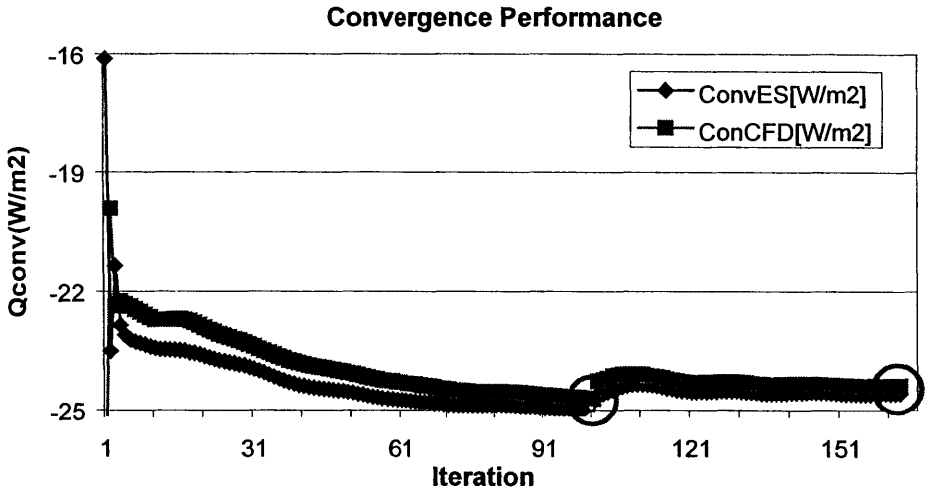

Figure 7.18 Convergence of one-time-step dynamic coupling over two days using method-1 (Case5) (ending points in circles)

7.3.5 Effect of Control Sensor Location on the Coupling Simulation

The study further investigates the control performance of indoor air temperature sensor in a coupled simulation. In principle, a separate CFD usually has no control function and merely predicts the distributions of airflow, temperature and contaminant concentration in a space with prescribed boundary conditions. By coupling with ES, CFD can adjust the room airflow and heat transfer patterns by changing the location of temperature control point. In the CFD part of a coupled simulation, a user can select a sensor location (a temperature reference point) whose temperature will be maintained at the controlled value during the calculation. The indoor air temperature gradient between

this controlled point and the air close to each surface is then transferred to ES for the calculation of supply energy requirement. Different sensor locations produce different indoor air temperature distributions and therefore demand different energy supplies for the space.

Figure 7.19 illustrates how the variation of the sensor location in CFD can change the temperature distribution in the space. It is obvious that, for this winter situation, the case with the sensor located at the bottom of the space requires more energy than the one with the sensor at the top of the space, because the warm supply air is at the top level of the space.

7.3.6 Effect of Uniform Surface Assumption on the Coupling Simulation

The theoretical study indicates that, to be consistent with the nodal model of ES, CFD has to use a uniform surface temperature or uniform heat flux assumption at the inter-coupled boundaries. The uniform assumption may not be accurate for most cases. It is meaningful to study the influence of this assumption on coupling solutions.

The influence of the uniform assumption is obviously case-dependent. For the cases with large gradients of surface temperature or heat flux, the influence may be large. The present test case has about 2 °C air temperature difference between the top and bottom level of the space. The study examines the influence of the uniform surface temperature assumption on solutions by evenly dividing the dominant south surface of the test case into three pieces from the top to the bottom. The results are compared with those with one uniform south surface temperature.

As shown in Table 7.6 and Figures 7.20 and 7.21, the two cases have no substantial differences in total sensible energy requirement, flow pattern, convergence performance, and computing time. The effect of the uniform assumption is localized at the area near the boundary. The findings are further verified by more case studies, such as those with displacement ventilation where significant temperature stratification usually exist. Those results and analysis will be further presented in Chapter 9.

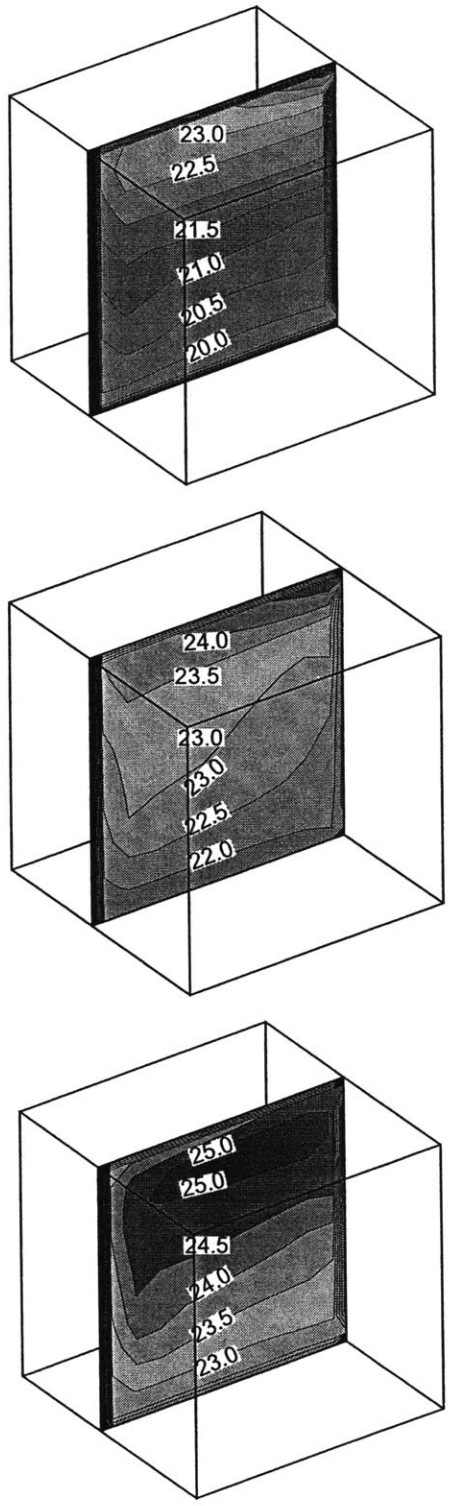

Figure 7.19 Temperature and velocity distribution at the middle section of the room, $T_{control}$=23°C
(a) top: control point at the top of room; (b) middle: control point in the center of room;
(c) bottom: control point at the bottom of room)

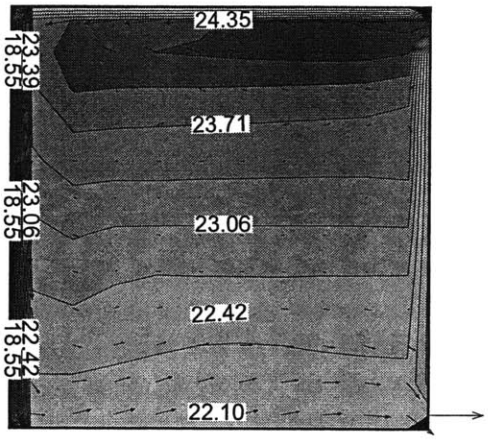

Figure 7.20 Temperature and velocity distribution at the middle section of an empty room with a one-piece south-facing exterior wall

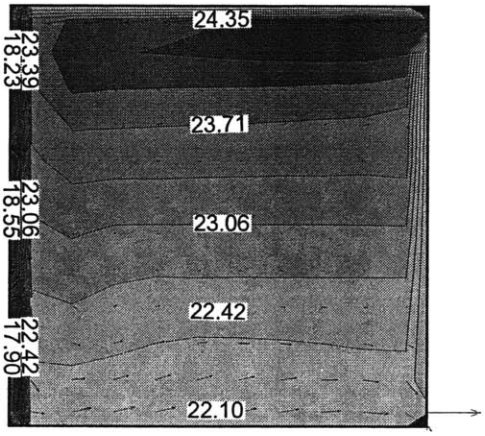

Figure 7.21 Temperature and velocity distribution at the middle section of an empty room with a three-piece south-facing exterior wall

Table 7.6 Results comparison for empty room with uniform/non-uniform surface temperature assumptions

South Wall	Q_{total} (W)	T_{south} (C)			$\Delta T=T_a-T_{room}$ (C)			h_{south} (W/m^{2}K)			Q_{south} (W/m^2)			R_{CFD} (<)	Time (s)
		Top	Mid	Low	Top	Mid	Low	Top	Mid	Low	Top	Mid	Low		
1-Piece	383	18.04	18.04	18.04	-0.004	-0.004	-0.004	4.84	4.84	4.84	24.0	24.0	24.0	0.23%	85
3-Piece	382	17.81	18.24	17.29	0.624	-0.003	-0.651	4.34	5.83	4.24	25.2	27.7	21.5	0.24%	85

Note: Q_{total} – total energy requirement for space; T_{south} – south wall surface temperature; T_a – indoor air temperature close to south wall; T_{room} – room control temperature; h_{south} – convective heat transfer coefficient at south wall; Q_{south} – convective heat flux from the south wall; R_{CFD} – final residuals in CFD; Time – computing time.

7.3.7 Effect of Negative Convection Coefficient on the Coupling Simulation

The theoretical study discussed the effect of negative convective heat transfer coefficient, which may arise in coupling method-2, on the convergence and stability of a coupled simulation. The analysis indicates that the negative convective heat transfer coefficient, h, may cause convergence and stability problems, although not necessarily. Larger negative h may have higher possibility of adverse effects.

To verify this conclusion, this section deliberately designs a case that may have a negative h at some surface using coupling method-2. The case is exactly the same as the previous one except with a colder winter design condition in Alaska, which may lead to a negative h in the room. The new iteration and control algorithm and the zero-equation model are employed in this simulation. The study tests the case with both method-1 and method-2 to compare the simulation results.

Table 7.7 shows the primary results of the calculations. The results from method-1 and method-2 look very close, so does the computing cost. Method-2 does generate a negative h at the bottom surface; however, the value is small (-0.5 W/m^2K), which has little impact on the convergence of the current simulation. The h values at the south surface from both methods are similar, which states that the temperature distribution is quite uniform in this case and the temperature gradient between the air close to the surface and the central control point is small.

More numerical experiments in the research verify that a large and negative h does cause the instability and divergence of simulation. No solutions can be obtained under those circumstances, as indicated by the theoretical analysis.

Table 7.7 Results of Alaska office case

	Q_{total} (W)	Q_{surfES} (W/m^2)	$Q_{surfMCFD}$ (W/m^2)	$Q_{surfCFD}$ (W/m^2)	$\Delta Q_{surface}$ (W/m^2)	$T_{southES}$ (C)	$T_{southCFD}$ (C)	h_{south} (W/m^2K)	h_{bottom} (W/m^2K)		R_{CFD} (<)	Time (s)
M-1	747	51.99	51.87	51.51	0.48	15.30	15.30	7.11	6.56		0.10%	47
M-2	749	52.01	51.97	51.97	0.04	15.29	15.29	6.74	-0.50		0.10%	43

Note: M-1: Method-1; M-2: Method-2

Q_{total} – total energy requirement for space; Q_{surfES} – convective heat flux at south wall from ES; $Q_{surfMCFD}$ – convective heat flux at south wall from CFD based on mean h and T; $Q_{surfCFD}$ – integral convective heat flux at south wall from CFD; ΔQ_{surf}= Q_{surfES}- $Q_{surfCFD}$; $T_{roomCFD}$ – control room air temperature in CFD; $T_{southES}$ – south wall surface temperature from ES; $T_{southCFD}$ – south wall surface temperature from CFD; h_{south} – convective heat transfer coefficient at south wall; h_{bottom} – convective heat transfer coefficient at floor; R_{CFD} – final residuals in CFD; Time – computing time.

7.4 Conclusions from Theoretical Analysis and Numerical Experimentation

This chapter investigates the existence, uniqueness, accuracy, convergence, and stability of numerical solutions of ES-CFD coupling simulation. Both the theoretical analysis and numerical experimentation verify that the iteration between ES and CFD programs can lead to a correct and converged solution.

The study analyzes the mathematical and numerical performance of four different data coupling methods. Although mathematically identical, these methods have different influences on the accuracy, convergence, stability, and computing time of a coupled simulation. In general, coupling method-1, which transfers enclosure interior surface temperatures from ES to CFD and returns convective heat transfer coefficient and indoor air temperature gradients from CFD to ES, is more stable than other coupling methods. The method can unconditionally satisfy the convergence condition when the heat transfer coefficient h is larger than zero. Coupling method-3, which transfers enclosure interior surface temperatures from ES to CFD but returns convective heat flux from CFD to ES, is most computationally expensive, because it performs explicit iteration in ES while the others are implicit. Coupling method-2, which transfers enclosure interior surface temperatures from ES to CFD and returns the nominal convective heat transfer coefficient based on the temperature gradients between surface and mean indoor air/control air temperatures from CFD to ES, has very similar performance as method-1, except that it may bring negative h values for some particular cases. The large negative h value may cause convergence and stability problem of the simulation. Coupling method-4, which transfers interior convective heat flux from ES to CFD and returns convective heat transfer coefficient and indoor air temperature gradients from CFD to ES, cannot properly control indoor air temperature. This investigation has developed an improved iterative coupling and control algorithm to solve the problem. The new algorithm, in fact, accelerates the convergence of all the coupling methods. Moreover, the iteration and control algorithm developed allows easy control of the indoor environment and space energy requirement by adjusting the thermal sensor location. The investigation further demonstrates that a reasonable convergence criteria can help quickly achieve accurate solutions of a coupled simulation.

CHAPTER 8

CASE STUDIES: VALIDATIONS AND APPLICATIONS

This chapter reports the validations of the coupled program with experimental data from four full-scale building experiment facilities. The comparison of the numerical solutions with the experimental data reveals the advantages of the integrated building simulation over the separate ES and CFD applications. The chapter further demonstrates the capabilities of the coupled program through two practical building design projects.

The four full-scale building experiments used to validate the coupled program include the study of:

(1) cooling load in a room with displacement ventilation (Chen 1988);
(2) natural convection in a room without and with radiator (Lomas et al 1994);
(3) convective heat transfer coefficients in a room with radiator (Wallenten 1998);
(4) mixed convection in a glazed atrium (Hiramatsu et al 1996).

By comparing uncoupled and coupled simulation results with experimental data, the research tries to examine the performance of the E+MIT-CFD program, in terms of the solution accuracy, convergence and reliability. The study further demonstrates the capability and importance of the coupling simulation for the design of energy efficient buildings and systems through two design projects:

(1) ventilation system design for a large-scale indoor auto racing complex;
(2) displacement ventilation system design for a Boston office building.

8.1 Cooling Load in a Room with Displacement Ventilation

8.1.1 Case Description

The uniform indoor air temperature assumed by ES models is not true for most indoor spaces. The assumption may cause serious problems in predicting building heating/cooling load for cases with air temperature stratification. Chen (1988) conducted an experimental and numerical investigation on a full-scale climate chamber studying the influence of temperature profiles on the heating/cooling load prediction. The experimental chamber, shown in Figure 8.1, is 5.6 m long, 3.0 m wide, and 3.2 m high. Table 8.1 shows the material properties of the room enclosures. The thermal conditions of spaces above and below the room were controlled to be the same as those of the test chamber. The walls can be electrically heated so that the heat loss through them is zero, simulating adiabatic conditions. The room temperature was initialized at 23.0 °C, after which a step heat input of 950 W was uniformly applied to the Venetian blinds to simulate solar radiation. The room was cooled by displacement ventilation at a rate of 7 ACH. The temperature at the center of the occupied zone (x = 2.8 m, y = 1.5 m, z = 0.9 m) was controlled at 23.0 °C.

Chen's study measured the cooling load at the starting period. With uniform temperature assumption, ES overpredicted the cooling load. This was because the air temperature difference between the ceiling and the controlled point was larger than that between the floor and the controlled point. Thus, more heat was transferred into the ceiling than obtained from the floor during the initial hours of cooling. With the assumption of uniform air temperature distribution, the heat transferred to the ceiling is the same as that obtained from the floor. The extra heat was considered to be a part of the cooling load and therefore the ES overpredicted the cooling load. Chen then used the non-linear temperature gradient functions generated by curve-fitting the CFD results to produce a reasonable prediction of the cooling load (Chen 1988).

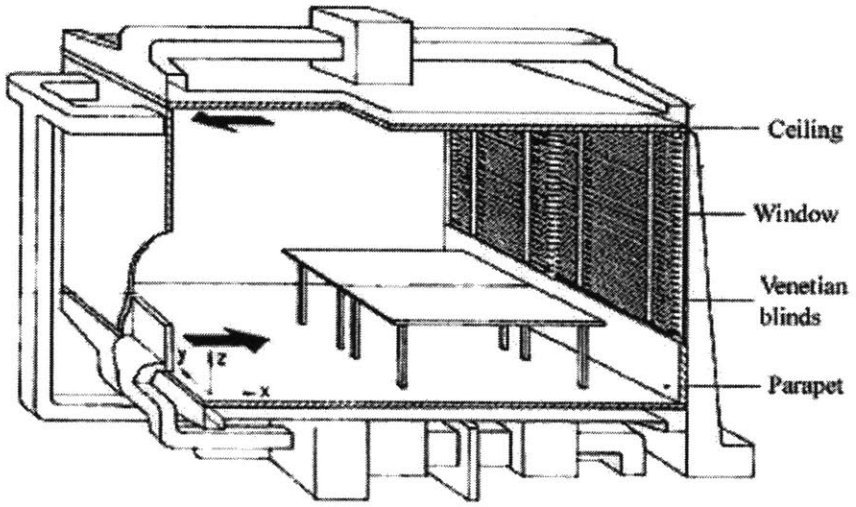

Figure 8.1 Delft climate chamber

Table 8.1 Room enclosure materials

Enclosure	Thickness (m)	Density (kg/m^3)	Specific Heat (J/kg-K)	Thermal Conductivity (W/m-K)
Ceiling	0.175	2300	840	1.9
Floor	0.175	2300	840	1.9
Rear wall	0.140	700	840	0.23
Side walls	0.140	700	840	0.23
Parapet	0.100	30	1470	0.035
Window	Outside glass: thickness 0.6 cm, absorption coeff. 0.018 Inside venetian blinds: slat angle 45°, slat width 5.5 cm The height between two slats 5.0 cm, absorption coeff. 0.3			

8.1.2 Simulation and Results

This study uses the coupled program to simulate the cooling load of the room with the static bin coupling strategy. The indoor air temperature gradient functions obtained by Chen (1988) were implemented in E+MIT-CFD as the bin that ES can directly exploit.

Since the investigation focuses on the cooling load of the space, the direct load calculation model of EnergyPlus, the "purchased air" model, was employed, which does not require the specification of systems. Although the "purchased air" model implies a variable air volume system, whereas the experiment had a constant air volume system, the macro-effect on the room energy balance being concerned is unchanged.

The study models the heat source of the space – the heated Venetian blinds – as an electrical heater. The radiative/convective heat split was introduced using experimentally determined heat transfer coefficients (Chen 1989). These coefficients were based on measured temperatures and heat fluxes at steady state, and yielded a 70 percent convective load. In reality, the radiative/convective split varies with time, with the radiative portion decreasing as the room walls heat up. However, since there is no transient heat transfer split coefficient available, the load was initially calculated with 70 percent convection for the whole process. The entire energy simulation was performed with a time step of ten minutes.

Figure 8.2 presents the predicted cooling load with and without coupling, compared with the measurement. The cooling load approaches the steady-state value of 950 W as the space and walls heat up. The simulation without coupling significantly overpredicts the cooling load, as explained above. The results with the static bin coupling agree with the experimental data, although the fixed 70 percent convective load still overestimates the cooling load for the first three hours of the experiment. The fixed 70 percent convective split may not be accurate for this dynamic cooling process. The heat load from the blinds initially has a larger radiative portion since the walls are cooler than they are at steady-state. To account for this, a coupled simulation was performed with an arbitrary hourly schedule for the radiative/convective load split, with the convective load increasing from 54 to 70 percent, such that the simulation results match the experimental data. This arbitrary schedule was then used for the separate ES, which still significantly overpredicts the cooling load.

This validation verifies that the non-uniform indoor air temperature distribution is important to the heating/cooling load calculation of some buildings. The coupling of CFD and ES can improve the accuracy of building simulation. The static bin coupling strategy is an effective and efficient coupling method if appropriate bin functions are available. Although this validation did not involve a direct coupling of CFD with ES, similar results can be obtained if such a coupling is employed (Chen 1988).

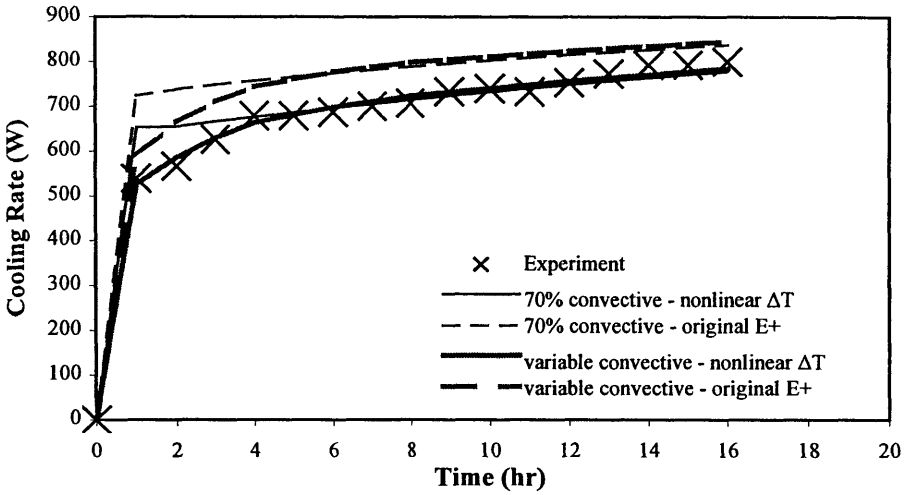

Figure 8.2 Transient cooling load for Delft climate chamber

8.2 Natural Convection in a Room without or with a Radiator

8.2.1 Case Descriptions

This study further validates the coupled program by using the International Energy Agency (IEA) Annex 21/Task 12 test facility (Lomas et al. 1994). The test facility was built for the particular purpose of providing reliable measurement data for empirical validation of building energy simulation programs.

Located at Cranfield airfield 70 km northwest of London, the IEA test rooms comprised eight semi-detached rooms with roof spaces, as shown in Figure 8.3. Three of them were highly monitored test rooms with single glazing window, double glazing window and opaque infill panel at the south wall, respectively. The rooms were of lightweight, timber framed construction with a concrete slab floor elevated above the ground, and were tightly sealed to prevent infiltration. Experimental data including surface temperature, room air temperature, relative humidity, and solar radiation were collected carefully over an unheated period of ten days in May 1990 and a heated period of ten days in October 1987. The first three days were considered as a start-up period to lessen the effects of initial conditions. In the heating scenario, an oil-filled electric panel radiator with a maximum power of 680 W was used to heat the rooms to a set-point of 30°C from 06:00 to 18:00. The complete geometric and operational information of the test site can be found in IEA reports (Lomas et al. 1994). The experimental data has been used to assess the performance of many building simulation programs. Considerable differences among the simulations were found and few predictions can lay within the error bands for all the measured data. The present study investigates both the unheated and heated cases with double glazing south window to demonstrate the dynamically coupled simulation.

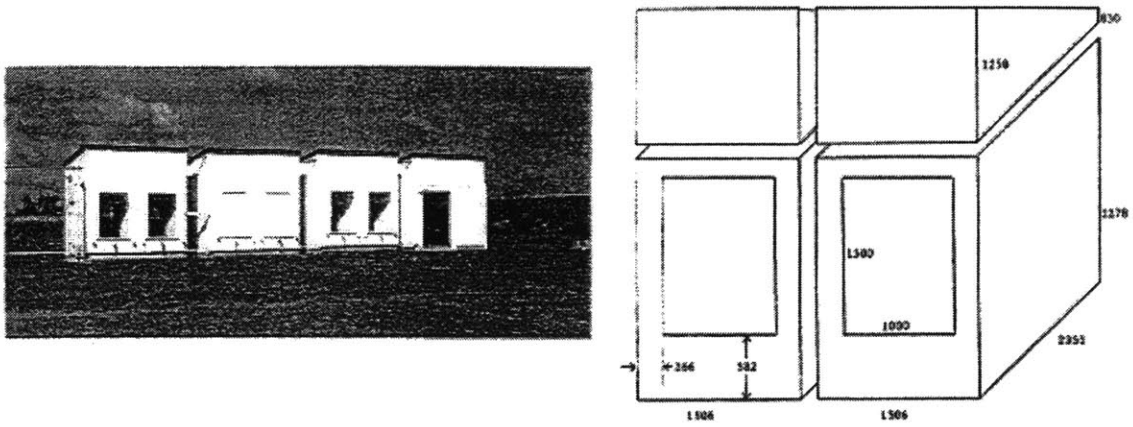

Figure 8.3 IEA empirical validation test rooms

8.2.2 Simulation and Results of the Room without a Radiator

The study first investigates the natural convection and heat transfer in the test room without radiator. Figure 8.4 shows the built simulation model of the test facility with the geometry and materials information from the IEA report. The model consists of two zones – test room and roof space. The envelopes of the facility are exposed to the outdoor environment except the west wall that is adiabatic because of the identical next room. Exterior shading from the neighboring test buildings is also included by using a detached shading surface. Detailed modeling algorithms for solar radiation, building envelopes and indoor air in EnergyPlus (Crawley et al. 2000) were employed in the energy simulation with a ten-minute time step, under the real outdoor climate conditions for the experimental period (5/21-5/30, 1990). In a coupled simulation, CFD only modeled the test room, which was divided into 14×21×19=5,586 non-uniform grid cells. The coupled simulation used the full dynamic coupling strategy with data coupling method-1 to exchange information between ES and CFD. The coupling frequency was set at each hour for all ten days. The first three days worked as the warm-up period of the simulation and the results of the rest days were analyzed. The total computing time of the coupled simulation is about 1 hour 45 minutes on a PIII-900MHz desktop PC when using Xu's zero-equation turbulence model in CFD.

Figure 8.5 shows the variations of indoor air velocity and temperature in the middle plane of the room in a typical test day, predicted by CFD with the real-time boundary conditions obtained from ES. The figures exhibit how the outdoor conditions influence the indoor airflow patterns through the window. The indoor air temperature, although not completely uniform, has a very small gradient between the highest and lowest temperature within the room throughout the day. The air temperature is almost uniform in the core of the space whereas the larger temperature gradients occur at the regions close to the surfaces. The same uniform temperature patterns were observed in the measurement, which implies that the uniform air assumption of ES may be acceptable for this case.

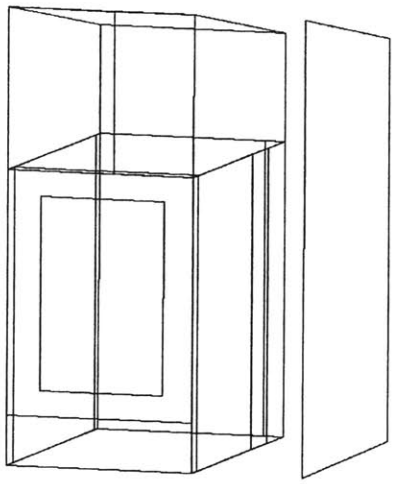

Figure 8.4 Simulation model of IEA empirical validation test room

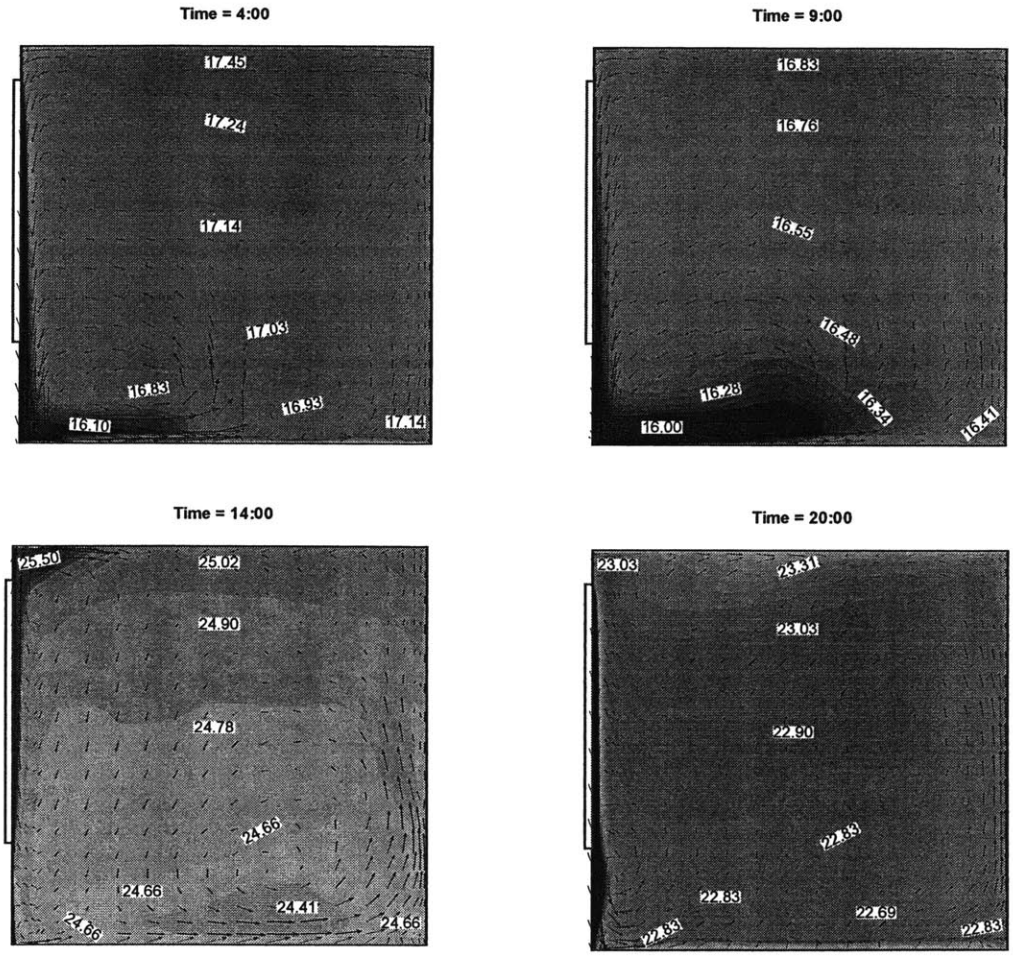

Figure 8.5 Airflow and temperature patterns vs. time in the middle plane of the room

Figure 8.6(a) compares the measured and calculated air temperature at the center of the room. The results show that EnergyPlus can produce reasonable solutions even without coupling for this case. But the coupled results have better agreement with the measurement, capturing a more accurate peak room temperature in the later afternoon. Figure 8.6(b) presents the predicted results by Negrao (1995) who used the integrated ESP-r program with the standard k-ε turbulence model.

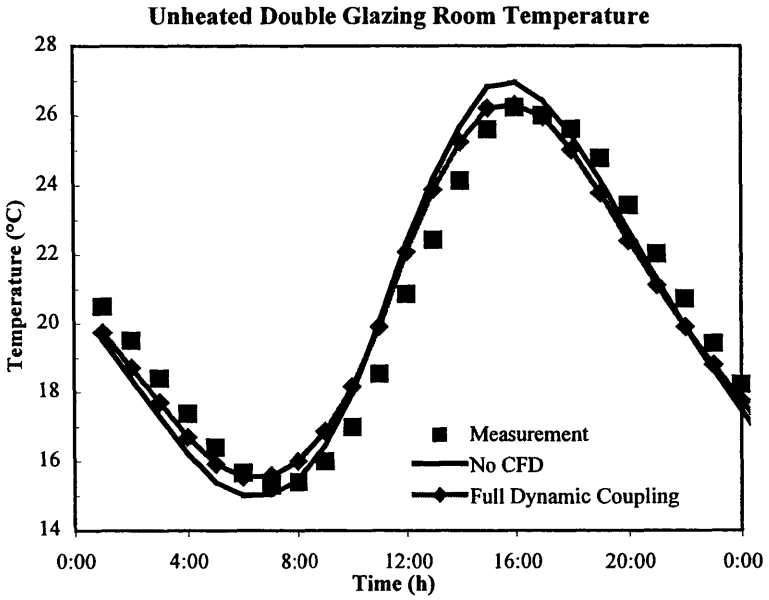

(a) from this study using integrated EnergyPlus

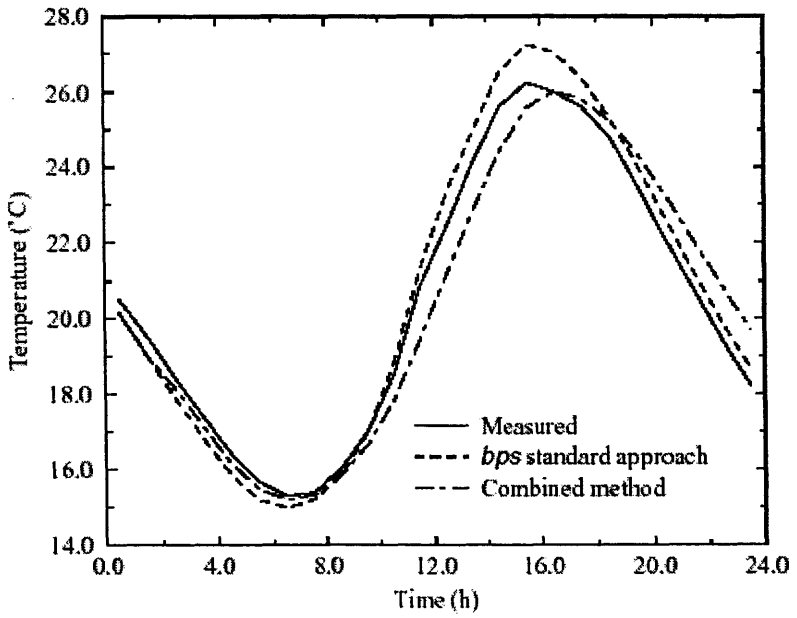

(b) from Negrao (1995) using integrated ESP-r (bps is the separate ES solver)

Figure 8.6 Air temperature of the test room.

The predicted interior surface temperatures of building envelopes show negligible difference between the coupled and non-coupled solutions, as shown in Figure 8.7 that uses the floor temperature as an example. Both the non-coupled and coupled results are close to the experimental data near the minimum value. But the discrepancies on the order of 2.0°C are observed at the region of the maximum value for both calculations. These discrepancies may be attributed to the simulation of solar radiation since it has significant impact on temperature at this time of the day. Negrao (1995) tested different solar models and found that the results were sensitive to the solar model. In addition, he raised the suspicion to the measurement because the measured floor temperature shows a tendency toward a high maximum value but suddenly at 13:00 this tendency changes to a lower maximum temperature.

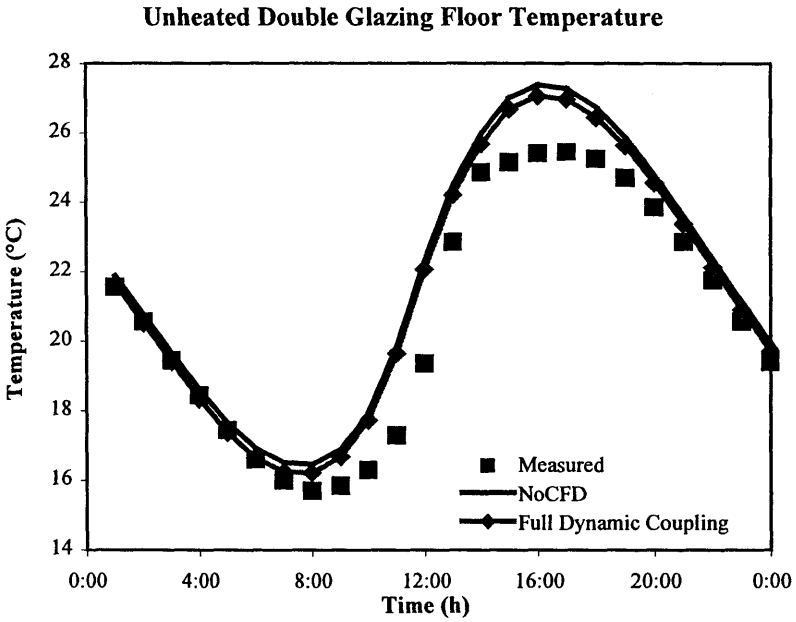

Figure 8.7 Interior surface temperature of the floor

Although it provides similar surface temperatures, the coupled simulation produces a quite different convective heat flux at the floor because of the different convective heat transfer coefficients, as presented in Figures 8.8 and 8.9. But the convective heats predicted show the similar trend and the same order of magnitude. The floor has the lowest heat flux around 12:00 when the floor temperature is closest to the indoor air temperature. The small difference of the floor and room air temperature results in the significant fluctuation of nominal convection coefficients computed by CFD, as seen in Figure 8.9. It may even lead to a negative convection coefficient. Large negative convection coefficients, if introduced into ES directly by using coupling method-2, may cause serious convergence and stability problems, as indeed occurred in the simulation.

In this case, the convection coefficients predicted by CFD, although larger than those from ES in general, have comparable orders of magnitude. This is because the

convection coefficient correlations used in EnergyPlus are specifically developed for natural convection. Acceptable convection coefficients and uniform indoor air distribution make the separate ES appropriate for this natural convection case, although the coupling provides slight improvement. The remaining discrepancy between the simulation and measurement may be attributed to other simulation models, e.g. solar models. The same conclusions were reached by Olsen (2002). His study using EnergyPlus indicated that all of the results fall within the error bounds for the unheated cases with the separate ES. Olsen's study further showed that even fairly significant changes in the convection coefficient do not have a large effect on the predictions. The errors between the simulation and measurement may be accounted for by uncertainties in input properties, the measurement error (±0.2°C), and the solar radiation model (Olsen 2002).

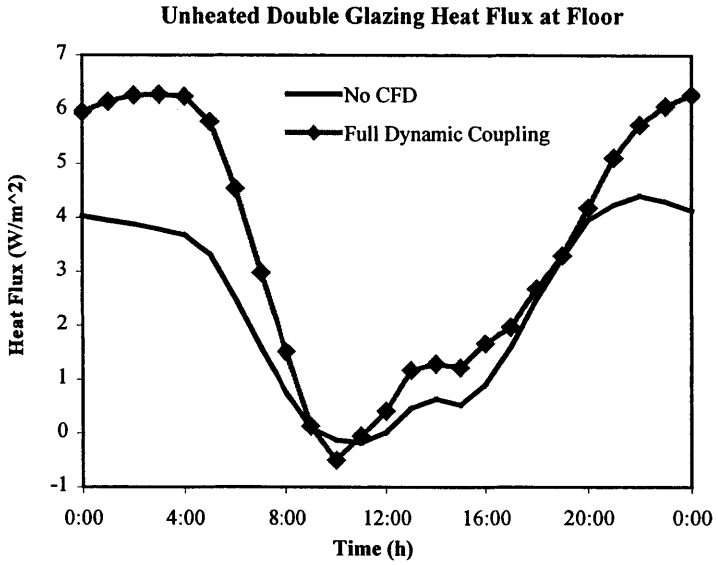

Figure 8.8 Internal convection heat flux at the floor

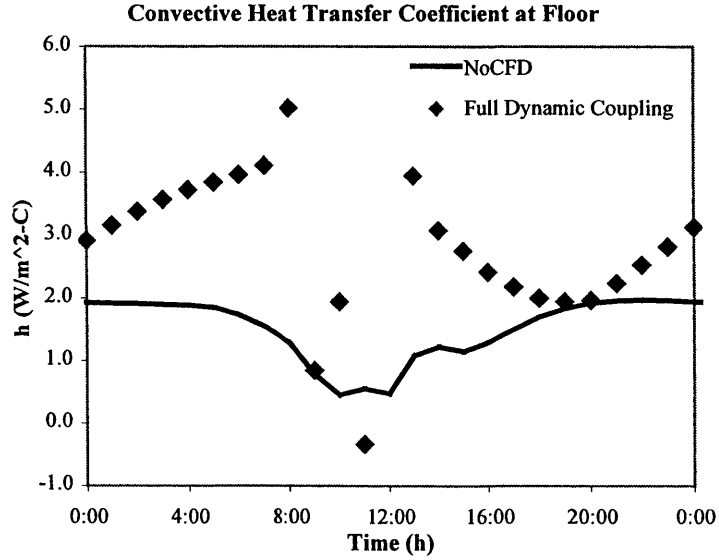

Figure 8.9 Convective heat transfer coefficient at the floor [$h=Q/(T_{surface}-T_{room})$]

To shorten the computing time of the coupled simulation, this study tests the dynamic bin coupling strategy with this validation case. In the dynamic bin coupling, the hourly quasi-dynamic coupling process was employed to model the first three days. The first two days were warm-up periods of the simulation. The dynamic results of indoor air temperature gradients and convective heat transfer coefficients in the third day were then saved and used for the energy simulation of the next seven days. This dynamic bin coupling strategy with quasi-dynamic coupling process significantly reduces the computing effort, which only needs about 15 minutes for the whole simulation with the same PCIII-900MHz computer. The results are very close to those produced with the full dynamic coupling for all ten days, as demonstrated by Figure 8.10. This is because the dynamics of airflow and heat transfer in the ten days are very similar due to the similar environmental and operational conditions. Finally, the other coupling methods, besides method-1, have also been examined. All the coupling methods can provide converged results with slight differences, as revealed by Figure 8.10.

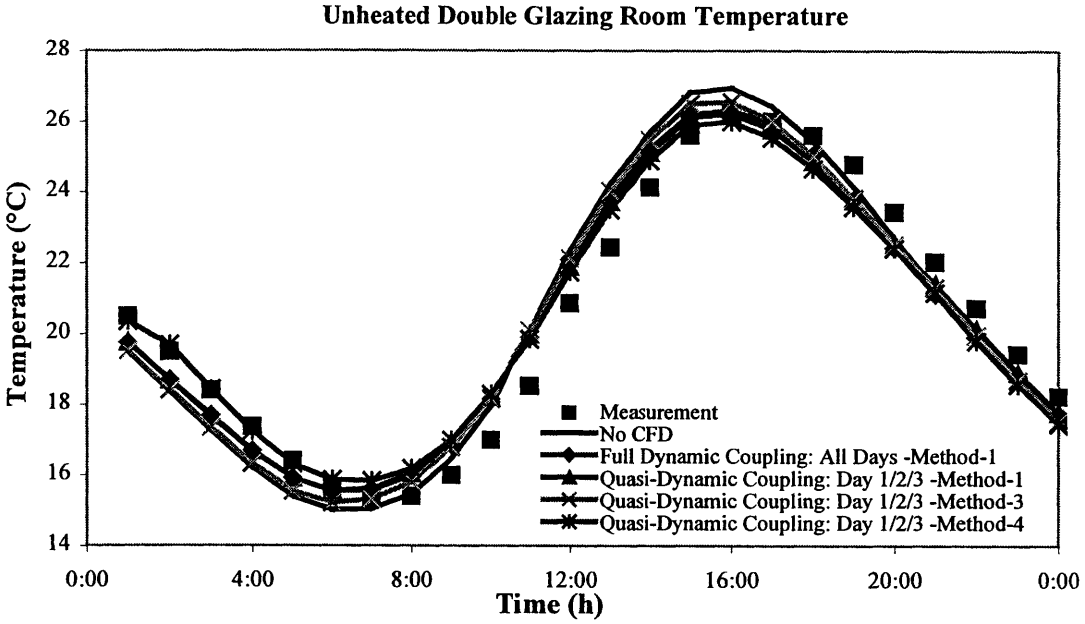

Figure 8.10 Air temperature of the test room with different simulation approaches

8.2.3 Simulation and Results of the Room with a Radiator

The simulation of the natural convection room without internal heating provides reasonable results even without the coupling because of the acceptable convection coefficient correlations and uniform indoor air temperature. However, a room with radiant heating would impose more challenges. The literatures (e.g. Lomas et al. 1994) report some interesting observations about the simulated and measured results:

- Most ES programs underpredicted the energy consumption.
- Predicted energy consumption varied considerably between programs (52% variance in the case of the double-glazed room).

- Most programs underpredicted the lowest and highest temperatures in the test room.

The IEA report (Lomas et al. 1994) discusses a number of issues that may contribute to these less-than encouraging results. The modeling of internal convection and the influence of temperature stratification are indicated as two of the primary causes for the discrepancies between programs and between simulated and measured results. This section thus simulates this heating case with the aim of identifying the effect of these two influence factors on the prediction.

The experimental facility of the heated case is exactly the same as that without heating, except that an oil-filled electrical panel radiator (L0.68×H0.57×T0.02 m) was placed under the window. The average maximum power output of the radiator was 680W. The heat output from the radiator was 60% radiative and 40% convective, which was calculated using standard empirical results for radiative and convective heat transfer from a vertical heated plate. In the experiment, the dynamic response of the radiator was represented by a first order system with a time constant of 22 minutes.

The study models the radiator using the "High Temperature Radiant System" model of EnergyPlus. Since the actual PID controller used in the experiment cannot be modeled by EnergyPlus, an operative temperature throttling range of 26-30°C, corresponding from full to zero power, was used to control the radiator. The simulation was performed under the real weather conditions of the test days (17th Oct. 1987 – 26th Oct. 1987). The hourly full dynamic coupling simulation was run for the ten consecutive days. The total computing time of the coupled simulation is about 3 hours 50 minutes with a PIII-900M desktop PC.

Figure 8.11 shows the indoor air temperature and velocity variations in a typical experimental day – Oct. 23. When the radiator is on, a plume of warm air will rise from the heater and flow along the south wall and window toward the ceiling. As a consequence, unlike the unheated case, some degree of air temperature stratification is found in the space. The greatest stratification between the ceiling and floor can be about 3.8°C. The same stratification was observed in the experiment: the stratification between top, middle and bottom sensor locations is at least 1°C 73% of the hours and at least 2°C 26% of the hours.

The predicted and measured mean air temperatures over a single day (October 23) are compared in Figure 8.12. In the experiment, the heater turned on at 6:00 but it would not heat up the air around the sensors in the room to the setpoint temperature of 30°C until approximately 11:00. This is because the radiative portion of the heat output would be absorbed by the internal surfaces before convecting into the air, resulting in a time lag in the response of the air temperature to heat injection. Both simulations captured the same heat transfer mechanics, although smaller lag times were predicted. The air temperature from the coupled simulation is closer to the measurement than that from the non-coupled simulation. The result from this study is slightly better than the result obtained by Beasoleil-Morrison (2000) who used the integrated ESP-r program. The small lag time (the predicted result is about 1 hour leading the measured value) is

probably because the current ES program cannot properly model the dynamic behaviors of the oil-filled radiator. With the present "step-function" radiator model of EnergyPlus, the time delay of power/temperature when the heater is switched on or off cannot be represented. It results in the fast temperature rise and drop in the simulation. This analysis can be partially verified by testing the case with different convective/radiant splits. The non-coupled results shown in Figure 8.13 reveal that the case with 0% radiant/100% convective split almost has no time lag to affect the indoor air temperature while even the case with 100% radiant/0% convective split still cannot have the same time lag as the measurement. Moreover, when the heater turns off at 18:00, the indoor air temperatures of all the three cases drop immediately without delay.

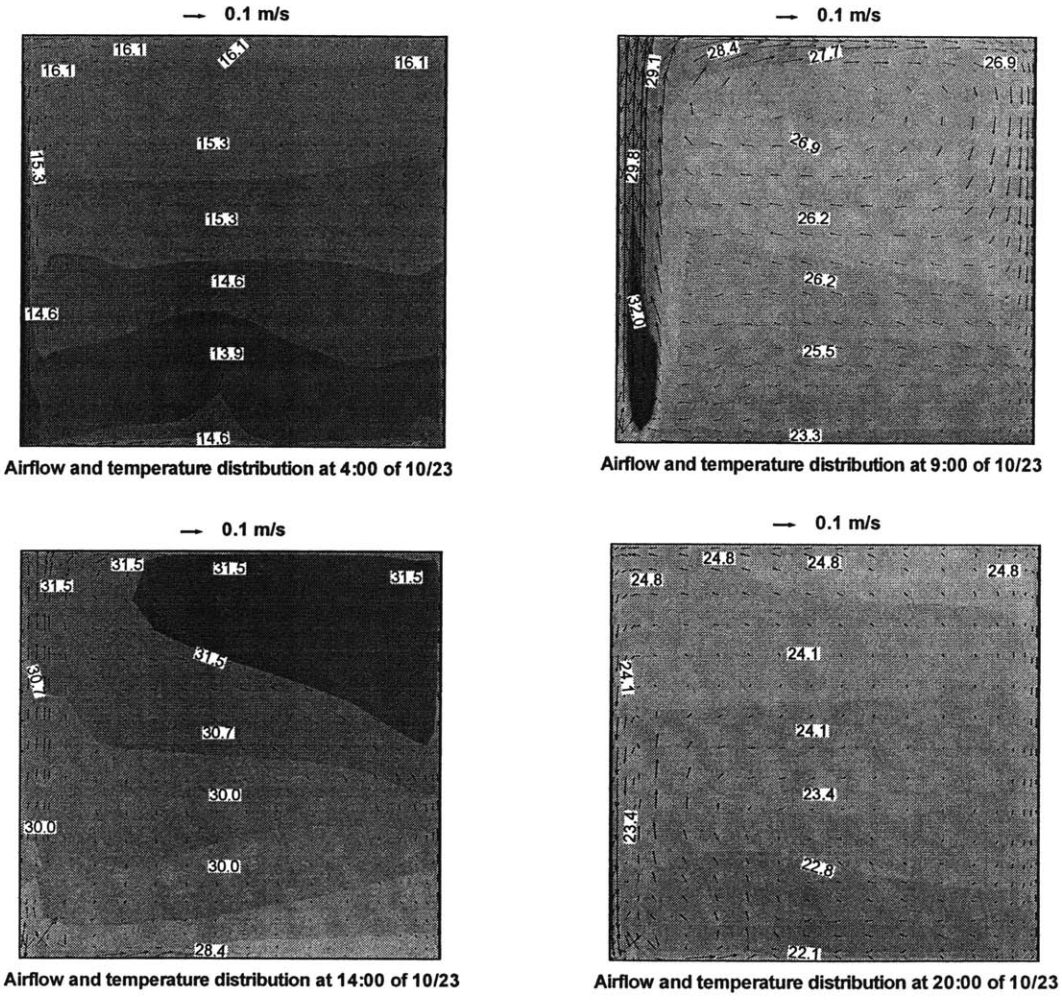

Figure 8.11 Velocity and temperature distributions in the middle plane of the test room

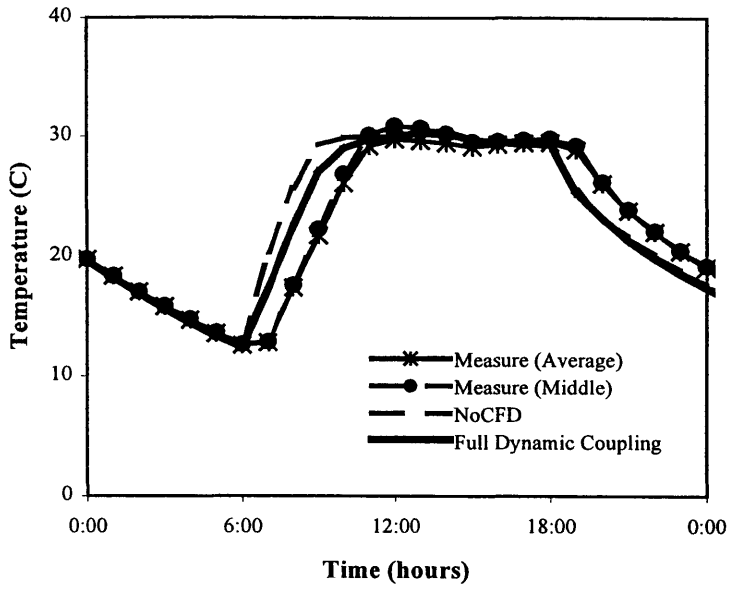

(a) from this study using integrated EnergyPlus

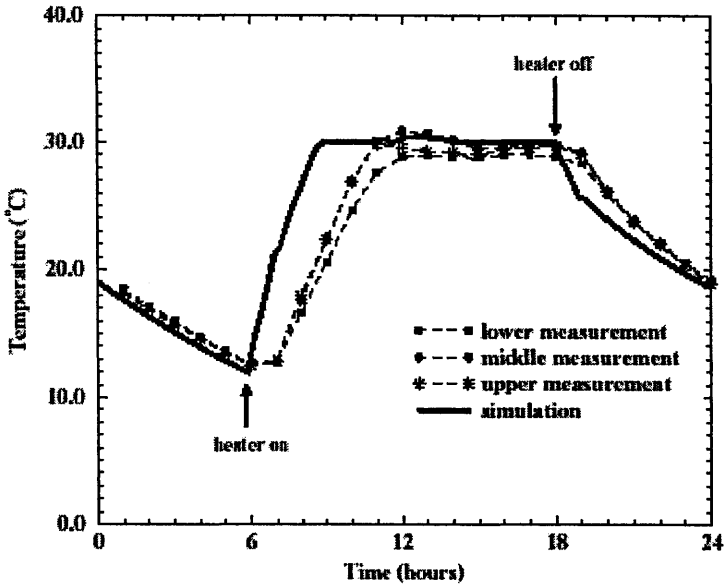

(b) from Ian Beasoleil-Morrison (2000) using integrated ESP-r

Figure 8.12 Computed and measured mean air temperature on October 23

Table 8.2 compares the daily-averaged convective heat transfer coefficients at floor, ceiling, south window, and north wall from the coupled and non-coupled simulations as well as those estimated using Khalifa correlations (1989). The coupled solutions are closer to the calculated results using Khalifa correlations that were particularly developed for the radiator-heating scenarios. Beausoleil-Morrison (2000) indicated that Khalifa correlations overestimate the h value for the window above the radiator.

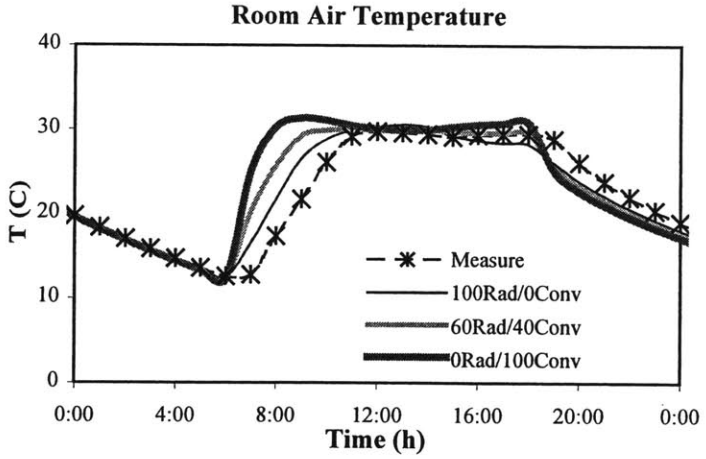

Figure 8.13 Different time delays of room air temperature rise using different convection/radiation splits of the heater

Table 8.2 Daily-averaged convection coefficients at selected enclosures

	Floor	Ceiling	South window	North wall
h_{ES} (W/m^{2}K)	1.7	1.3	2.3	1.1
h_{CFD} (W/m^{2}K)	3.7	4.0	4.8	1.9
$h_{empirical}$* (W/m^{2}K)		3.0	9.0	2.1

* developed by Khalifa (1989) for radiator-heating scenario

Although distinct convection coefficients and obvious air temperature stratifications are obtained by the coupled simulation, the coupled simulation still underpredicted the radiator energy consumption that was predicted to be 70.4 MJ for seven days, 21.2% less than the measured value of 89.4 MJ (the uncertainty bands of the measurement were reported to be from 78.1 MJ to 92.7 MJ). The coupled result has slight improvement compared to the uncoupled prediction that was 66.5 MJ. Olsen (2002) obtained very similar results by using EnergyPlus. He explained that this is primarily due to the lack of any time lag in the radiator model, which allows the air to heat up faster than it actually does, and thus allows the radiator energy consumption to decrease more rapidly.

This study then particularly investigates the sensitivity of the prediction to the convective heat transfer coefficient. The simple coefficient correlations (Eq.(3.8)-(3.12)) and detailed coefficient correlations (Eq.(3.5)-(3.7)) in EnergyPlus were, respectively, used for the non-coupled simulation. In addition, two sets of artificially enlarged convection coefficients that double and triple the constants of the simple correlations were employed to test the effect of large convection coefficients on the predictions. The results reveal that the convective heat transfer coefficient itself has very limited influence on the solutions, as shown in Figure 8.14 and 8.15. This, to some extent, demonstrates

the indoor air temperature gradients may mainly contribute to the slight improvement of the coupled results for this case.

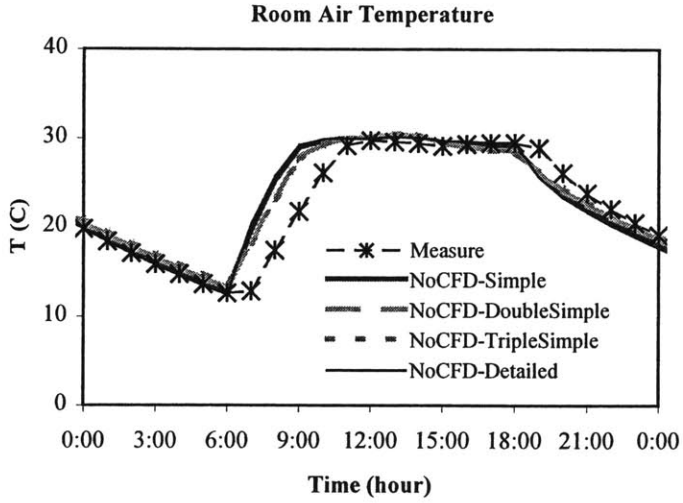

Figure 8.14 Computed and measured room air temperature on Oct. 23

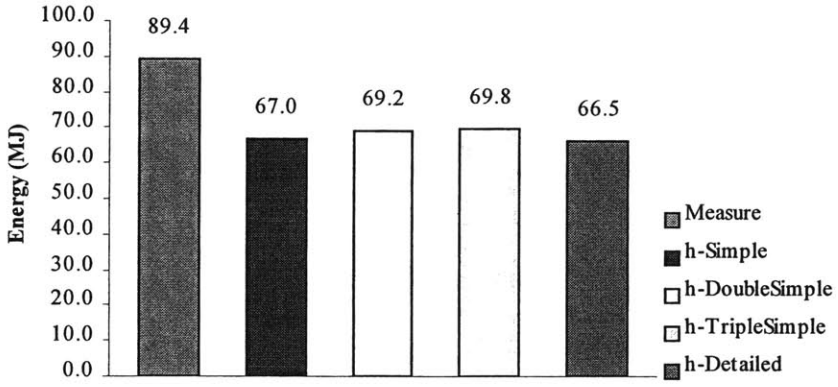

Figure 8.15 Computed and measured radiator energy consumption of seven days

In summary, this validation shows that the separate ES can predict the thermal performance of buildings with natural convection in an acceptable accuracy. The coupled simulation can slightly improve the accuracy of the results. More importantly, the coupled simulation provides the spatial and temporal distributions of indoor air velocity, temperature and concentration that are important for designing a comfortable and healthy indoor environment. However, a coupled simulation takes much longer computing time than a separate ES. A dynamic bin coupling strategy may substantially reduce this computing cost while providing reasonable results, if the changes of environmental and operational conditions between days are small. The study indicates that the convection coefficients, although under-determined by EnergyPlus, are probably not the source of the errors between the simulation and measurement. The solar model and radiator model may have more important impact for this case.

8.3 Natural Convection Coefficients in a Room with a Radiator

8.3.1 Case Descriptions

The IEA validation cases show that the convection coefficients predicted by CFD are much larger than those from the correlations in ES. Although the credibility of the convective heat transfer coefficients from CFD with simple zero-equation turbulence models have been examined using Fisher's experiments (1995), it is always desired to have the knowledge of the dynamic behaviors of the coefficients under the real environmental conditions. Few experimental data sets exist for the validation of the convection coefficient calculation under dynamic operational conditions, rather than well-controlled laboratory conditions. Wallenten (1998) conducted such an experiment in a full-size test room located in Lund, Sweden.

The test room was one of seven similar rooms inside an experimental building located in Lund, Sweden. The room had the dimensions 3×3.6×2.4 m. The south wall with a 1×1.1m window and the roof were exposed to the ambient climate. The floor was on top of a basement that held a constant temperature of 18 °C. The neighboring rooms at west and east were completely identical. The parameters of the enclosure materials and windows were completely described in Wallenten's experimental report (1998). Wallenten used various heating and ventilation strategies to condition the room throughout the experimental program. This study only investigates the unventilated room with a normal 3-pane south window. A small radiator was placed either 0.2 m from the north (back) wall in the center of the wall or 0.12 m from south wall under the window as illustrated in Figure 8.16. In the experiment, the radiator was controlled by its own bimetallic thermostat that allowed the average effect at 180W.

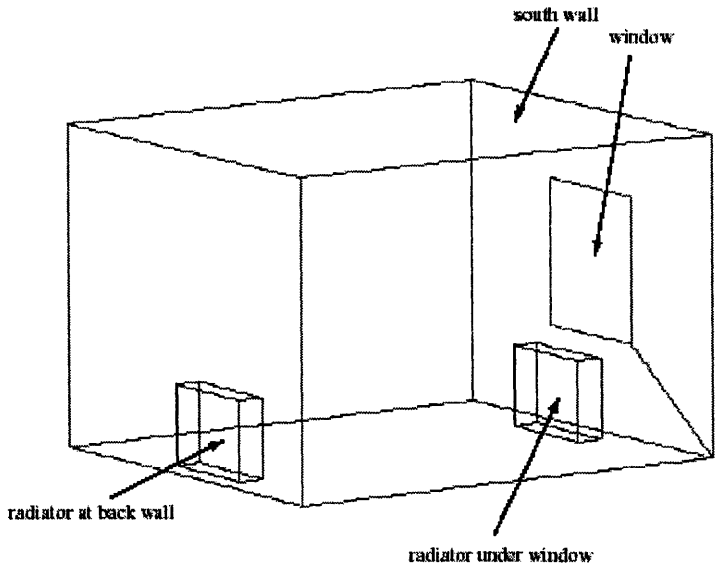

Figure 8.16 Schematic of Wallenten test room

The room was well instrumented to monitor surface, air and interstitial wall temperatures. Convection coefficients were then derived from these data using a surface heat balance that considered convection, internal long wave radiation, and conduction through the wall. In order to examine the realistic operating conditions, the dynamic heat conduction and internal long wave radiation were taken into the consideration as they were. This, however, raised the uncertainty to the calculation of convection coefficients (the accuracy of h is at best ±15% for window and ±20% for wall), which were evidenced by the scatter of h values. As a result, these scattered data are not suitable for quantitative comparison but they do demonstrate the matched trend or range between the simulated and measured results.

8.3.2 Simulation and Results

The study applied the non-coupled and coupled simulation to three different scenarios: (1) radiator-off; (2) radiator-on under the window; and (3) radiator-on at the back wall. The simulation was conducted for a seven-day experimental period in January with a ten-minute time step in ES. A climate file typical of the region was employed as no Lund weather data was available for the period of the experiments. In the calculation, the radiator was modeled using the "High Temperature Radiant System" model with 60/40 convective/radiative split. Since the radiator was on for all the simulation days, the time lag deficiency of this model is not important. In the CFD of a coupled simulation, the indoor space was divided into 26×29×24=18,096 non-uniform grid cells. Xu's zero-equation turbulence model was used to simulate the turbulence. The hourly full dynamic coupling with data coupling method-1 was adopted for all seven days. The total computing time of the coupled simulation is about 7 hour and 30 minutes with a PIII-900M PC.

The experiment found that the location of the radiator has a significant impact on convection coefficients at the window. Much higher h_c values were observed when the radiator was placed under the window than when it was placed at the back wall. Quantifying the differences is difficult due to the data scatter, but Wallenten recommends a multiplier as high as 3.5. The predicted results of this study are shown in Figure 8.17-8.18, where $h_c=q_c/(T_{ref}-T_{surface})$ and T_{ref} is the air temperature at the center of the room. When the radiator is off, the calculated h_c values at the window with coupling are similar to those without coupling, indicating the detailed coefficient correlations used in EnergyPlus are appropriate for natural convection without the radiator. However, these correlations cannot properly reflect the difference of h_c values between the case with the radiator under the window and the case with the radiator at the back wall. The h_c values provided by CFD are much higher than those from the correlations, with greater values occurring when the radiator is placed under the window. The difference is about 2 times, which is less than the observation but much more obvious than the simulated results by Beausoleil-Morrison (2000) who used the adaptive h_c correlations of the ESP-r program during the simulation.

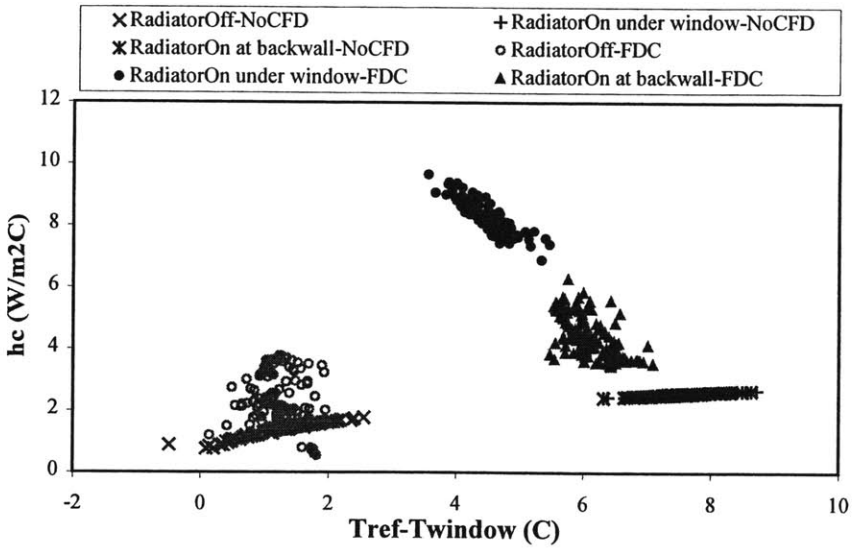

Figure 8.17 Predicted h_c at window for Wallenten test room
(NoCFD: ES only; FDC: full dynamic coupling of ES and CFD)

Figure 8.18 illustrated the predicted and measured h_c at the south wall when the radiator is placed at the back wall. The experiment observed that the heat output from the radiator significantly affected the convective regime and much higher h_c values were found when the radiator was operating. The simulation without coupling cannot capture this phenomenon because of the use of the same correlations for all the scenarios. The coupled results reveal the distinct separation of h_c values between the radiator-on case and radiator-off case. The results show good agreement with the measurement and with the simulated results from Beausoleil-Morrison (2000) using the artificial toggle of the h_c correlations according to the radiator's operational state.

This validation case further demonstrates the difference of convective heat transfer between the coupled simulation and the non-coupled simulation. The coupled simulation, even with simple zero-equation turbulence models in CFD, can provide more reasonable prediction of convective heat than the separate ES.

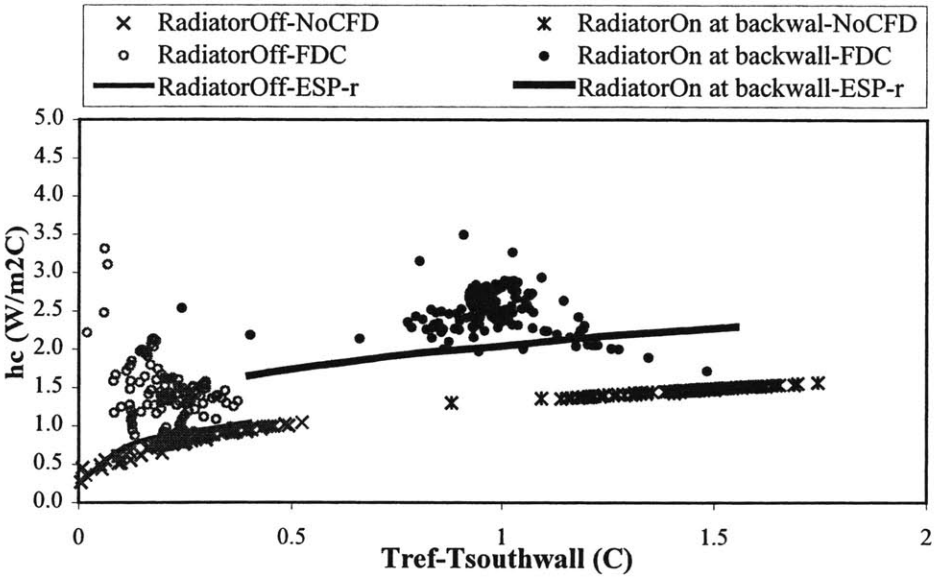

(a) prediction

(NoCFD: ES only; FDC: full dynamic coupling with E+MIT-CFD;
ESP-r: simulation with ESP-r program by Beausoleil-Morrison, 2000)

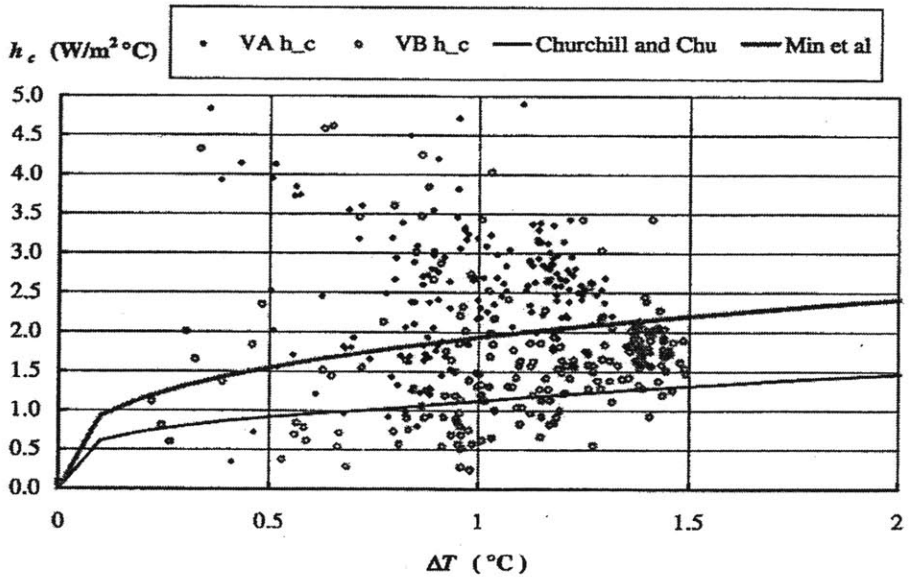

(b) measurement

(VA: measurement point 2.25m from floor and 0.6m from sidewall; VB: measurement point 1.46m from floor and 0.6m from sidewall; Churchill and Chu, Min at al: empirical correlations)

Figure 8.18 Predicted and measured h_c at south wall when the radiator is placed at the back wall in Wallenten test room (3×3.6×2.4m)

8.4 Mixed Convection in a Glazed Atrium

8.4.1 Case Descriptions

The validations on natural convection cases with or without a heater demonstrate the performance and feasibility of the dynamic coupling program developed. It is desirable to have one more validation for a ventilated building under real environmental conditions. The case used for this purpose in this section is a test facility of a full-scale glazed atrium in Japan (Hiramatsu et al 1996), as pictured in Figure 8.19. The case has plenty of measurement data for both building envelope and indoor air, which have been widely used as a reference.

Figure 8.20 illustrates the geometry and the configuration of the atrium. The atrium had glazed ceiling, south, west, and east walls. The floor and the north wall were insulated. The detailed material properties can be found in Murakami's experimental report (1994). The experiment studied natural and cooling ventilation. The present study only investigates the cooling scenarios by using opening A to supply cool fresh air and using opening B to exhaust warm indoor air. All the other openings were closed. The cooling system for the atrium had a maximum power of 32 kW and the maximum air supply volume of 4050 m^3/hr. The atrium was empty and had no partitions.

The experiment with the air cooling conditions was conducted on April 5th, 1994. The mean supply air velocity at opening A was 1.4 m/s, and the set-up supply air temperature was 15 °C. The experiment measured the outdoor air temperature, wind speed, solar radiation, indoor air temperature and velocity, interior surface temperature, as well as the solar radiation through the glazed walls.

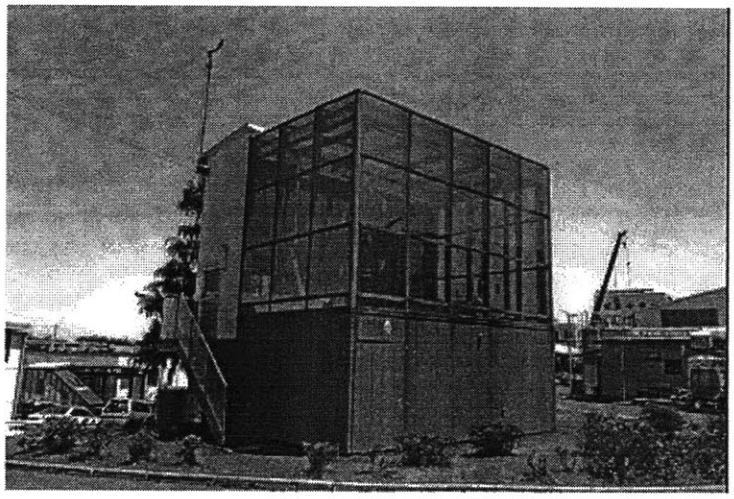

Figure 8.19 The appearance of the experimental atrium in Japan (Hiramatsu et al 1996)

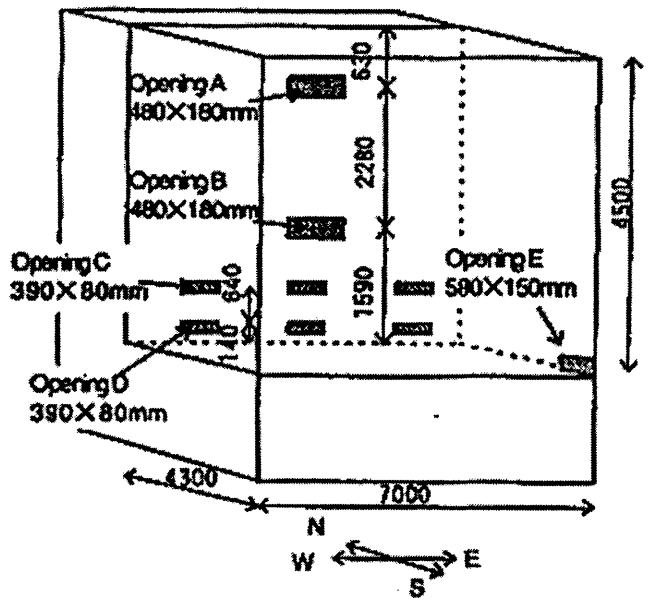

Figure 8.20 The atrium size and openings (unit: mm)

8.4.2 Simulation and Results of the Atrium without Room Air Temperature Control

The experiment supplied air at constant mass flow rate and air temperature to the space and tested the varying indoor environment during the day. The test atrium was modeled in this study with the same configuration, materials and conditions as the experiment. Since the climate data of the experimental day was not available, the required weather file was rebuilt based on the measured outdoor temperature and solar gains, as illustrated in Figure 8.21.

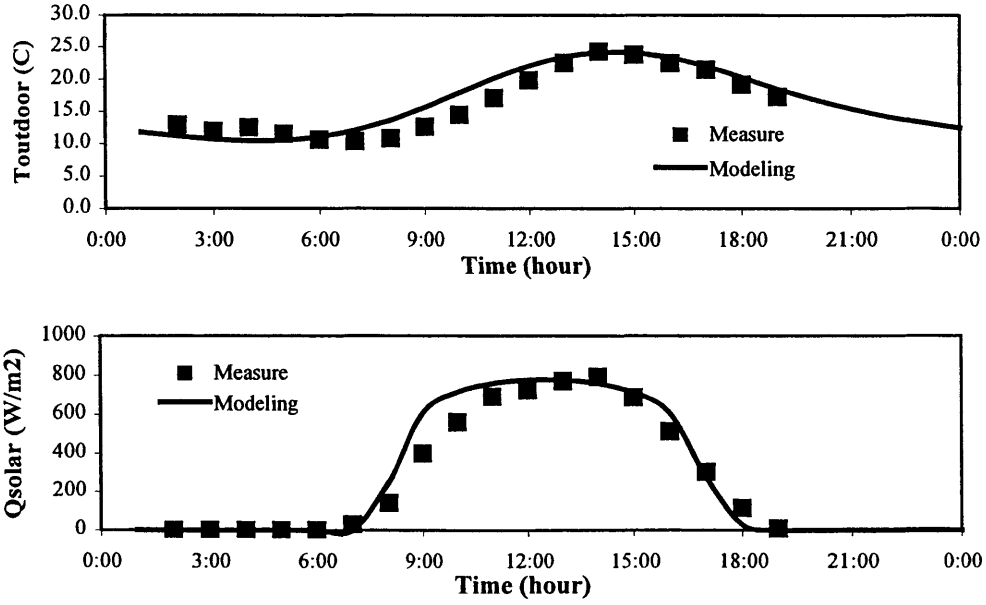

Figure 8.21 Modeled and measured weather conditions

In the simulation, the ES with ten-minute time steps was performed for the experimental day and the previous warm-up days. Detailed coefficient correlations of EnergyPlus were used in the separate ES. In the coupled simulation, CFD modeled the space with two sets of non-uniform grids: 19×10×14=2,660 and 31×18×27=15,066 cells. Xu's zero-equation turbulence model was used again to describe the turbulence. The hourly full dynamic coupling with coupling method-1 was operated for the experimental day only (not for the warm-up days) to reduce the computing cost. The results with two grids are similar, indicating the grid-independence of the solutions. The total computing time of the coupled simulation with the coarse grid is about 1 hour 30 minutes with a PIII-900MHz PC.

Figure 8.22 shows the calculated and measured indoor air temperature at the center of the atrium. The varying trends of the indoor air temperature during the day from both simulations agree with the measurement. The highest indoor air temperature is found between 14:00-15:00. The coupled simulation produces a higher peak temperature (about 2°C higher) than the non-coupled simulation. This is mainly because the non-coupled simulation underestimates the convective heat from the enclosures. Figure 8.23 demonstrates the convective heat from the south window with different simulation approaches, as an example. A significant difference of the convective heat is noticed, especially around noon when the difference is about 2 times. Consequently, the window interior surface temperature from the coupled simulation is lower (closer to the measurement) than that from the non-coupled simulation, as shown in Figure 8.24. The distinction of window temperatures between two approaches is not as much as that of convective heat, indicating radiation between the surfaces contribute significantly in this case. Note that the peak indoor air temperature predicted by the coupled simulation is still lower than the measured one. One primary reason is probably that the supply air temperature in the experiment had a significant swing with the average range of 3.7°C and the supply air temperature was even as high as 25°C around 14:00.

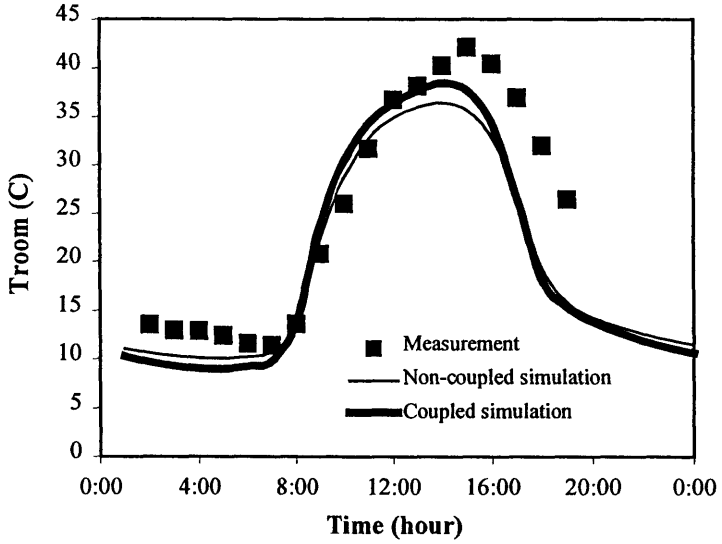

Figure 8.22 Calculated and measured indoor air temperature at the center of the atrium

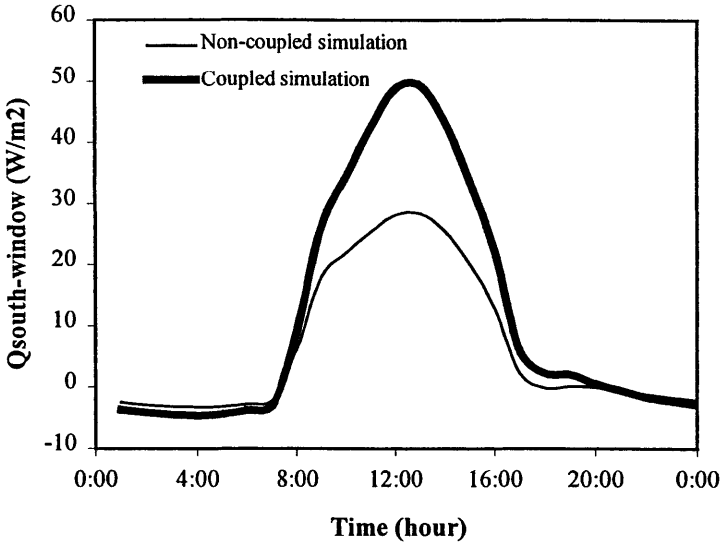

Figure 8.23 Calculated convective heat from the south window of the atrium

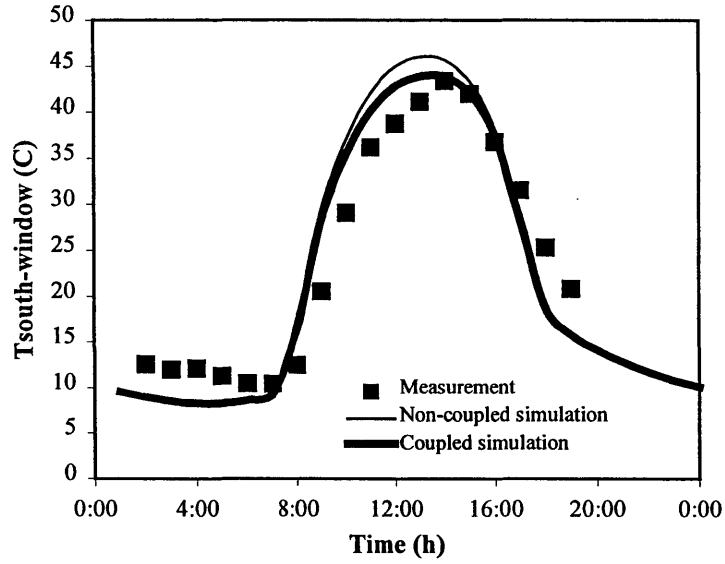

Figure 8.24 Calculated and measured south window interior surface temperature

Figure 8.25 and 8.26 further compare the calculated and measured interior surface temperatures of the floor and north wall. In general, the coupled results show a better agreement with the measurement. With the real-time boundary conditions provided by ES, CFD can predict the dynamic airflow patterns during the day, as exhibited in Figure 8.27. The predicted airflow patterns show very good agreement with the measurement presented in Figure 8.28. Because the supply air temperature is higher than the indoor air temperature during the nighttime, the supply air moves towards the ceiling after it leaves the diffuser due to the positive buoyancy effect. As the indoor air temperature rises in the

daytime, the supply air cannot horizontally reach the opposite glass wall and falls towards the floor after it enters the space. The indoor air temperature distributions at 10:00 and 12:00 are illustrated in Figure 8.29. The temperature gradient of 3°C between the top and bottom of the air space is found for both time points.

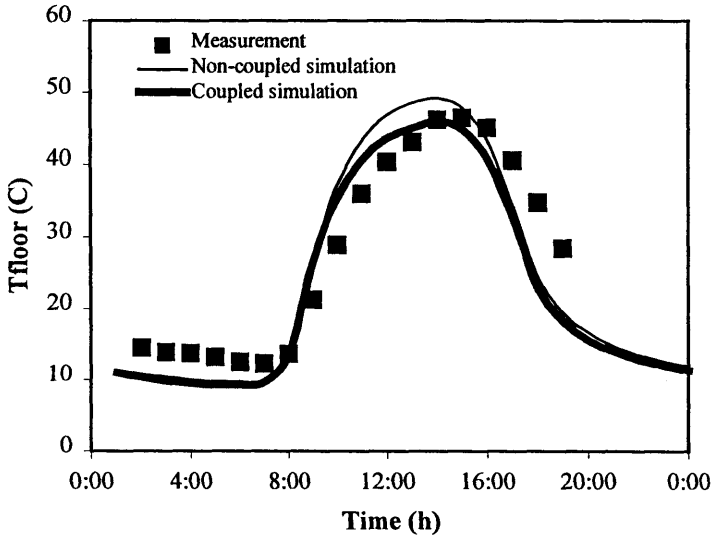

Figure 8.25 Calculated and measured floor interior surface temperature

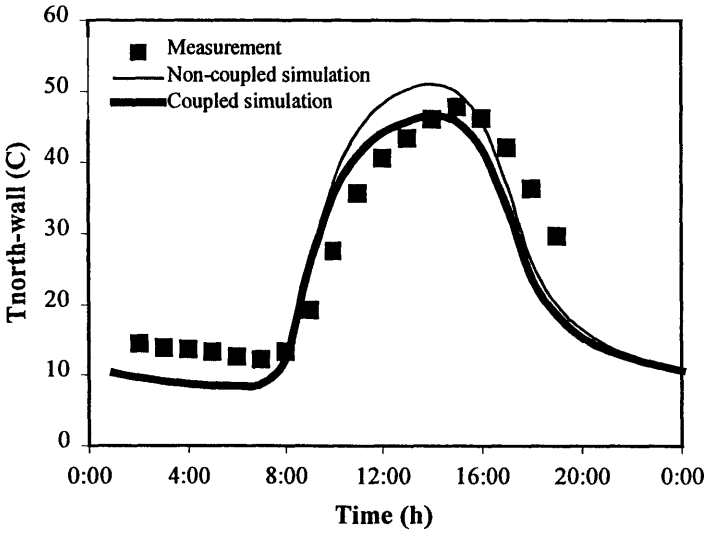

Figure 8.26 Calculated and measured north back wall interior surface temperature

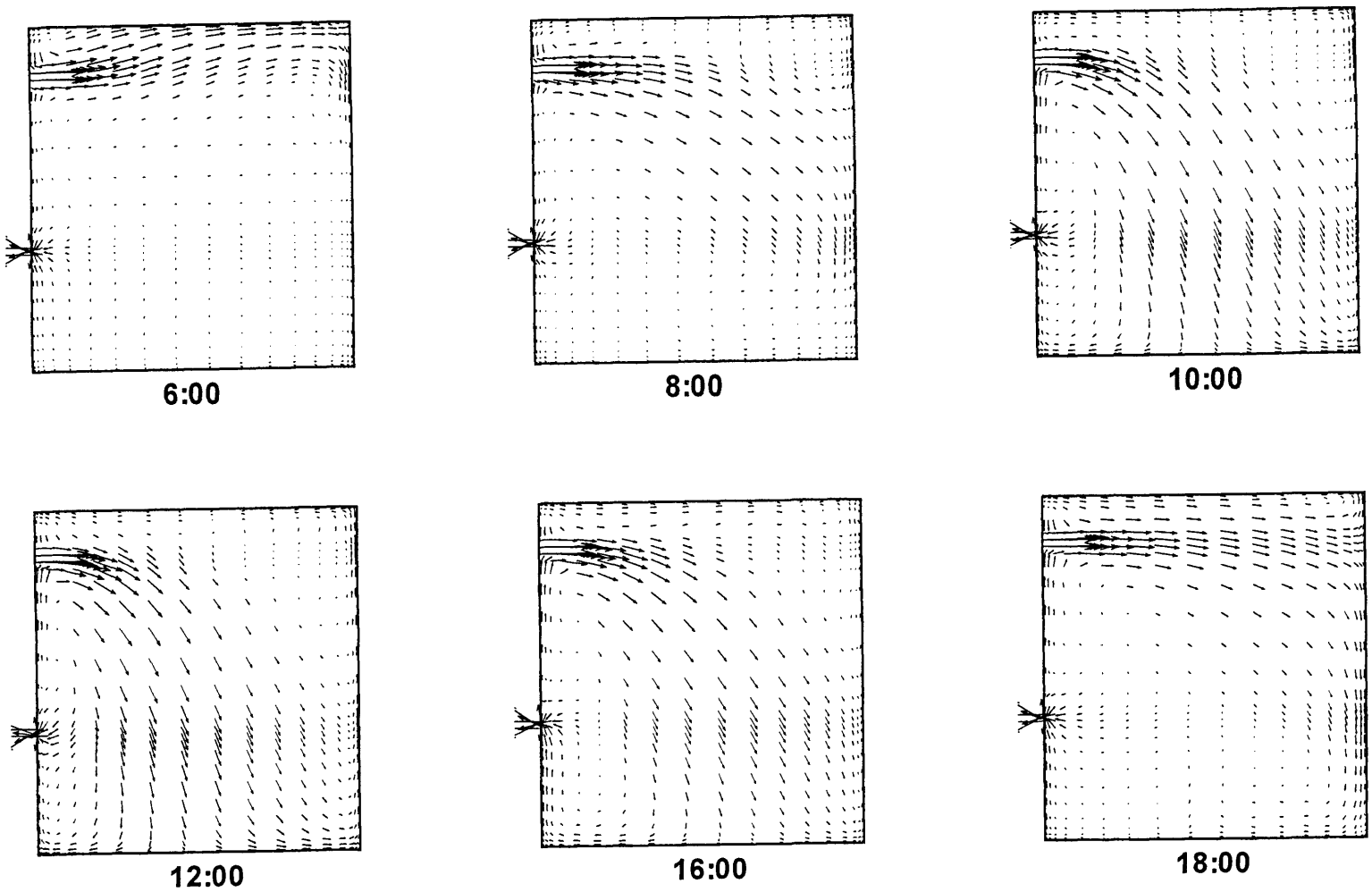

Figure 8.27 Predicted dynamic air velocity distribution in y-z middle plane of the room

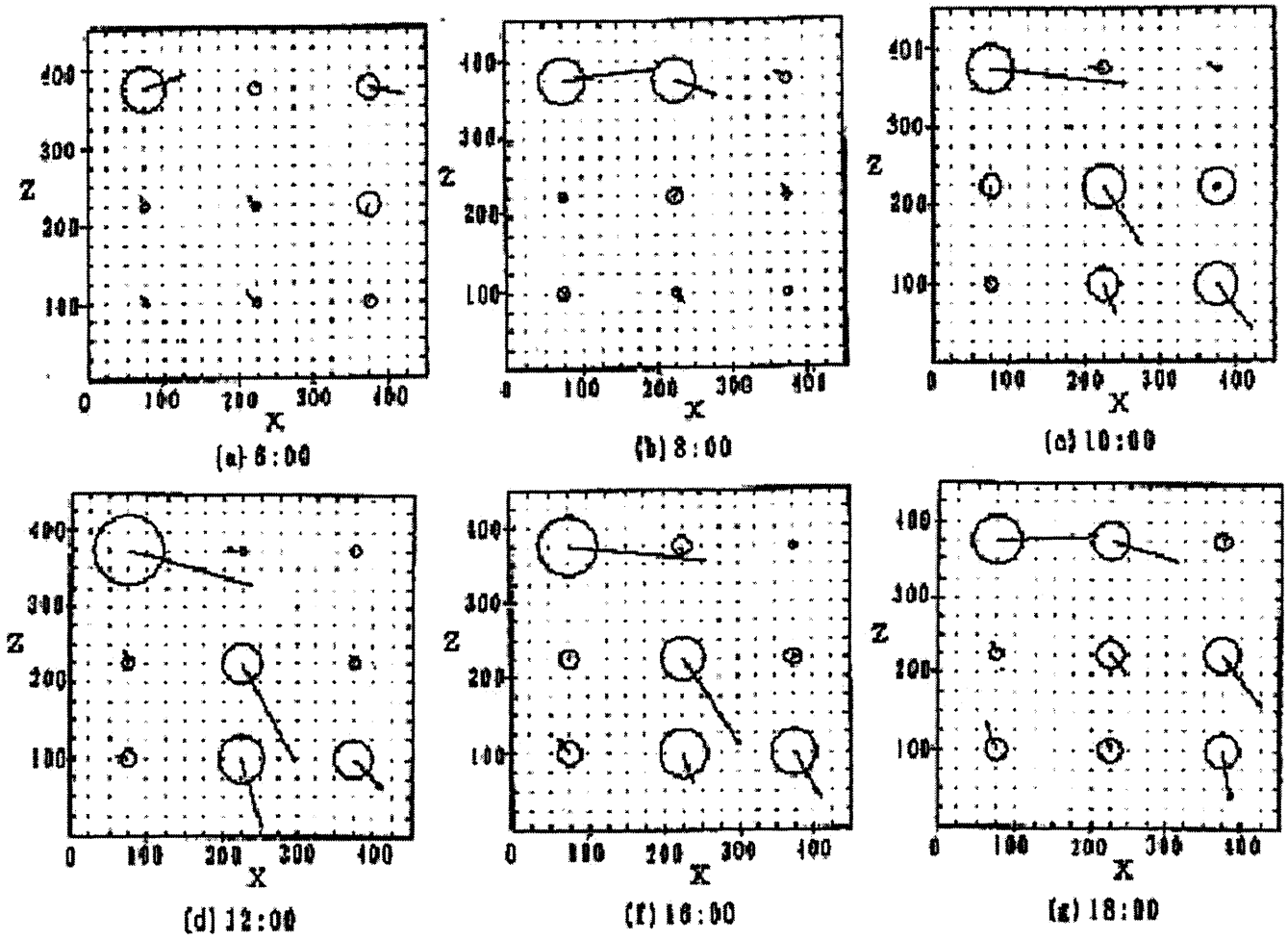

Figure 8.28 Measured air velocity distribution in y-z middle plane of the room
(Arrow shows air velocity vector, radius of the circle shows strength of turbulence for three directions)

Furthermore, the study compares the profiles of calculated and measured indoor air temperature and velocity. Figure 8.31 and 8.32 show the profiles of air temperature and velocity at the measurement locations as illustrated in Figure 8.30 and 8.32. Reasonable agreement is achieved for most of the results.

In summary, this validation study further demonstrates that the coupled simulation can effectively provide the complementary boundary conditions for ES and CFD and thus results in more accurate and informative predictions of building performance.

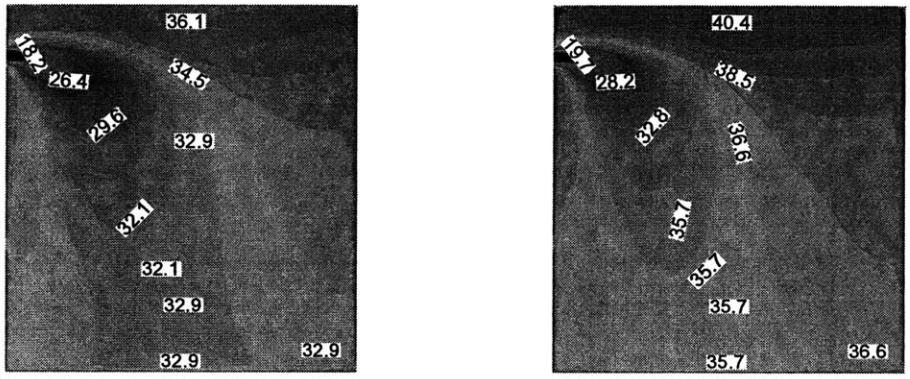

(a) 10:00 (b) 12:00

Figure 8.29 Predicted air temperature distribution in y-z middle plane of the room

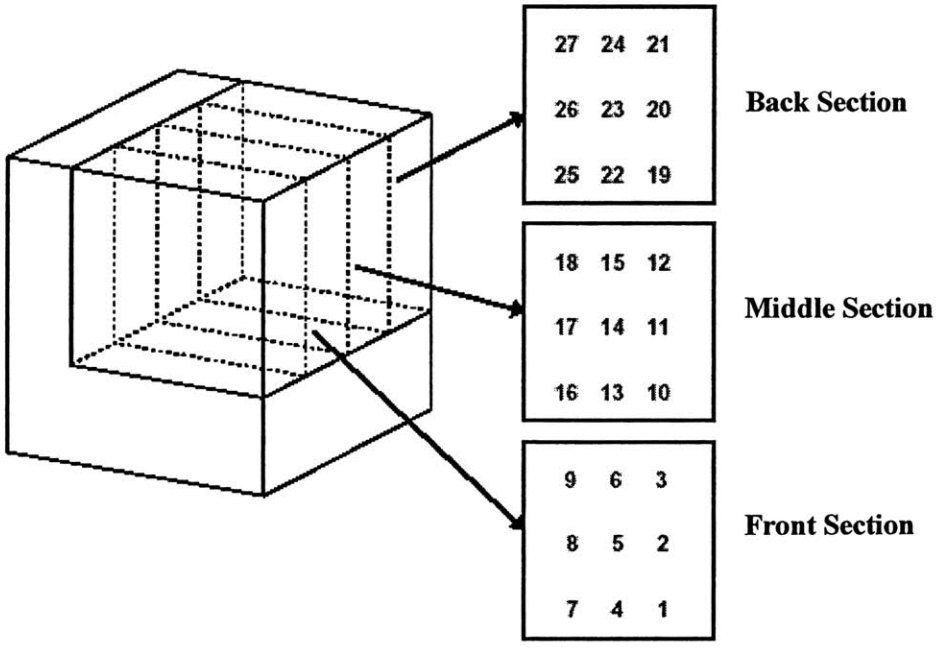

Figure 8.30 Measurement locations of indoor air temperature

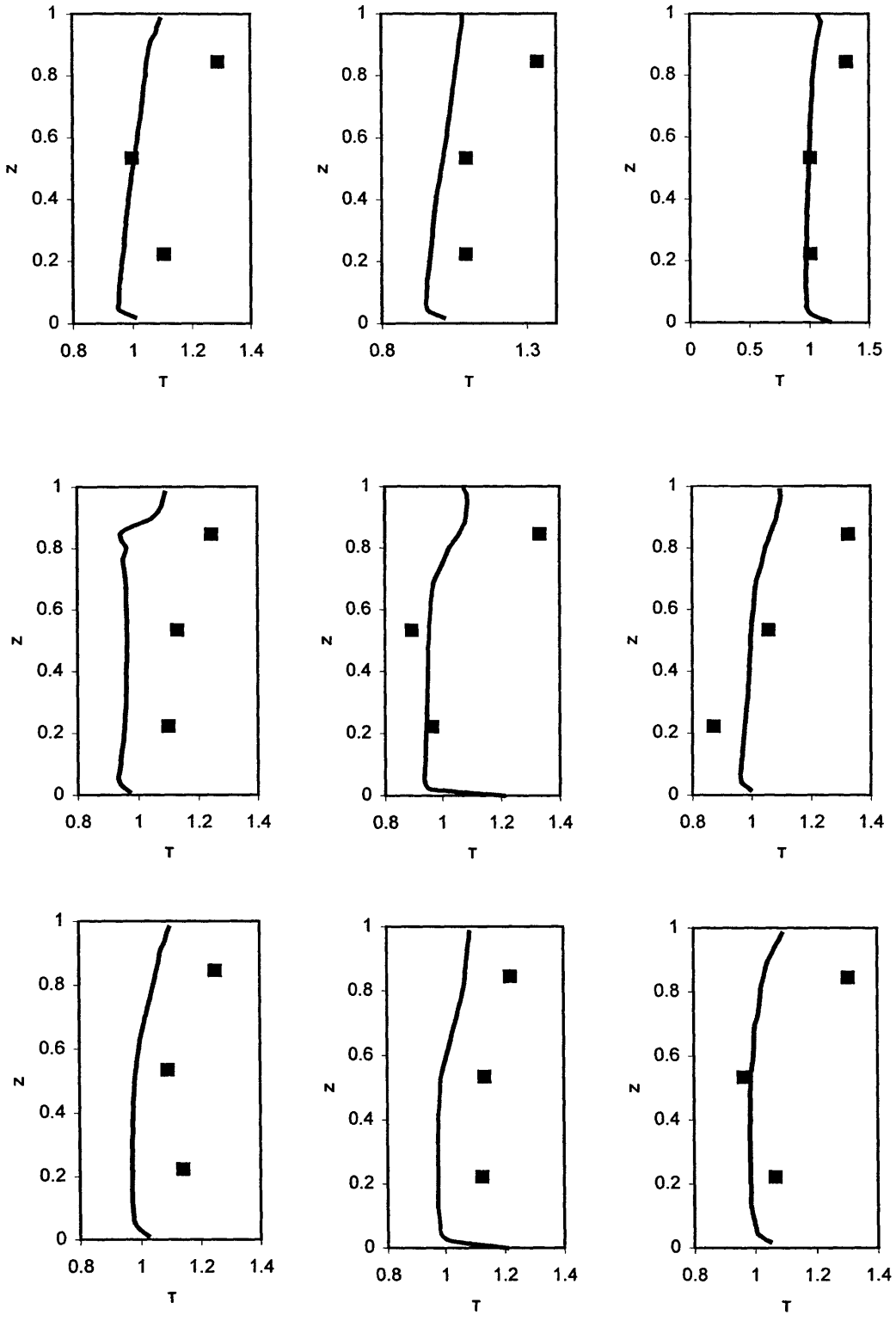

Figure 8.31 Predicted and measured air temperature profiles at 10:00 (Z=height/H, $T=(T_{air}-T_{in})/(T_{out}-T_{in})$, dot-measurement, line-calculation) (top: back section; middle: middle section; bottom: front section)

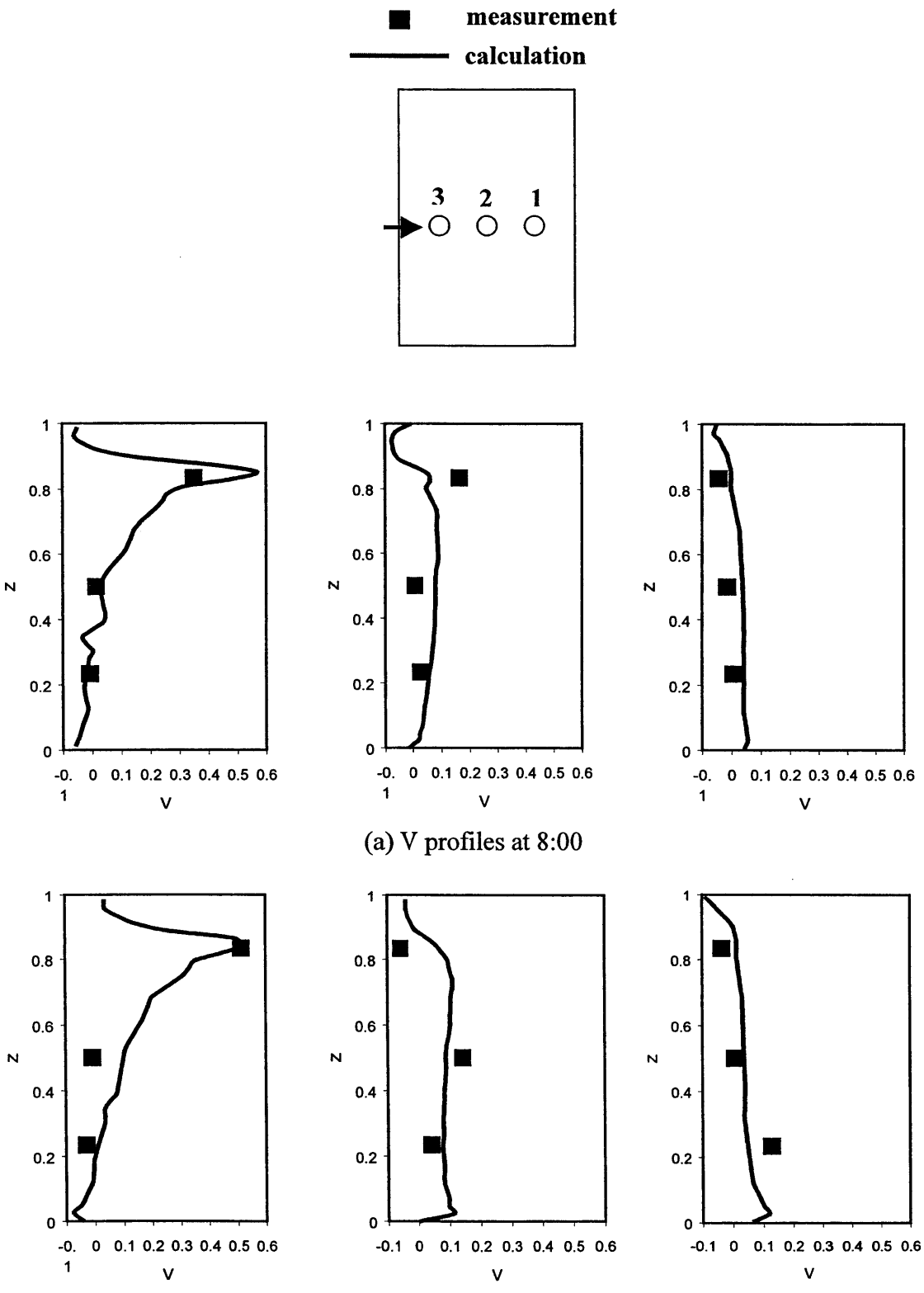

(a) V profiles at 8:00

(b) V profiles at 10:00

Figure 8.32 Predicted and measured air velocity profiles
(Z=height/H, $V=V_{air}/V_{in}$)

8.4.3 Simulation and Results of the Atrium with Room Air Temperature Control

The study further uses this facility to demonstrate the coupled simulation with an indoor air temperature control process as an example of demonstrating the capability of the coupled program. The case is exactly the same as the previous one, except that a variable air volume (VAV) cooling system with a constant supply air temperature of 15°C, instead of the fixed AC system, is used to air-condition the space. The atrium is controlled to have an upper limit of room temperature at 25°C. If the indoor air temperature at the center of the room is higher than this threshold value, the VAV system will be trigged to supply the cool air as needed.

Since this is not a real experimental scenario and no experimental data are available, the separate ES and the full dynamic coupling simulation were performed for a comparative study. The coarse grid and Xu's zero-equation turbulence model were used in the coupled simulation. In the coupling, CFD provides ES the convective heat transfer coefficients and indoor air temperature gradients as well as the exhaust air temperature while ES provides CFD the interior surface temperatures and cooling energy requirement. The air supply and exhaust openings in CFD can automatically switch on and off in response to the on/off operation of the system in ES.

Figure 8.33 presents the predicted indoor air temperatures at the center of the room and exhaust air temperatures. The cooling system is activated only between 10:00 and 18:00 when the indoor air temperature is higher than the prescribed control temperature at 25°C. Since the outdoor air temperature during this period is lower than 25°C and there is no internal heat gain, the heat is mainly from the solar radiation. The predicted indoor air temperatures from the non-coupled and coupled simulation are almost the same. The high supply air velocity, due to the large amount of cooling load and the small supply opening, rapidly removes the heat from the envelops and creates a fairly uniform air temperature in the core of the space, as shown in Figure 8.34. In a non-coupled simulation, the exhaust air temperature is the same as the room air temperature because of the complete mixing assumption. The exhaust air temperature from the coupled simulation is also close to the central air temperature, indicating the uniform temperature distribution in the core region of the atrium.

Figure 8.35 compares the cooling energy calculated by the non-coupled and coupled simulations. The coupled simulation obtains a much higher energy requirement (202MJ) than the non-coupled simulation (94MJ) for the day. This is because much larger convective heats from the enclosures are predicted by the coupled simulation. The convective heats from the enclosures are the sole heat sources for the atrium. Figure 8.36 illustrated the convection behaviors at the south window and the floor, as examples. A much higher convective heat from the south window is found in the coupling due to the strong cold airflow along the window. The convection coefficients predicted by CFD are similar to those from the empirical correlations of ES when the cooling system is off. However, the empirical correlations provide unreasonably small h values when the cooling system is on. The large convective heat from the window by the coupled simulation leads to the significant decrease of the interior surface temperature. Similarly,

the separate ES underestimates the convective heat from the floor, but the difference is not as large as that at the south window. This is because the air velocity and air temperature close to the floor are smaller and warmer than those close to the south window. This small difference, however, still creates a large difference of the floor temperature, indicating the convective heat may be more important for an opaque surface than a glazed surface in the determination of surface temperature.

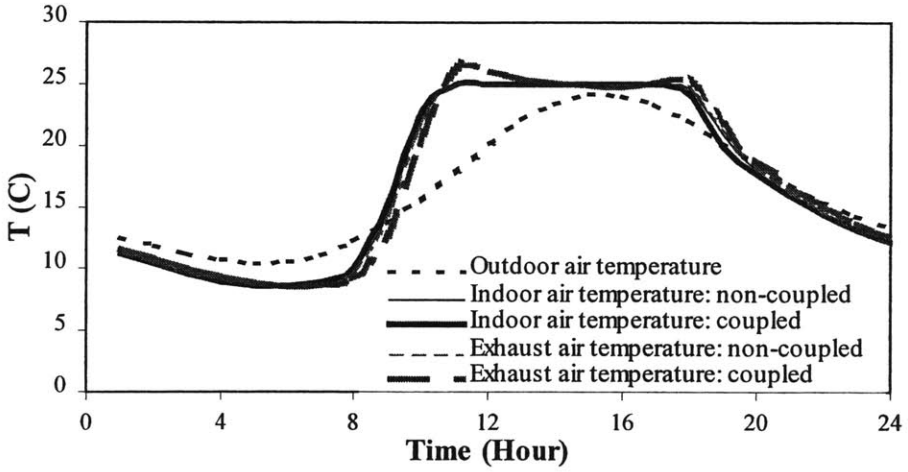

Figure 8.33 Outdoor air, indoor air and exhaust air temperature for the atrium with a VAV cooling system

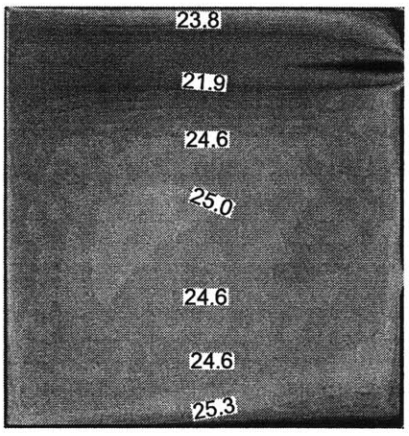

Figure 8.34 Predicted indoor air temperature distribution in the middle section of the atrium at 12 pm

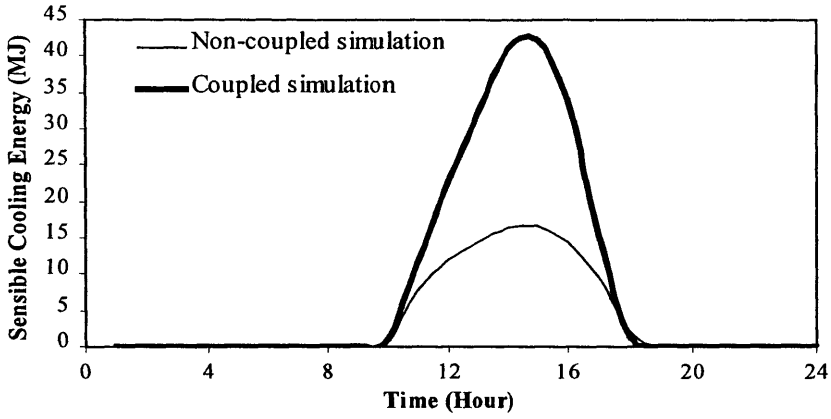

Figure 8.35 Predicted sensible cooling energy for the atrium with a VAV cooling system

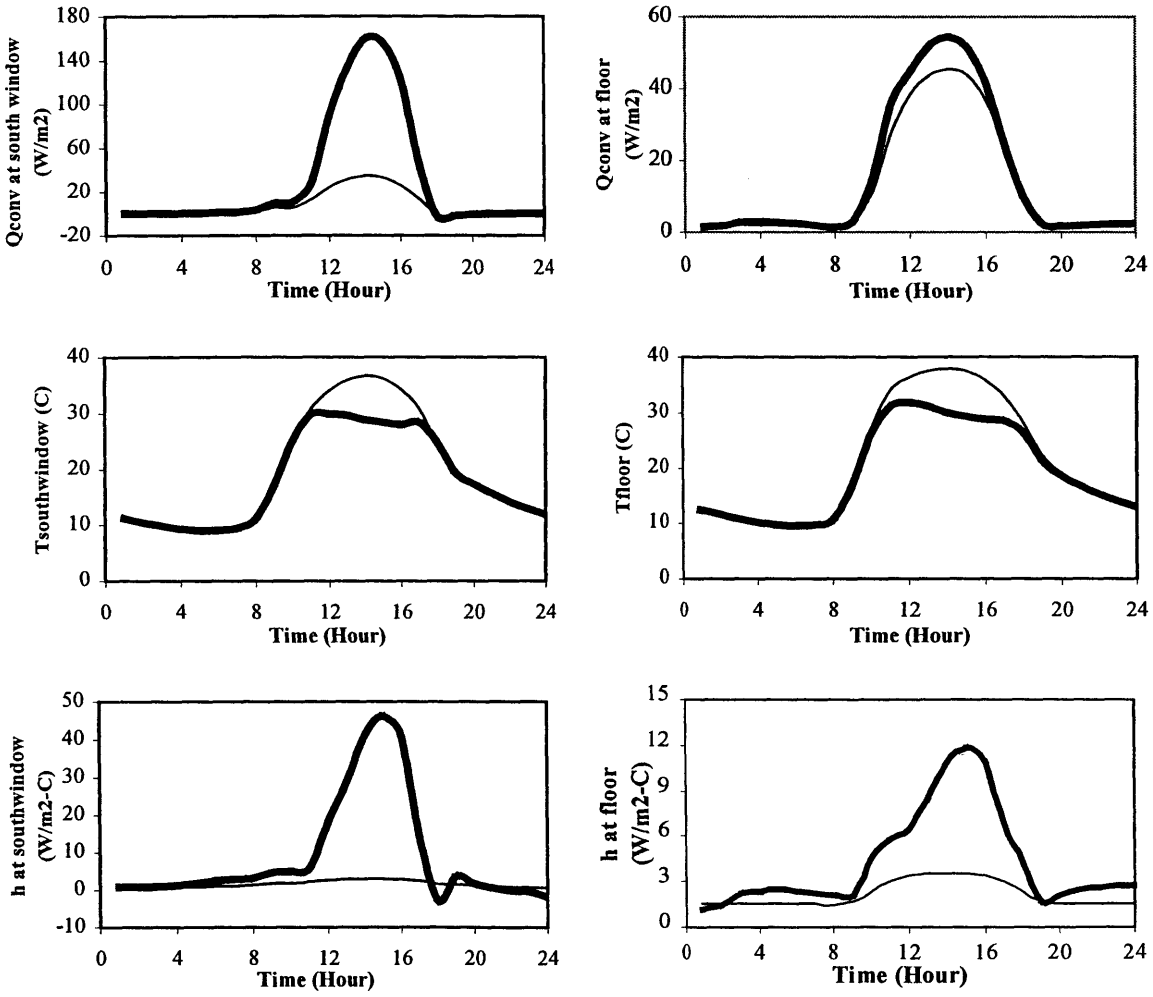

Figure 8.36 Predicted convection heats, interior surface temperatures and convection coefficients at south window and floor of the atrium with a VAV cooling system (thin line – non-coupled results; thick line – coupled results)

8.5 Ventilation System Design for a Large-Scale Indoor Auto Racing Complex

8.5.1 Case Descriptions

The previous four sections presented the case studies with various experimental facilities. The validations and applications demonstrated the good performance of the coupling program developed. The coupled simulations provide more accurate and informative predictions on building thermal and airflow behaviors than the separate simulations. This section applies the coupling program to help optimize the ventilation system design for the world's first full-scale indoor auto-racing facility, planned to be built in Pennsylvania. The application will demonstrate the applicability of the coupling simulation to such kind of large-scale building and system design.

The indoor auto racing facility is primarily a single space building with a floor area of over 0.2×10^6 m^2 and a ceiling height of 46 m, as shown in Figure 8.37. The space is being designed to accommodate a variety of future possible occupancy conditions for a wide variety of events – 60,000 spectators in the grandstands and/or 60,000 spectators in the infield, as well as lesser occupancies within various areas of the infield. The facility will have special lighting and large screen displays for televised events, food and retail concessions stands, etc. The track facility is designed for a maximum of 45 racing cars running simultaneously on the track at a maximum speed of 242 km/h (150 mph) and an average speed of 217 km/h (135 mph). Such a large-scale and complicated building with a variety of indoor components strongly challenges the experience and capability of ventilation system designers, even with the aid of simulation tools.

The modeling of this facility is quite challenging because of the high speed of racing cars, the huge scale difference between the building and the internal objects (such as spectators), and the enormous amount of heat and chemical components generated from the fuel used by the cars. Special numerical techniques and simplifications are needed to create a simulation model that translates the real world into a description of the flow physics suitable for numerical processing. Moreover, the integrated simulation of CFD and ES is necessary for this project because:

(1) The convective heat from the enclosures, although smaller than the enormous amount of heat from spectators, lights, and cars, is still considerable because of the unusual surface convective heat transfer coefficients. The coefficients may be significantly large due to the strong forced convection caused by the racing cars.
(2) An accurate and detailed prediction of the non-uniform indoor environment is essential for the indoor air quality and thermal comfort analysis.
(3) Even 1% prediction error of the energy consumption is considerable (around 300kW) due to the large capacity of the facility.

The integration of ES and CFD can supply the complementary information to each other and reach a more precise and informative prediction of building thermal and indoor environmental performance with different ventilation system designs. The present study focuses on the cooling scenarios in the summer racing season. To design an

effective and efficient cooling and ventilation system for this complex, the study first investigates the steady state building and indoor environment, which implies a long-time racing event with steady outdoor conditions. Under this circumstance, the thermal capacity of the air and the thermal mass has no influence on the cooling load and indoor environment. The cooling load is equal to the convective internal heat gains and heat gains from the enclosures. With the optimally designed ventilation system, the study then simulates the actual racing event with limited racing hours, which reveals the dynamic characteristics of building envelopes, indoor air, and energy consumption.

8.5.2 Steady Simulation and Results

The steady scenario, although not realistic, provides an extreme condition that can be used to determine systems and size equipment with less computing cost. In order to convert the reality to a model suitable for numerical simulation, special simplifications and techniques have been developed to construct the auto-racing complex model with the major thermo-fluid components. The auto-racing facility has been modeled in a blueprint-similar but abstract manner, as compared in Figure 8.37. The simulation model and the architectural model look alike, but there are differences. For example, the curved racetrack was simulated in the model using square blocks. Rather than using moving boundary techniques to handle the moving cars, the impact of moving cars on the indoor environment has been reasonably approximated by concentrating on their velocity momentum and their effects as heat and contaminant sources. As a result, the model simulated these 45 cars as "still" objects with momentum, heat and contaminant source characteristics. This approach has been proven to be acceptable and practical in the study by Yang et al (2000), which used this technique to simulate a moving ice resurfacer in an ice rink and obtained satisfactory results. A further simplifying process used in this study was to group the 45 racing cars into 15 groups of three cars each so as to reduce the data inputs. The 15 groups of cars were uniformly distributed on the track and assumed to be traveling at the same average speed of 217 km/h (135 mph) and with the same heat and contaminant generation rates (e.g. 750 horsepower or 599 kW per car and 3 kg/hour lead from the gasoline used by 45 cars). As for the spectators, because of the scale-difference and input-quantity limitations, it is impossible to simulate so many spectators individually in the model. Therefore, focusing on the macro influence of the spectators on the indoor environment, all of the spectators have been simplified into several solid blocks of resistance, heat and moisture sources, with an average occupied area of 0.5 m^2 for each person. The total heat generated by each person in such an event is 150 W, and the moisture generation rate is 0.055 kg/h per person. Because the size of air supply diffusers is much smaller than those of other components in the building and also the types of diffusers have not been specified at the early design stage, the investigation employed the uniform air-supply assumption for all the diffusers with the use of the momentum method (Chen and Moser 1991) assuming 50% real supply area of the gross diffuser opening area.

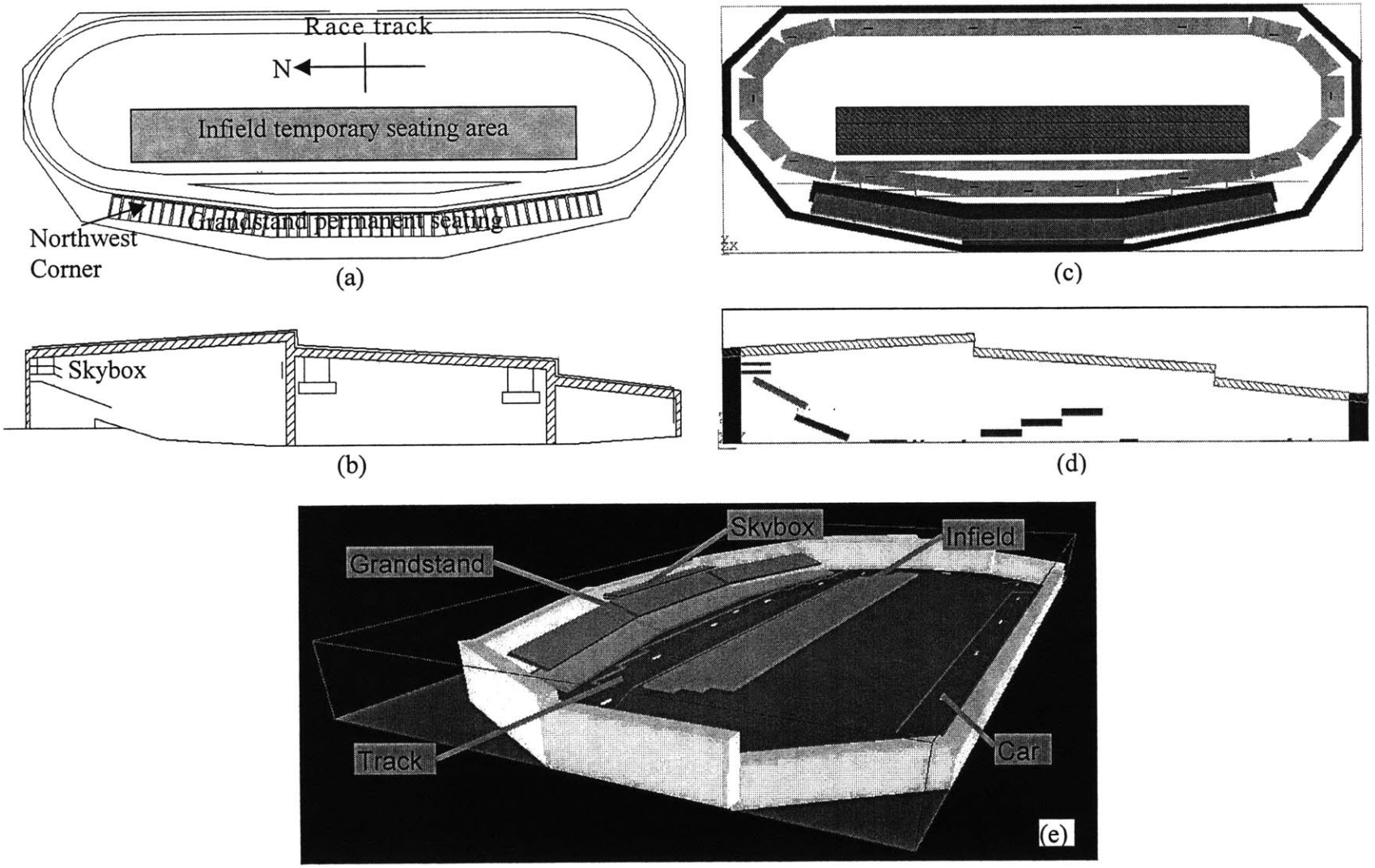

Figure 8.37 The architectural blueprint and CFD model for the auto-racing complex: (a) blueprint plane, (b) blueprint middle section, (c) CFD model plane, (d) CFD model middle section, (e) 3D CFD model

With these simplifications, a base ventilation system design for this space was established, as illustrated in Figure 8.38. The initial concept included supplying fresh air to the grandstands (occupied zone #1) and the infield (occupied zone #2); in addition, air-curtains between the track and the occupied zones were envisioned to help isolate the occupied zones from the hot and contaminated plumes generated by the cars. The rising hot and polluted air plumes were then to be mechanically exhausted from a series of large exhaust fans located along two clerestories at the roof level. The grandstand area of the base design assumed a traditional overhead duct system to supply fresh air, while the infield area was assumed to be ventilated by a displacement ventilation system that supplies fresh air underneath the seats. Rather than attempting to provide full air-conditioning of the entire facility space during a racing event, the design goal was to use the required ventilation air to provide partial "spot-cooling" of occupied areas, which would provide comfort levels similar to that experienced by racing fans in a conventional outdoor race track. Table 8.3 gives the air supply parameters for the base case. The ventilation system for the complex must be designed to work under a worst-case scenario. For this facility, the worst summer scenario is a major auto-racing event with a maximum number of racing cars on the track and the maximum number of spectators inside the complex, under the summer design conditions of Pittsburgh, PA.

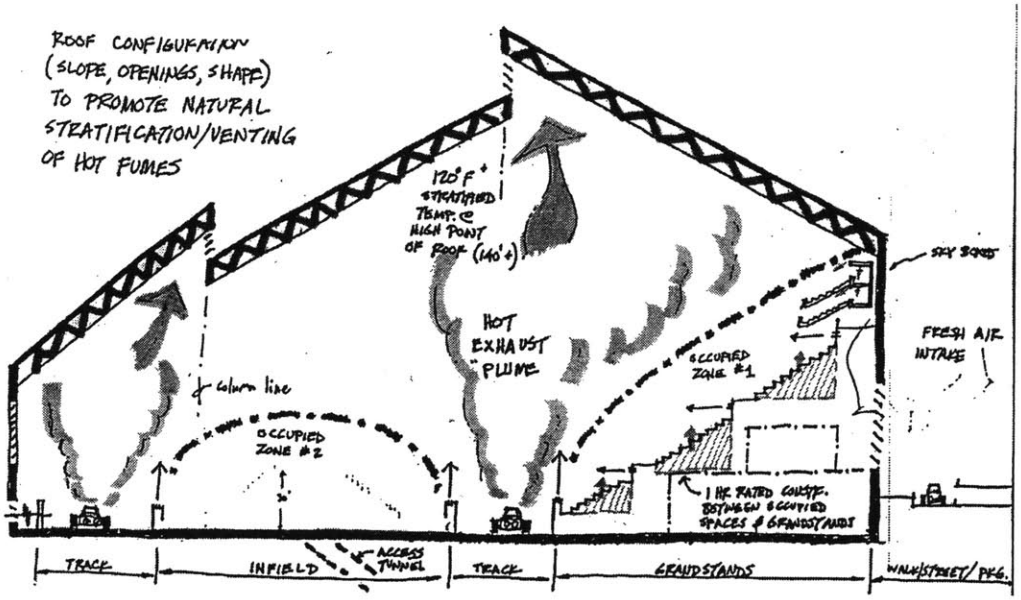

Figure 8.38 Illustration of the ventilation strategy

Table 8.3 The ventilation systems and the air supply parameters used

Case	Grandstands			Infield			Air Curtain		
	Supply Method	Flow Rate (Mcfm /m^3/s)	Supply Temp (°F/°C)	Supply Method	Flow rate (Mcfm /m^3/s)	Supply Temp (°F/°C)	Curtain Length	Flow rate (Mcfm /m^3/s)	Supply Temp (°F/°C)
BaseCase	Duct	1.0/472	50/10	Displace	1.0/472	50/10	Full	1.0/472	86/30
FinalCase	Duct	1.5/708	50/10	Displace	1.2/566	65/18	Partial	0.3/142	50/10

The CFD simulation is then required to help evaluate the initial system design and improve the base case, step by step, toward an optimal design. In order to provide reasonable thermal boundary conditions for CFD calculations, the ES is essential. However, since one CFD calculation under steady-state conditions may take about 10 hours to obtain a reasonable result for this case with a grid resolution of 100×100×55, it is impractical to perform any dynamical coupling process. The study thus employed the two-step static coupling process. In this ES-CFD-ES two-step static coupling, ES first calculates the surface temperatures and cooling loads using the default convective heat transfer coefficient correlations. With these surface temperatures and cooling loads as boundary conditions, CFD calculates the heat and airflow distributions in the space. The indoor air temperature gradients and convection heat transfer coefficients obtained from the CFD results are then fed back to ES to obtain more accurate cooling loads for sizing the ventilation systems. If necessary, one more CFD calculation can be conducted with the updated thermal boundary conditions.

Figure 8.40(a) shows the air temperature in the mid-section of the facility under the steady state condition for the base case with the boundary conditions provided by ES. Since the cars run counterclockwise around the track as shown in Figure 8.39, the car-induced winds coming out of the turn at the northwest corner cause the highly polluted and hot air from the track to penetrate into the grandstand area at that location. Table 8.4 summarizes the air temperature in the mid-section of the grandstands, the infield, and the northwest corner. The air temperature is generally high in all the occupied zones, and the air temperature at the northwest corner of the grandstands is the highest due to the car-induced air movement. The corresponding relative humidity is less than 40% for the base case. Figure 8.41(a) shows the lead concentration distribution normalized to a source strength in the mid-section under the steady-state condition. The airflow pattern shown in Figure 8.39 demonstrates that the air curtain is too weak to block the wind generated by the cars and isolate the polluted and hot plumes from the occupied zones, although it does help to cool the air from the track and further dilute the pollutants associated with the car exhausts.

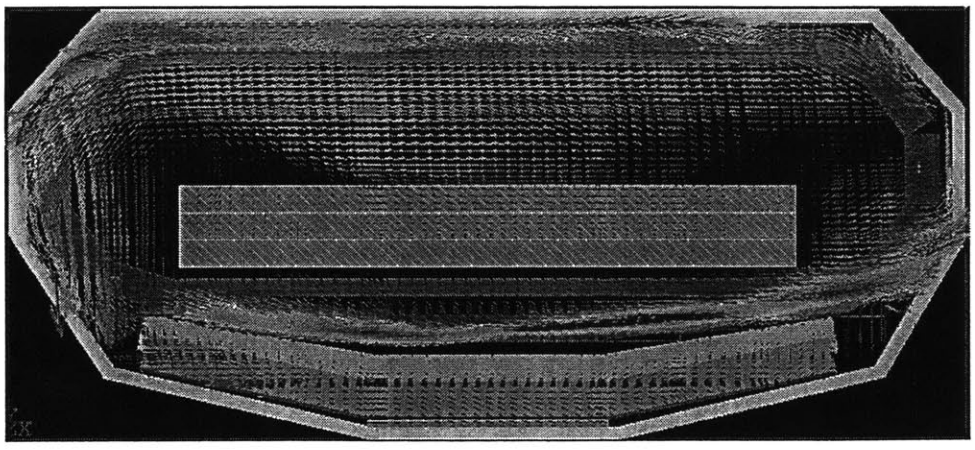

Figure 8.39 The air velocity distribution for the base case at 5 m height above the tracks

Table 8.4 The air temperature computed by CFD for different occupied zones (°F/°C)

Case	Grandstands	Infield	Northwest Corner
BaseCase	95/35	97/36	107/42
FinalCase	88/31	90/32	95/35

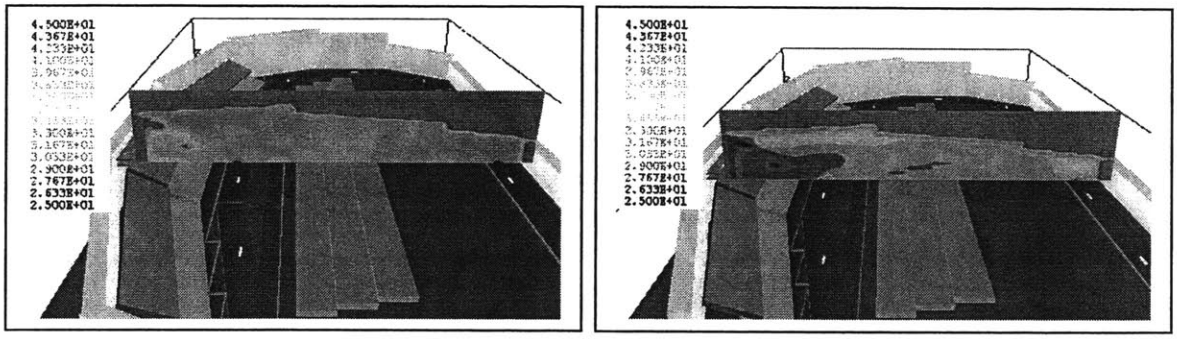

(a) (b)

Figure 8.40 The air temperature distribution in the middle section: (a) BaseCase; (b) FinalCase (unit: ˚C)

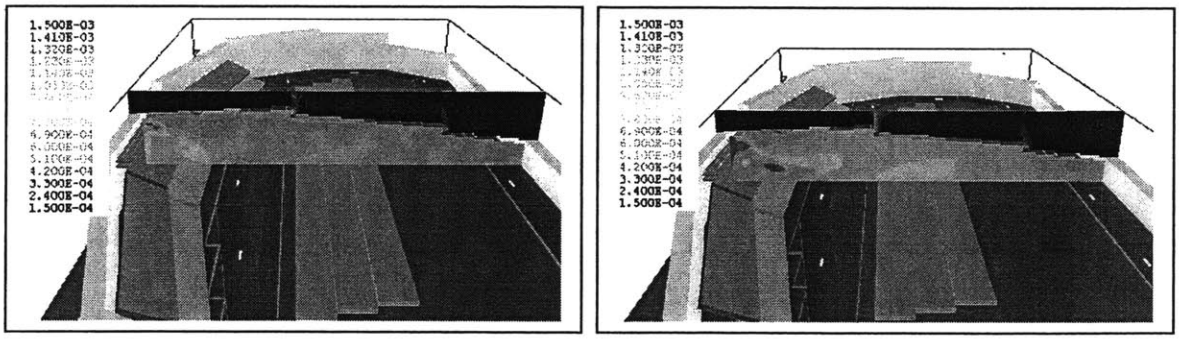

(a) (b)

Figure 8.41 The lead concentration distribution in the middle section: (a) BaseCase; (b) FinalCase (unit: gLead/kgAir)

Different improvement approaches have been investigated through a number of CFD simulations and comparisons. The study finally identified a more practical design that can achieve a better indoor air quality and thermal comfort with the same ventilation rate and system capacity. In this proposed final design, the grandstand uses the overhead duct system with a supply air temperature of 10°C and a supply flow rate of 707m^3/s (1.5x10^6cfm). The infield uses the displacement ventilation system with a supply air temperature of 18°C and a supply flow rate of 566m^3/s (1.2x10^6cfm). A partial air

curtain with a flow rate of $142m^3/s$ ($3x10^5cfm$) and a temperature of 10^oC is used in the northwest corner of the facility. Figures 8.40(b) and 8.41(b) show the distributions of the air temperature and lead concentration, respectively, with this system. Obviously, the final case provides a relatively low lead level. Most importantly, the air temperature in the facility is moderate, as seen in Table 8.4. Although the temperature in the northwest corner is the highest, the air velocity in that area is also the highest. The overall thermal comfort level is rather uniform in the occupied zones. The temperatures are a little higher than normal comfort standards. However, considering the temperature is for an "outdoor" shaded space and the case is for the worst summer scenario, the thermal comfort should be accepted by spectators. As the planning process for the project evolved concurrently with these early CFD studies, it became apparent that major racing events would not likely be scheduled for an indoor facility during peak summer conditions, when outdoor racing events are very popular. This will allow the design team to significantly reduce the size and capital cost of the central refrigeration plant, while refining the HVAC system to further improve the comfort conditions within the facility during off-peak months.

The CFD results with the final system design were then used for the ES calculation to identify the effect of CFD results on building energy simulation. Figure 8.42 shows the predicted enclosure surface temperatures and the required peak cooling energy with and without CFD results. Under the steady state, the required cooling energy is 30.67 MW by the coupled simulation while it is 27.05 MW by the separate ES. The difference of 3,620 KW is considerable, mainly attributed to the dramatic difference of the convective heat transfer coefficients used. Table 8.5 compares the convective heat transfer coefficients computed by CFD with those used in ES, as well as showing the indoor air temperature gradients predicted by CFD. The coefficients from ES are undoubtedly too small for such a strong forced convection case, while those from CFD seem more reasonable. The convective heat transfer coefficient on the west wall is about the same as that from ES due to the low air velocity behind the grandstands.

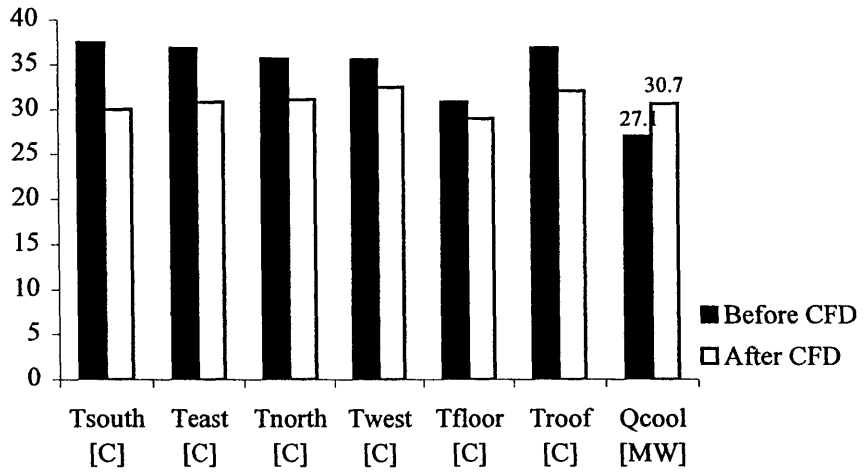

Figure 8.42 Comparison of the surface temperatures and cooling load computed with and without CFD results

Table 8.5 Indoor air temperature gradients and convection coefficients from CFD and ES

Wall	$\Delta T=T_{air}-T_{room}$ (°C)	h from CFD (W/m^2C)	h from ES (W/m^2C)	Estimated h^* (W/m^2C)
South	-0.72	84.6	2.55	68
East	0.36	86.7	2.51	76
North	0.62	47.1	2.33	68
West	-2.63	4.1	2.32	
Ground	-0.95	240.5	1.42	76
Roof	0.18	12.5	1.45	

Note: T_{air} is the air temperature close to the surfaces, T_{room} is the air temperature in the core zone of the space, h is defined based on the surface temperature and T_{room}. h^* is estimated according to the formula for very strong airflow over a large plate (Lienhard 1999)

Figure 8.42 also shows the change of the surface temperatures with and without the coupling. Some of the changes are as large as 5~7°C, such as that for the south wall. Based on the new surface temperatures and cooling load determined by ES, another CFD calculation should be performed to update the indoor air temperature gradients and convection coefficients. For this case, it is estimated that these changes in boundary conditions may not be determinative to the CFD solutions. The two-step static coupling simulation, therefore, is reasonably fine for the design purpose.

More detailed analysis of thermal behaviors of the walls are presented in Figure 8.43. The south and east walls have the most apparent differences between the coupled and non-coupled results. It is because these two walls are closest to the racing tracks and fully exposed to the strongest air movements from the cars, as revealed by the velocity distribution in Figure 8.39. This can be further verified by the high h values at these two walls in Table 8.5. In contrast, the west wall encounters the minimum impact from the racing cars since the wall hides behind the grandstands. The convection at this wall is mainly natural rather than forced. Therefore, the h value produced by CFD is similar to that from the separate ES and the change of the predicted convection heat is small.

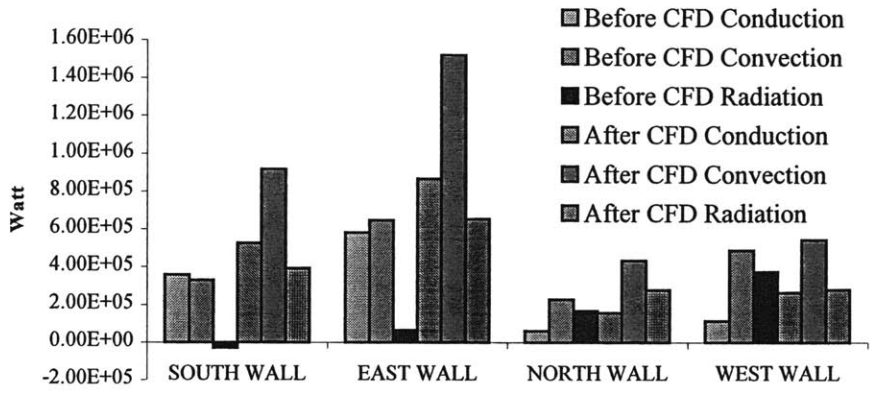

Figure 8.43 Thermal behaviors of walls computed with and without CFD results

8.5.3 Unsteady Simulation and Results

An actual racing event usually lasts merely three to five hours during a day. Under this circumstance, the thermal capacity of indoor air, building envelopes and spectator seats will have significant impact on the building thermal performance. These thermal masses can store the heat gained from various heat sources (occupants, cars, lights, equipment, solar, etc...) and release them at a later time. As a consequence, it may reduce the total energy requirement for a racing event. Such a realistic scenario is then investigated here using both the coupled and non-coupled simulation. Three-hour racing event is arranged to occur during 10:00-13:00 of the summer design day. The properties of the thermal masses of the building, besides the indoor air, are listed in Table 8.6. The thermal conductivity values are the same as those used in the steady-state simulation. Each occupant is assumed to have $0.5m^2$ sitting area. The static bin coupling strategy was used in the coupled simulation. That is, the convection coefficients and indoor air temperature gradients generated in the steady CFD simulation were used in the coupled simulation for the three racing hours. The static bin coupling strategy can dramatically reduce the computing time. This strategy is suitable for this case in which the environmental and occupied conditions have little or no change during the racing hours. Moreover, the indoor airflow patterns dominated by the car movements can reach quasi-steady state rapidly. This results in the small variation of the h values during the event, which are determined by the velocity distribution in CFD that uses the zero-equation turbulence model.

Table 8.6 Properties of thermal masses in the auto racing complex

Enclosure	Thickness (m)	Density (kg/m^3)	Specific Heat (J/kg-K)	Thermal Conductivity (W/m-K)
Roof	0.1	480	1250	0.0437 (R13)
Ground	0.1	608	830	0.5682 (R1)
Wall	0.2	840	1250	0.2841 (R4)
Seats	0.2	608	830	0.0758 (R15)

The study at first investigates the influence of the racing event on the mean indoor air temperature using the non-coupled simulation. Figure 8.44 presents the non-coupled results of indoor air temperature with and without the racing event. Without the event, the indoor air temperature has slight swing during the day although the outdoor air temperature waves significantly, indicating good insulation of the building envelopes. Meanwhile, the thermal masses postpone the time of the peak indoor air temperature from the early-afternoon to the mid-night. When the racing event starts at 10:00 in the racing days, the indoor air temperature rises. However, due to the thermal storage effect, the air temperature does not reach the upper threshold temperature value of 30°C until 11:10. At that moment, the cooling system is activated to maintain the indoor air temperature at the constant 30°C until the event is over. Part of the stored heat will be released back to the indoor space after the event. Because the present study simulated the continuous days with the same racing events, the heat did not completely dismiss to the

surroundings before the next racing event came, resulting in the indoor air temperature in the early morning being higher than that without racing event.

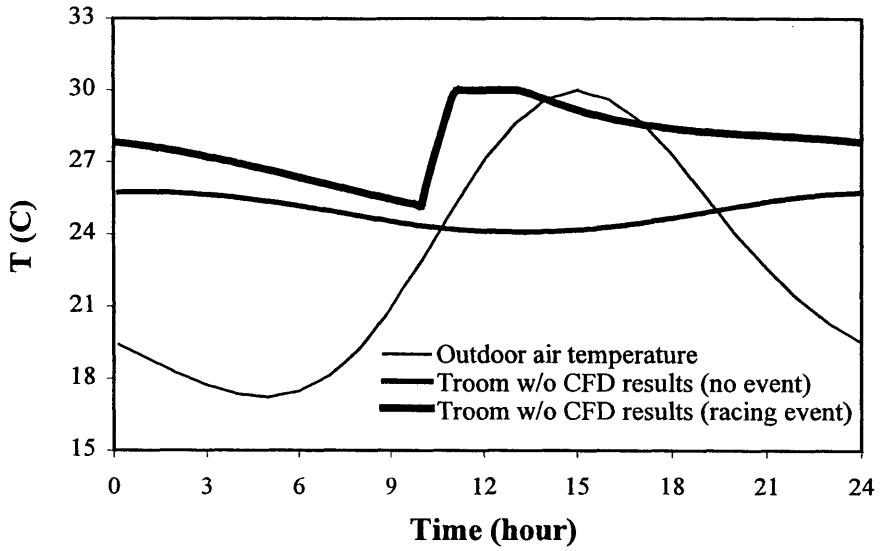

Figure 8.44 Indoor and outdoor air temperature with and without racing event

Figure 8.45 compares the indoor air temperature computed with and without CFD results during the racing hours. The indoor air temperature obtained from the coupled simulation is similar to that from the non-coupled simulation when it is lower than 27°C although significantly different convection coefficients and air temperature gradients were used in the coupled simulation. This reflects the lag of the thermal response time of building thermal masses. After that point, the difference between two approaches is apparent. The coupled results show a longer time lag (about 20-30 minutes later than the non-coupled results) for the indoor air to reach the controlled temperature. This implies that more thermal storage effect was achieved in the coupled simulation. This effect results in considerable decrease of the supply cooling energy, as seen in Figure 8.46. The total cooling energy consumed during the racing event predicted by the coupled simulation is 117 GJ (32,500 kW-hour), which is about 38.5% less than the value of 162 GJ (45,000 kW-hour) predicted by the non-coupled simulation. This significant distinction is primarily due to the different surface convective heats obtained, which determine the effectiveness of the heat transfer between the indoor air and thermal masses. The coupled simulation produces much higher convective heats from all the rigid surfaces than the non-coupled one because of the larger convection coefficients and the indoor air temperature gradients from CFD results, as demonstrated in Figure 8.47. The figure shows that the ground slab works as the most important heat reservoir during the racing event. The heat absorbed by the slab significantly increases the temperature of the thermal mass, as indicated by Figure 8.48. The heat will be released to the indoor space and the deep ground at a later time after the racing event.

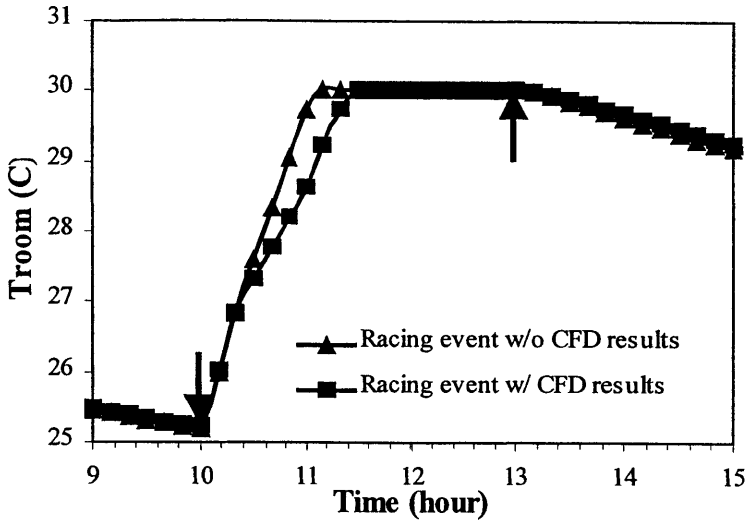

Figure 8.45 Mean indoor air temperature during the racing day computed with and without CFD results

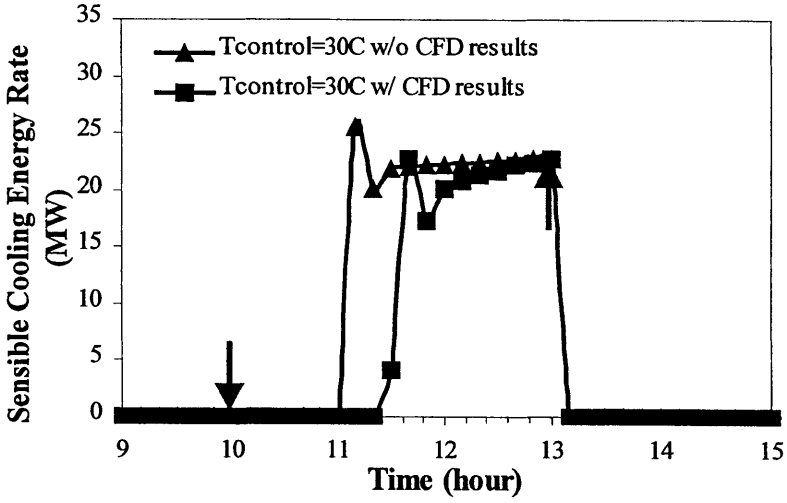

Figure 8.46 Sensible cooling energy rate during the racing event computed with and without CFD results

This study shows the significant difference between the static and dynamic predictions of building thermal behaviors, indicating the importance of thermal storage effect. The present simulation with the static bin coupling strategy provides a basic and reasonable estimate of building energy consumption. More accurate results for building envelopes, indoor environmental quality and energy consumption can be obtained through the dynamic coupling; however, it is extremely expensive in computing cost for this case.

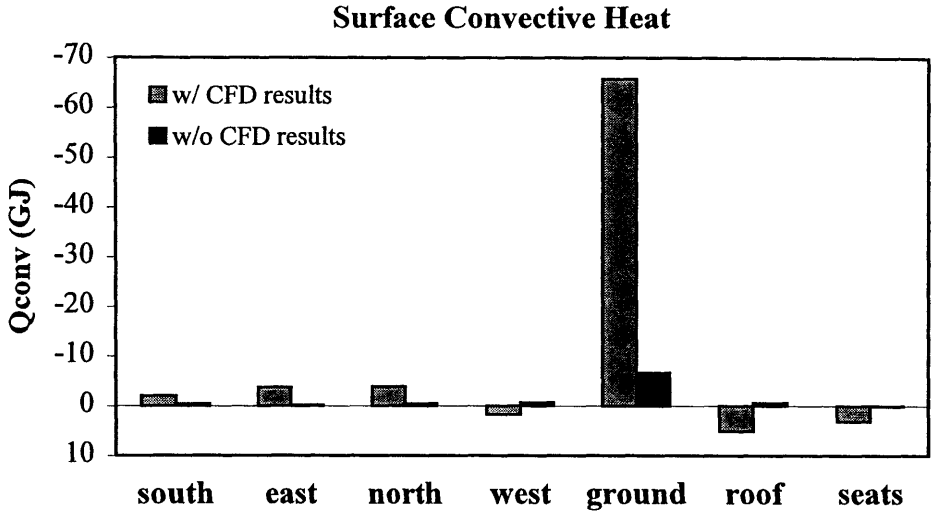

Figure 8.47 Convective heat transfer from surfaces during the racing event computed with and without CFD results

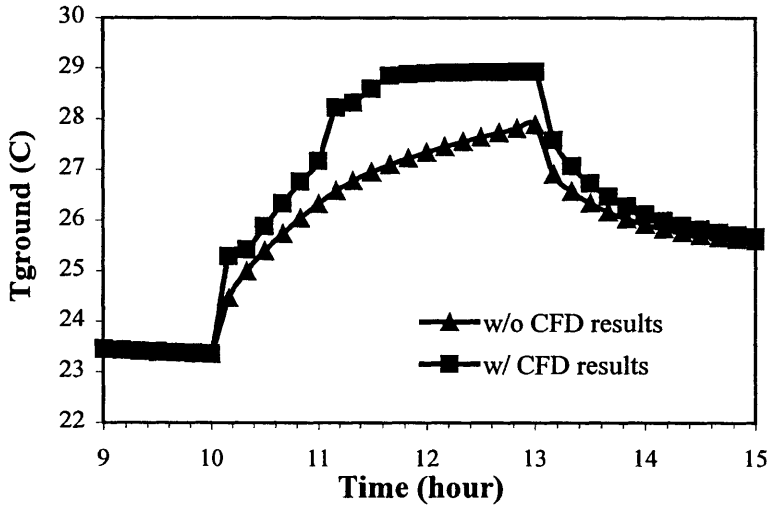

Figure 8.48 Ground temperature during the racing event computed with and without CFD results

8.6 Displacement Ventilation in a Boston Office Building

8.6.1 Case Descriptions

For most buildings with dynamic operational and environmental conditions, dynamic coupling simulation is always necessary. This section uses a typical office building in Boston to demonstrate the applicability of the coupling program to this type of building with diverse ventilation systems. The investigation focuses on one of the

representative one-occupant offices in such an office building. The office is in a middle floor of the building, with completely identical neighboring rooms. The geometry and configuration of the office is illustrated in Figure 8.49. The room has only one south-facing exterior wall with a large window. The properties of the enclosure materials are summarized in Table 8.7. An occupant (100W) and a working computer (270W) exist during the whole day, both of which have a 30% radiant/70% convective heat split. The room is conditioned 24 hours a day with a VAV side-wall displacement ventilation system. The supply air temperature is 16°C and the desired room air temperature is 25°C. The room is investigated under the summer design conditions in Boston.

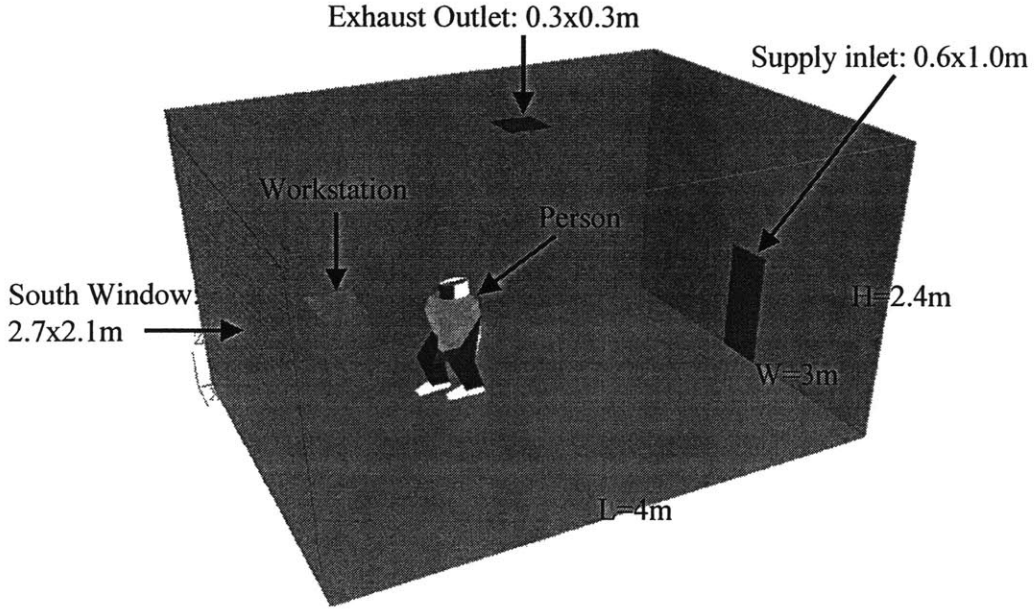

Figure 8.49 Schematic of the one-occupant office

Table 8.7 Material properties of the office

Enclosure	Thickness (m)	Density (kg/m^3)	Specific Heat (J/kg-K)	Thermal Conductivity (W/m-K)
Roof/Ceiling	0.175	2300	840	0.0523 (R19)
Wall	0.14	1600	840	0.0612 (R13)
Glass	0.006			0.9

8.6.2 Simulation and Results

The study compares the performance and results of non-coupled and coupled simulations. In the non-coupled simulation, detailed convection coefficient correlations of EnergyPlus were used to predict the convective heats from building enclosures. In the coupled simulation, both full dynamic and quasi-dynamic coupling strategies were tested, with the coupling frequency of each hour. The CFD in the coupled simulation used a

non-uniform grid of 19×25×17=8,075 cells and the zero-equation turbulence model to simulate the indoor air movement with the boundary conditions (supply air mass flow rate and envelope surface temperatures) from the ES. The ES obtains the updated convection heat coefficients and indoor air temperature gradients and the exhaust air temperature from each CFD calculation. To reduce the computing time of the coupled simulation, besides calling CFD every hour in the formal simulation day, only the first day of the warm-up period had the CFD coupling. The CFD results were saved and used for the simulation of the rest of the warm-up days in ES. The total computing time is about 9 hours for the full dynamic coupling simulation and about 1 hour 45 minutes for the quasi-dynamic coupling simulation with a Pentium III 900 MHz PC.

The simulation results expose the apparent variations of the cooling load and indoor airflow patterns during the summer design day. Less cooling energy is required in the nighttime because of the cold outdoor temperature and no solar gains, as shown in Figure 8.50. The peak cooling energy is predicted around 13:00 by both the coupled and non-coupled calculations. However, the coupled results have a larger peak load than the non-coupled results. The total cooling energy required in the day is 59.1 MJ by the coupled simulation and is 55.2 MJ by the non-coupled simulation. The difference seems not significant (6.6%). However, since the actual exhaust air temperature at the ceiling, predicted by the coupled simulation, is much higher than the mean room air temperature, the required supply airflow rate is much smaller from the coupled simulation than from the non-coupled simulation, as illustrated by Figures 8.51 and 8.52. The difference of the total supply air mass between these two simulations is over 15%. This implies that the fan and chiller could be oversized if using the non-coupled results.

The results from Figures 8.50-8.52 also indicate that the quasi-dynamic coupling cannot provide the proper solutions because the limited iteration steps (100 steps) in each CFD can not lead to a converged solution at every coupling step. The problem can be overcome by using more iteration steps (500 steps) in each CFD calculation. The new results are comparable to those from the full dynamic coupling. However, the computing time of the quasi-dynamic coupling with 500 CFD iterations increases to be about 8 hours, which is almost the same as that of the full dynamic coupling.

The influence of the CFD results on building thermal performance becomes clearer when detailed thermal characteristics of building envelopes are analyzed. Figure 8.53 presents the total convective heat gains from each enclosure interior surface during the day. Distinct differences are found between the coupled and non-coupled solutions, especially at the floor. Explicit temperature gradient and large convection coefficient at the floor caused by the sidewall displacement ventilation introduce significant heat into the office space. Because of the cold air near the floor, the floor has a relatively lower temperature than the other opaque surfaces, instead of a higher temperature from the non-coupled simulation. The low floor temperature leads to about 1°C temperature drop for all the other opaque surfaces by the radiation effect, as shown in Table 8.8. As a result, less heat is transferred from these surfaces to the indoor space. These heat reductions offset the increase of heat gain from the floor, resulting in the limited increase of the total cooling load in the coupled simulation. Table 8.8 also indicates that the convection

coefficients at the other surfaces predicted by CFD are similar to those from ES. This should attribute to the characteristics of displacement ventilation: low supply air velocity and dominant buoyancy effect. Figure 8.54 further demonstrates the variations of floor temperature and convective heat during the day. The difference between the coupled and non-coupled results is explicit, even during the nighttime. The cold supply air above the floor is the major reason for this difference, which the separate ES cannot simulate because of the complete mixing assumption.

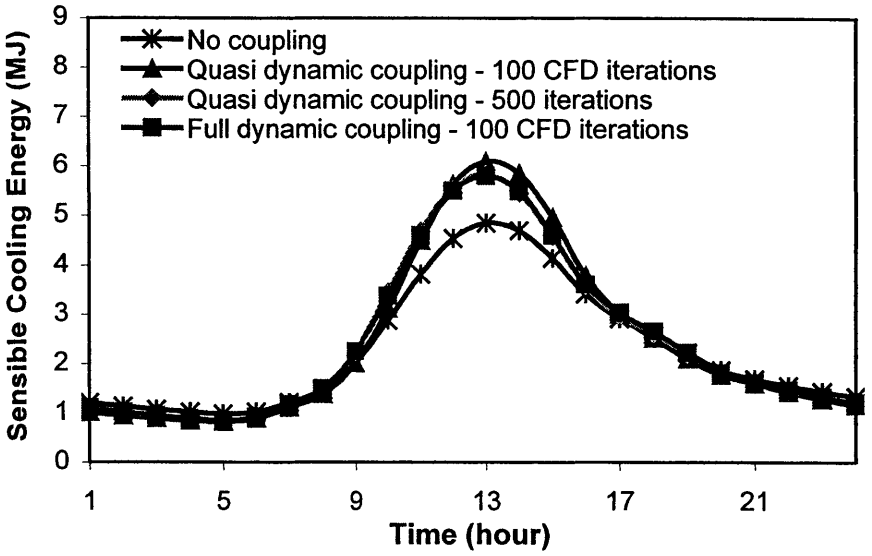

Figure 8.50 Predicted sensible cooling load for the office during the summer day

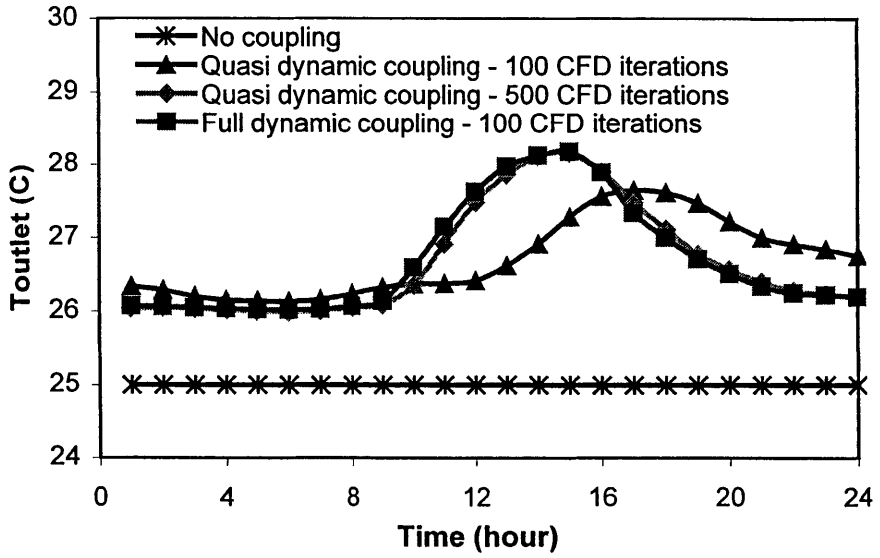

Figure 8.51 Predicted exhaust air temperature in the office during the summer day

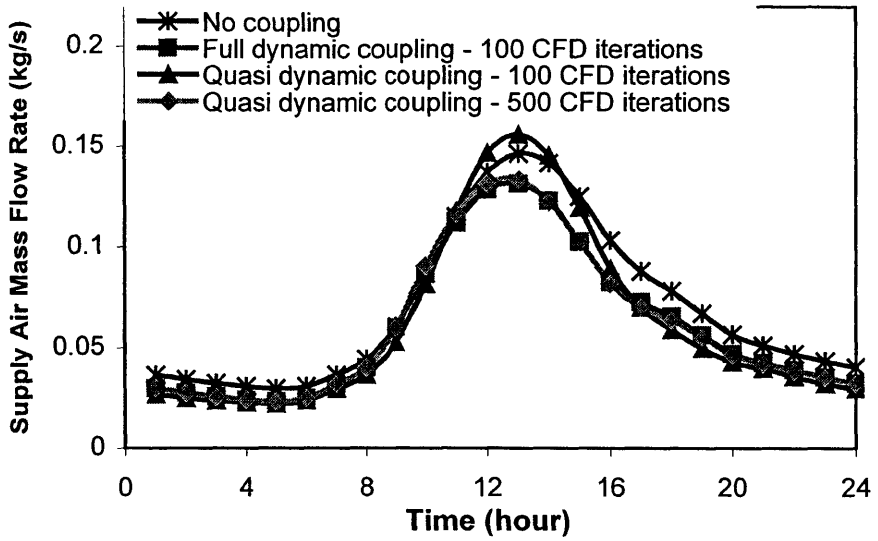

Figure 8.52 Supply airflow rate predicted with and without CFD results

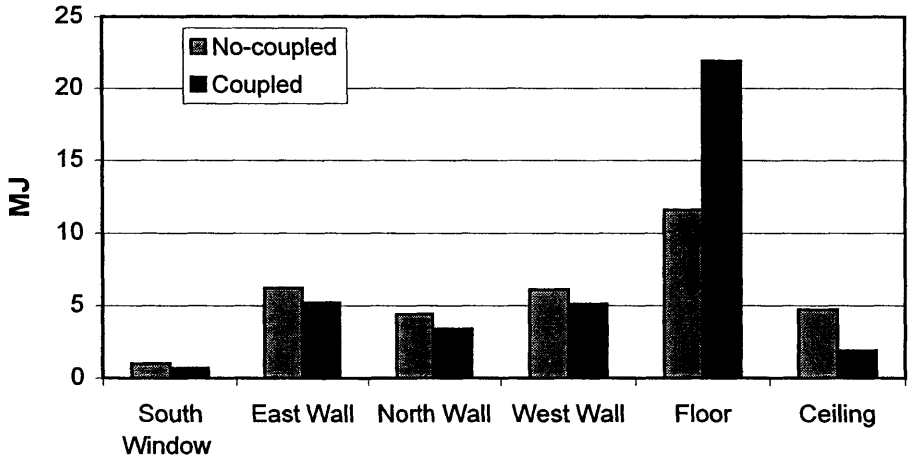

Figure 8.53 Total convective heat transfer from the enclosures of the office in the summer design day

On the other hand, with the dynamic boundary conditions (supply airflow rate and surface temperatures) provided by ES, the CFD in the coupled simulation can effectively and accurately predict the dynamic indoor air movement through the entire summer design day. Figure 8.55 presents the distributions of the indoor air velocity and temperature at the peak load time of 13:00, as an example. The airflow pattern exhibits the typical flow characteristics of displacement ventilation: the large circulation above the floor and the significant vertical air temperature gradient.

Table 8.8 Day-averaged enclosure interior surface temperature and convection coefficients predicted with and without CFD results

Enclosure	No-coupled results		Coupled results	
	$T_{surface}$ (C)	h (W/m^2C)	$T_{surface}$ (C)	h (W/m^2C)
South window	25.7	1.9	25.3	3.0
East wall	28.5	1.9	27.3	2.2
North wall	28.4	1.9	27.2	2.1
West wall	28.5	1.9	27.3	2.2
Floor	29.2	2.3	26.5	17.6
Roof	28.7	1.1	27.6	0.3

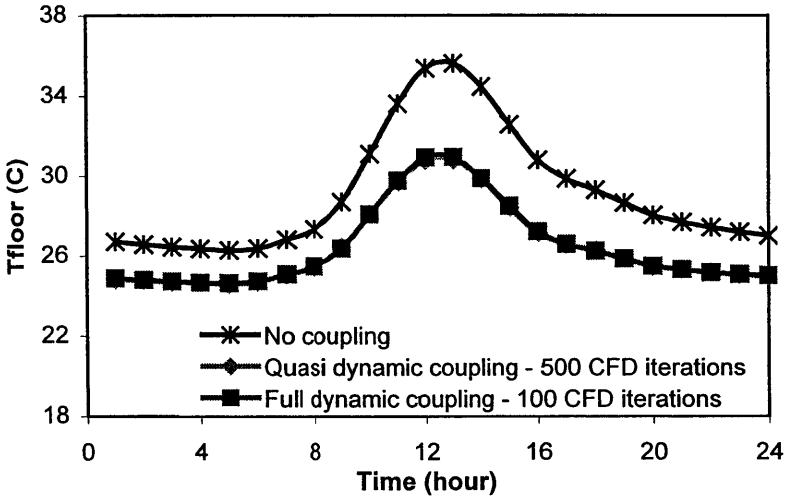

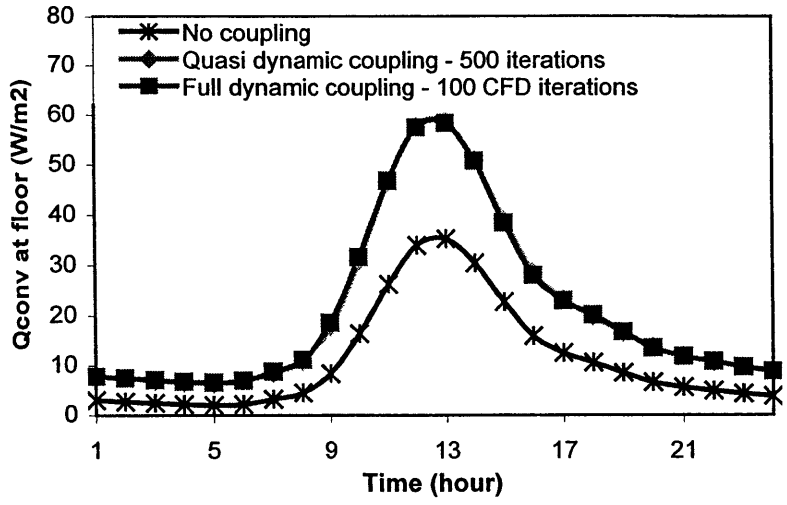

Figure 8.54 Floor interior surface temperature and convection heat flux predicted with and without CFD results

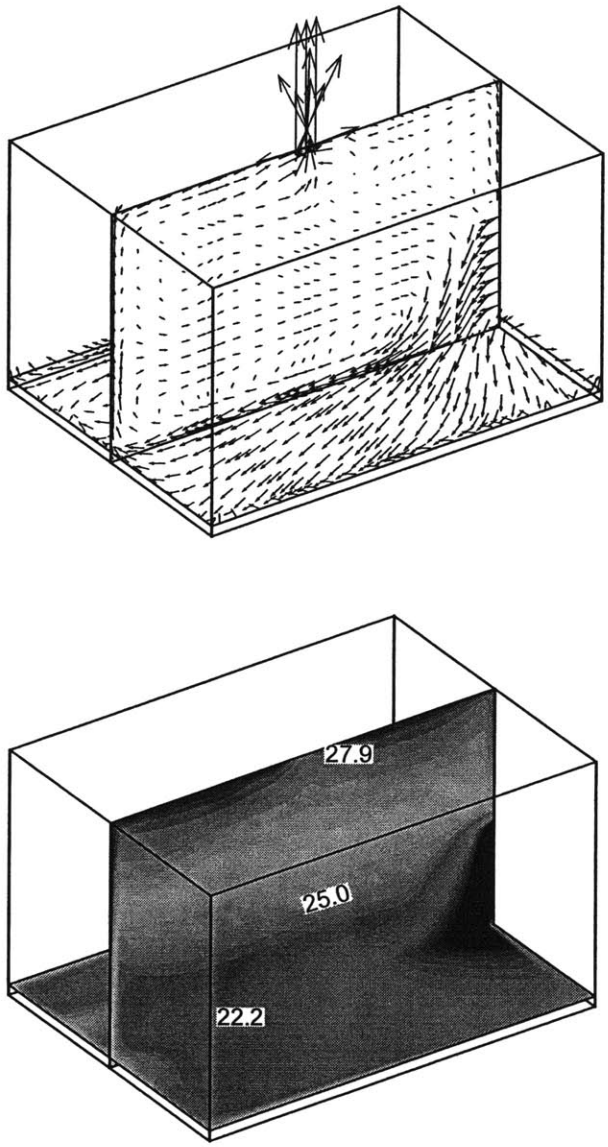

Figure 8.55 Velocity and temperature distribution in the office at 13 pm of the summer design day in Boston by using displacement ventilation system

8.7 Summary

This chapter used four experimental facilities to validate the coupling program developed. The cases studied range from natural, forced to mixed ventilation. The validations verify that the program developed can provide reasonable and reliable predictions on building performance. In general, the coupled simulation produces more accurate and detailed results than the separate simulations:

(1) CFD receives more precise and real-time thermal boundary conditions and can predict the dynamic indoor environment conditions that are important for the assessment of indoor air quality and thermal comfort.

(2) ES obtains more accurate convection heat from enclosures and can provide more accurate estimate of building energy consumption and dynamic thermal behaviors of building envelopes.

The study reveals that indoor air temperature gradients and convective heat transfer coefficients have a large impact on the whole building simulation. The coefficient correlations used in the separate ES may significantly deviate from the real situations and result in a mistaken prediction of building performance.

The application cases presented in this chapter further demonstrate the capability and importance of the coupling program for the design of energy efficient buildings and systems. Both the validations and applications examined and compared different coupling strategies. All of the coupling strategies implemented can provide reasonable solutions, in which the full dynamic coupling provides the most complete and accurate solutions while the static and dynamic bin coupling greatly reduce the computing cost with acceptable solution accuracy. The selection of an appropriate coupling strategy for a specific building directly determines the accuracy and efficiency of a simulation, which will be the subject of next chapter.

CHAPTER 9

SENSITIVITY ANALYSIS OF COUPLING SIMULATION

This chapter first discusses the building and environmental elements that may affect the necessity and effectiveness of the coupling simulation of ES and CFD. The characteristics of these elements along with the solution accuracy requirement determine whether a coupled simulation is essential for a specific building and which coupling strategy can provide a best solution with the compromise of accuracy and efficiency. The chapter conducts the sensitivity studies of coupling simulation to these characteristics, based on which general suggestions are provided for the appropriate usage of the coupling simulation.

9.1 Coupling-Relevant Building and Environmental Characteristics

Building behaviors are determined by comprehensive building and environmental characteristics. Extensive studies on the most influential factors for energy consumption in buildings have been conducted, such as those by Korobov (1960), Lomas (1994) and Saporito (1999). However, not all the factors for energy consumption have significant influence on the determination of a suitable coupling simulation strategy. The change of some building characteristics, such as building shape, may not explicitly affect the performance of a particular coupling simulation process.

This study is interested in the building and environmental characteristics that may directly influence the performance of various coupling simulation strategies. The goal of the study is to identify the most efficient and reliable coupling strategy for a building with specific combination of these building and environmental characteristics.

According to the principles of ES and CFD coupling, the relationship tightness level of building energy and airflow models determines whether a coupled simulation is necessary and which coupling strategy is most appropriate for a particular building. Otherwise, the building energy simulation and airflow modeling can be operated individually to evaluate the comprehensive building performance. More specifically, the necessity and effectiveness of ES-CFD coupling are determined by:

(1) the dependence of building envelope heat transfer and cooling/heating load on indoor air movement and air temperature stratification;
(2) the sensitivity of indoor air movement and air temperature stratification to thermal boundary conditions.

A coupled simulation is desired if the inter-coupled information between ES and CFD is important to either ES or CFD or both. The dynamic performance of the inter-coupled information determines the best coupling strategy for a building. For example, if the inter-coupled data are constant or with small fluctuation, a one-step or two-step static coupling process may be sufficient. Otherwise, a dynamic coupling may be necessary.

Therefore, all the physical conditions from outdoor to indoor that may influence the inter-coupled variables (e.g. convective heat from enclosures) should be examined for the possible effects on building energy and airflow predictions. As illustrated in Figure 9.1, the primary building and environmental characteristics, whose variation may have potential impact on the envelop heat transfer and indoor environment, may include:

- Outdoor weather conditions;
- Building envelope materials;
- Building window-wall area ratio;
- Building function;
- Space geometry;
- Internal loads;
- HVAC systems.

These influential factors can be further grouped into five categories according to their macro-effects on buildings, as summarized in Table 9.1. The first category is environmental conditions that are mainly represented by the outdoor air temperature and solar radiation for the thermal consideration. The second is different HVAC systems used, such as radiation heating and cooling systems, traditional mixing HVAC systems, displacement ventilation systems, and natural/ mechanical ventilation systems. The third is building occupancy and system operating conditions that represent the capacity and dynamics of building energy consumption mainly determined by building functions. The fourth is building envelope information including material properties and window-wall area ratio. The last one is building geometry with different floor areas and ceiling heights. The combination of these characteristics determines the whole building thermal and indoor airflow behaviors, where the individual characteristics may have distinctive influence. Consequently, it is important to investigate the relationship of the building performance and the coupling simulation with these building and environmental characteristics.

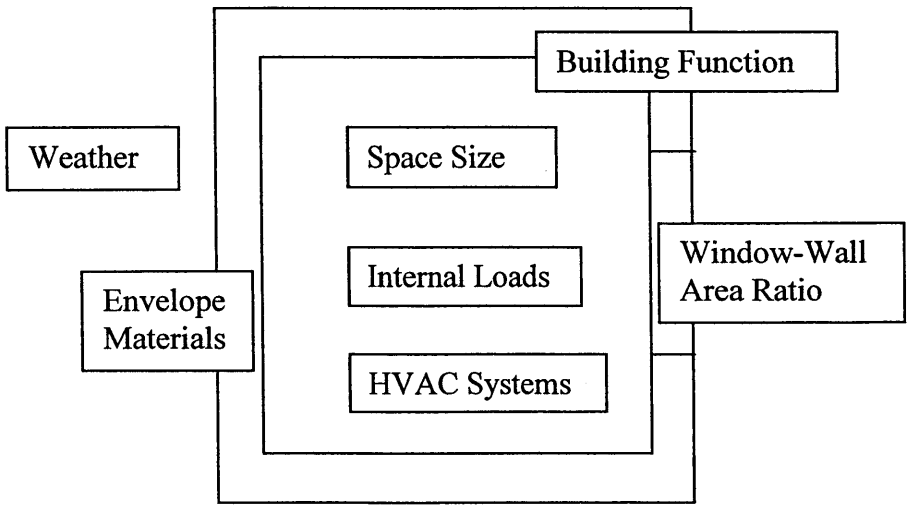

Figure 9.1 Illustration of coupling-relevant building and environmental characteristics

Table 9.1 Coupling-relevant building and environmental characteristics and potential variations

Category	Characteristic	Potential Variations
Environmental conditions	outdoor air temperature	large fluctuation, small fluctuation
	solar radiation	yes (summer design day), no (winter design day)
HVAC systems	radiation heating/cooling	
	mixing ventilation	CAV, VAV
	displacement ventilation	CAV, VAV
	natural/mechanical ventilation	
Occupying and operating conditions	internal load	heavy, medium, light
	schedule	day & night (residential), day only (commercial)
Building envelope materials	wall, ceiling, floor	heavy, medium, light
	window-wall area ratio	full, partial, none
Building geometries	floor area	regular, large
	ceiling height	regular, high

9.2 Sensitivity Studies of Coupling Simulation to the Building and Environmental Characteristics

The previous section indicates the building and environmental characteristics that may potentially affect the building thermal behaviors and result in the thermal interaction between building envelope and indoor air. This interaction may lead to the necessity of a coupled simulation. However, it is not clear yet how the individual characteristics may influence the building performance and the coupling simulation. This section conducts the sensitivity study of coupling simulation to each major building and environmental characteristic indicated. The main objectives of this sensitivity study are to address:

(1) how the building and environmental characteristics influence the building envelope and indoor air thermal behaviors;
(2) whether a coupled simulation is necessary for a building with specific characteristics;
(3) which coupling strategy can provide a best solution (accuracy and efficiency) for a building with specific characteristics.

A sensitivity study requires a base model, upon which the influential parameters can be intentionally adjusted item by item to examine the particular effect of the individual parameters on the whole system. Such a base model has been created by the present sensitivity study, which is basically the same as the one-occupant office used in the case study at section 8.6. Table 9.2 lists the primary characteristic parameters of the base model. The study only investigates the cooling scenarios since the heating scenarios have analogous behaviors. The investigation particularly focuses on ventilated buildings with different air-conditioning systems because the previous case studies indicate that the

coupling may have marginal benefits for buildings with natural convection. For most ventilated buildings, the HVAC systems used dominate building indoor environments and also influence building envelope thermal behaviors. Therefore, HVAC system is the most important influential factor to the coupling simulation. Same conditions of other building characteristics (e.g. window area) may have distinct influence on a building with different systems. The study thus respectively investigates the impact of building and environmental characteristics on a building and simulation under different HVAC system conditions. Three typical ventilation systems are comparably investigated: traditional ceiling-jet mixing ventilation system, side-wall-supply displacement ventilation system, and floor-supply displacement ventilation system, as illustrated in Figure 9.2.

Table 9.2 Primary characteristic parameters of the base case

	Base Case	
Environment Conditions	Outdoor air temperature	Boston summer design day conditions
	Solar radiation	
Occupancy and Operating Conditions	Internal loads	100 W occupant, 270 W computer
	Schedule	All-day
Building Envelope Materials	wall, ceiling, floor	R-19 ceiling and floor, R-13 walls, Light materials
	South window	$2.7\times2.1=5.67m^2$, Clear 6mm glass
Building Geometries	Floor area	$3\times4=12m^2$
	Ceiling height	2.4m

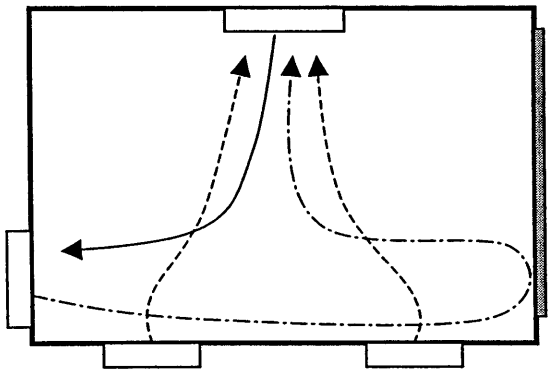

Figure 9.2 Illustration of three different ventilation systems for the office space (solid line: ceiling-jet mixing ventilation system; dash dot line: side-wall-supply displacement ventilation system; dash line: floor-supply displacement ventilation system)

With a base model using a specific ventilation system, the individual building and environmental characteristics can then be adjusted for the sensitivity analysis. In theory, the sensitivity study needs a continuous change of each characteristic parameter within a reasonable range to acquire sufficient information for quantitative assessment of the influence of individual characteristics. For example, the south window in the base case should experience continuous variation of window area from full to zero. This may demand tremendous computing efforts. In addition, it is difficult to quantify the change of some variables, such as solar radiation. The present study merely tests a limited number of variations for each characteristic parameter to accumulate basic and qualitative knowledge of appropriate use of the coupled simulation. Particularly, the investigation tests some extreme conditions for most variables, such as with and without solar radiation, with and without window, to qualitatively analyze the influence of each characteristic on coupling simulation. Table 9.3 summarizes the major variation cases studied for the ventilated room with different systems.

Table 9.3 Major variation cases studied for a room with different ventilation system

HVAC Systems	**Ceiling-jet mixing ventilation**	**Side-wall-supply displacement ventilation**	**Floor-supply displacement ventilation**
	constant-air-volume system		
	variable-air-volume system		
Environment conditions	constant outdoor air temperature		
	cloudy day (no solar radiation)		
Occupancy and operating conditions	no internal load		
	day only operation (9:00-18:00)		
Building envelope materials	all heavy materials (thermal mass)		
	no south window but R-13 south wall		
	no south window but R-7 south wall		
Building geometries	quadruple floor area		
	double ceiling height		

In order to demonstrate the benefits of a coupled simulation over a non-coupled simulation, both simulations are performed for each base and variation case. In the coupled simulation, all types of the coupling strategies implemented are used to identify the most suitable coupling process for a particular building. More specifically, for the base case and each variation case, the following simulations are performed in sequence:

(1) Non-coupled simulation;

(2) Coupled simulation with:

- Full dynamic coupling (FDC);
- Quasi dynamic coupling (QDC);
- One-time-step dynamic coupling (ODC);
- Dynamic bin coupling (DBC).

Since the theoretical analysis and numerical experiments in Chapter 7 indicate that data coupling method-1 is the most reliable and efficient data-exchange method, this method has been used for all the coupled simulations in this sensitivity study.

9.2.1 Office with Ceiling-Jet Mixing Ventilation System

The ceiling-jet ventilation system is a widely used HVAC design, which usually supplies fresh air from ceiling-mounted diffusers and exhausts indoor air from near-floor outlets. Because of the strong supply air, the room air is fairly well-mixed. In practice, different types of ceiling diffusers are available, which may lead to different indoor airflow patterns, as investigated by Srebric (2000). This sensitivity study only tests two general and abstract forms of diffusers with the same rectangular geometry: horizontal supply diffuser and vertical supply diffuser, as illustrated in Figure 9.3. The vertical supply diffuser is used in the base case with a constant supply air volume rate at $0.36m^3/s$. The supply air temperature can be automatically adjusted based on the cooling energy requirement. The control air temperature at the center of the room is 20°C. The vertical supply diffuser may not be practical in reality because of the draft risk, but it is acceptable for this sensitivity study that aims to create a complete mixing environment with less concern of thermal comfort. Table 9.4 presents the variation cases investigated.

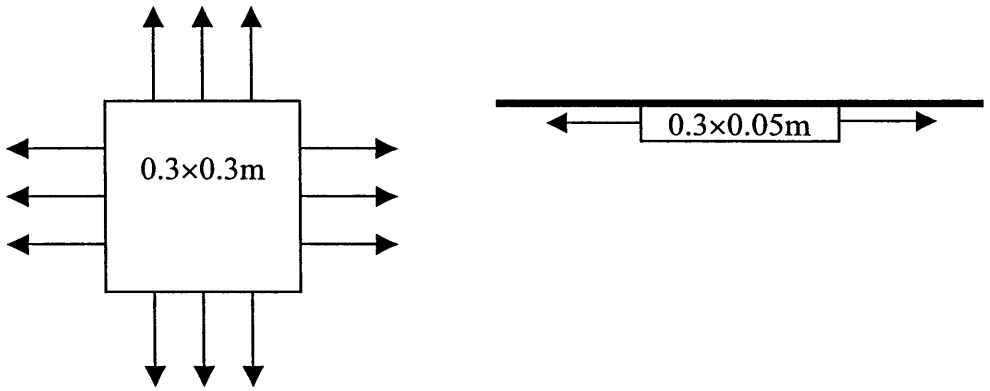

(a) horizontal supply ceiling diffuser

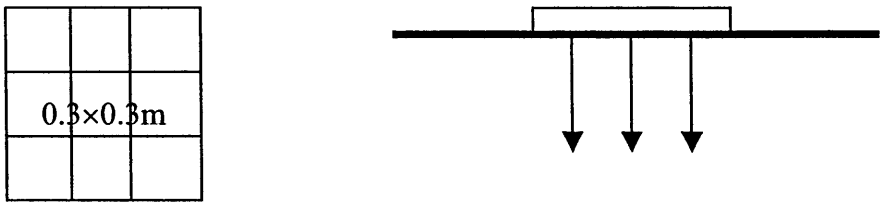

(b) vertical supply ceiling diffuser

Figure 9.3 Illustration of two ceiling-mounted air-supply diffusers

Table 9.4 Summary of the base and variation cases for the office with ceiling-jet mixing ventilation system

	Base Case		Variation Cases
HVAC systems	***Ceiling-jet mixing ventilation system***	Vertical supply diffuser, CAV system, $\dot{V} = 0.36 m^3/s$, $T_{control}$=20°C	**V-1**: horizontal supply diffuser
			V-2: VAV system, T_{supply}=18°C
			V-3: $T_{control}$=25°C
Environment conditions	Outdoor air temperature	Boston summer design day conditions	**V-4**: Boston summer cloudy day and constant $T_{outdoor}=T_{max}$
	Solar radiation		**V-5**: Boston summer cloudy day (no solar radiation)
Occupancy and operating conditions	Internal loads	100 W occupant, 270 W computer	
	Schedule	Day and night (24 hours)	**V-6**: day only (9:00-18:00)
Building envelope materials	Wall, ceiling, floor	R-19 ceiling and floor, R-13 walls, all light materials (no thermal mass)	**V-7**: R-19 ceiling and floor, R-13 walls, all heavy materials (thermal mass)
	South window	2.7×2.1=5.67m^2, clear 6mm glass	**V-8**: no window but R-13 south wall
			V-9: no window but R-7 south wall
Building geometries	Floor area	3×4=12m^2	**V-10**: quadruple 6×8=48 m^2
	Ceiling height	2.4m	**V-11**: double 4.8m

Figure 9.4 presents the total cooling load in the day predicted by the non-coupled and hourly full dynamic coupled simulation. The figure shows the effect of building characteristics on the building cooling energy. The solar radiation at the window is clearly a dominant heat source to the space. The case of a cloudy day (V-5) or without the window (V-8 and V-9) can reduce the cooling load as large as about half. The results also expose that the calculated load has no significant difference from that of the base case when using the horizontal supply diffuser (V-1) or VAV system (V-2) or heavy envelope materials (V-7). Both the quadruple floor area case (V-10) and double ceiling height case (V-11) double the area of the exterior-facing south wall and the window, resulting in the notable increase of cooling load (about 60-70%). The case with only daytime operating hours (V-6) has limited energy-savings (about 25%) because the major cooling energy is required during the daytime.

Figure 9.4 also shows that all the coupled cooling loads are larger than the uncoupled results due to the convection coefficients and the indoor air temperature gradients transferred from CFD to ES. As indicated by Figure 9.5, the difference can be

as large as 25%. Eight of the twelve cases have the significant difference above 10%. The case with constant high outdoor temperature (V-4) has the largest error of the cooling load between two simulations because of the continuous high convective heat from CFD. The case with horizontal supply diffuser (V-1) also has about 20% prediction difference of the cooling load. This is because the cold supply air attaches to the enclosure surfaces and flows downward to the floor, enhancing the convection between the cold air and surfaces, as illustrated in Figure 9.6.

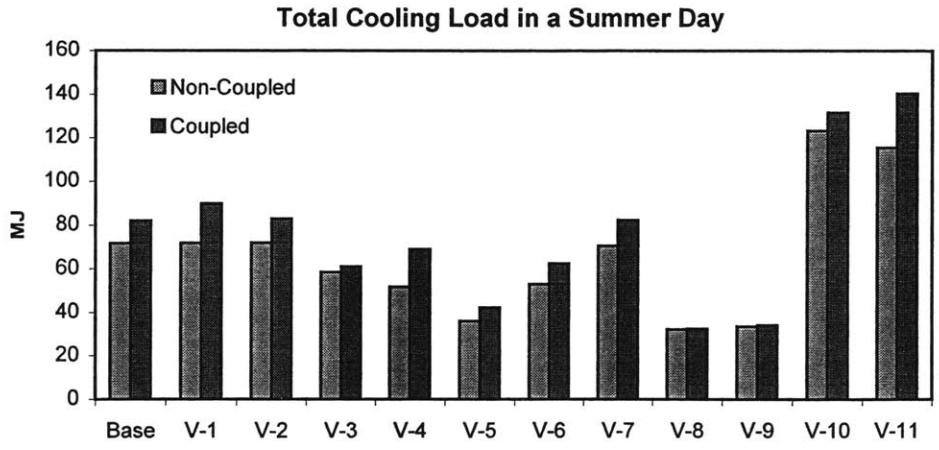

Figure 9.4 Total cooling load in a summer day with different building conditions

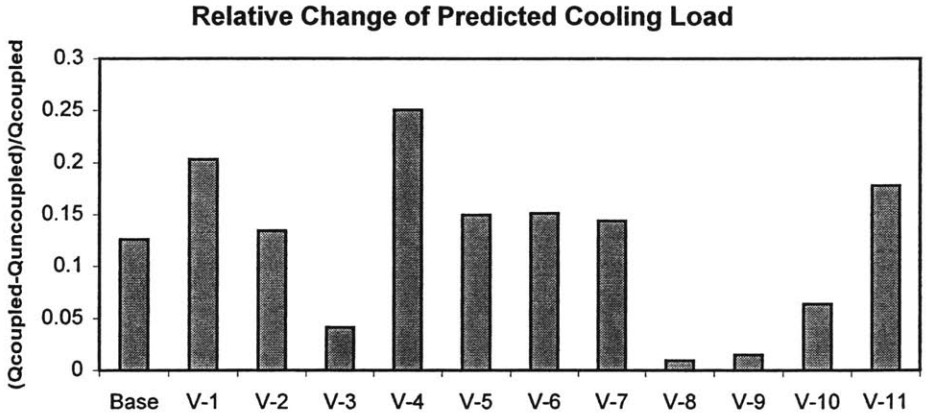

Figure 9.5 Relative errors of predicted cooling load with coupled and non-coupled simulations for different building conditions

The cases with small energy difference (<10%) are V-3 (the case with high indoor air control temperature), V-8 and V-9 (the cases without the south window), and V-10 (the case with quadruple floor area). The reason for the small changes is that the temperature gradients near the enclosures (especially the south wall and window) for V-3, V-8 and V-9 are smaller even compared to the cloudy day case (V-5) that has the same magnitude of low cooling load. Figure 9.7 shows the temperature profiles in the center of

the room from the south window to the north wall for V-3, 5, 8, and 9. V-5 has the sharpest temperature gradient at the south window. Since the supply air velocity is fixed with a CAV system, the airflow pattern is basically unchanged and the temperature gradients determine the convective heat gains from the enclosures. The small energy difference for the quadruple floor area case (V-10) is mainly because the supply air with the original speed can reach limited indoor space. As a result, the airflow velocity close to the envelopes is much smaller than that for the base case.

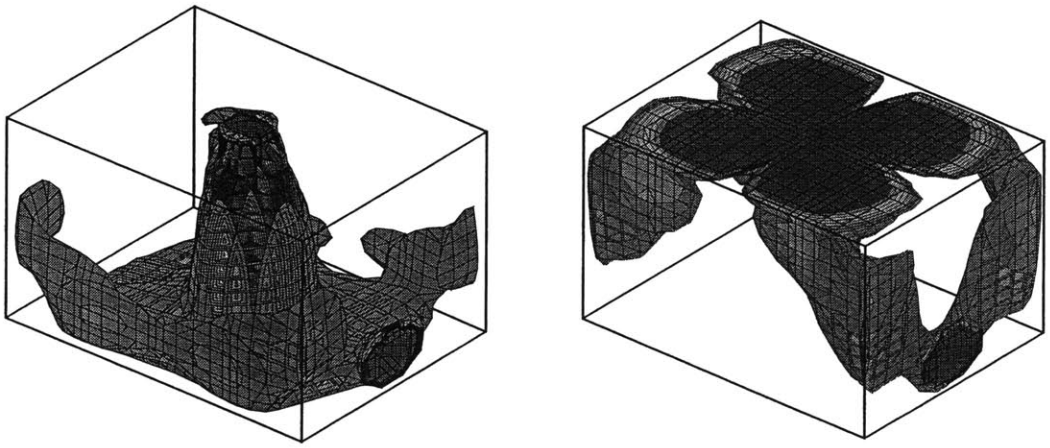

Figure 9.6 Airflow speed contour (V>0.5m/s) at 12 pm
(left: vertical supply diffuser – Base Case; right: horizontal supply diffuser – V-1)

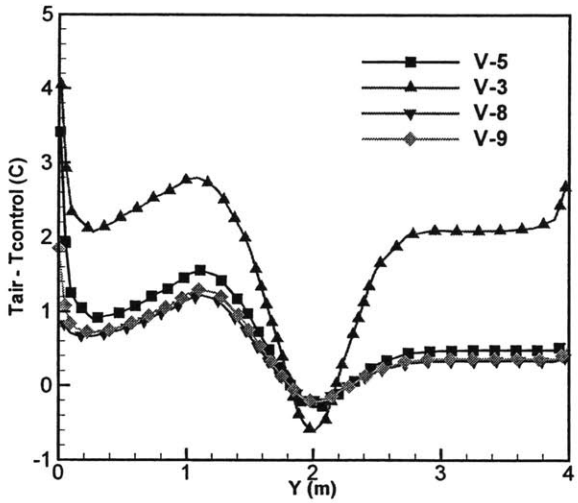

Figure 9.7 Indoor air temperature profile in the center of the room from south wall/window (Y=0) to north wall (Y=4m)

Although the coupled results of the cooling load have no significant change from the uncoupled ones for V-3, 8, 9, and 10, some differences of the results are still noticed. For example, Table 9.5 presents the calculated daily-averaged interior surface

temperatures for case V-8 that has a R-13 south wall without window. The difference of the temperatures between the non-coupled and coupled simulation is about 1°C.

Table 9.5 Daily-averaged interior surface temperatures predicted by coupled and non-coupled simulations for the case with a whole R-13 south wall

Enclosures	Interior Surface Temperature (°C)	
	Non-coupled results	Coupled results
South wall	21.8	20.8
North wall	21.5	20.4
West wall	21.5	20.6
East wall	21.5	20.4
Floor	21.4	20.4
Ceiling	21.6	20.5

The study further investigates the performance of different coupling strategies. In theory, hourly full dynamic coupling can provide the most precise simulation results; however, it takes the longest time to complete a calculation. The computing time becomes more considerable if a coupling is used for the warm-up period, which may eventually make a coupled simulation impractical for most building design applications. The other coupling strategies, such as quasi-dynamic coupling and one-time step dynamic coupling, may significantly reduce the computing time. However, it is unclear whether these coupling processes can produce the same results as the full dynamic coupling. It is meaningful to apply all kinds of coupling strategies to the base and variation cases, with the particular interest to address

(1) whether the coupling is necessary for the warm-up days of a simulation day;
(2) whether the other coupling processes can provide reasonably similar results as the full dynamic coupling but with less computing cost;
(3) whether the coupling frequency can be reduced without significantly affecting the solutions.

The investigation results on this ceiling-jet mixing ventilation office show that:

(1) The coupling in the warm-up days before the formal simulation day is necessary, especially for the buildings with considerable thermal masses. Otherwise, the results during the initial hours of the formal simulation day will significantly deviate from the real solutions, resulting in the inconsistence of solutions at 0:00 and 24:00 of the simulation day, as indicated by Figures 9.8 and 9.9.
(2) The dynamic bin coupling strategy can greatly reduce the computing cost for the warm-up period. Rather than using coupled simulation for all the warm-up days, the dynamic bin coupling method performs the coupled simulation only for the first day of the warm-up period. The recorded dynamic CFD information is then used for the rest of the warm-up days. Figures 9.8 and 9.9 show that the results by this strategy are the same as those achieved by using the coupled simulation for all the days. However, the computing time is reduced by more than half, as seen in Table 9.6.

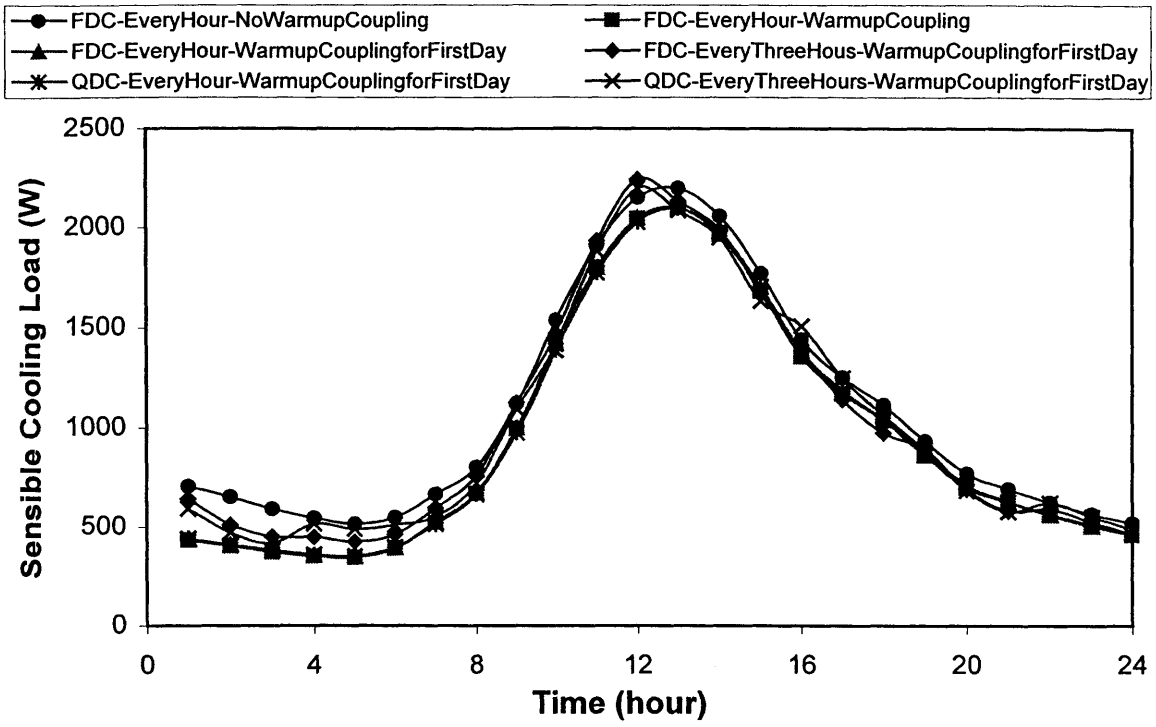

Figure 9.8 Predicted sensible cooling load during the summer day for the variant case with heavy envelope materials (V-7) with different dynamic coupling strategies

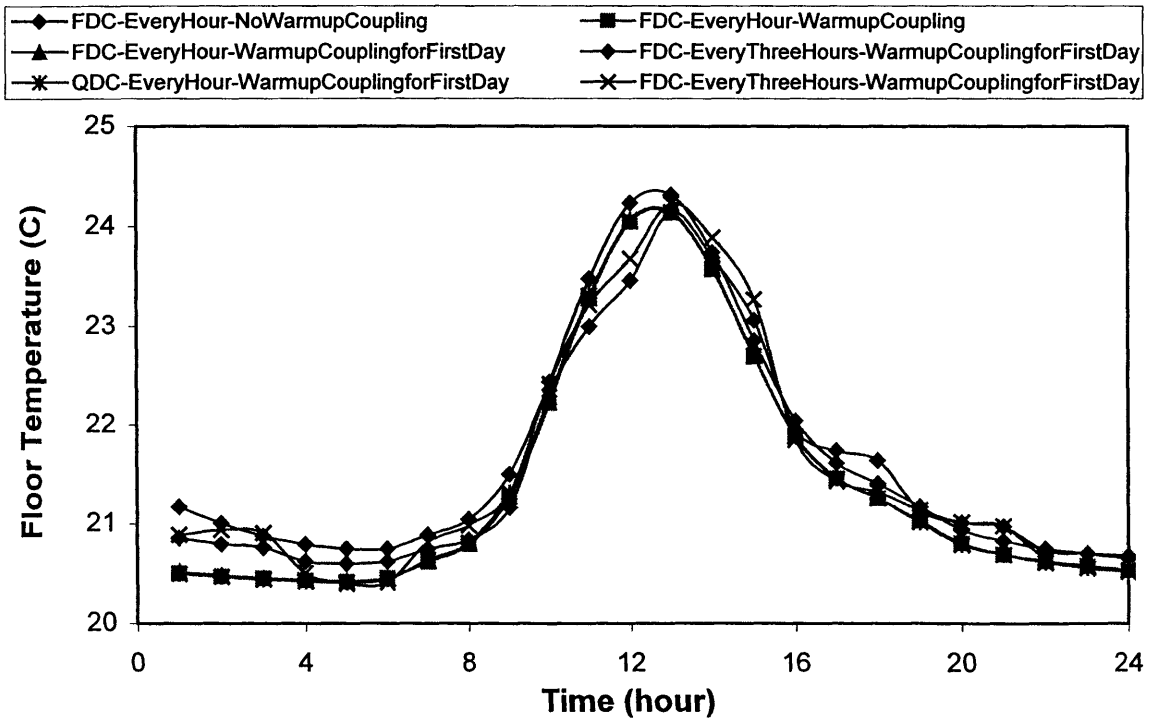

Figure 9.9 Predicted floor temperature during the summer day for the variant case with heavy envelope materials (V-7) with different dynamic coupling strategies

(3) The quasi-dynamic coupling can provide solutions very similar to the full dynamic coupling while dramatically reducing computing costs, as indicated by Figures 9.8, 9.9, 9.10, and Table 9.6. However, if the indoor environment or building envelope encounters significant changes between two time steps, as during the start-up and shut-down period of the daytime operation case (V-6), using CFD results at the last time step to the current time step of ES may cause serious prediction problems.

(4) Reduced coupling frequency (for example, every three hours) further saves computing time but the results show some degree of difference and non-smoothness as revealed in Figures 9.8 and 9.9. Taking V-7 case as an example, the total cooling energy predicted with the every-three-hour full dynamic coupling method is about 6% larger than that with the hourly full dynamic coupling method.

(5) One-time-step dynamic coupling is not suitable for most cases with dynamic environmental and/or operational conditions. But it is ideal for cases with small variability of building thermal behaviors, such as the cases with the whole R-13 and R-7 south walls (V-8 and V-9) in which the building indoor environment is under the limited influence of outdoor dynamic conditions, as demonstrated by Figure 9.11. The one-time step dynamic coupling can reduce the computing time to less than ten minutes for case V-8 and V-9, as examples.

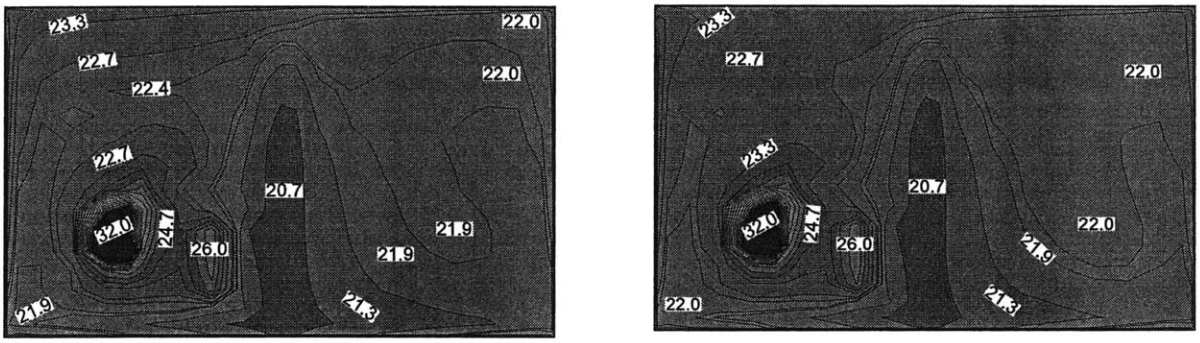

Figure 9.10 Indoor air temperature distribution at 12 pm in the Y-Z plane across the occupant and equipment of the case with heavy envelope materials (V-7) (left: by hourly full dynamic coupling simulation; right: by hourly quasi-dynamic coupling simulation)

Table 9.6 Computing time for the case with heavy envelope materials (V-7) using different dynamic coupling strategies

Dynamic coupling strategy	**Computing time**
FDC-EveryHour-NoWarmupCoupling	5 hours 55 minutes
FDC-EveryHour-WarmupCoupling	24 hours 20 minutes
FDC-EveryHour-WarmupCouplingforFirstDay	11 hours 48 minutes
FDC-EveryThreeHours-WarmupCouplingforFirstDay	5 hours
QDC-EveryHour-WarmupCouplingforFirstDay	1 hour 41 minutes
QDC-EveryThreeHours-WarmupCouplingforFirstDay	38 minute

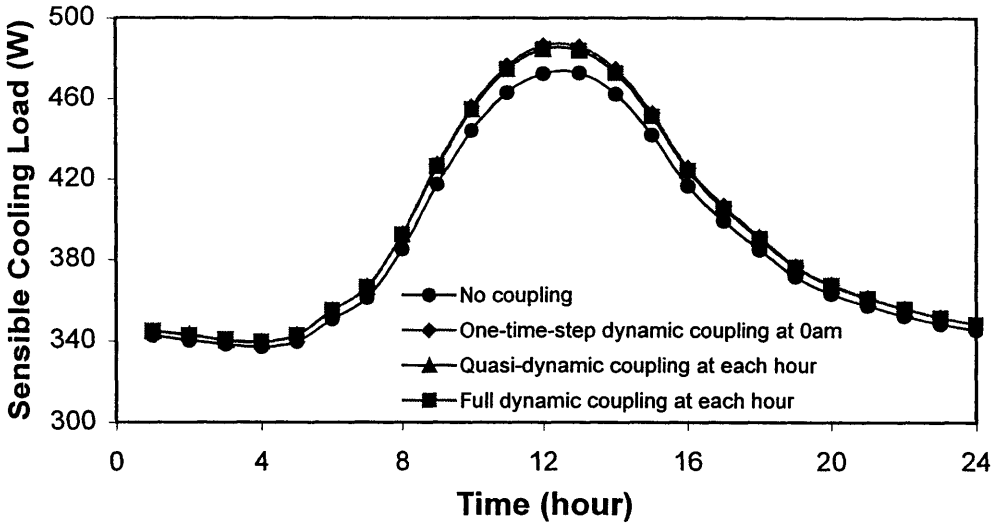

Figure 9.11 Predicted sensible cooling load for the case with R-7 south wall (V-9)

9.2.2 Office with Side-Wall-Supply Displacement Ventilation System

Displacement ventilation is an advanced ventilation approach. As explained in detail in Chapters 4 and 8, displacement ventilation can provide a cleaner indoor environment with less energy consumption due to the dominant upward flow and vertical air temperature stratification. The most common displacement ventilation system uses a horizontal discharge diffuser at a low sidewall position to supply fresh air into the indoor space. The supply air has a slightly lower temperature than the room temperature and a fairly low supply velocity. When the air flows over the floor and rises as it is heated by sources such as people and equipment, the indoor heat and contaminants can be removed directly without circulation and exhausted from the ceiling vent.

This study uses a box diffuser of 0.6m(W)×1.0m(H) in the middle of the north wall above the floor to supply air at 16°C by a variable air volume (VAV) control system. The indoor air temperature at the center of the room is controlled at 25°C. Table 9.7 summarizes the primary descriptions of the base case and its variations for sensitivity analysis. Similar simulation and analysis processes as those for the ceiling-jet cases have been conducted for this study. Both the non-coupled and coupled simulations were performed for each test case. All the coupling strategies implemented have been examined in order to identify a best coupling approach for each particular case.

The study shows that the total cooling load predicted by the coupled simulation has only marginal increase from that predicted by the non-coupled simulation for all the cases, as revealed by Figure 9.12. The reasons have been analyzed in Section 8.6.2:

(1) The dominant buoyancy-driven indoor airflow has relatively small convective heat transfer coefficients for most building enclosures except the floor. These coefficients can be reasonably simulated by the natural convection empirical correlations of the ES program, as presented in Table 8.8.

(2) In the coupled simulation, the increased convective heat from the floor is offset by the reduced convective heats from the other enclosures. The reduction is attributed to the overall surface temperature drop due to the significant decrease of the floor surface temperature, as demonstrated by Figure 8.53 and Table 8.8.

However, because of the distinctive vertical indoor air temperature stratification, the exhaust air temperature at the ceiling is much higher than the mean room air temperature, as demonstrated in Figure 9.15. As a consequence, the supply air mass flow rate with the VAV system can be greatly reduced by the coupling, as shown in Figure 9.13 and 9.14. The results indicate that the difference between the coupled and uncoupled predictions can be as large as over 40%. The high ceiling case (V-11), which has the most significant vertical temperature gradient as exhibited in Figure 9.15, has the maximum deviation of predicted supply air mass between the coupled and uncoupled results. The improvement with the coupling is not significant for the cases with less cooling loads because of the corresponding small indoor air temperature gradients.

Table 9.7 Summary of the base and variation cases for the office with side-wall-supply displacement ventilation system

	Base Case		Variation Cases
HVAC systems	***Side-wall-supply displacement ventilation system***	Side-wall box diffuser, VAV system, T_{supply}=16°C, $T_{control}$=25°C	**V-1**: CAV system, $\dot{V} = 0.12\,m^3/s$
Environment conditions	Outdoor air temperature	Boston summer design day conditions	
	Solar radiation		**V-2**: Boston summer cloudy day (no solar radiation)
Occupancy and operating conditions	Internal loads	100 W occupant, 270 W computer	**V-3**: no internal objects
	Schedule	Day and night (24 hours)	**V-4**: day only (9:00-18:00)
Building envelope materials	Wall, ceiling, floor	R-19 ceiling and floor (middle floor), R-13 walls, all light materials (no thermal mass)	**V-5:** R-19 ceiling and floor (middle floor), R-13 walls, all heavy materials (thermal mass)
			V-6: top floor (R-19 roof)
	South window	2.7×2.1=5.67m^2, clear 6mm glass	**V-7**: no window but R-13 south wall
			V-8: no window but R-7 south wall
			V-9: three-pieces window and walls: top, middle, bottom
Building geometries	Floor area	3×4=12m^2	**V-10**: quadruple 6×8=48 m^2
	Ceiling height	2.4m	**V-11**: double 4.8m

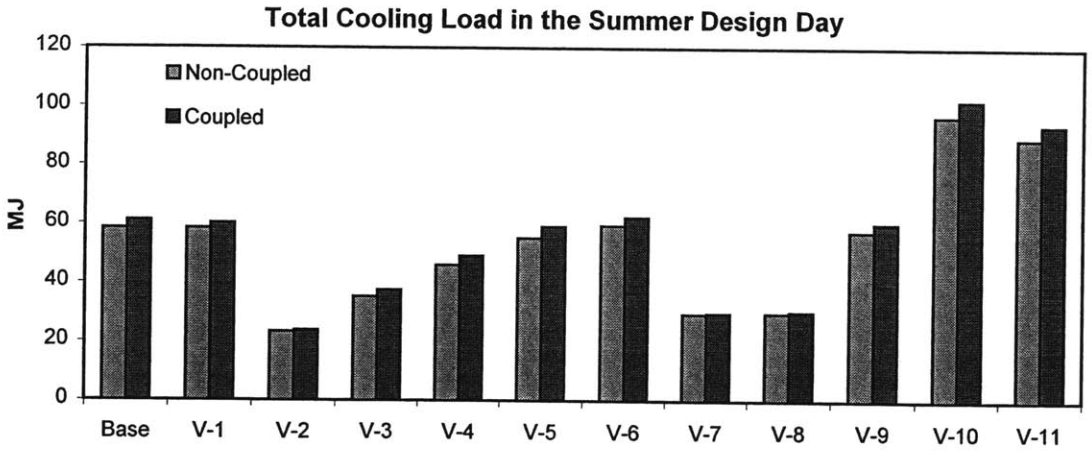

Figure 9.12 Predicted total cooling load from coupled and non-coupled simulations

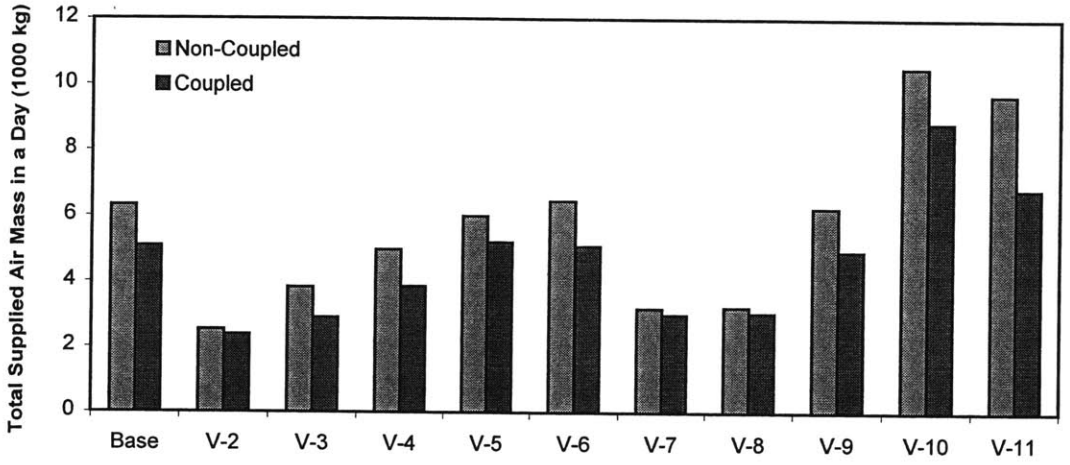

Figure 9.13 Comparison of total supplied air mass in the summer day for different cases

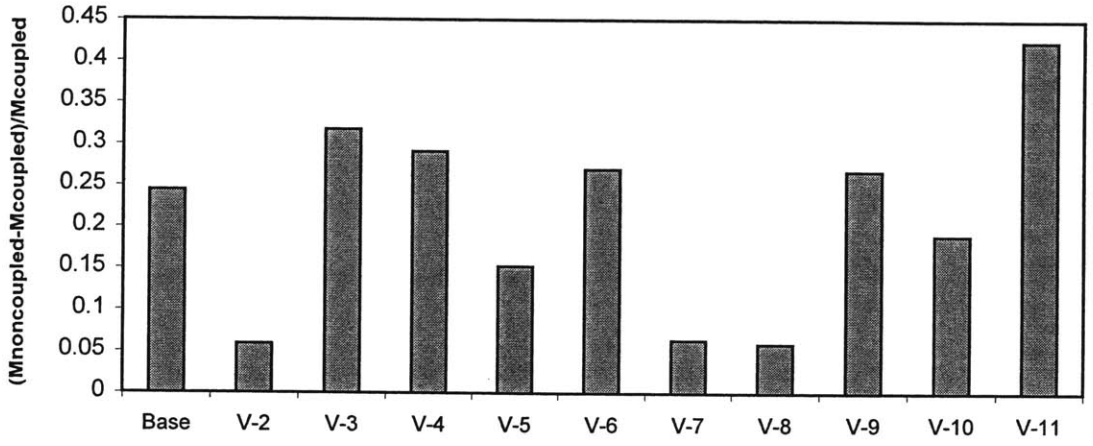

Figure 9.14 Relative change of supply mass between coupled and uncoupled solutions

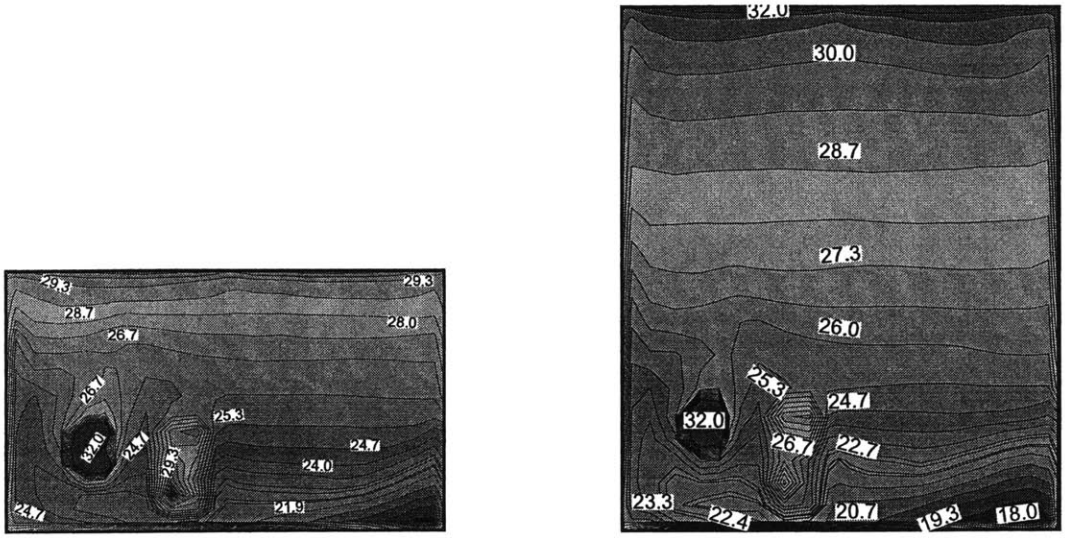

Figure 9.15 Indoor air temperature distribution at 12 pm in the Y-Z plane across the occupant and equipment for the base case and double ceiling height case (V-11)

The case without internal heat objects (V-3) verifies that the heat from building enclosures is of the same order as that from the internal heat sources. Because no heat sources exist in the occupying zone, the vertical air temperature stratification is larger such that the relative change of the coupled and uncoupled results of supply mass is larger than that for the base case.

The study investigates the effect of the uniform surface assumption on the coupled solution by dividing each wall and window into three pieces from top to bottom (V-9). The results reveal that the uniform assumption has little impact on the coupled simulation although explicit surface temperature gradients do exist. As Figure 9.16 shows, the uniform surface temperature equals the average of the gradient values and the air temperature profiles close to the surface from two simulations are almost the same.

The study also finds that exposing the ceiling (roof) to the outdoor environment (V-6) will not change the simulation results. This is probably because of good insulation of the ceiling and weak convective heat at the ceiling due to the slow air movement and small temperature difference between the ceiling and the air close to the ceiling.

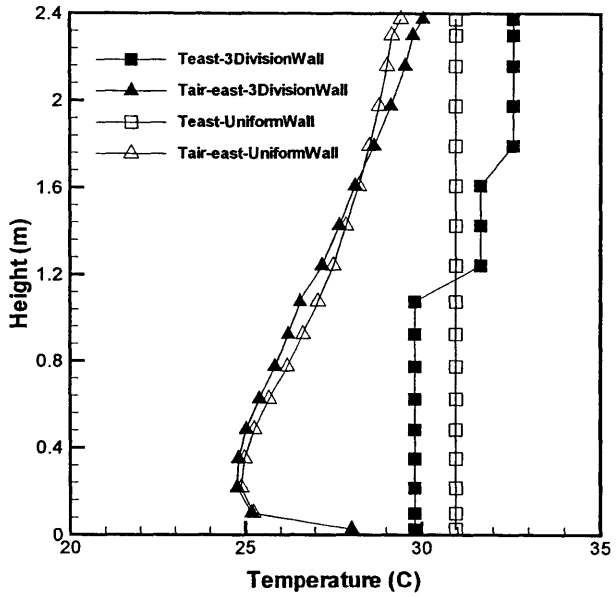

Figure 9.16 Profiles of east wall temperature and air temperature close (0.025m) to the east wall at 12 pm with uniform and non-uniform surface assumption

The study intensively compares the performance of different coupling strategies. As indicated in Section 8.6.2 of Chapter 8, the quasi-dynamic coupling with limited CFD interior iteration steps (100 steps) cannot provide proper solutions for this displacement ventilation case. This is because the dominant buoyancy-driven air movement in displacement ventilation requires more iteration in each CFD to achieve a converged and stable solution. The study finds that the quasi-dynamic coupling with more iteration steps (500 steps) in each CFD can obtain similar results as the full dynamic coupling. This is true even for the case with a whole R-13 south wall (V-7), which has relatively small fluctuation of indoor environment conditions. Figure 9.17 presents the floor temperature of case V-7 predicted using different coupling methods but without applying coupling to the warm-up period. The figure clearly demonstrates:

(1) Large difference exists between the coupled and uncoupled results;
(2) One-time-step dynamic coupling provides somehow different results because the CFD results obtained at 0:00 (the beginning of a day) may not be appropriate for the rest of the day;
(3) Quasi-dynamic coupling with 100 CFD iteration steps shows the explicit converging process during the morning hours and tends to approach the full dynamic coupling results in the later afternoon;
(4) Quasi-dynamic coupling with 500 CFD iterations has results very close to those from full dynamic coupling except at the initial hours because of the historical thermal effect;
(5) Both quasi-dynamic and full dynamic coupling simulations show the importance of the coupling for the warm-up days because otherwise inconsistent solutions are obtained at 0:00 and 24:00.

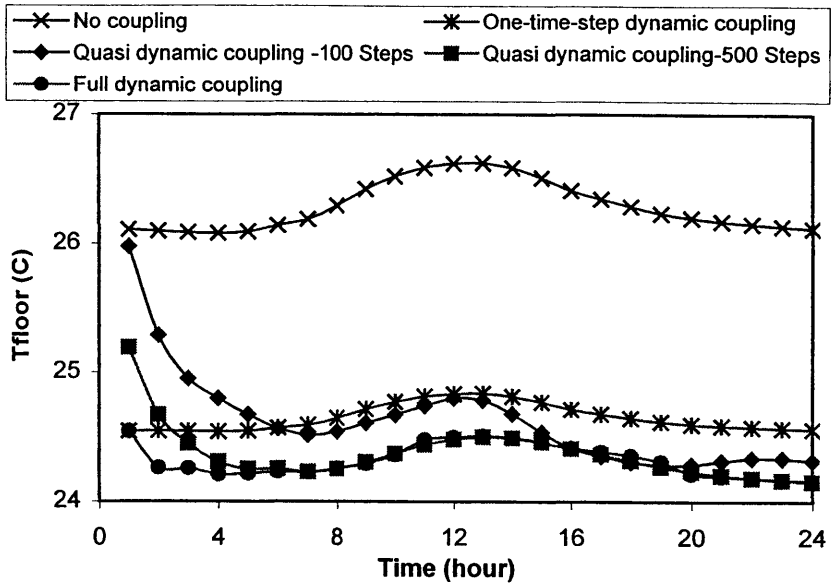

Figure 9.17 Predicted floor temperature for the R-13 south wall case (V-7)

The same conclusions can be drawn for the other cases, such as the case with heavy envelope materials (V-5) presented in Figure 9.18. Although it provides similar results as the full dynamic coupling, the quasi-dynamic coupling with sufficient CFD interior loops has no substantial saving of the total computing time, as presented in Table 9.8. The results show that the coupling at the frequency of every two hours can provide reasonably good solutions while saving about half of the time. But the coupling at the frequency of every three hours may result in obvious non-smoothness of the solutions.

Table 9.8 Computing time for the case with heavy envelope materials (V-5) with different dynamic coupling strategies

Dynamic coupling strategy	**Computing time**
FDC-EveryHour-NoWarmupCoupling: 100 CFD Steps	4 hours 46 minutes
FDC-EveryHour-WarmupCouplingforFirstDay: 100 CFD Steps	9 hours 51 minutes
FDC-Every2Hours-WarmupCouplingforFirstDay: 100 CFD Steps	5 hours 40 minutes
QDC-EveryHour-NoWarmupCoupling: 500 CFD Steps	3 hours 53 minutes
QDC-EveryHour-WarmupCouplingforFirstDay: 500 CFD Steps	7 hour 57 minutes
QDC-EveryHour-WarmupCouplingforFirstDay: 100 CFD Steps	1 hour 45 minutes
QDC-Every2Hour-WarmupCouplingforFirstDay: 500 CFD Steps	3 hour 39 minutes
QDC-Every2Hour-WarmupCouplingforFirstDay: 100 CFD Steps	43 minutes
OTS-0am-WarmupCouplingforFirstDay: 100 CFD Steps	48 minute

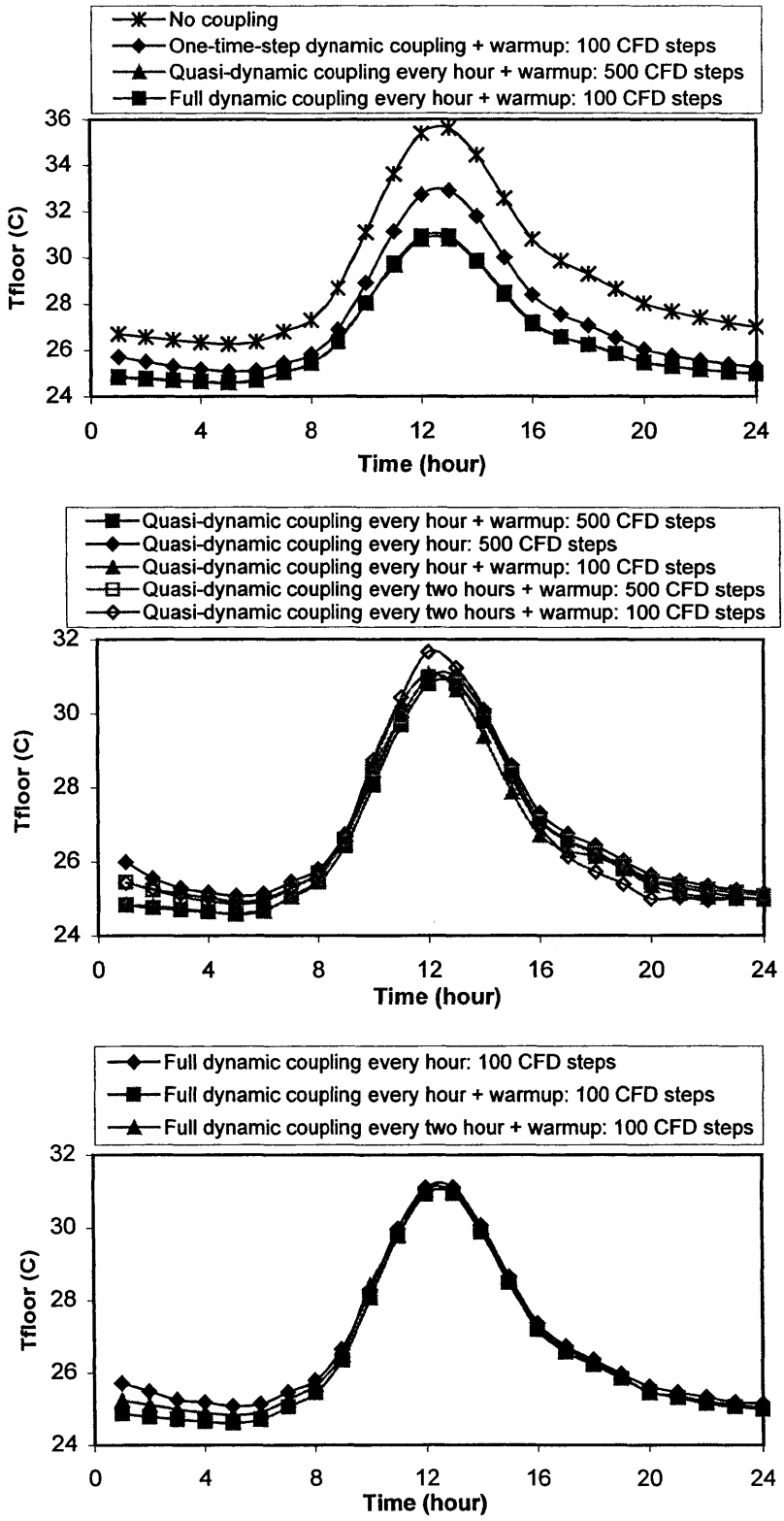

Figure 9.18 Predicted floor temperature for the case with heavy envelope materials (V-5) using different dynamic coupling strategies

9.2.3 Office with Floor-Supply Displacement Ventilation System

One major advantage of displacement ventilation is that the one-dimensional upward airflow in the occupied zone, due to the positive buoyancy, can remove heat and contaminants without mixing. However, displacement ventilation with sidewall diffuser introduces a large recirculation at the lower part of the space (Chen at al 1998), which is adverse to the one-dimensional upward flow. This recirculation can result in cross-contamination between occupants. The floor-supply displacement ventilation system has thus been developed to solve the recirculaion problem (Kobayashi 2001). A typical floor-supply displacement ventilation system supplies fresh air through a perforated floor or small supply air diffusers on the floor and exhausts upward thermal plumes from the ceiling vent. This study uses the office with a floor-diffuser-supply displacement ventilation system to study the performance of coupling simulation. Two 0.3×0.3m floor diffusers are installed on the floor, as sketched in Figure 9.2. The study investigates two types of floor diffusers: (1) vertical supply diffuser; (2) swirl supply diffuser, as illustrated in Figure 9.19. Table 9.9 summarizes the base case and its variations studied.

(a) Vertical supply floor diffuser

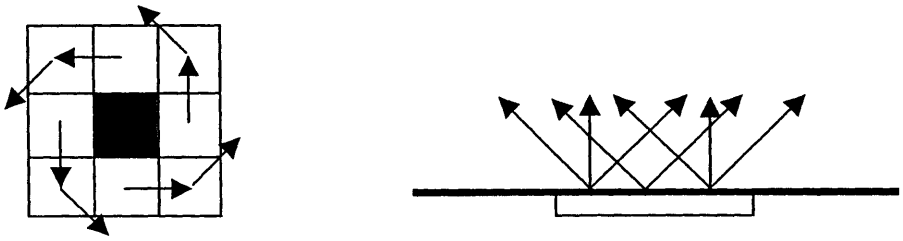

(b) Swirl supply floor diffuser

Figure 9.19 Illustration of two kinds of floor diffusers

The simulation results show that the cooling load predicted for the office with floor-supply displacement ventilation is almost the same as that for the office with side-wall-supply displacement ventilation. Similar to the side-wall-supply case, the cooling load calculated by the coupled and non-coupled simulation for this case have no significant difference, as shown in Figure 9.20. The type of floor diffuser (vertical or swirl supply diffuser) and the diffuser control systems (VAV or CAV) have almost no influence on the cooling load calculation. However, the indoor airflow and temperature distributions do appear different when using different floor diffusers, as demonstrated by Figures 9.23 and 9.24.

Table 9.9 Summary of the base and variation cases for the office with floor-supply displacement ventilation system

	Base Case		Variation Cases
HVAC systems	***Floor-supply displacement ventilation system***	Floor square vertical supply diffusers, VAV system, T_{supply}=19°C, $T_{control}$=25°C	**V-1**: floor square swirl supply diffusers
			V-2: CAV system, $\dot{V} = 0.126 m^3/s$
Environment conditions	Outdoor air temperature	Boston summer design day conditions	
	Solar radiation		**V-3**: Boston summer cloudy day (no solar radiation)
Occupancy and operating conditions	Internal loads	100 W occupant, 270 W computer	
	Schedule	Day and night (24 hours)	**V-4**: day only (9:00-18:00)
Building envelope materials	Wall, ceiling, floor	R-19 ceiling and floor, R-13 walls, all light materials (no thermal mass)	**V-5:** R-19 ceiling and floor, R-13 walls, all heavy materials (thermal mass)
	South window	2.7×2.1=5.67m^2, clear 6mm glass	**V-6**: no window but R-13 south wall
			V-7: no window but R-7 south wall
			V-8: three-pieces window and walls: top, middle, bottom
Building geometries	Floor area	3×4=12m^2	
	Ceiling height	2.4m	**V-9**: double 4.8m

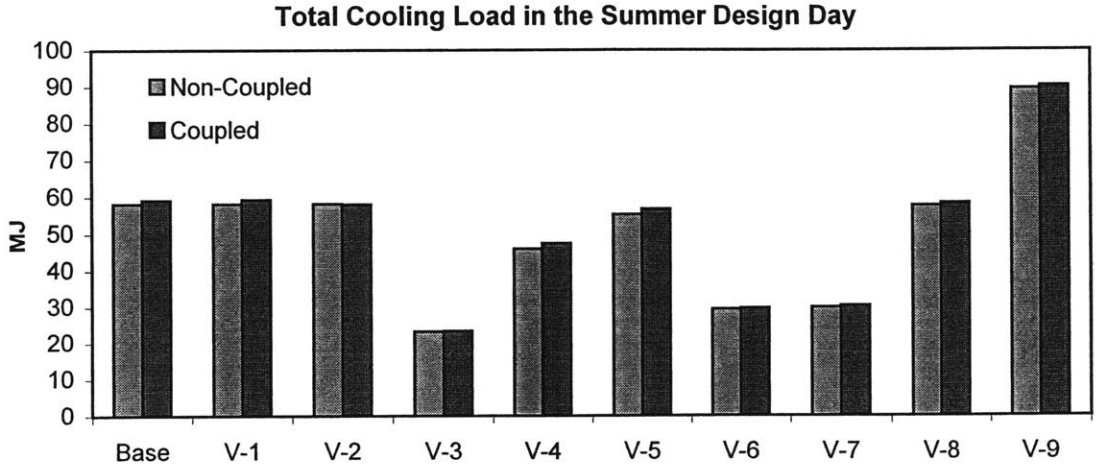

Figure 9.20 Predicted total cooling load from coupled and non-coupled simulations

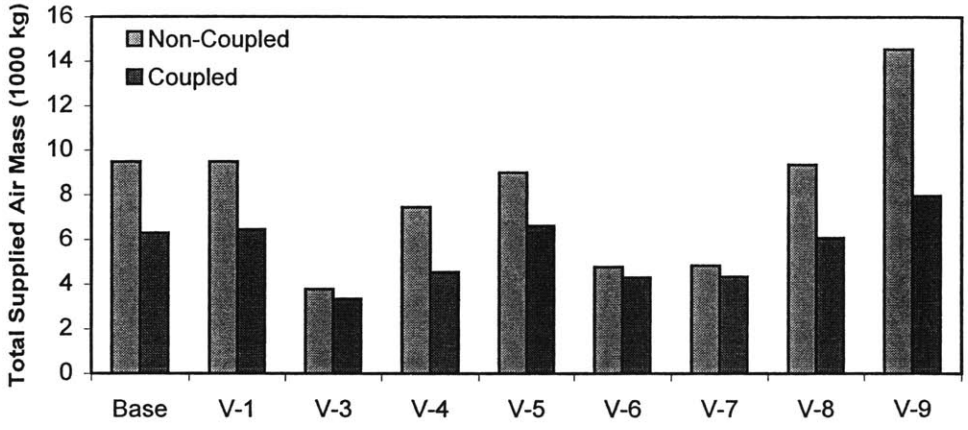

Figure 9.21 Comparison of total supplied air mass in the summer day for different cases

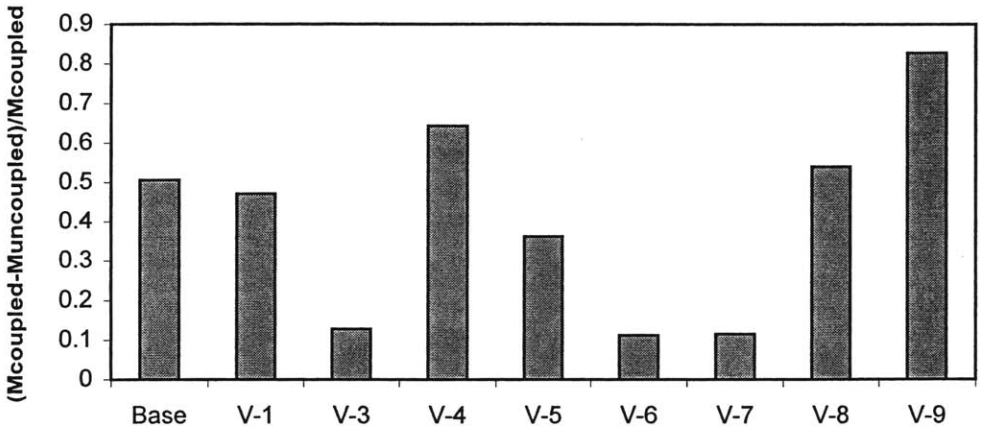

Figure 9.22 Relative change of supply mass between coupled and uncoupled solutions

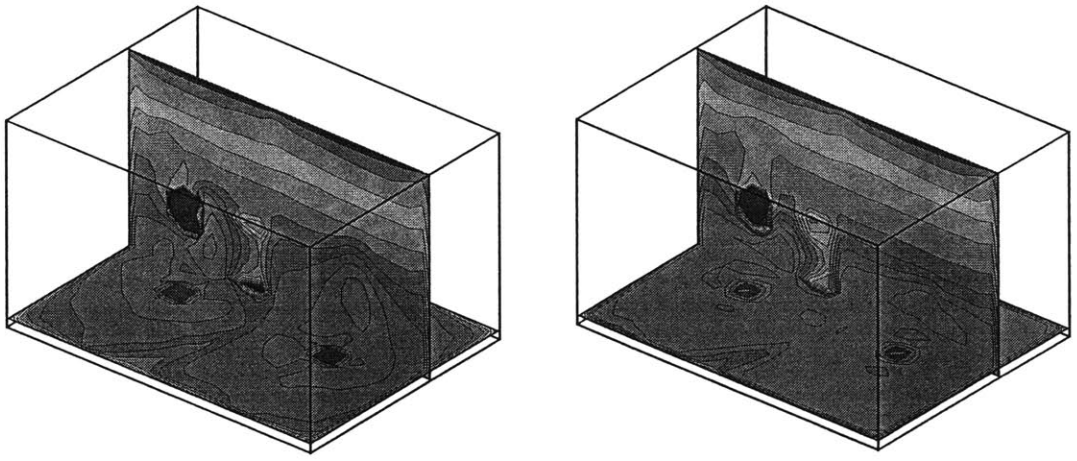

(a) using vertical floor diffuser (b) using swirl floor diffuser

Figure 9.23 Indoor air temperature distributions at 12pm at the section across the occupant body and the computer and the section close to the floor

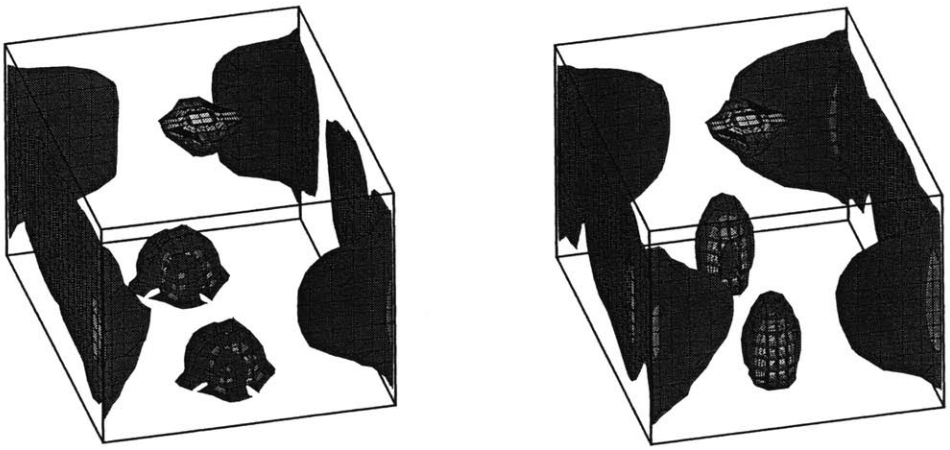

(a) using vertical floor diffuser (b) using swirl floor diffuser

Figure 9.24 Contours of indoor airflow speed (>0.2m/s) at 12pm

As with the side-wall-supply case, the total mass of supply air predicted by the coupled simulation is much smaller than that by the non-coupled simulation due to the high exhaust air temperature. The relative change of the solutions is even higher than that in the side-wall-supply case, as shown in Figure 9.22. For example, for the base case, the relative change is 24% for the side-wall-supply case and 50% for the floor-supply case; and for the double ceiling height case, the relative change is 42% for the sidewall-supply case and 83% for the floor-supply case. This implies a larger difference between the exhaust air temperature and mean room air temperature for the floor-supply displacement ventilation, as verified by Figure 9.25. Figure 9.24 and 9.25 further verify that the floor-supply displacement ventilation will not cause more serious thermal discomfort of air draft and cold feet than the side-wall-supply displacement ventilation unless very close to the diffusers.

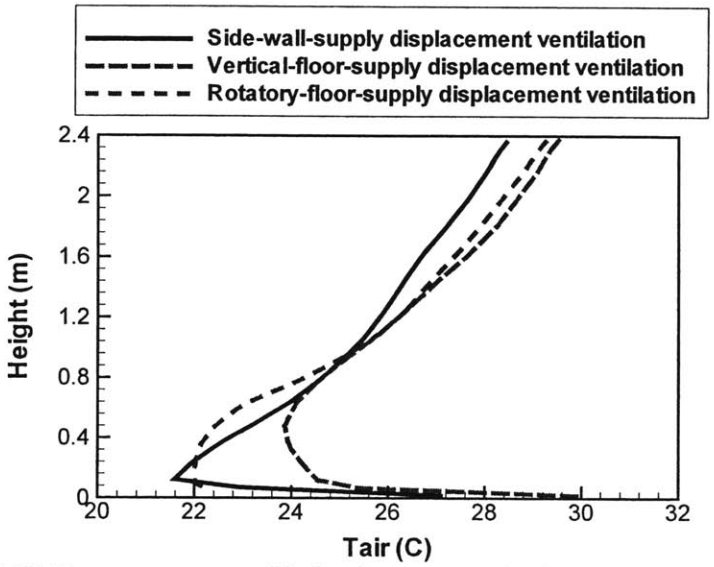

Figure 9.25 Temperature profile in the center of office at 12:00 for the base case

Figure 9.26 presents the predicted floor temperature for different cases. The results verify again that the uniform surface assumption has little impact on the simulation results. The swirl supply diffuser provides slightly lower floor temperature because the cold supply air can reach more floor area. The CAV system has a marginally higher floor temperature due to the different supply conditions. The case with heavy building envelopes postpones the peak floor temperature from 12:00 to 13:00 and the temperature fluctuation is moderate.

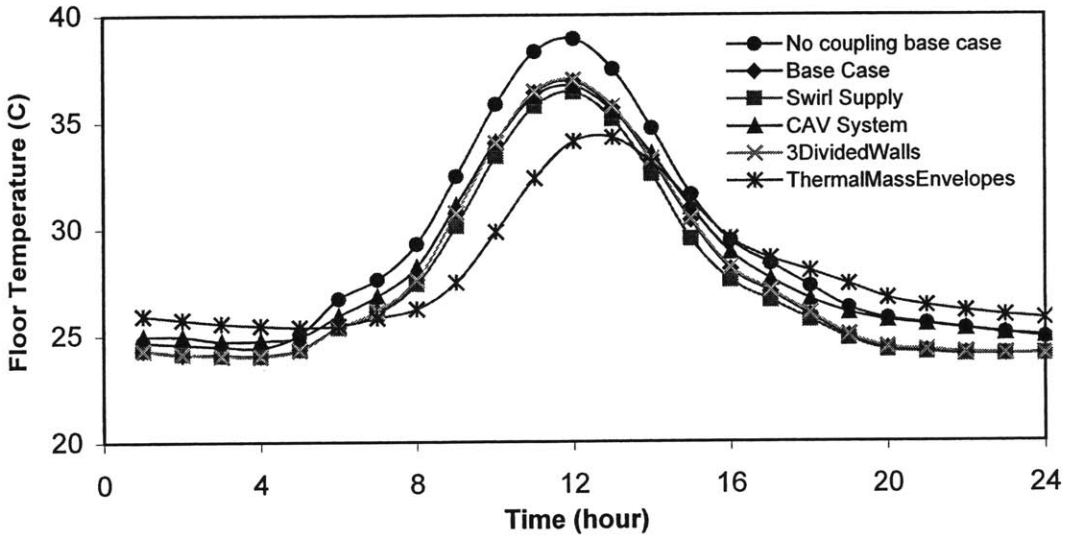

Figure 9.26 Floor temperature with full dynamic coupling simulation

The investigation of various coupling simulation strategies for this floor-supply case reaches the same conclusions as those obtained in the side-wall-supply case. The one-time-step coupling is not sufficient for accurate prediction of dynamic building behaviors, even for the cases with slight fluctuation of thermal performance. More iteration in each CFD is essential for the quasi-dynamic coupling to reach a converged solution at each coupling step. However, this fine iteration in CFD is superfluous for the full dynamic coupling because the stable-approaching iteration between CFD and ES will provide sufficient CFD iterations before a converged solution is eventually reached. It turns out that the quasi-dynamic coupling saves little time over the full dynamic coupling although the solutions obtained are fairly similar. The study further indicates that the coupling frequency of every two hours is a minimum requirement to acquire a smooth and reasonable solution. Figure 9.27 presents the convective heat flux at the floor predicted by different coupling strategies with the heavy envelope case (V-5) and Table 9.10 compares the computing time for each calculation. It is noticed that at least 4-5 hours are required to achieve a reasonable solution for this case.

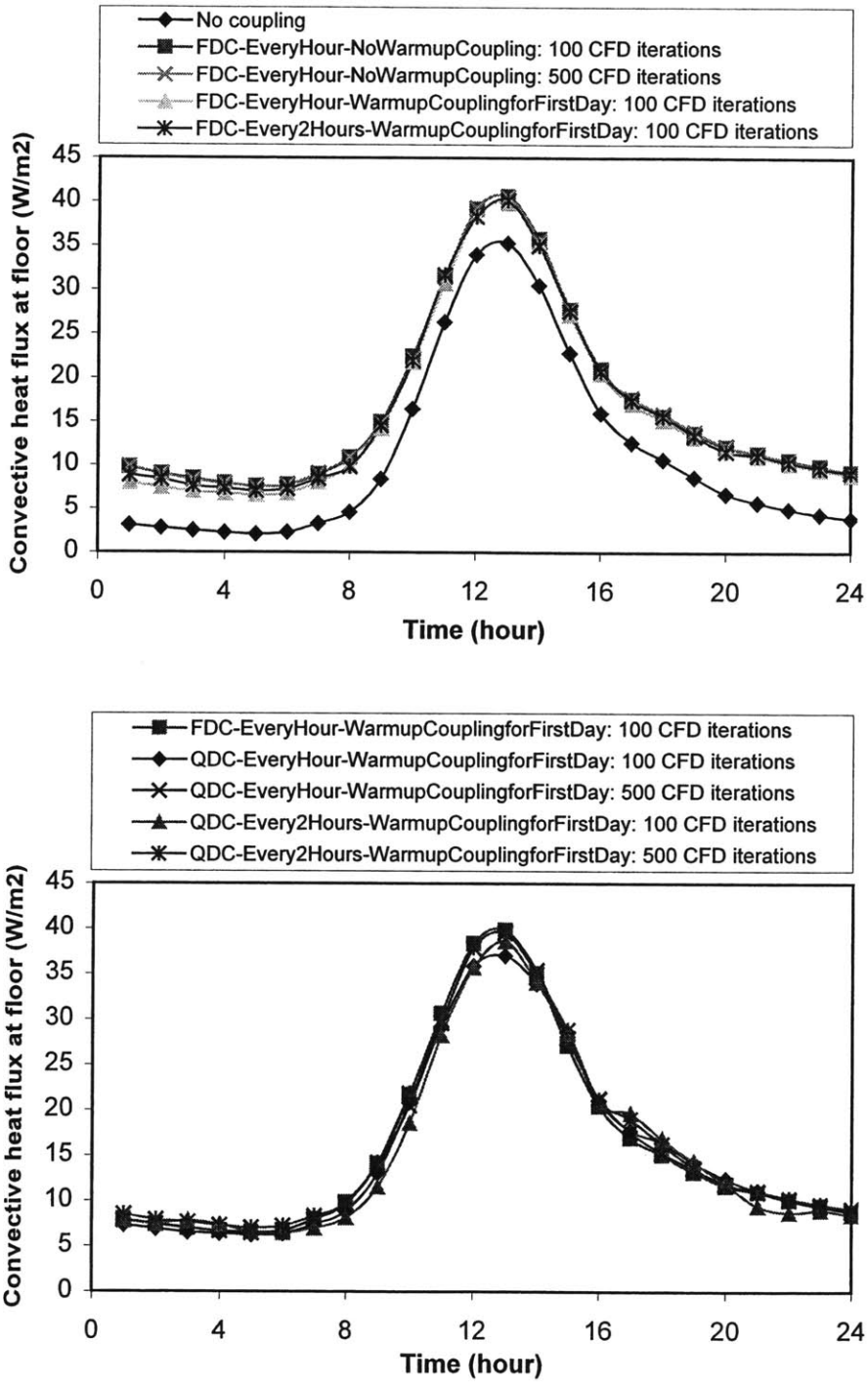

Figure 9.27 Convective heat flux at the floor for the case with heavy envelope materials (V-5)

Table 9.10 Computing time for the case with heavy envelope materials (V-5) with different dynamic coupling strategies

Dynamic coupling strategy	Computing time
FDC-EveryHour-NoWarmupCoupling: 100 CFD Iterations	6 hours 6 minutes
FDC-EveryHour-NoWarmupCoupling: 500 CFD Iterations	17 hours 32 minutes
FDC-EveryHour-WarmupCouplingforFirstDay: 100 CFD Iterations	11 hours 5 minutes
FDC-Every2Hours-WarmupCouplingforFirstDay: 100 CFD Iterations	5 hours 6 minutes
QDC-EveryHour-WarmupCouplingforFirstDay: 500 CFD Iterations	7 hour 1 minutes
QDC-EveryHour-WarmupCouplingforFirstDay: 100 CFD Iterations	1 hour 23 minutes
QDC-Every2Hour-WarmupCouplingforFirstDay: 500 CFD Iterations	4 hour 5 minutes
QDC-Every2Hour-WarmupCouplingforFirstDay: 100 CFD Iterations	49 minutes

9.3 General Suggestions for Using ES-CFD Coupling Simulation

The sensitivity studies and the validations and applications in the previous chapter extensively examine the performance of various coupling simulation strategies. These practices help form the basic knowledge about the appropriate selection of a particular simulation approach for a specific building. In general, the building and environmental characteristics and solution accuracy requirement determine the best simulation strategy. Usually, at the early stage of a building design, a non-coupled simulation may be sufficient because many building details have not been determined and a quick and rough prediction of building performance is desired. When the design advances further, a more accurate simulation of integrated building behaviors is expected and a coupled simulation may be required.

A coupled simulation provides a more accurate and informative prediction of building performance but needs a much longer computing time. It is the user's choice to determine the best compromise between accuracy and cost. Based on the case studies and sensitivity analysis, this study summarizes the average solution improvement ranges and computing costs of the coupled simulation in Table 9.11 for different scenarios. The general measurement errors are also included in the table as a reference. Although the data of Table 9.11 may vary with cases studied and methodologies used, the table provides users a gross sense about the potential benefits and cost of a coupled simulation.

The sensitivity analysis indicates that buildings with significant indoor airflows, such as those with mixing ventilation, may encounter considerable change of energy consumption by using coupling. Significant indoor air temperature stratifications may influence slightly the cooling load but significantly the supply airflow rate. The building and environmental characteristics that may cause notable change of envelope and indoor air conditions determine the coupling level between ES and CFD.

Table 9.11 Average solution improvement and computing cost of coupled simulation

		Natural Convection	Mixing Ventilation	Displacement Ventilation
$\lvert T_{room-couple} - T_{room-noncouple} \rvert$ (°C)		~0.5	~2	~2
$\lvert T_{surface-couple} - T_{surface-noncouple} \rvert$ (°C)		~0.5	~1-5	~2-5
$\left\lvert \frac{Q_{couple} - Q_{noncouple}}{Q_{couple}} \right\rvert$		~5-10%	~10-25%	~2-5%
$\left\lvert \frac{\dot{M}_{couple} - \dot{M}_{noncouple}}{\dot{M}_{couple}} \right\rvert$			~10-30%	~20-50%
Computing cost with hourly full dynamic coupling for each simulation day (second/grid)		0.1-0.2	2.0-2.6	2.0-2.7
Measurement accuracy	T	±0.2-0.5°C	±0.5-1°C	±0.3°C
	Q	±2-10%	±10%	

Note: T is the peak temperature. Q is the heating/cooling energy requirement, $\dot{M}$ is the supply air mass flow rate. Measurement accuracy data are from the experimental reports by Lomas et al. (1994), Hiramatsu et al. (1996), Fisher (1995), Wallenten (1998), and Chen et al. (1998).

According to the investigation results, this research has established some general guidelines for the appropriate usage of a coupled simulation. The major concerns and corresponding suggestions about coupling simulation have been summarized below.

(1) In which circumstance are a separate ES and CFD or a static coupling sufficient?

A separate ES and CFD is appropriate if

a. building design and calculation is at the early stage;
b. building has fairly mixed indoor environment and properly calibrated convective heat transfer coefficient correlations;
c. indoor airflow is dominated by internal heat gains.

For these calculations, a one-way or two-way static coupling can always be used to manually exchange relevant information between ES and CFD. The static coupling avoids the substantial iteration between ES and CFD and thus significantly reduces the computing cost.

(2) In which circumstance is a dynamic coupling necessary?

A dynamic coupled simulation is desired if

a. building has obvious indoor air temperature stratifications and/or perceptible indoor air movement;
b. indoor air environment is heavily dependent on the thermal boundary conditions.

(3) Which coupling strategy should be used?

The selection of coupling strategy is determined by building features and simulation requirements.

a. In general, one-time-step dynamic coupling is not suitable for most cases with dynamic environmental and/or operational conditions. But it is ideal for the cases with small fluctuations of building thermal behaviors, such as the case with good insulations that makes the indoor environment receive little influence from the varying outdoor conditions and the case in the winter design day that has constant outdoor conditions. One-time-step dynamic coupling uses much less computing time than full dynamic coupling.
b. Full dynamics coupling conducts the most complete coupling between ES and CFD and thus results in the most accurate and informative predictions of building behaviors. However, it is most expensive in computing cost.
c. Quasi-dynamic coupling can provide solutions very similar to full dynamic coupling while significantly reducing computing cost for most cases because of no iteration in each coupling step. However, for some cases with unstable airflows, more iteration in CFD is required in order to reach a converged solution at each coupling step. This fine iteration in CFD is superfluous for full dynamic coupling because the stable-approaching iteration between CFD and ES will allow CFD to have sufficient iterations during the converging process at each coupling step. As a result, quasi-dynamic coupling for these cases saves very limited time compared to full dynamic coupling. In addition, if a building encounters a significant change of thermal behaviors, using CFD results at the previous step (especially with large time steps) for the current step of ES may lead to notable prediction errors.
d. Bin coupling method is a highly efficient coupling strategy. Static bin coupling is recommended if corresponding reliable bins are available and the dynamic indoor environment is not studied.
e. Since it is impossible to generate sufficient bins for diverse building conditions, dynamic bin coupling can be used to generate real-time bins for typical simulation days and the dynamic bins can then be used for the similar days. Quasi-dynamic or full dynamic or even one-time-step dynamic coupling can be employed to produce those dynamic bins in the typical days. Dynamic bin coupling can dramatically reduce the computing time, especially for the simulation on a long term (e.g. a year). Similar environmental and building operational conditions are the premise to the use of this approach.

(4) Which coupling frequency should be used?

The study indicates that the coupling frequency at every two hours is a minimum requirement in order to acquire a smooth and reasonable solution. The coupling at the frequency of every three hours results in obvious non-smoothness of the solutions. Hourly coupling is the frequency most recommended by this study. More frequent exchange of information between ES and CFD may not be necessary because of the small change of the inter-coupled conditions between two close coupling steps.

(5) *Is it necessary to use coupling for the warm-up period of a simulation for a typical design day?*

The coupling in the warm-up days before the formal simulation of a design day is necessary, especially for buildings with considerable thermal masses. Otherwise, the results at 0:00 of the simulation day will not be consistent to the results at 24:00 of the day. Buildings with very light materials may not need the coupling in the warm-up days because of the small thermal history effect from the ending hours of the last warm-up day to the beginning hours of the simulation day. Usually, the dynamic bin method can be used in the warm-up period to reduce the computing time due to the similarity of environmental and operational conditions of the warm-up days.

Finally, as a summary of this section, Table 9.12 lists all the coupling strategies and indicates their potential application scopes. As always, strictly dividing cases into different categories is difficult. Accumulation of knowledge and experience on similar cases is essential to the quick achievement of an accurate solution.

Table 9.12 ES-CFD coupling strategies and corresponding application scopes

Coupling Strategy	Applications
Static Coupling: One Step	For buildings with loose relationship between envelopes and indoor air, in which the change of inter-related variables is not significant. Only one side needs information from the other. For example, CFD may need boundary conditions from ES but ES is fairly insensitive to CFD results in an air-conditioned room with low velocity mixing ventilation.
Static Coupling: Two Step	For buildings with loose relationship between envelopes and indoor air, in which the change of inter-related variables is not significant. Both need information from each other.
Dynamic Coupling: One-Time-Step	For buildings with tight relationship between envelopes and indoor air but with small fluctuation of indoor and outdoor conditions. For instance, the study of residential buildings under winter design conditions, where the indoor load and outdoor weather have small variation during a day while the continuously operating HVAC system may tightly link the energy consumption with the indoor airflow.
Dynamic Coupling: Quasi	For most buildings with tight relationship between envelopes and indoor air and under continuous weather and load changes. These changes will significantly affect the building envelope and indoor air conditions.
Dynamic Coupling: Full	For buildings with very tight relationship between envelopes and indoor air and under significant weather and load changes. These changes will result in remarkable fluctuations of building envelope and indoor air conditions. Good for design day study due to the expensive computing cost.
Bin Coupling: Static	For most buildings without dramatic changes of heat/cooling load and outdoor air temperature, in which the appropriate bins are available and indoor environment are not concerned. Particularly feasible for long term simulations
Bin Coupling: Dynamic	For buildings with similar environmental, occupancy and operational conditions in a period of time. Good for long term simulations.

CHAPTER 10

CONCLUSIONS AND RECOMMENDATIONS

This chapter summarizes the primary results and conclusions from this study and indicates the problems associated with the coupling that may need further investigation.

10.1 Conclusions

CFD and building energy simulation (ES) programs provide plentiful and complementary information about building thermal performance, such as space cooling/heating load, distributions of indoor air velocity, temperature, and contaminant concentrations. This information is important to determine thermal comfort, indoor air quality, and energy consumption of a building that enable design of energy efficient, comfortable and healthy indoor environments.

This research explored the fundamentals, implementations and applications of the ES-CFD thermal coupling. The study developed a prototype of an integrated building simulation tool by incorporating a CFD program into an ES program.

(1) Why couple ES and CFD programs

Separate applications of ES and CFD programs need special assumptions in the calculations, such as the perfect mixing assumption of indoor air for ES. These assumptions may have significant impact on the solutions for some cases. An integration of CFD and ES can eliminate many of the assumptions because of the complementary nature of ES and CFD results. Therefore, it can result in a more accurate and detailed prediction of building performance.

Two different approaches are available to couple the CFD and ES models. A CFD program can be extended to include the functions of ES by solving heat transfer in solid materials and incorporating an appropriate radiation model, HVAC system model, and plant model. The extended CFD method sounds powerful but is very computationally expensive. This study has focused on the coupling of individual ES and CFD programs, in which CFD handles indoor air movement while ES solves heat radiation between surfaces and heat conduction in solid materials. This coupling approach can considerably save computing costs while providing comparable solutions, because:

(a) ES deals with heat conduction in building envelopes with various simplified methods, such as the simplification of one-dimensional heat conduction, which is reasonable for most envelope areas except corners.
(b) CFD in this approach can model airflows at specific time steps of interest, acting as "snap-shots" of the airflows with corresponding boundary conditions obtained from ES, instead of predicting all transient airflows with small time steps.

(c) CFD in this approach can be used for indoor spaces of particular interest rather than the whole building.

In general, the complementary and exchangeable information between ES and CFD programs may include:

(a) From ES to CFD:
- Supply energy requirements, such as dynamic supply air mass flow rate, air temperature, and/or radiator power;
- Enclosure interior surface temperatures;

(b) From CFD to ES:
- Convective heat fluxes from enclosure interior surfaces to indoor air;
- Convective heat transfer coefficients at enclosure interior surfaces;
- Indoor air temperature gradients;
- Exhaust air temperature at outlet.

By exchanging this information, a coupled simulation of ES and CFD can determine the following parameters that are interesting to system designers, consultants, researchers, and architects by one calculation:

- *Thermal comfort:*
  Air velocity distribution
  Air temperature distribution
  Relative humidity distribution
  Mean radiant temperature distribution

- *Indoor air quality:*
  Contaminant concentration distribution
  Ventilation effectiveness distribution

- *HVAC system design and energy analysis:*
  Space cooling/heating load
  Coil load
  Energy consumption of the HVAC systems

(2) Coupling challenges and strategies

The idea of ES and CFD program coupling seems straightforward. However, different physical models and numerical schemes used in ES and CFD impose challenges to the integration practice. The major challenge is the three discontinuities between ES and CFD programs. The first one is time scale discontinuity: ES has a characteristic time-scale of hours for heat transfer in building enclosure, while CFD has a few seconds for room air. The second one is space model discontinuity: the indoor environmental conditions predicted for each space in ES are spatially averaged, while CFD presents field distributions of the variables. The last one is computing speed

discontinuity: the computing time for ES is a few seconds per zone for an annual energy analysis and requires little computer memory, while a CFD calculation for a zone may take a few hours and require a large amount of memory.

In order to bridge these discontinuities between ES and CFD, this study has developed corresponding special coupling strategies. For the time scale discontinuity, the present study partitions the whole calculation into a long-time process for ES and a short-time scale process (strictly speaking, a quasi-static process at a given time-step) for CFD. The space model discontinuity is bridged by using appropriate numerical approximation. Although the numerical approximation method may influence the coupling performance depending on the problems studied, sufficient subdivisions of enclosure surfaces in ES can always diminish this effect. As for the computing speed discontinuity, beside using simpler mathematic models and numerical methods, such as zero-equation turbulence models, to reduce the CFD computing time, the study has proposed the staged coupling strategies to minimize the CFD calling times during a coupled simulation.

The staged coupling strategies consist of *static coupling process*, *dynamic coupling process*, and *bin coupling process*, as listed in Figure 10.1. The static coupling process has one-step or two-step information exchange between ES and CFD programs. With only a few coupling steps, the static coupling can be performed manually, which does not require arduous modifications of individual ES and CFD programs. The dynamic coupling process involves continuous coupling between two programs at each time step, which is further divided into three different categories. The first one is one-time-step dynamic coupling process that focuses on the coupling at one specific time step of interest. At that time step, the iteration between ES and CFD is carried out to reach a converged solution. The second one is quasi-dynamic coupling process. In a quasi-dynamic coupling, ES and CFD couple with each other without iteration at each time step in a period of time. That is, CFD receives the boundary conditions from the previous ES calculation at the current n^{th} time step and returns the thermal information of indoor air to ES at the next $(n+1)^{th}$ time step. The third one is full dynamic coupling process that iterates ES and CFD a number of times at each time step to reach a converged solution before moving on to the next time step.

The bin coupling process is an approach used to reduce computational costs. It provides ES the information that is pre-computed by CFD and saved in the bins for continuous energy calculation. Two bin coupling processes – static bin coupling process and dynamic bin coupling process – have been developed by this study. In a static bin coupling, the indoor air thermal information required by ES are pre-calculated by CFD as the functions of cooling/heating loads (for conditioned periods) or indoor-outdoor air temperature difference (for unconditioned periods). ES then determines these parameters for a particular calculation by directly interpolating the CFD results from the static function bins. Dynamic bin coupling, rather than generating curve-fitted functions and constructing a comprehensive bin system in advance, predicts the airflow details in some typical days by either quasi-dynamic or full dynamic coupling process. These results are then used in ES for the days with similar conditions.

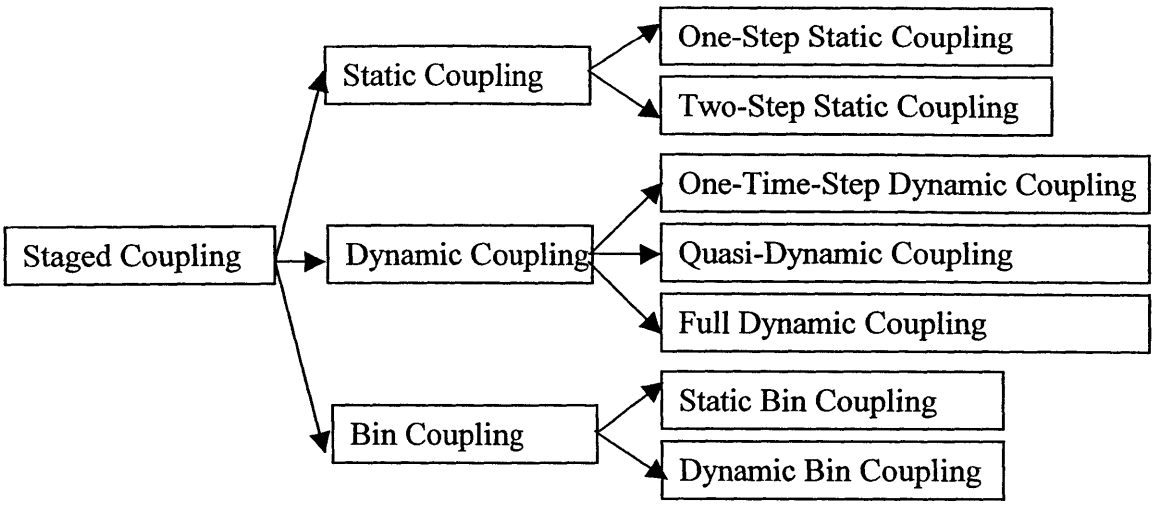

Figure 10.1 Tree of the staged coupling strategies

In practice, the building characteristics and the purpose of simulation determine the most suitable coupling process for a particular building. Sometimes, several coupling processes may be used together to achieve the best solution for a specific case.

(3) Coupling methods, algorithm, and solutions

In all of the coupling processes proposed above, the study indicated that the convective heat from building enclosure is the key link between ES and CFD. This information can be exchanged between ES and CFD in several different manners. The study analyzed all potential data-exchange methods and compared the performance of these methods theoretically and numerically. Table 10.1 summarizes the data coupling methods investigated and the comparisons of their performance.

Table 10.1 Summary of data coupling methods and their performance

Coupling Method	From ES to CFD	From CFD to ES	Convergence	Stability	Speed
1	Surface temperature	Convection coefficient and air temperature gradient	√√√	√√√	√√√
2	Surface temperature	Nominal convection coefficient	√√	√√	√√√
3	Surface temperature	Surface heat flux	√	√√	√
4	Surface heat flux	Convection coefficient and air temperature gradient	√	√	√

Note: one √ = fair; two √ = good; three √ = excellent.

Through theoretical analysis and numerical experimentation, the study verified that the solution of a coupled ES and CFD simulation does exist and is unique. The investigation also concluded that the iteration between ES and CFD programs with different data coupling methods can lead to a correct and converged solution.

However, the research also indicated that although mathematically identical, the various data coupling methods have different impacts on the accuracy, convergence, stability, and computing time of a coupled simulation. In general, coupling method-1 is more stable than the other coupling methods. The method can unconditionally satisfy the convergence condition when the heat transfer coefficient h is positive. Coupling method-2 has very similar performance as method-1, except that it may bring negative h values for some particular cases. The theoretical analysis indicated that the large negative h value may cause divergence and instability problems of simulation. Coupling method-3 is most computationally expensive, because it performs explicit iteration in ES while the others are implicit. The explicit iteration updates variables slowly and thus needs more CFD calls. Moreover, the explicit iteration usually means less stability in computation. Coupling method-4 requires special treatments to control indoor air temperature and to calculate the inter-coupled variables, resulting in more unstable performance than others.

The investigation found that a reasonable simulation convergence criterion could help quickly achieve accurate solutions of a coupled simulation. The study developed an improved iterative coupling and control algorithm that can accelerate the convergence of all the coupling methods. The algorithm also allows easy control of the indoor environment and space energy requirements by adjusting the thermal sensor location. The algorithm consists of three essential treatments:

(a) In each CFD calculation, CFD runs for up to one hundred iteration times without the requirement of convergence, because the supply air enthalpy (or, mass flow rate with a VAV system) is always updated during the coupling before reaching the final solution. The final CFD solution at each coupling step will be well converged if the boundary conditions approach the stable values.
(b) The entire CFD temperature field is modified based on the difference between the required air temperature and calculated air temperature at the control point.
(c) The modified outlet temperature from CFD is used in ES to generate the new inlet supply air enthalpy for the next CFD run.

The reasons that the algorithm is able to accelerate the convergence for all the coupling methods are:

(a) Superfluous iterations and critical criteria within each CFD run are not necessary since the boundary conditions are updated all the time.
(b) The modification of the temperature field forces it to approach the required temperature (the control temperature specified) more quickly. The effect is similar to providing a more reasonable initial temperature field for each CFD run.
(c) The modified outlet temperature, which is closer to the final result than that from the original CFD without the artificial modification, helps to capture the correct inlet enthalpy faster.

(4) Implementation of ES-CFD program coupling

All the coupling strategies and coupling methods proposed have been implemented by coupling the MIT-CFD solver with the EnergyPlus program. As a result, a coupling simulation program, named E+MIT-CFD, has been established.

The MIT-CFD solver was newly developed by this study, because the existing CFD programs need significant modifications (even on data and code structures) before they can be incorporated into an ES program. The program employs many standard CFD methods and adopts a number of advanced CFD techniques, allowing accurate, reliable and fast prediction of various airflows. The well-designed data and code structure of the program make it easy to plug into an arbitrary building energy simulation program. The EnergyPlus program, developed by Lawrence Berkeley National Laboratory, is a new-generation building energy analysis and thermal load simulation program, with many advantages over its parent programs of BLAST and DOE-2.

The development of E+MIT-CFD employed the modularity concept of modern programming. Rather than directly connecting ES and CFD programs, an interface module was created to contain the interface variables and conduct the data-exchange operations. The ES and CFD programs were then connected to the interface module, without the necessity of re-organizing their own data and program structures. This modular structure allows the minimum modifications in individual ES and CFD programs for coupling purpose, and thus avoids significant changes of the coupling program each time the individual ES and CFD models get updated. This characteristic also allows easy replacement of the ES and/or CFD solver with other programs in the coupling program.

(5) Validations and applications

The new MIT-CFD program has been validated by using five typical building indoor airflows with experimental data. The cases studied include typical natural, forced, and mixed convections in a cavity, mixing and displacement ventilation in a room. The validations verified the CFD solver is capable of simulating most building indoor airflows and heat transfers with reasonable accuracy and computing cost. The simple turbulence models, such as zero-equation module, can provide reasonable convective heat transfer from rigid surfaces with an appropriate grid system. The study indicated that a finer grid may not always lead to a better solution when using zero-equation turbulence model. In general, the scales of 0.05~0.1m and 0.002~0.005m are recommended for the first grid close to a surface when using Xu's zero-equation turbulence model to simulate forced convection and natural convection flows, respectively.

The study validated the coupling program developed with experimental data from four full-scale building experiment facilities. The cases investigated range from natural convection to forced convection and from mixed ventilation to displacement ventilation. The validations verified that the program developed can provide reasonable and reliable predictions on building performance. In general, the coupled simulation produces more accurate and detailed results than the separate simulations:

- CFD receives more precise and real-time thermal boundary conditions and can predict the dynamic indoor environment conditions that are important for the assessment of indoor air quality and thermal comfort.
- ES obtains more accurate convection heat at enclosures and can provide more accurate estimate of building energy consumption and dynamic thermal behaviors of building envelopes.

The study reveals that indoor air temperature gradient and convective heat transfer coefficient have great impact on the whole building simulation. The empirical coefficient correlations used in the separate ES may significantly deviate from the real situations and result in a mistaken prediction of building performance. The application studies further demonstrate the capability and importance of the coupling program for the design of energy efficient buildings and systems.

(6) General user guidelines

In order to establish some basic guidelines for the development and application of ES and CFD coupling, this research further analyzed the sensitivity of coupling simulation to major building and environmental characteristics. These characteristics include environmental conditions, HVAC systems, building occupancy and operating conditions, envelope materials, and building geometries. According to the investigations, the study provides general suggestions for the appropriate usage of a coupled simulation, as briefly repeated below.

(1) Under which circumstance is a separate ES and CFD sufficient?

a. building design and calculation is at the early stage;
b. building has fairly mixed indoor environment and properly calibrated convective heat transfer coefficient correlations;
c. indoor airflow is dominated by internal heat gains.

For these calculations, a one-way or two-way static coupling or a static bin coupling can always be used to manually exchange relevant information between ES and CFD as needed.

(2) Under which circumstance is a dynamic coupling necessary?

a. building has obvious indoor air temperature stratifications and/or perceptible indoor air movement;
b. indoor air environment is heavily dependent on the thermal boundary conditions.

(3) Which coupling strategy should be used?

a. In general, one-time-step dynamic coupling is not suitable for most cases with dynamic environmental and/or operational conditions. But it is ideal for the cases with small fluctuations of building thermal behaviors. One-time-step dynamic coupling uses much less computing time than full dynamic coupling.
b. Full dynamics coupling conducts the most complete coupling between ES and CFD and thus results in the most accurate and informative predictions of building performance. However, it is most expensive in computing cost.

c. If a building has no significant change of thermal behaviors, quasi-dynamic coupling can provide solutions very similar to full dynamic coupling and largely reduce the computing time for most cases because of no iteration in each coupling step. However, for some cases with unstable airflows, more iteration in CFD is required to reach a converged solution at each coupling step, resulting in very limited time saving of quasi-dynamic coupling.
d. Bin coupling method is a highly efficient coupling strategy. Static bin coupling is recommended if reliable bins are available and dynamic indoor environment is not concerned.
e. Dynamic bin coupling is a realistic and efficient coupling approach, which generates real-time bins for typical simulation days. The dynamic bins saved can then be used for the similar days. Quasi-dynamic or full dynamic or even one-time-step dynamic coupling can be used to produce those dynamic bins in typical days. Dynamic bin coupling can dramatically reduce computing costs, especially for the simulation on a long term (e.g. a year). Similar environmental and building operational conditions are the premise to the use of this approach.

(4) Which coupling frequency should be used?

The coupling frequency of every two hours is a minimum requirement in order to acquire a smooth and reasonable solution, although hourly coupling is suggested. More frequent exchange of information between ES and CFD may not be necessary because of the small change of the inter-coupled conditions between two close coupling steps.

(5) Is it necessary to use coupling for the warm-up period of a simulation for a typical design day?

The coupling in the warm-up days before the formal simulation of the design day is necessary, especially for buildings with considerable thermal masses. Otherwise, inconsistent solutions may be obtained at 0:00 and 24:00 of the design day. Buildings with very light materials may not need coupling for the warm-up days because of the small thermal history effect from the ending hours of the last warm-up day to the beginning hours of the design day. Usually, dynamic bin method can be used in the warm-up period to reduce the computing time due to the similarity of environmental and operational conditions of the warm-up days.

10.2 Recommendations for Future Research

This study developed a prototype of an integrated building simulation tool. To improve the qualities and enhance the capabilities of the program developed, further study is expected in these areas:

- *Further validation and improvement of the coupling program.* More realistic buildings with complex geometries and mixing usages of different HVAC systems should be used to examine the capability and robustness of the coupling program developed. Examples of this kind of building would be: multi-room family houses

using window-based AC units and natural/mechanical ventilation; multi-zone high-rise commercial buildings with displacement ventilation for the core zone of the buildings and chilled beam/radiator for the perimeter zone; and residential buildings with central HVAC systems and atrium. In addition, more accurate zero-equation turbulence models are always desired in the CFD solver. Since a universal turbulence model is impossible to obtain, the program can implement different zero-equation turbulence models that are calibrated for different indoor airflows. A self-adaptation algorithm can be developed to automatically switch the model during a simulation based on the airflow characteristics (e.g. Rayleigh and Reynolds number). Furthermore, the current coupling program uses three individual interfaces to generate the input files for the CFD, ES and coupling platform, respectively. It is highly desirable to have a consolidated interface for one coupled simulation.

- *Integration of zonal airflow models with the coupling program.* In an integrated simulation, CFD uses most of the computing time. The time may rise dramatically when more zones need the airflow information. In order to be acceptable for most engineering and design purposes, zonal airflow models, which need less computing efforts than CFD, can be integrated with CFD to cooperatively handle air movement problems in buildings and exchange information with ES programs. Zonal airflow models introduce more dynamics into the prediction of mean airflows compared to nodal models, but are less sophisticated than CFD. Zonal airflow models are distinguished from CFD in that they are generally quite coarse, do not necessarily attempt an accurate prediction of the flow field, and utilize more reduced forms of the governing differential equations. In zonal modeling, flow equations are formulated that attempt to account for how flow rates might change based on temperature differences, length scales, and initial momentum. Special "flow laws" may be required to complement the simplification and approximation of the flow equations, especially at those regions associated with a special flow driving mechanism, such as the areas close to walls and jets. These "flow laws" are generally simple correlations chosen or generated by the model developers. Although heavily dependent on the physically valid hypotheses and previous experiments, zonal airflow models are very versatile and can effectively provide airflow information with little investment and user-training. By integrating zonal airflow models into the coupling program, the computational effort can be significantly reduced because CFD is then only to predict the detailed airflow information for the crucial zones of a building while zone airflow models are to produce fast and general airflow predictions for all the other zones.

- *Connections of air pressures at building openings to weather data and building characteristics.* The current coupling simulation program has not been able to substantially handle natural ventilation designs. The major problem is that the air pressure difference at openings, due to the wind, cannot be determined. This air pressure at openings determines the potential mass flow rates and air flow directions through these openings. How to obtain these air pressure conditions, which are strongly related to the weather conditions and building characteristics (e.g. orientation, shape), should be resolved.

- *More system connections between the ES and CFD program.* The present coupling of CFD and ES has been focused on the thermal performance of the air space and envelope of a building, with few connections to the systems serving the building. The CFD results, such as the exhaust air temperature, will undoubtedly affect the simulation results of the system and plant models in ES. The work to integrate CFD solutions with system and plant models needs to be done.

REFERENCES

Allard F. and Inard C. 1992. "Natural and mixed convection in rooms: prediction of thermal stratification and heat transfer by zonal models," Room Air Convection and Ventilation Effectiveness, ASHRAE.

ASHRAE. 1997. "1997 ASHRAE handbook fundamentals," ASHRAE, Atlanta.

ASHRAE. 2000. "ASHRAE analytical test suite – building fabric," 1052RP Final Report, December.

Assem S.D. 1991. "Advanced matrix theory for scientists and engineers," Abacus Press, Gordon and Breach Science Publishers.

Awbi H.B. 1998. "Calculation of convective heat transfer coefficients of room surfaces for natural convection," Energy and Buildings, 28: 219-227.

Baker A.J. 1983. "Finite element computational fluid mechanics," Hemisphere Publishing, New York.

Beausoleil-Morrison I. 2000. "The adaptive coupling of heat and air flow modeling within dynamic whole-building simulation," Ph.D. Thesis, University of Strathclyde, Glasgow, UK.

Beausoleil-Morrison I. et al. 2001. "Further developments in the conflation of CFD and building simulation," Seventh International IBPSA Conference (BS2001), 2: 1265-1274, Rio de Janeiro, Brazil, August.

Bejan A. 1995. "Convection heat transfer," 2nd Ed., John Wiley and Sons Inc..

Bland B.H. 1992. "Conduction in dynamic thermal models: analytical tests for validation", Building Services Engineering Research and Technology, 13(4): 197-208.

Bland B.H. 1993. "Conduction tests for the validation of dynamic thermal models of buildings," BEPAC Technical Note 93/1, August.

Bohn M.S., Kirkpatrick A.T. and Olson D.A. 1984. "Experimental study of three dimensional laminar convection at high Reyleigh Number," ASME Journal of Heat Transfer, 106: 339-345.

Bouia H. and Dalicieux P. 1991. "Simplified modeling of air movements inside dwelling room," Proceedings of the Building Simulation Conference, August. (now IBPSA)

Boussinesq J. 1877. "Essai sur la theorie des eaux courantes," Mem. Presentes Acad. Sci. 23-46, Paris.

Broderick C.R. and Chen Q. 2001. "A simple interface to CFD codes for building environment simulations," Proceedings of Building Simulation Conference, 1: 577-584, Rio de Janeiro, Brazil.

Building Systems Laboratory. 1999. "BLAST 3.0 users manual," Urbana-Champaign, Illinois: Building Systems Laboratory, Department of Mechanical and Industrial Engineering, University of Illinois.

Charvat P. et al. 2001. "Numerical modeling of airflow and temperature fields in a glazed attic," Seventh International IBPSA Conference (BS2001), 1: 441-448, Rio de Janeiro, Brazil, August 13-15.

Cheesewright R., King K.J., and Ziai S. 1986. "Experimental data for validation of computer codes for prediction of two-dimensional buoyant cavity flows," In Significant questions in buoyancy affected enclosure or cavity flows, (Ed. by J.A.C. Humphrey, C.T. Adedisian and B.W. le Tourneau), ASME, 75-81.

Chen Q. 1988. "Indoor airflow, air quality and energy consumption of buildings," Ph.D. Thesis, Delft University of Technology, The Netherlands.

Chen Q. 1989. "Convective heat transfer in rooms with mixed convection," Proceeding of International Seminar on Air Flow Patterns in Ventilated Spaces, 69-82, Liege, Belgium, February.

Chen Q. 1995. "Comparison of different k-ε models for indoor airflow computations," Numerical Heat Transfer, Part B: Fundamentals, 28: 353-369.

Chen Q. 1996. "Prediction of room air motion by Reynolds-stress models," Building and Environment., 31(3): 233-244

Chen Q., Glicksman L.R., Yuan X., et al. 1998. "Performance evaluation and development of design guidelines for displacement ventilation," Final Report for ASHRAE RP-949, MIT, MA.

Chen Q. and Jiang Z. 1992. "Significant questions in predicting room air motion," ASHRAE Trans. 98(l): 929-939.

Chen Q. and Kooi, J. van der. 1988. "ACCURACY - a computer program for combined problems of energy analysis, indoor airflow and air quality," ASHRAE Transactions, 94(2): 196-214.

Chen Q. and Moser A. 1991. "Simulation of a multiple-nozzle diffuser," Proceedings of the 12th AIVC Conference on Air Movement and Ventilation Control within Buildings, 2: 1-13, Ottawa, Canada.

Chen Q., Peng X., and van Paassen A.H.C. 1995. "Prediction of room thermal response by CFD technique with conjugate heat transfer and radiation models," ASHRAE Transactions, 3884: 50-60.

Chen Q. and Srebric J. 2002. "A procedure for verification, validation, and reporting of indoor environment CFD analyses," International Journal of HVAC&R Research, 8(2): 201-216.

Chen Q. and Xu W. 1998. "A zero-equation turbulence model for indoor airflow simulation. Energy and Buildings," 28: 137-144.

Churchill S.W. and Chu H.H.S. 1975. "Correlating equations for laminar and turbulent free convection from a vertical plate," Int. J. Heat Mass Transfer, 18: 1323-1329.

Clarke J.A. 1985. "Energy simulation in building design," Adam Hilger, Bristol.

Clarke J.A., Dempster W.M., and Negrao C.O.R. 1995 a. "The implementation of a computational fluid dynamics algorithm within the ESP-r system," Proc. Building

Simulation '95, 166-75, Madison, USA, Int. Building Performance Simulation Association.

Clarke J.A., Hensen J.L.M., and Negrao C.O.R. 1995 b. "Predicting indoor air flow by combining network approach, CFD and thermal simulation," Proc. 16th AIVC Conference 145-53.

Clarke J.A. and Tang D. 1990. "An investigation of the functional conflation of building energy simulation and computational fluid dynamics," Project Proposal to the UK SERC (now EPSRC), ESRU, University of Strathclyde.

Clovis R.M. 2001. "Issues on the integration of CFD to building simulation tools," Seventh International IBPSA Conference (BS2001), 1: 29-40, Rio de Janeiro, Brazil, August 13-15.

Craft T.J. 1998. "Developments in a low-Reynolds-number second-moment closure and its application to separating and reattaching flows," Int. J. Heat Fluid Flow, 19: 541-548.

Crawley D.B., Lawrie L.K., Pedersen C.O., and Winkelmann F.C. 2000. "EnergyPlus: energy simulation program," ASHRAE Journal, 42(4): 49-56.

Crawley D.B. et al. 2001. "EenergPlus: new capabilities in a whole-building energy simulation program," Seventh International IBPSA Conference (BS2001), 1: 51-58, Rio de Janeiro, Brazil, August 13-15.

Davidson L. and Nielsen P.V. 1996. "Large eddy simulations of the flow in a three-dimensional ventilated room," Proc. Roomvent '96, 2: 161-168.

Deardorff J.W. 1970. "A numerical study of three-dimensional turbulent channel flow at large Reynolds numbers," J. Fluid Mech., 42: 453-480.

Department of Energy. 2002. "Building Energy DataBook," http://buildingsdatabook. eren.doe.gov/, USA.

Diamond S.C., Horak H.L., Hunn B.D., et al. 1977. "DOE-1 program manual," Report ANL/ENG-77-04, Los Alamos Scientific Laboratory.

Dorgan C.B., Dorgan C.E., Kanarek M.S., and Willman A.J. 1998. "Health and productivity benefits of improved indoor air quality," ASHRAE Trans., 104(1): 4161.

Duff I.S., Erisman A.M., and Reid J.K. 1986. "Direct methods for sparse matrices," Oxford Science Publication.

Emmerich S. 1997. "Use of computational fluid dynamics to analyze indoor air quality issues," National Institute of Standards and Technology, Report NISTIR 5997, USA.

Emmerich S. and McGrattan K. 1998. "Application of a large eddy simulation model to study room airflow," ASHRAE Trans., 104(1).

Emvin P. 1997. "The full multigrid method applied to turbulent flow in ventilated enclosures using structured and unstructured grids," Ph. D. Thesis, Charlmers University of Technology, Sweden.

Energy Information Administration. 1995. "State energy data report 1995," Tables 3-7, USA.

ESRU (Energy Systems Research Unit). 1999. "The ESP-r system for building energy simulations: user guide version 9 series," ESRU Manual U99/1, University of Strathclyde, Glasgow, UK.

Fanger P.O., Melikov A.K., Hanzawa H., and Ring J. 1989. "Turbulence and draft," ASHRAE J., 31(7): 18-23.

Feustel H.E. 1998. "COMIS – an international multizone air-flow and contaminant transport model," Lawrence Berkeley National Laboratory, USA, Report LBNL-42182.

Feustel H.E. (Editor) 1999. "Energy and Buildings – special issue devoted to multizone air-flow modeling," Energy and Buildings, 30(1).

Fisher D.E. 1995. "An experimental investigation of mixed convection heat transfer in a rectangular enclosure," Ph.D. Thesis, University of Illinois at Urbana-Champaign, USA.

Fisher V. and Rosler M. 1996. "Investigation and application of coupled building and room air flow simulation," Proc. Roomvent '96, 2: 215-222.

Fisk W.J. 2000. "Health and productivity gains from better indoor environments and their relationship with building energy efficiency," Annual Review Energy Environ., 25: 537-66.

Fluent Inc. 2001. "Airpak: simply-powerful airflow modeling," http://airpak.fluent.com/.

Gao Y. 2002. "Coupling of a multizone airflow simulation program with computational fluid dynamics for indoor environmental analysis," Master Thesis, Massachusetts Institute of Technology, USA.

GATC. 1967. "Computer program for analysis of energy utilization in postal facilities: volume 1 user's manual," General American Transportation Corporation, Niles, USA.

Griffith B.T. 2002, "Incorporating nodal and zonal room air models into building energy calculation procedures," Master Thesis, Massachusetts Institute of Technology, USA.

Groleau D. and Marenne C. 2001. "A multi-zone unsteady thermal simulation tool based on a 3D modelling of the building," Seventh International IBPSA Conference (BS2001), 1: 585-592, Rio de Janeiro, Brazil, August 13-15.

Haghighat F., Lin Y. and Megri A.C. 2001. "Development and validation of a zonal model – POMA," Building and Environment, 36: 1039-1047.

Hanjalic K. and Jakirlic S. 2002. "Second-moment turbulence closure modeling," Closure Strategies for Turbulent and Transitional Flows, B.E. Launder and N.H. Sandham (Eds.), Cambridge University Press, Cambridge, 47-101.

Harrington L. 2001. "Computer modelling of night-time natural ventilation," Thesis. Loughborough, UK.

Hiramatsu T., Harada T., Kato S. et al. 1996. "Study of thermal environment in experimental real-scale atrium," ROOMVENT '96, 1: 523-530, July 17-19.

Hittle D.C. 1979. "Building loads analysis and system thermodynamics (BLAST) users manual (Version 2.0)," Technical Report E-153, Vol. 1 and 2, U.S. Army Construction Engineering Research Laboratory (USA-CERL), Champaign, IL.

Inard C., Bouia H., and Dalicieux P. 1996. "Prediction of air temperature distribution in buildings with a zonal model," Energy and Buildings, 24: 125-132.

Jiang Y. 2002, "Study of natural ventilation in buildings with large eddy simulation," Ph.D. Thesis, Massachusetts Institute of Technology, USA.

Jiang Y. and Chen Q. 2001. "Study of natural ventilation in buildings by large eddy simulation," Journal of Wind Engineering and Industrial Aerodynamics, 89(13): 1155-1178.

Jiang Y. and Chen Q. 2002. "Study of particle dispersion in buildings with large eddy simulation," Proceedings of Indoor Air 2002, The 9th International Conference on Indoor Air Quality and Climate, Monterey, California.

Jones P.J. and Whittle G.E. 1992. "Computational fluid dynamics for building air flow prediction—current status and capabilities," Building and Environment, 27(3): 321-338.

Khalifa A.J.N. 1989. "Heat transfer processes in buildings," Ph.D. Thesis, University of Wales College of Cardiff, Cardiff UK.

Klems J.H. 1999. "Shape of T_S vs Q_C curves," Proposal of Bild-it Project, Lawrence Berkeley National Laboratory.

Kobayashi N. 2001. "Floor-supply displacement ventilation system," Master Thesis, Massachusetts Institute of Technology, USA.

Kolmogorov A.N. 1942. "Equations of turbulent motion of an incompressible fluid," IZv. Akad. Nauk SSSR Ser. Phy. 6(1/2): 56-58.

Korobov N.M. 1960. "Property and calculation of optimal coefficients," Doklady Akademi Nauk SSSR, 132: 1009-1012 (English translation: Soviet Mathematics Doklady, 1(1960): 696-700).

Kusuda T. 1976. "NBSLD, the computer program for heating and cooling loads in buildings," NBS Building Science Series No. 69-R, Washington DC, USA.

Ladeinde F. and Nearon M. 1997. "CFD applications in the HVAC&R industry," ASHRAE Journal, 39(1): 44-4.

Larsen S.F. and Lesino G. 2001. "A new code for the hour-by-hour thermal behavior simulation of buildings," Seventh International IBPSA Conference (BS2001), 1: 75-82, Rio de Janeiro, Brazil, August 13-15.

Launder B.E. and Spalding D.B. 1974. "The numerical computation of turbulent flows," Computer Methods in Applied Mechanics and Energy, 3: 269-289.

LBNL (Lawrence Berkeley National Lab). 2001. "EnergyPlus users manual".

Lebrun J. 1970. "Physiological requirements and physical conditions for air conditioning by concentrated static source," Ph.D. Thesis, Universite de Liege, France.

Lemaire A.D., Chen Q., Ewert M., et al. 1993. "Room air and contaminant flow, evaluation of computational methods," IEA Energy Conservation in Buildings and Community Systems Programme Annex 20 Subtask 1 Summary Report.

Leonard B.P. 1979. "A stable and accurate convective modeling procedure based on quadratic interpolation," Comput. Meths. Appl. Mech. Eng., 19: 59-98.

Leschziner M.A. 1990. "Modelling engineering flows with Reynolds stress turbulence closure," J. Wind Eng. and Industrial Aerodynamics, 35: 21-47.

Liddament M.W. 1991. "A review of building air flow simulation," AIVC Technical Note 33, Air Infiltration and Ventilation Centre, UK.

Lienhard J. 1999. "A heat transfer textbook," The third edition, Massachusetts Institute of Technology, Cambridge, MA.

Lin Y. 1999. "POMA – a zonal model for airflow and temperature distribution analysis," Masters Thesis, Concordia University, Montreal, Quebec, Canada.

Lomas K.L. and Eppel H. 1994. "Developing and proving sensitivity analysis techniques for thermal simulation of buildings," BEPAC'94, 253-280.

Lomas K.J., Eppel H., Martin C., and Bloomfield D. 1994. "Empirical validation of thermal building simulation programs using test room data," Volume 1 & 2 : Final Report, IEA Energy Conservation in Buildings and Community Systems Programme Annex 21 and IEA Solar Heating and Cooling Programme Task 12. (IEA 1994)

Mendes N. et al. 2001. "DOMUS 1.0: a Brazilian PC program for building simulation," Seventh International IBPSA Conference (BS2001), 1: 83-90, Rio de Janeiro, Brazil, August 13-15.

Meyers G.E. 1980. "Long-time solutions to heat conduction transients with time dependent inputs," Journal of Heat Transfer, 102: 115-120.

Mitalas G.P. and Stephenson D.G. 1967. "Room thermal response factors," ASHRAE Trans., 73(2).

Moser A. 1992. "Numerical simulation of room thermal convection - review of IEA Annex-20 results," Proceeding of International Symposium on Room Air Convection and Ventilation Effectiveness.

Moser A. 1994. "The IEA works on guidelines for ventilation of large enclosures," Proc. UK, Building Research Establishment, BEPAC Conference, Building Environmental Performance - Facing the Future.

Mundt E. 1996. "The performance of displacement ventilation systems-experimental and theoretical studies," Ph.D. Thesis, Royal Institute of Technology, Stockholm, Sweden.

Murakami S. 1998. "Overview of turbulence models applied in CWE-1997," J. Wind Eng. Ind. Aerodyn., 74-76: 1-24.

Murakami S., Kato S., and Kondo Y. 1990. "Examining k-e EVM by means of ASM for

a 3-D horizontal buoyant jet in enclosed space," Int. Symp. on Eng. Turbulence Modelling and Measurements, Dubrovnik: ICHMT.

Murakami S., Mochida A., Ooka R., et al. 1996. "Numerical prediction of flow around a building with various turbulence models: comparison of k-ε EVM, ASM, DSM, and LES with wind tunnel tests," ASHRAE Trans., 102(1).

Musy M., Wurtz E., and Sergent A. 2001. "Buildings air-flow simulations: automatically-generated zonal models," Seventh International IBPSA Conference (BS2001), 1: 593-600, Rio de Janeiro, Brazil, August 13-15.

NASA. 1975. "NECAP: NASA energy/cost analysis program," Vol. I-User's manual and Vol. II-Engineering manual. NASA Report CR-2590. Houston.

Negrao C.O.R. 1995. "Conflation of computational fluid dynamics and building thermal simulation," Ph.D. Thesis, University of Strathclyde, Glasgow, UK.

Neymark J. and Judkoff R. 2000. "International energy agency building energy simulation test and diagnostic method for HVAC equipment models (HVAC BESTEST)," Vol. 1: Cases E100-E200 (Draft), November. (IEA 2000)

Nielsen P.V. 1974. "Flow in air-conditioned rooms," Ph.D. Thesis, Technical University of Denmark, Copenhagen, Denmark.

Nielsen P.V. 1989. "Progress and trends in air infiltration and ventilation research," Proc. 10th AIVC Conf., Convetry: Air Infiltration and Ventilation Centre.

Nielsen P.V. 1998. "The selection of turbulence models for prediction of room airflow," ASHRAE Transactions, SF-98-10-1.

Nielsen P.V., Restivo A. and Whitelaw J.H. 1978. "The velocity characteristics of ventilated rooms," J. Fluids Engineering, Transactions of ASME, 100: 291-298.

Nielsen P.V. and Tryggvason T. 1998. "Computational fluid dynamics and building energy performance simulation," Proc. Roomvent '98, 1: 101-107, Stockholm, Sweden.

Nieuwstadt F.T.M. 1990. "Direct and large-eddy simulation of free convection," Proc. 9th Int. Heat Transfer Conf., 1: 37-47, Jerusalem.

Nieuwstadt F.T.M., Eggles J.G.M., Janssen R.J.A., and Pourquie M.B.J.M. 1994. "Direct and large-eddy simulations of turbulence in fluids," Future Generation Computer Systems, 10: 189-205.

NIOSH (National Institute for Occupational Safety and Health). 1999. http://www.cdc.gov/niosh/nrinev.html.

Noel J., Roux J., and Schneider P.S. 2001. "CODYBA, a design tool for buildings performance simulation," Seventh International IBPSA Conference (BS2001), 1: 67-74, Rio de Janeiro, Brazil, August 13-15.

NREL (National Renewable Energy Laboratory). 1998. "Buildings research - developing energy efficiency and renewable energy technologies for buildings," NREL Research, Colorado.

Off F., Moser A., and Suter P. 1996. "Transient numerical modelling of heat transfer by radiation and convection in atrium with thermal inertia," Proc. Roomvent '96, 3: 153-162.

Olson D. A., Glicksman L.R. and Ferm H. M.1990. "Steady-state natural convection in empty and partitioned enclosures at high Rayleigh numbers," J. Heat Transfer, Trans. ASME 112, 640-647

Olsen E.L. 2002. "Performance comparison of U.K. low-energy cooling systems by energy simulation," Master Thesis, Massachusetts Institute of Technology, USA.

Patankar S.V. 1980. "Numerical heat transfer and fluid flow," New York: Hemisphere/ McGraw-Hill.

Patankar S.V. and Spalding D.B. 1972. "A calculation procedure for heat, mass and momentum transfer in three-dimensional parabolic flows," Int. J. of Heat and Mass Transfer, 15: 1778-1806.

Prandtl L. 1926. "Ueber die ausgebidete turbulenz," Proc. 2nd Int. Congress for Applied Mechanics, 62-74, Zurich.

Rees S.J. and Haves P. 2001, "A nodal model for displacement ventilation and chilled ceiling systems in office spaces," Building and Environment, 36: 753-762.

Renz U. and Terhaag U. 1990. "Predictions of air flow pattern in a room ventilated by an air jet, the effect of turbulence model and wall function formulation," Proc. Roomvent '90, 18.1-18.15, Oslo: NORSK VVS.

Rhie C.M. and Chow W.L. 1983. "Numerical study of the turbulent flow past an airfoil with trailing edge separation," AIAA J., 21: 1525-1532.

Roache P.J. 1972. "Computational fluid mechanics," Hemosa, Albuquerque, New Mexico.

Saporito A. 1999. "A multi-parameter study into the heating energy consumption of commercial and institutional buildings," Ph.D. Thesis, South Bank University, London, UK.

Schild P. 1997. "Accurate prediction of indoor climate in glazed enclosures," Ph.D. Thesis, Norwegian University of Science and Technology, Trondheim, Norway.

Schwenke H. 1975. "Ueber das verhalten elener horizontaler zuluftstrahlen imbegrenzten raum," Luft- und Kaltetechnik, 5: 241-246.

Seem J.E. 1987. "Modeling of heat transfer in buildings," Ph.D. Thesis, University of Wisconsin-Madison, USA.

Sowell E.F. and Hittle D.C. 1995. "Evolution of building energy simulation methodology," ASHRAE Trans., 101: 850-855.

Spalding D.B. 1972. "A novel finite-difference formulation for differential expressions involving both first and second derivatives," Int. J. Num. Meth. Eng., 4: 551-559.

Spengler J.D. and Chen Q. 2000. "Indoor air quality factors in designing a healthy building," Annual Review of Energy and the Environment, 25: 567-600.

Srebric J. 2000. "Simplified methodology for indoor environment design," Ph.D. Thesis, Massachusetts Institute of Technology, USA.

Srebric J., Chen Q., and Glicksman L.R. 1999. "Validation of a zero-equation turbulence model for complex indoor airflows," ASHRAE Transactions, 105(2): 414-427.

Srebric J., Chen Q., and Glicksman L.G. 2000. "A coupled airflow-and-energy simulation program for indoor thermal environmental studies," ASHRAE Transactions, 106(1): 465-476.

Stephenson D.G. and Mitalas G.P. 1971. "Calculation of heat conduction transfer functions for multi-layer slabs," ASHRAE Transactions, 77(2): 117-126.

Tennekes H. and Lumley J.L. 1972. "A first course in turbulence," London: MIT Press.

Thakur S. and Shyy W. 1999. "Reynolds stress models for flows in complex geometries: review and application," AIAA 30th Fluid Dynamics Conference, 99-3782.

Thompson C.P. and Leaf G.K. 1988. "Application of a multigrid method to a buoyancy-induced flow problem," Multigrid Methods – Theory, Applications and Supercomputing. S.F. McCormick. New York: arcel Dekker Inc.

Togari S., Arai Y., and Miura K. 1993. "A simplified model for predicting vertical temperature distribution in a large space," ASHRAE Trans., 99(l): 84-99.

Wallentén P. 1998. "Heat flow in building components: experiment and analysis," Ph.D. Thesis, Lund University, Sweden.

Warren P. 2000. "Multizone air flow modeling (COMIS)," IEA-ECB Annex 23, Document TSR-06-2000, ISBN 1 902177 15 5.

Whittle G.E. 1986. "Computation of air movement and convective heat transfer within buildings," Int. J. Ambient Energy, 3: 151-164.

Winkelmann F.C., Birdsall B.E., Buhl W.F., et al. 1993. "DOE-2 Supplement, Version 2.1E, LBL-34947, November 1993," Lawrence Berkeley Laboratory, Springfield, Virginia: National Technical Information Service.

Witte M.J., Henninger R.J., Glazer J., and Crawley D.B. 2001. "Testing and validation of a new building energy simulation program," Proceedings of Building Simulation 2001, August, Rio de Janiero, Brazil, IBPSA.

Wittwer C. 1999. "ColSim - simulation von regelungssystemen in aktiven thermischen anlagen," Ph.D. thesis, http://www.ubka.uni-karlsruhe.de.

Wurtz E., Nataf J.M. and Winkelmann F. 1998. "Two- and three-dimensional natural and mixed convection simulation using modular zonal models," IJHMT, 42: 923-940.

Xu W. 1998. "New turbulence models for indoor airflow simulation," Ph.D. Thesis, Massachusetts Institute of Technology, USA.

Xu W. and Chen Q. 1998. "Numerical simulation of air flow in a room with differentially heated vertical walls," ASHRAE Transactions, 104(1): 168-175.

Yang C., Demokritou P., Chen Q., Spengler J.D., and Parsons A. 2000. "Ventilation and air quality in indoor ice skating arenas," ASHRAE Transactions, 106(2): 338-346.

Yuan X., Chen Q. and Glicksman L.R. 1998. "A critical review on displacement ventilation," ASHRAE Transactions, 104(1): 78-90.

Yuan X., Chen Q., and Glicksman L.R. 1999. "Models for prediction of temperature difference and ventilation effectiveness with displacement ventilation," ASHRAE Transactions, 105(1): 353-367.

Zhu J. 1991. "A low diffusive and oscillation-free convection scheme," Communications in Applied Numerical Methods, 7: 225-232 .

NOMENCLATURE

A	area of surface
A	coefficient matrix
b	source
B	coefficient matrix
C	gas contaminant concentration
C_p	specific heat of air
D	distance to surface
f	math function
g	gravity, math function
h	heat transfer coefficient; height
H	height
i	index of enclosure surfaces
I	surface flux of variable
IterCFD	CFD iteration number
k	turbulence kinetic energy
K	conductivity
l	distance to surface
L	length; thickness
$\dot{m}$	supply air mass flow rate
N	number of enclosure surfaces
P	air pressure
Pr	Prandtl number
q	heat flux
Q	heat transfer; energy requirement
Q	interior surface heat convection tensor
R	residuals
S	source
T	temperature
T	temperature tensor
t	time
U	air velocity component
V	room volume; air velocity
V	velocity vector
x	distance; coordinate
y	distance to surface

Greek Symbols

α	thermal diffusivity; concentration diffusivity; under-relaxation factor
β	gas thermal expansion coefficient
δ	thickness of boundary layer
ε	turbulence dissipation rate
μ	turbulence kinetic viscosity
ν	turbulence dynamic viscosity
ρ	air density

Δ	difference
Φ	general variable
Γ	diffusion coefficient

Subscripts

a	indoor air close to surface
c	convection; cold
cond	conduction
conv	convection
D	distance to surface
h	hot
i	index of enclosure surfaces; coordinate direction
in	inlet
j	coordinate direction
k	index of enclosure surfaces; coordinate direction
n	iteration step
o	exterior surface
r	radiation; room
rad	radiation
room	room-averaged
s	interior surface
s-rad	solar radiation and radiation from internal heat sources
t	turbulence; temperature

Superscripts

n	nth iteration step
n+1	(n+1)th iteration step

APPENDIX: DEVELOPMENT AND OPERATION OF E+MIT-CFD

This appendix introduces, in detail, the development and structure of the E+MIT-CFD program developed, as well as the instructions to use the program. The appendix also introduces the procedures to replace the current MIT-CFD solver with an arbitrary CFD program in this coupling program, which may encourage the integration of commercial CFD solvers with EnergyPlus.

A.1 Development of E+MIT-CFD

Chapter 5 introduces the developed coupling program and the major development procedures. This appendix expands the content of Chapter 5 and presents the details of the program and its development so as to provide users and other coupling program developers deep knowledge of the program.

As discussed in Chapter 5, in order to automate the coupling of the simulations, the CFD program needs to be incorporated into the ES program. ES program simulates the whole building performance for a long period of time while CFD program focuses on the "snap-shot" of the airflow and heat transfer in a single space. Figure A.1 demonstrates the frame structure of the EnergyPlus program embedded with MIT-CFD (i.e. E+MIT-CFD). The italic sections involve the coupling between the two programs.

To form an integrated tool, both the ES and CFD programs need modifications. The ES and CFD programs connect to each other by exchanging the inter-coupled information, such as, interior surface temperature and/or surface heat flux from ES to CFD, and interior surface convective heat transfer coefficient and indoor air temperature gradient from CFD to ES. Hence, the essential changes for EnergyPlus and MIT-CFD are to create two new functions:

(1) passing new and updated information to the partner;
(2) receiving and updating information from the partner into the current calculation.

The present study proposes various coupling strategies and data coupling methods for the flexibility of application. As a consequence, EnergyPlus and MIT-CFD require corresponding changes to accommodate the new terms created, update the information exchanged, and output the inter-coupled results.

ManageSimulation

InitExchangeData

Do Environment Loop
Do Day Loop
Do Hour Loop
Do Timestep Loop

ManageWeather
ManageExteriorEnergyUse
ManageHeatBalance

ManageSurfaceHeatBalance
InitSurfaceHeatBalance
UpdateHconvIn(ZoneCFD) *[UpdateHConvIn from CFD]*
CalcHeatBalanceOutsideSurf
CalcHeatBalanceInsideSurf
[AddConvForSurfaceHeatBalance, AddConvForAirHeatBalance, OutputTsurf]

ManageAirHeatBalance
InitAirHeatBalance
CalcHeatBalanceAir
ManageHVAC
ManageZoneAirUpdate('Predict')
SimHVAC
ManageZoneAirUpdate('Correct')
CorrectZoneAirTemp
[OutputQEnergyDemand,Troom]

IF (CFD And ThisTimeStep)
CFDSimulation
JudgeConvergence [Based on Q, Twall]
If (DatabaseMethod Or Convergent) Return
CFDSmulator [UpdateBoundaryConditions, UpdateOutputs]
If (Not Convergent) Then
GoBackTo ManageSurfaceHeatBalance

ManageThermalComfort

End Do Timestep Loop
End Do Hour Loop
End Do Day Loop
End Do Environment Loop

Figure A.1 Frame structure of EnergyPlus embedded with MIT-CFD (E+MIT-CFD)

A.2 Changes in EnergyPlus

With a focus on the thermal connection between building envelope and indoor air, five of 120 modules in EnergyPlus (Version 1.0.0) have been modified to achieve the integration with MIT-CFD. The following details the changes made in these modules (all the modifications in the original codes are marked with the lines "zzzz" at the head and tail of the modified codes).

1 SimulationManager

a) Add the link to **DataExchangeCFDAndES:** USE DataExchangeCFDAndES;
b) Add the computing time counter = CTIM1(ending time) – CTIM0(starting time);
c) Open additional files for coupling performance outputs;
d) Initialize the created coupling data before each simulation by calling the Subroutine **InitExchangeData**, which also temporarily hosts the dialog and input functions of "Coupling Choices".

```
!zzzzzzzzzzzzzzzzzzzzzzzzzzzzzzzzzzzzzzzzzzzzzzzzzzzzzzzzzzzzzzzzzzzzzzzzzzzzzzzzzzzzzzzzzzzzzzzzzzzzzz
WRITE(*,*)'*************** WANT TO COUPLE WITH CFD? ***************'
WRITE(*,*)'*************** YOUR REPLY [Y/N]: '
READ(*,*)REPLY
IF(REPLY(1:1).EQ.'Y'.OR.REPLY(1:1).EQ.'y') THEN
CFD=.TRUE.
ELSE
CFD=.FALSE.
ENDIF

IF(CFD) THEN

WRITE(*,*)'*************** COUPLE DURING WARM-UP PERIOD? *********'
WRITE(*,*)'*************** YOUR REPLY [Y/N]: '
READ(*,*)REPLY
IF(REPLY(1:1).EQ.'Y'.OR.REPLY(1:1).EQ.'y') THEN
WarmupCFD=.TRUE.
ELSE
WarmupCFD=.FALSE.
ENDIF

WRITE(*,*)'*************** WHICH ZONE TO DO COUPLING? *************'
WRITE(*,*)'|ZONE NUMBER: 1, 2, 3, ...                    |'
WRITE(*,*)'*************** YOUR SELECTION [NUM]: '
READ(*,*) ZONECFD

WRITE(*,*)'*************** SELECT COUPLING STRATEGY ***************'
WRITE(*,*)'|1- VIRTUAL DYNAMIC COUPLING                  |'
WRITE(*,*)'|2- ONE-TIME-STEP DYNAMIC COUPLING            |'
WRITE(*,*)'|3- QUASI DYNAMIC COUPLING                    |'
WRITE(*,*)'|4- FULL DYNAMIC COUPLING                     |'
WRITE(*,*)'*************** YOUR SELECTION [1/2/3/4]: '
READ(*,*) STRATEGY

IF(STRATEGY==1) THEN   ! Virtual dynamic coupling
WRITE(*,*)' '
WRITE(*,*)'*************** SELECT FUNCTION DATABASE ***************'
WRITE(*,*)'|1- SUMMER COOLING CASE                       |'
WRITE(*,*)'|2- WINTER HEATING CASE                       |'
WRITE(*,*)'*************** YOUR SELECTION [1/2]: '
READ(*,*) DATABASE
WRITE(*,*)' '
WRITE(*,*)'*************** SELECT SPECIAL FUNCTION ****************'
WRITE(*,*)'|1- CONSTANT T DISTRIBUTION                   |'
WRITE(*,*)'|2- LINEAR T(Q) FUNCTION                      |'
WRITE(*,*)'|3- NON-LINEAR T(Q) FUNCTION                  |'
```

```
      WRITE(*,*)'************** YOUR SELECTION [1/2/3]: '
      READ(*,*) FuncMethod
      FunctionMethod=.TRUE.
      CFDFLAG=2
      ENDIF

      IF(STRATEGY==2) THEN    ! One-time-step dynamic coupling
      WRITE(*,*)' '
      WRITE(*,*)'************** SELECT THE TIME STEP ******************'
      WRITE(*,*)'|ANY HOUR DURING 1-24                              |'
      WRITE(*,*)'************** YOUR SELECTION [1-24]: '
      READ(*,*) ONETIME
      CFDFLAG=2
      ENDIF

      IF((STRATEGY==3).OR.(STRATEGY==4)) THEN    ! Quasi-dynamic and full dynamic coupling
      WRITE(*,*)' '
      WRITE(*,*)'************** SELECT COUPLING FREQUENCY *************'
      WRITE(*,*)'|1-PER DAY; 2-PER HOUR; 3-PER TIME STEP; 4-SCHEDULED |'
      WRITE(*,*)'************** YOUR SELECTION [1/2/3/4]: '
      READ(*,*) CFDFLAG

      IF(CFDFLAG==4) THEN     ! Scheduled coupling frequency
      WRITE(*,*)' '
      WRITE(*,*)'************** INPUT SCHEDULED COUPLING DAYS *********'
      WRITE(*,*)'|COUPLING DAYS DURING A PERIOD OF TIME             |'
      WRITE(*,*)'************** YOUR SCHEDULED DAY [1,2,3,...,366]: '
      ! Pick up days requiring coupling: such as 1,100,200,300;
      ! 0 after any number means done selection;
      ! If the first number is 0, coupling is required for all the days simulated.

      DO i=1,366
        READ(*,*)CFDSchedule(i)
        IF(CFDSchedule(i)==0) GOTO 100
      ENDDO
100   IF(CFDSchedule(1)==0) THEN
        DO i=1,366
        CFDSchedDay(i)=1
        ENDDO
      ELSE
        DO i=1,366
        IF(CFDSchedule(i).NE.0) CFDSchedDay(CFDSchedule(i))=1
        ENDDO
      ENDIF

      DO i=1,366
      CFDSchedule(i)=0
      ENDDO

      WRITE(*,*)'************** INPUT SCHEDULED COUPLING HOURS ********'
      WRITE(*,*)'|COUPLING HOUR OF 24 HOURS EACH DAY               |'
      WRITE(*,*)'************** YOUR SCHEDULED HOUR [1,2,3,...,24]: '
      ! Pick up hours requiring coupling: such as 1,5,9,13,19;
      ! 0 after any number means done selection;
      ! If the first number is 0, coupling is required for all 24 hours.

      DO i=1,24
        READ(*,*)CFDSchedule(i)
        IF(CFDSchedule(i)==0) GOTO 200
      ENDDO
200   IF(CFDSchedule(1)==0) THEN
        DO i=1,24
        CFDScheHour(i)=1
        ENDDO
      ELSE
        DO i=1,24
        IF(CFDSchedule(i).NE.0) CFDScheHour(CFDSchedule(i))=1
        ENDDO
      ENDIF
      ENDIF
```

```
ENDIF

IF((STRATEGY==3).OR.(STRATEGY==4).OR.(STRATEGY==2)) THEN     ! If non virtual dynamic coupling
WRITE(*,*)' '
WRITE(*,*)'************** SELECT DATA COUPLING METHOD ***********'
WRITE(*,*)'|1- ES->T; CFD->h & dT                    |'
WRITE(*,*)'|2- ES->T; CFD->h(corrected)              |'
WRITE(*,*)'|3- ES->T; CFD->Q                         |'
WRITE(*,*)'|4- ES->Q; CFD->h & dT                    |'
WRITE(*,*)'************** YOUR SELECTION [1/2/3/4]: '
READ(*,*) MCOUPLE
ENDIF

ENDIF
!zzzzzzzzzzzzzzzzzzzzzzzzzzzzzzzzzzzzzzzzzzzzzzzzzzzzzzzzzzzzzzzzzzzzzzzzzzzzzzzzzzzzzzzzzzzzz
```

2 HeatBalanceSurfaceManager

a) Add the link to **DataExchangeCFDAndES:** USE DataExchangeCFDAndES;

b) In the Subroutine **ManageSurfaceHeatBalance**, add three links to Subroutines **UpdateHconvInAndTair**, **CFDSimulation**, **ConvectionCoefficients**; update the interior surface heat transfer coefficients from CFD at the beginning of each ES calculation if coupling simulation; determine whether to perform CFD simulation at the current time step of ES according to the selected coupling strategy; and flow back for one more ES-CFD iteration at the current coupling step if the convergence of solutions is not achieved.

```
SUBROUTINE ManageSurfaceHeatBalance
......
......
!zzzzzzzzzzzzzzzzzzzzzzzzzzzzzzzzzzzzzzzzzzzzzzzzzzzzzzzzzzzzzzzzzzzzzzzzzzzzzzzzzzzzzzzzzzzzz
IF (CFD) THEN    ! Assign the coupling frequency
    IF(CFDFLAG==1) RUNCFDFLAG=BeginDayFlag                          ! Per day
    IF((CFDFLAG==2).OR.(CFDFLAG==4)) RUNCFDFLAG=BeginHourFlag  ! Per hour
    IF(CFDFLAG==3) RUNCFDFLAG=.TRUE.                            ! Per time step
ENDIF
!zzzzzzzzzzzzzzzzzzzzzzzzzzzzzzzzzzzzzzzzzzzzzzzzzzzzzzzzzzzzzzzzzzzzzzzzzzzzzzzzzzzzzzzzzzzzz

 CALL InitSurfaceHeatBalance  ! Initialize all heat balance related parameters

!zzzzzzzzzzzzzzzzzzzzzzzzzzzzzzzzzzzzzzzzzzzzzzzzzzzzzzzzzzzzzzzzzzzzzzzzzzzzzzzzzzzzzzzzzzzzz
     ITERATE=0
111  CONTINUE

     IF (CFD) THEN

       IF(Convergence) THEN        ! Turn on the flag for saving history at the start of a simulation
          OneTimeStore =.TRUE.
          OneTimeStoreR=.TRUE.
       ELSE
          OneTimeStore =.FALSE.
          OneTimeStoreR=.FALSE.
       ENDIF

       CALL UpdateHconvIn(ZoneCFD)        ! Update h from CFD via interface module
       IF(SUMHA(ZoneCFD)==0.0)  CALL InitInteriorConvectionCoeffs(REAL(TempSurfInTmp))  ! Avoid h=0

     END IF
!zzzzzzzzzzzzzzzzzzzzzzzzzzzzzzzzzzzzzzzzzzzzzzzzzzzzzzzzzzzzzzzzzzzzzzzzzzzzzzzzzzzzzzzzzzzzz

     ! Solve the zone heat balance 'detailed' solution
     ! Call the outside and inside surface heat balances
 CALL CalcHeatBalanceOutsideSurf
 CALL CalcHeatBalanceInsideSurf
```

```
    ! The air heat balance must be called before the temperature history
    ! updates because there may be a radiant system in the building
 CALL ManageAirHeatBalance

    ! IF NECESSARY, do one final "average" heat balance pass.  This is only
    ! necessary if a radiant system is present and it was actually on for
    ! part or all of the time step.
 CALL UpdateFinalSurfaceHeatBalance

!zzzzzzzzzzzzzzzzzzzzzzzzzzzzzzzzzzzzzzzzzzzzzzzzzzzzzzzzzzzzzzzzzzzzzzzzzzzzzzzzzzzzzzzzzzzzzzzzzzzzzzz
IF (CFD) THEN    ! Call CFD solver according to the coupling strategy selected

        IF(WarmUpFlag.and.(.NOT.WarmupCFD)) THEN   ! w/o warm-up coupling

        ELSE
            IF(RunCFDFlag) THEN
                IF(STRATEGY==2) THEN          ! One-time-step coupling
                        IF(HourOfDay==ONETIME) THEN
                        CALL CFDSimulator     ! Call CFD solver via interface module
                        IF(Convergence == .false.) GOTO 111
                        ENDIF
                ELSE      ! Quasi-dynamic and full dynamic coupling
                        IF(CFDFLAG==4) THEN      ! Scheduled coupling frequency
                                IF(CFDSchedDay(DayOfSim)==1) THEN
                                  IF(CFDScheHour(HourOfDay)==1) THEN
                                    CALL CFDSimulator     ! Call CFD solver via interface module
                                    IF(Convergence == .false.) GOTO 111
                                  ENDIF
                                ENDIF
                        ELSE
                                CALL CFDSimulator     ! Call CFD solver via interface module
                                IF(Convergence == .false.) GOTO 111
                        ENDIF
                ENDIF
            ENDIF
        ENDIF

ENDIF
!zzzzzzzzzzzzzzzzzzzzzzzzzzzzzzzzzzzzzzzzzzzzzzzzzzzzzzzzzzzzzzzzzzzzzzzzzzzzzzzzzzzzzzzzzzzzzzzzzzzzzzz

    ! Before we leave the Surface Manager the thermal histories need to be updated
......
......
 RETURN
END SUBROUTINE ManageSurfaceHeatBalance
```

c) In the Subroutine **CalcHeatBalanceInsideSurf**, add the link to the Subroutine **UpdateHconvInAndTair**; introduce the additional or updated terms related to interior surface convections into the interior surface heat balance equation:

$$q_i + q_{ir} = \sum_{k=1}^{N} q_{ik} + q_{i,c} \qquad (A.1)$$

where,

$$q_{i,c}=h_{i,c}(T_i-T_{i,air})=h_{i,c}(T_i-T_{room})-h_{i,c}\,(T_{i,air}-T_{room})=h_{i,c}(T_i-T_{room})-h_{i,c}\Delta T_{i,air} \qquad (A.2)$$

If data exchange method-1, 2 or 4 is used, the additional convective heat transfer $QAdditionalConv=h_{i,c}\Delta T_{i,air}$ as well as the updated $h_{i,c}$ are placed into the interior surface heat balance equation. If data exchange method-3 is used, $q_{i,c}$ obtained from CFD is directly introduced into the interior surface heat balance equation.

For example, for the calculation of heat transfer through regular CTF surface and/or EMPD surface in the program, the modified codes are:

```
!zzzzzzzzzzzzzzzzzzzzzzzzzzzzzzzzzzzzzzzzzzzzzzzzzzzzzzzzzzzzzzzzzzzzzzzzzzzzzzzzzzzzzzzzzzzzzzzzzzzzzzzzzzzz
IF(CFD.AND.(MCOUPLE==3).AND.(ZoneNum.EQ.ZoneCFD).AND.(.NOT.FIRSTRUN)) THEN
! Using data exchange method-3
TempSurfInTmp(SurfNum)                          &
= (CTFConstInPart(SurfNum)                      & ! Constant portion of conduction eq (history terms)
 +DBLE(QRadThermInAbs(SurfNum))                 & ! LW radiation from internal sources
 +DBLE(QRadSWInAbs(SurfNum))                    & ! SW radiation from internal sources
 - DBLE(QSurface(SurfNum))                      & ! Convection from surface to zone air
 +DBLE(NetLWRadToSurf(SurfNum))                 & ! Net radiant exchange with other zone surfaces
 +Construct(ConstrNum)%CTFSourceIn(0)           & ! Heat source/sink term for radiant systems
          *QsrcHist(SurfNum,1)                  & ! (if there is one present)
 +DBLE(QHTRadSysSurf(SurfNum))                  & ! Radiant flux from a high temperature radiant heater
 +DBLE(IterDampConst)*TempInsOld(SurfNum) )     & ! Iterative damping term (for stability)
 /( Construct(ConstrNum)%CTFInside(0)           & ! Conduction term (both partition sides same temp)
  -Construct(ConstrNum)%CTFCross(0)             & ! Conduction term (both partition sides same temp)
  +DBLE(IterDampConst) )                          ! Convection and damping term

ELSE
! Using other data exchange methods and even no coupling
TempSurfInTmp(SurfNum)
= ( CTFConstInPart(SurfNum)                     & ! Constant portion of conduction eq (history terms)
  +DBLE(QRadThermInAbs(SurfNum))                & ! LW radiation from internal sources
  +DBLE(QRadSWInAbs(SurfNum))                   & ! SW radiation from internal sources
  +DBLE(HConvIn(SurfNum))*MAT(ZoneNum)          & ! Convection from surface to zone air
  +DBLE(QAdditionalConv(SurfNum))               & ! Additional convection term
  +DBLE(NetLWRadToSurf(SurfNum))                & ! Net radiant exchange with other zone surfaces
  +Construct(ConstrNum)%CTFSourceIn(0)          & ! Heat source/sink term for radiant systems
            *QsrcHist(SurfNum,1)                & ! (if there is one present)
  +DBLE(QHTRadSysSurf(SurfNum))                 & ! Radiant flux from a high temperature radiant heater
  +DBLE(IterDampConst)*TempInsOld(SurfNum) )    & ! Iterative damping term (for stability)
  /( Construct(ConstrNum)%CTFInside(0)          & ! Conduction term (both partition sides same temp)
   -Construct(ConstrNum)%CTFCross(0)            & ! Conduction term (both partition sides same temp)
   +DBLE(HConvIn(SurfNum))+DBLE(IterDampConst) ) ! Convection and damping term

ENDIF
!zzzzzzzzzzzzzzzzzzzzzzzzzzzzzzzzzzzzzzzzzzzzzzzzzzzzzzzzzzzzzzzzzzzzzzzzzzzzzzzzzzzzzzzzzzzzzzzzzzzzzzzzzzzz
```

Similar modifications are made for other types of surfaces. After ES produces the new interior surface temperatures, the results are exported for the next CFD run and the new convection terms are prepared for the indoor air energy balance equation of ES.

```
!After calculate the interior surface temperature for all surfaces
!zzzzzzzzzzzzzzzzzzzzzzzzzzzzzzzzzzzzzzzzzzzzzzzzzzzzzzzzzzzzzzzzzzzzzzzzzzzzzzzzzzzzzzzzzzzzzzzzzzzzzzzzzzzz
IF(CFD) THEN
        DO SurfNum = 1, TotSurfaces
            IF (.NOT. Surface(SurfNum)%HeatTransSurf) CYCLE  ! Skip non-heat transfer surfaces
            TempWall(SurfNum)=TempSurfInTmp(SurfNum)
        END DO

! Prepare new convection terms for indoor air via interface module
        CALL AddConvForAirHeatBalance

END IF
!zzzzzzzzzzzzzzzzzzzzzzzzzzzzzzzzzzzzzzzzzzzzzzzzzzzzzzzzzzzzzzzzzzzzzzzzzzzzzzzzzzzzzzzzzzzzzzzzzzzzzzzzzzzz
```

3 ZoneTempPredictorCorrector

a) Add the link to **DataExchangeCFDAndES:** USE DataExchangeCFDAndES;

b) In the Subroutine **PredictSystemLoads**, since the history of indoor air temperature has impact on the current indoor air temperature calculation and ES updates the indoor air temperature records immediately after the new ones are available, the past indoor air temperatures should be saved at the beginning of iterative coupling simulation at each coupling time step. Then, if a converged solution is not achieved at the current iteration, ES and CFD will iterate again from the beginning of this time step. At this moment, the saved values are recovered to allow ES calculate the current indoor air temperature with the right air temperature history.

```
!zzzzzzzzzzzzzzzzzzzzzzzzzzzzzzzzzzzzzzzzzzzzzzzzzzzzzzzzzzzzzzzzzzzzzzzzzzzzzz
IF(CFD) THEN
  IF(WarmUpFlag.and.(.NOT.WarmupCFD)) THEN
  ELSE
    IF(Convergence) THEN
         IF(OneTimeStore==.TRUE.) THEN
                    MATOld(ActualZoneNum)  =MAT(ActualZoneNum)
                    XMATOld(ActualZoneNum) =XMAT(ActualZoneNum)
                    XM2TOld(ActualZoneNum) =XM2T(ActualZoneNum)
                    XM3TOld(ActualZoneNum) =XM3T(ActualZoneNum)
                    XM4TOld(ActualZoneNum) =XM4T(ActualZoneNum)
                    IF(ActualZoneNum==NumofZones) OneTimeStore = .FALSE.
         ENDIF
    ELSE   ! If not converged, recover the history of indoor air temperature
         IF(OneTimeStore==.FALSE.) THEN
                    MAT(ActualZoneNum) =MATOld(ActualZoneNum)
                    XMAT(ActualZoneNum)=XMATOld(ActualZoneNum)
                    XM2T(ActualZoneNum)=XM2TOld(ActualZoneNum)
                    XM3T(ActualZoneNum)=XM3TOld(ActualZoneNum)
                    XM4T(ActualZoneNum)=XM4TOld(ActualZoneNum)
                    IF(ActualZoneNum==NumofZones) OneTimeStore = .TRUE.
         ENDIF
    ENDIF
  ENDIF
ENDIF
!zzzzzzzzzzzzzzzzzzzzzzzzzzzzzzzzzzzzzzzzzzzzzzzzzzzzzzzzzzzzzzzzzzzzzzzzzzzzzz
```

c) In the Subroutine **CorrectZoneAirTemp**, the third order Taylor finite difference approximation was used to model the temperature derivative term in the indoor air energy balance equation:

$$C_z \frac{dT_z}{dt} = \sum_{i}^{N_{sl}} \dot{Q}_i + \sum_{i=1}^{N_{surfaces}} h_i A_i (T_{si} - T_z) + \sum_{i=1}^{N_{zones}} \dot{m}_i C_p (T_{zi} - T_z) + \dot{m}_{inf} C_p (T_\infty - T_z) + \dot{m}_{sys} C_p (T_{sup} - T_z) \tag{A.3}$$

where

$C_z \frac{dT_z}{dt}$ = energy stored in zone air

$\sum_{i}^{N_{sl}} \dot{Q}_i$ = sum of the convective internal loads

$\sum_{i=1}^{N_{surfaces}} h_i A_i (T_{si} - T_z)$ = convective heat transfer from the zone surfaces

$\sum_{i=1}^{N_{zones}} \dot{m}_i C_p (T_{zi} - T_z)$ = heat transfer due to interzone air mixing

$\dot{m}_{inf} C_p (T_\infty - T_z)$ = heat transfer due to infiltration of outside air

$\dot{Q}_{sys}$ = system output

Then the zone air temperature can be calculated by

$$T_z^t = \frac{\sum_i^{N_{sl}} \dot{Q}_i + \sum_{i=1}^{N_{surfaces}} h_i A_i T_{si} + \sum_{i=1}^{N_{zones}} \dot{m}_i C_p T_{zi} + \dot{m}_{inf} C_p T_\infty + \dot{m}_{sys} C_p T_{sup} - \left(\frac{C_z}{\delta t}\right)\left(-3T_z^{t-\delta t} + \frac{3}{2} T_z^{t-2\delta t} - \frac{1}{3} T_z^{t-3\delta t}\right)}{\frac{11}{6}\frac{C_z}{\delta t} + \sum_{i=1}^{N_{surfaces}} h_i A_i + \sum_{i=1}^{N_{zones}} \dot{m}_i C_p + \dot{m}_{inf} C_p + \dot{m}_{sys} C_p} \tag{A.4}$$

By using the convection information and actual exhaust air temperature obtained from CFD, the above equation can be re-arranged as

$$T_z^t = \frac{\sum_i^{N_{sl}} \dot{Q}_i + \sum_{i=1}^{N_{surfaces}} h_i A_i (T_{si} - \Delta T_{i,air}) + \sum_{i=1}^{N_{zones}} \dot{m}_i C_p T_{zi} + \dot{m}_{inf} C_p T_\infty + \dot{m}_{sys} C_p (T_{sup} - T_{exhaust-CFD}) - \left(\frac{C_z}{\delta t}\right)\left(-3T_z^{t-\delta t} + \frac{3}{2} T_z^{t-2\delta t} - \frac{1}{3} T_z^{t-3\delta t}\right)}{\frac{11}{6}\frac{C_z}{\delta t} + \sum_{i=1}^{N_{surfaces}} h_i A_i + \sum_{i=1}^{N_{zones}} \dot{m}_i C_p + \dot{m}_{inf} C_p} \tag{A.5}$$

Therefore, two more terms $-\sum_{i=1}^{N_{surfaces}} h_i A_i \Delta T_{i,air}$ and $-\dot{m}_{sys} C_p T_{exhaust-CFD}$ are introduced to the numerator of the right hand of the equation and one term $\dot{m}_{sys} C_p$ is deducted from the denominator. $-\sum_{i=1}^{N_{surfaces}} h_i A_i \Delta T_{i,air}$ is implemented into the program through the interface subroutine **AddConvForAirHeatBalance** called in **CalcHeatBalanceInsideSurf**. The relative changes about $-\dot{m}_{sys} C_p T_{exhaust-CFD}$ in the code for both the plenum and controlled zones are:

```
!zzzzzzzzzzzzzzzzzzzzzzzzzzzzzzzzzzzzzzzzzzzzzzzzzzzzzzzzzzzzzzzzzzzzzzzzzzzzzzzzzzzzzzzzzzzz
IF(CFD.AND.(ZoneNum.EQ.ZoneCFD).AND.(.NOT.FIRSTRUN)) THEN

CoefSumhat = CoefSumhat +
Node(ZoneEquipConfig(ControlledZoneNum)%InletNode(NodeNum))%MassFlowRate &
*(Node(ZoneEquipConfig(ControlledZoneNum)%InletNode(NodeNum))%Temp-TCFDOutlet) &
*cpairfn(ZoneAirHumRat(ZoneNum),Node(ZoneEquipConfig(ControlledZoneNum)%InletNode(NodeNum))%Temp) &
/Zone(ZoneNum)%Multiplier

ELSE

CoefSumha = CoefSumha +
Node(ZoneEquipConfig(ControlledZoneNum)%InletNode(NodeNum))%MassFlowRate &
*cpairfn(ZoneAirHumRat(ZoneNum),Node(ZoneEquipConfig(ControlledZoneNum)%InletNode(NodeNum))%Temp) &
/Zone(ZoneNum)%Multiplier
CoefSumhat = CoefSumhat +
Node(ZoneEquipConfig(ControlledZoneNum)%InletNode(NodeNum))%MassFlowRate &
```

```
*Node(ZoneEquipConfig(ControlledZoneNum)%InletNode(NodeNum))%Temp &
*cpairfn(ZoneAirHumRat(ZoneNum), Node(ZoneEquipConfig(ControlledZoneNum)%InletNode( NodeNum))%Temp) &
/Zone(ZoneNum)%Multiplier

ENDIF
!zzzzzzzzzzzzzzzzzzzzzzzzzzzzzzzzzzzzzzzzzzzzzzzzzzzzzzzzzzzzzzzzzzzzzzzzzzzzzzzzzzzzzzzzzz
```

After new indoor air temperature and new heating/cooling load are calculated in this subroutine, the results are exported for the next CFD simulation.

```
!zzzzzzzzzzzzzzzzzzzzzzzzzzzzzzzzzzzzzzzzzzzzzzzzzzzzzzzzzzzzzzzzzzzzzzzzzzzzzzzzzzzzzzzzzz
IF(CFD.AND.(ZoneNum.EQ.ZoneCFD)) THEN
! Sensible load is the enthalpy into the zone minus the enthalpy that leaves the zone.

  IF(.NOT.FIRSTRUN) THEN
    CpAir = cpairfn(ZoneAirHumRat(ZoneNum), TCFDOutlet)

    SNLOAD=ZoneEnthalpyIn-(cpair*Node(ZoneNodeNum)%MassFlowRate*TCFDOutlet) &
                          +NonAirSysEquipHeatAdd(ZoneNum)
    SNLoadHeatRate(ZoneNum) = MAX(REAL(SNLOAD),0.0)
    SNLoadCoolRate(ZoneNum) = Abs(MIN(REAL(SNLOAD),0.0))
    SNLoadHeatEnergy(ZoneNum) = MAX(REAL(SNLOAD),0.0)*TimeStepSys*3600.
    SNLoadCoolEnergy(ZoneNum) = Abs(MIN(REAL(SNLOAD),0.0)*TimeStepSys*3600.)
  ENDIF

  TempRoom=ZT(ZoneNum)
  EnthalpyInlet=ZoneEnthalpyIn
  QEnergyDemand =SNLOAD

END IF
!zzzzzzzzzzzzzzzzzzzzzzzzzzzzzzzzzzzzzzzzzzzzzzzzzzzzzzzzzzzzzzzzzzzzzzzzzzzzzzzzzzzzzzzzzz
```

4 HVACManager

a) Add the link to **DataExchangeCFDAndES:** USE DataExchangeCFDAndES;

b) In the Subroutine **ManageHVAC,** change the control condition of "DoOutputReporting" from "(.not. WarmUpFlag)" to "((.not.WarmUpFlag).and. Convergence)". That is, only when the real simulation (not warm-up calculation) reaches a converged solution during a coupled simulation, the results are outputted/recorded. Since the defaulted value for "Convergence" is "True" when the coupling is not required, the control condition is the same as the original one under this circumstance.

```
!zzzzzzzzzzzzzzzzzzzzzzzzzzzzzzzzzzzzzzzzzzzzzzzzzzzzzzzzzzzzzzzzzzzzzzzzzzzzzzzzzzzzzzzzzz
  IF ((.NOT.WarmUpFlag).and.Convergence) THEN
    IF (DoOutputReporting) THEN
         CALL UpdateDataandReport(HVACTSReporting)
    END IF
    IF (ZoneSizingCalc) THEN
         CALL UpdateZoneSizing(DuringDay)
    END IF
  END IF
!zzzzzzzzzzzzzzzzzzzzzzzzzzzzzzzzzzzzzzzzzzzzzzzzzzzzzzzzzzzzzzzzzzzzzzzzzzzzzzzzzzzzzzzzzz
```

5 Window5Manager

a) Add the link to **DataExchangeCFDAndES:** USE DataExchangeCFDAndES;

b) In the Subroutine **CalcWindowHeatBalance,** calculate the window inside air temperature with using the air temperature close to the window from CFD, instead of using the mean room air temperature.

```
! Calculate Inside air temperature
!zzzzzzzzzzzzzzzzzzzzzzzzzzzzzzzzzzzzzzzzzzzzzzzzzzzzzzzzzzzzzzzzzzzzzzzzzzzzzzzz
tin = MAT(ZoneNum) + 273.15  +  DeltaTair(SurfNum)
!zzzzzzzzzzzzzzzzzzzzzzzzzzzzzzzzzzzzzzzzzzzzzzzzzzzzzzzzzzzzzzzzzzzzzzzzzzzzzzzz
```

Most modifications in these modules are only to call the corresponding operations in the interface modules, or, to insert the new terms that are generated in the interface modules. This makes the implementation of new coupling methods rather easy, and also facilitates the future improvement of either ES or CFD programs.

Other changes may be required to consider the effect of the exhaust air temperature on the energy estimation, which include the modifications in the modules: **ZoneEquipmentManager** and **PurchasedAirManager**.

6 ZoneEquipmentManager

a) Add the link to **DataExchangeCFDAndES:** USE DataExchangeCFDAndES;

b) In the Subroutine **SizeZoneEquipment,** use "TCFDOutlet" passed from CFD, instead of the mean room air temperature, to calculate the "DeltaTemp" between supply air and exhaust air, which is used to the update supply air mass flow rate.

```
SysOutputProvided = ZoneSysEnergyDemand(ActualZoneNum)%RemainingOutputRequired
DeltaTemp = Node(SupplyAirNode)%Temp - Node(ZoneNode)%Temp
CpAir = CpAirFn(Node(SupplyAirNode)%HumRat,Node(SupplyAirNode)%Temp)

!zzzzzzzzzzzzzzzzzzzzzzzzzzzzzzzzzzzzzzzzzzzzzzzzzzzzzzzzzzzzzzzzzzzzzzzzzzzzzzzz
IF(CFD.AND.(ActualZoneNum.EQ.ZoneCFD).AND.(.NOT.FIRSTRUN)) THEN
   DeltaTemp = Node(SupplyAirNode)%Temp - TCFDOutlet
ENDIF
!zzzzzzzzzzzzzzzzzzzzzzzzzzzzzzzzzzzzzzzzzzzzzzzzzzzzzzzzzzzzzzzzzzzzzzzzzzzzzzzz

IF ( ABS(DeltaTemp) > SmallTempDiff ) THEN
    Node(SupplyAirNode)%MassFlowRate = SysOutputProvided / (CpAir*DeltaTemp)
ELSE
    Node(SupplyAirNode)%MassFlowRate = 0.0
ENDIF
```

c) In the Subroutine **CalcZoneLeavingConditions,** update the return air temperature with "TCFDOutlet" from CFD, instead of the mean room air temperature.

7 PurchasedAirManager

a) Add the link to **DataExchangeCFDAndES:** USE DataExchangeCFDAndES;

b) In the Subroutine **CalcPurchAirLoads,** use "TCFDOutlet" passed from CFD, instead of the mean room air temperature, to calculate the "DeltaTemp" between supply air and exhaust air, which is used to update the supply air mass flow rate of purchased air. The modifications are similar with those in Subroutine **SizeZoneEquipment.**

If HVAC systems are taken into the consideration in a coupled simulation, more modifications on those individual system modules in ES may be needed. Below shows an example of such modifications made on the high temperature radiant system module.

8 RadiantSystemHighTemp

a) Add the link to **DataExchangeCFDAndES:** USE DataExchangeCFDAndES;

b) In the Subroutine **UpdateHighTempRadiantSystem,** since the power history of radiator has impact on the current heat power calculation and ES updates the power history immediately after a new heat power is generated, the power history of radiator needs to be saved at the beginning of iterative coupling simulation at each coupling time step. If a converged solution is not achieved after the current iteration, ES and CFD will iterate again from the beginning of this time step. At this moment, the saved values are recovered to allow ES calculate the current heat power with the right power history.

```
!zzzzzzzzzzzzzzzzzzzzzzzzzzzzzzzzzzzzzzzzzzzzzzzzzzzzzzzzzzzzzzzzzzzzzzzzzzzzzzzz
IF(CFD) THEN
   IF(WarmUpFlag.and.(.NOT.WarmupCFD)) THEN
   ELSE
      IF(Convergence) THEN
            IF(OneTimeStoreR==.TRUE.) THEN
               QHTRadSrcAvgOld(RadSysNum) =QHTRadSrcAvg(RadSysNum)
               LastQHTRadSrcOld(RadSysNum)=LastQHTRadSrc(RadSysNum)
               OneTimeStoreR = .FALSE.
            ENDIF
      ELSE    ! If not converged, recover the power history of radiator
            IF(OneTimeStoreR==.FALSE.) THEN
               QHTRadSrcAvg(RadSysNum) =QHTRadSrcAvgOld(RadSysNum)
               LastQHTRadSrc(RadSysNum)=LastQHTRadSrcOld(RadSysNum)
               OneTimeStoreR = .TRUE.
            ENDIF
      ENDIF
   ENDIF
ENDIF
!zzzzzzzzzzzzzzzzzzzzzzzzzzzzzzzzzzzzzzzzzzzzzzzzzzzzzzzzzzzzzzzzzzzzzzzzzzzzzzzz
```

c) In the Subroutine **ReportHighTempRadiantSystem,** the dynamic heat power of the high temperature radiant system calculated in ES is exported to CFD to correspondingly update the heat flux conditions of the radiator in the indoor space.

```
!zzzzzzzzzzzzzzzzzzzzzzzzzzzzzzzzzzzzzzzzzzzzzzzzzzzzzzzzzzzzzzzzzzzzzzzzzzzzzzzz
         IF(CFD) DynamicHeat=HighTempRadSys(RadSysNum)%HeatPower
!zzzzzzzzzzzzzzzzzzzzzzzzzzzzzzzzzzzzzzzzzzzzzzzzzzzzzzzzzzzzzzzzzzzzzzzzzzzzzzzz
```

A.3 Changes in MIT-CFD

As shown in Figure A.1, EnergyPlus calls MIT-CFD whenever needed through one of the interface modules – CFDSimulation. After checking the convergence of the whole simulation, the CFDSimulation module will automatically connect to the main program of the CFD solver – CFDMainProgram in another module. A user can easily turn an independent CFD program into the CFDMainProgram module by changing the "Main Program" title into a "Subroutine" title.

As mentioned in section A.1, MIT-CFD should also create two new function subroutines. One is the UpdateBoundaryConditions subroutine at the beginning of each CFD calculation to update the relevant boundary conditions based on the last ES solutions. The other is the UpdateOutputs subroutine at the end of each CFD calculation to update the information to be transferred back to ES. Some other modifications may apply based on the special situations of individual CFD codes, such as the time and place of data saving and screen display, in order to be consistent with EnergyPlus and save computing and storing time. The following details the information updated in the UpdateBoundaryConditions and UpdateOutputs subroutines.

1 **UpdateBoundaryConditions:** the CFD boundary conditions updated during a coupled simulation may include:
   a) surface temperature or surface heat flux, according to the selected data exchange methods;
   b) inlet conditions;
      - For a constant-air-volume system, air supply airflow rate V is specified and the supply air temperature T_{supply} is determined by
      $$T_{supply} = Q_{heat\_extraction}/(\rho C_p A V) + T_{outlet} \quad (A.6)$$
      - For a variable-air-volume system, T_{supply} is constant and the V is determined by
      $$V = Q_{heat\_extraction}/(\rho C_p A)\,(T_{supply}-T_{outlet}) \quad (A.7)$$
   c) pressure and temperature conditions for natural ventilation;
   d) heat flux for dynamic internal thermal objects.

2 **UpdateOutputs:** the information obtained in CFD, which may be used for ES calculation, include:
   a) convective heat transfer coefficients at each surface;
   b) air temperature close to the surfaces or air temperature gradient $\Delta T_{i,air}=T_{i,air}-T_{room}$;
   c) surface temperature or surface heat flux, depending on the selected data exchange methods;
   d) exhaust air temperature;
   e) volume-weighted mean air temperature;
   f) cooling capacity of natural ventilation.

A.4 Interface Modules

EnergyPlus and MIT-CFD call data-exchange subroutines to invoke the data transfer processes, while the interface modules implements the substantial exchange of the information. The interface modules include a common data module – DataExchangeCFDAndES and two data-exchange operation modules – UpdateHconvInAndTair and CFDSimulation. The common data module holds all the interface variables connecting EnergyPlus and CFD, as summarized in Table A.1 along with the brief explanations of these variables. With incorporating these new interface variables, the original EnergyPlus and CFD codes do not need to change their own data structures and variable names. The data-exchange operation modules work as the bridge

between EnergyPlus and CFD and perform most of the data transfer functions in the coupling. As a result, the ES and CFD programs need limited modifications to plug with the interface modules, rather than directly connecting to each other. It allows the easy update and maintenance of individual ES and CFD programs. It is also convenient to create new subroutines in the interface modules to study new data exchange methods and coupling strategies. The following describes in detail what UpdateHconvInAndTair and CFDSimulation modules do to bridge the ES and CFD programs and transfer information between them.

1 **UpdateHconvInAndTair** module consists of several subroutines. Each of them conducts a particular function to transfer the information from CFD to ES, such as:

a) Subroutine **UpdateHconvIn** dynamically provides the proper convective heat transfer coefficients to each ES calculation by importing the results from the last CFD calculation or extracting them from appropriate static or dynamic bins, depending on the coupling strategy used.

```
!zzzzzzzzzzzzzzzzzzzzzzzzzzzzzzzzzzzzzzzzzzzzzzzzzzzzzzzzzzzzzzzzzzzzzzzzzzzzzzzzzzzzzz
SUBROUTINE UpdateHconvIn(ZoneNumb)

   SUMHA(ZoneNumb) = 0.0      ! Initialize SUMHA for ZoneCFD
   FirstS=Zone(ZoneNumb)%SurfaceFirst-1  ! First surface in the zone

 DO SurfNum = Zone(ZoneNumb)%SurfaceFirst, Zone(ZoneNumb)%SurfaceLast

   IF(FunctionMethod) THEN       ! Vitural dynamic coupling
        HConvIn(SurfNum) = HconvInFunction(QEnergyDemand,SurfNum)
   ELSE
        HConvIn(SurfNum) = CFDHConvIn(SurfNum)      !Import h from CFD
        IF(CFDFLAG==4.and.CFDSchedDay(DayOfSim)==0)  &       !Import h from Bin
                HConvIn(SurfNum) = SaveCFDHConvIn(SurfNum,HourOfDay)
   END IF

   SUMHA(ZoneNumb)=SUMHA(ZoneNumb)+Surface(SurfNum)%Area*HConvIn(SurfNum)

 END DO   ! ...end of DO loop over the zone surfaces.

END SUBROUTINE UpdateHconvIn
!zzzzzzzzzzzzzzzzzzzzzzzzzzzzzzzzzzzzzzzzzzzzzzzzzzzzzzzzzzzzzzzzzzzzzzzzzzzzzzzzzzzzzz
```

b) Subroutine **AddConvForSurfaceHeatBalance** imports the indoor air temperature gradients from static or dynamic bins or the last CFD run and calculates the additional convection term QAdditionalConv=$h_{i,c}\Delta T_{i,air}$ for the inside surface heat balance equations of ES.

```
!zzzzzzzzzzzzzzzzzzzzzzzzzzzzzzzzzzzzzzzzzzzzzzzzzzzzzzzzzzzzzzzzzzzzzzzzzzzzzzzzzzzzzz
ENTRY AddConvForSurfaceHeatBalance

 DO SurfNum = 1, TotSurfaces
   ZoneNum = Surface(SurfNum)%Zone

     IF(ZoneNum.EQ.ZoneCFD) THEN
       IF(FunctionMethod)  &       ! Vitural dynamic coupling
         DeltaTair(SurfNum)=DeltaTairFunction(QEnergyDemand,SurfNum,FuncMethod)
       IF(CFDFLAG==4.and.CFDSchedDay(DayOfSim)==0)  &      !Import ΔT from Bin
         DeltaTair(SurfNum) = SaveDeltaTair(SurfNum,HourOfDay)

       QAdditionalConv(SurfNum) = HConvIn(SurfNum)*DeltaTair(SurfNum)

     ENDIF
```

```
  END DO
!zzzzzzzzzzzzzzzzzzzzzzzzzzzzzzzzzzzzzzzzzzzzzzzzzzzzzzzzzzzzzzzzzzzzzzzzzzzzzzzzzzzz
```

c) Subroutine **AddConvForAirHeatBalance** imports the indoor air temperature gradients from static or dynamic bins or the last CFD run and calculates the additional convection terms, such as $-\sum_{i=1}^{N_{surfaces}} h_i A_i \Delta T_{i,air}$ and $Q_{natural\text{-}ventilation}$, for the indoor air heat balance equation of ES.

```
!zzzzzzzzzzzzzzzzzzzzzzzzzzzzzzzzzzzzzzzzzzzzzzzzzzzzzzzzzzzzzzzzzzzzzzzzzzzzzzzzzzzz
ENTRY AddConvForAirHeatBalance

  DO SurfNum = 1, TotSurfaces
        ZoneNum = Surface(SurfNum)%Zone

    IF(ZoneNum.EQ.ZoneCFD) THEN
        IF(FunctionMethod)  &       ! Vitural dynamic coupling
          DeltaTair(SurfNum)= DeltaTairFunction(QEnergyDemand,SurfNum,FuncMethod)
        IF(CFDFLAG==4.and.CFDSchedDay(DayOfSim)==0)   &    !Import ΔT from Bin
          DeltaTair(SurfNum)= SaveDeltaTair(SurfNum,HourOfDay)

        SUMHAT(ZoneNum) = SUMHAT(ZoneNum) – &
                    HConvIn(SurfNum)*Surface(SurfNum)%Area*DeltaTair(SurfNum)
    ENDIF

  END DO

  SUMHAT(ZoneCFD) = SUMHAT(ZoneCFD) + QNV  ! Add natural ventilation power
!zzzzzzzzzzzzzzzzzzzzzzzzzzzzzzzzzzzzzzzzzzzzzzzzzzzzzzzzzzzzzzzzzzzzzzzzzzzzzzzzzzzz
```

UpdateHconvInAndTair module also includes some typical static function databases for static bin coupling, such as those developed by Chen (1988). Based on these, the convective heat transfer coefficients and the indoor air temperature gradients can be determined and used for the ES calculation.

2 **CFDSimulation** module is the gate to the main program of the CFD solver. As presented above, whenever ES calls CFD simulation, CFDSimulation module is activated. It will first evaluate the convergence status of the whole coupling simulation by comparing the difference of surface temperatures between this ES run and the last ES run on each single surface. If the largest temperature difference is smaller than the prescribed criteria, the coupling simulation at this coupling step is converged and no more CFD is needed. Otherwise, the CFD solver is called to perform a new CFD calculation. For the quasi-dynamic coupling, the convergence status is always set as "True" because of no requirement for iteration at each coupling step. In order to avoid the infinite (dead) iteration between ES and CFD, the module sets ten as the maximum iteration step and provides a warning if the iteration does not converge at a coupling step. In the current version of E+MIT-CFD, CFDSimulation module also produces the dynamic databases about convective heat transfer coefficients and the indoor air temperature gradients based on the CFD results on the typical days simulated. This part may be moved to UpdateHconvInAndTair module in the future since that module is mainly about extracting information from CFD to ES.

```
!zzzzzzzzzzzzzzzzzzzzzzzzzzzzzzzzzzzzzzzzzzzzzzzzzzzzzzzzzzzzzzzzzzzzzzzzzzzzzzzzzzzzz
SUBROUTINE CFDSimulator

! Judge whether the coupling is converged
        DO I=1, 100
        DTEMPWALL(I)=ABS(TempWALL(I)-TempWALL0(I))    !Compare T^n and T^n-1
        TempWall0(I)=TempWall(I)
        END DO

        AMAXD=0.
        DO I=1,100
        AMAXD=MAX(AMAXD,DTEMPWALL(I))    ! Find the max error
        ENDDO

        IF(AMAXD.LE.ConvergError) Convergence=.TRUE.
        IF(AMAXD.GT.ConvergError) Convergence=.FALSE.

        INITERATE=INITERATE+1    ! Calculate the total iteration times between ES and CFD
        IF(INITERATE.GT.10) Convergence=.TRUE.

        IF(STRATEGY==3) Convergence=.TRUE.    ! Quasi-dynamic coupling

        IF(FunctionMethod) RETURN    ! Return if virtual dynamic coupling

        CALL MAINPR    ! Call CFD main program

! Save h, ΔT, Qsurface at each hour to form the bin
        DO i=1,100
        SaveCFDHConvIn(i,HourOfDay)=CFDHConvIn(i)
        SaveDeltaTair(i,HourOfDay)=DeltaTair(i)
        SaveQSurface(i,HourOfDay)=QSurface(i)
        ENDDO

END SUBROUTINE CFDSimulator
!zzzzzzzzzzzzzzzzzzzzzzzzzzzzzzzzzzzzzzzzzzzzzzzzzzzzzzzzzzzzzzzzzzzzzzzzzzzzzzzzzzzzz
```

Table A.1 List of interface variables in DataExchangeCFDAndES module

Variable	Meaning
CFD	= True: operate FD coupling = False: no CFD coupling
EnergySimulation	= True: operate S calculation = False: no ES calculation
FunctionMethod	= True: use function database = False: do not need function database
Convergence	= True: a converged solution is reached = False: a converged solution is not reached
FirstRun	= True: first running of CFD simulation = False: not first running of CFD simulation
RunCFDFlag	= True: run CFD at current time step = False: do not run CFD at current time step
WarmupCFD	= True: operate CFD coupling during warm-up periods of ES = False: no CFD coupling during warm-up periods of ES
OneTimeStore	= True: save inside surface temperature history = False: otherwise
OneTimeStoreR	= True: save heat power history of high temperature radiator

	= False: otherwise
SaveCFDHConvIn	Saved convective heat transfer coefficients from CFD to construct the databases for virtual dynamic coupling
SaveDeltaTair	Saved indoor air temperature gradients from CFD to construct the databases for virtual dynamic coupling
SaveQSurface	Saved surface convective heat fluxes from CFD to construct the databases for virtual dynamic coupling
TempWALL	Surface temperatures from ES
CFDHConvIn	Convective heat transfer coefficients $h_{i,c}$ from CFD
DeltaTair	Indoor air temperature gradients $\Delta T_{i,air}$ from CFD
QAdditionalConv	Additional convective heat flux term: QAdditionalConv=$h_{i,c}\Delta T_{i,air}$
QSurface	Per unit area surface convective heat fluxes from CFD: QSurface=$h_{i,c}(T_i-T_{i,air})$
QSurfaceA	Surface convective heat fluxes from CFD: QSurfaceA=$h_{i,c}(T_i-T_{i,air})A_i$
TempWALL0	Surface temperatures from last ES
CFDHConvIn0	Convective heat transfer coefficients $h_{i,c}$ from last CFD
DeltaTair0	Indoor air temperature gradients $\Delta T_{i,air}$ from last CFD
TWallCFD	Surface temperatures from CFD
CoeffDeltaTair	Function coefficients for static function databases of indoor air temperature gradient
CoeffHConv	Function coefficients for static function databases of convective heat transfer coefficient
MATOld XMATOld XM2Told XM3TOld XM4TOld	History of mean room air temperature from ES
QHTRadSrcAvgOld LastQHTRadSrcOld	History of heat power of high temperature radiant system from ES
QEnergyDemand	Heating/cooling load from ES
QEnergyDemand0	Heating/cooling load from last ES
EnthalpyInlet	Enthalpy of supply air from ES
QNV	Cooling capacity of natural ventilation
TempRoom	Mean room air temperature from ES
VelocityInlet	Supply air velocity
TempInlet	Supply air temperature
VelocityOutlet	Exhaust air velocity
TRoomCFD	Mean room air temperature from CFD
TCFDOutlet	Exhaust air temperature from CFD
TCFDOut	Leaving air temperature of natural ventilation from CFD
ABlocks	Surface area of internal thermal objects calculated in CFD
ConvergError	Prescribed convergence criteria
Theating	Specified heating supply temperature
Tcooling	Specified cooling supply temperature

DynamicHeat	Dynamic heat power for internal thermal objects
CFDFLAG	Select coupling frequency: =1: coupling per day =2: coupling per hour =3: coupling per time step =4: scheduled coupling frequency
ZONECFD	Number of the zone to be simulated by CFD
FirstS	First surface number of the zone simulated by CFD
FuncMethod	Select special functions for virtual dynamic coupling: =1: constant temperature distribution =2: linear T(Q) function =3: non-linear T(Q) function
Strategy	Select coupling strategy: =1: virtual dynamic coupling =2: one-time-step dynamic coupling =3: quasi-dynamic coupling =4: full dynamic coupling
Database	Select function database for special functions: =1: summer cooling case =2: winter heating case
OneTime	One particular time step to be selected for one-time-step dynamic coupling strategy
InIterate	Inner coupling iteration number between ES and CFD
NRunStep	Total CFD running times in a coupled simulation
MCouple	Select data coupling method: =1: ES->T; CFD->h & dT =2: ES->T; CFD->h(corrected) =3: ES->T; CFD->Q =4: ES->Q; CFD->h & dT
CFDSchedule	Intermediate variable for recording scheduled coupling days and hours during a period of time
CFDSchedDay	=1: the day to use CFD coupling =0: otherwise
CFDScheHour	=1: the hour to use CFD coupling =0: otherwise

A.5 Operation of E+MIT-CFD

A.5.1 Prepare the input files

As mentioned in Chapter 5, in general, four input files: weather.epw and case.idf for EnergyPlus, grid.dat and input.cfd for MIT-CFD, are needed to perform a coupled simulation. If the simulation is for a design day, weather.epw is not necessary.

- **Input files for EnergyPlus**

In strict, the following input files are required to the EnergyPlus program.

Energy+.idd

The input data dictionary (IDD) is an ASCII (text) file containing a list of all possible EenryPlus objects and a specification of the data each object requires. This file is analogous to the DOE-2 keyword file.

case.idf

The input data file (IDF) is an ASCII file containing the data describing the building and HVAC system to be simulated.

Energy+.ini

This is the EnergyPlus initialization file. It is an optional ASCII input file that allows the user to specify the path for the directory containing Energy+.idd. This file, using the actual directories of the install, will be created during the install.

weather.epw

The EnergyPlus weather file is an ASCII file containing the hourly or sub-hourly weather data needed by the simulation program.

Among these four input files, *case.idf* and *weather.epw* vary with cases. EnergyPlus has three options for a user to create the input data files (IDFs):

(1) IDFEditor

This is a very simple, "intelligent" editor that reads the IDD and IDFs and allows creation/revision of IDF files.

(2) BLAST Translator

If one already has BLAST and/or BLAST input files, this program will produce the bulk of a translation to EnergyPlus. BLAST Translator generates a complete IDF file but does not include specifics for systems or plants. (It does include the System and Plant schedules that were in the BLAST deck).

(3) Manual Editing

For simple changes to an existing file, one can edit manually a file using the knowledge of the IDD, comments in the IDF file, and a text editor, such as NOTEPAD.

Weather data in EnergyPlus is a simple text-based format. The weather data format includes basic location information in the first eight lines: location (name, state/province/region, country), data source, latitude, longitude, time zone, elevation, peak heating and cooling design conditions, holidays, daylight saving period, typical and extreme periods, two lines for comments, and period covered by the data. The data are also comma-separated and contain much of the same data in the TMY2 weather data set. EnergyPlus does not require a full year or 8760 (or 8784) hours in its weather files. In fact, EnergyPlus allows and reads subsets of years and even sub-hourly (5 minute, 15 minute) data. EnergyPlus comes with a utility that reads standard weather service file types such as TD1440 and DATSAV2 and newer "typical year" weather files such as TMY2 and WYEC2.

More detailed information about the format, explanation, and creation of IDFs and weather data files could be found in EnergyPlus Manual, supplied along with EnergyPlus software.

- **Input files for MIT-CFD**

All CFD programs need grid system information and case specifications to run a simulation. MIT-CFD inputs these information from two separate files: grid.dat and input.cfd.

Grid.dat contains the (x,y,z) location of each mesh corner node in the computational domain simulated, within the general curvilinear coordinate system. The storing sequence is

```
WRITE(grid.dat, *) (((X(I,J,K),I=1,NI),J=1,NJ),K=1,NK)
WRITE(grid.dat, *) (((Y(I,J,K),I=1,NI),J=1,NJ),K=1,NK)
WRITE(grid.dat, *) (((Z(I,J,K),I=1,NI),J=1,NJ),K=1,NK)
```

where, NI,NJ, and NK are the maximum grid number in X, Y, Z directions.

Different methods and programs can be used to generate an appropriate grid. The SCI program provides a simple method to generate a rectangular grid system. It is straightforward in SCI to create and modify a grid system by defining the geometry scale and grid density, as shown in Figure A.2.

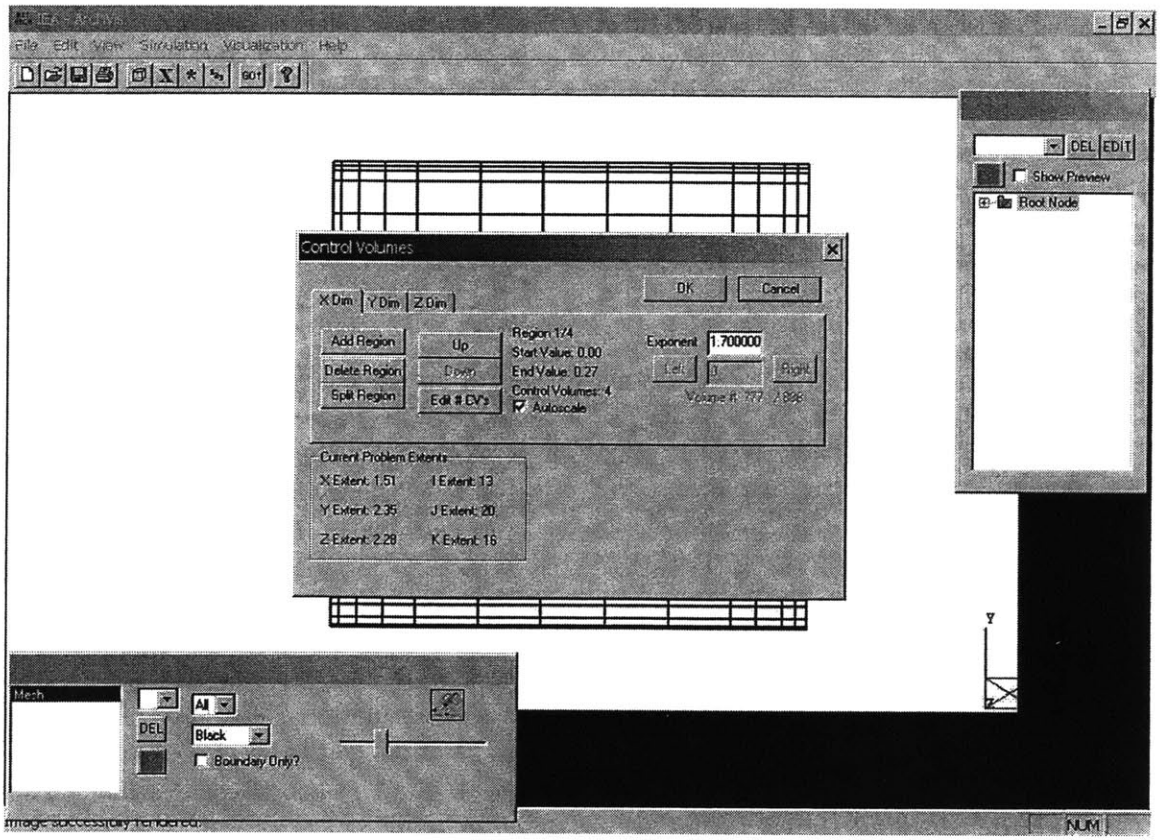

Figure A.2 Grid generation in SCI

Input.cfd includes all the other information necessary for a CFD modeling, which consists of problem specifications, property specifications, numerics specifications, and boundary conditions.

(1) Problem specifications

It indicates the flow physics, such as, steady or unsteady flow, laminar or turbulence flow, buoyancy flow, and so on. It also specifies the conservative equations to solve and the turbulence model to use.

(2) Property specifications

This part specifies all the property constants, such as density and viscosity of air, gravity, Prantl number, and the turbulence model constants.

(3) Numerics specifications

It includes the iterative control parameters, such as convergence criteria and maximum iterative steps, and all numerical methods to use, such as numerical scheme, relaxation factor, false time step, and initialization.

(4) Boundary conditions

Seven types of boundary conditions are available in MIT-CFD, including Inlet, Outlet, Wall, Symmetry, Blockage, Source, and Pressure. Two types of thermal boundary conditions, Dirichlet (temperature) and Newmann (heat flux) conditions, can be applied to all the above boundary conditions. When specifying the boundary conditions, besides the boundary condition type, a user also need to indicate the orientation and location of each boundary condition, as well as the relevant setup values.

Two options are available to create this input file:

(1) SCI

It is easy to follow the instructions in SCI to create the input.cfd. Most of the specifications indicated above are to leave the default value if the CFD program is being applied to the building field. SCI has one main window dynamically showing graphical responses of corresponding operations, and one small boundary-condition-specification window and one small display-control window. Under the "Simulation" manual, the options of "Mesh Definition", "Problem Description", "Simulation Properties", and "Iteration Control", exactly follow the sequences of creating CFD input files discussed above.

Note that SCI was developed for separate CFD simulation. The new parameters introduced in the input.cfd file due to the coupling have not yet been implemented into the SCI interface. Therefore, the following manual editing is necessary to input those parameters after using SCI to generate the original input.cfd.

(2) Manual Editing

Manual editing is an efficient way to modify an existing input file, using a text editor, such as NOTEPAD. A typical input.cfd is self-readable, with comment lines before each input field that clearly explain the meaning and proper input of each field in the file. It is easy to change the selections manually depending on the case studied.

A.5.2 Run the simulation

In order to operate a coupled simulation by using the graphic interface – *EP-Launch*, which is developed for the separate EnergyPlus simulation as shown in Figure A.3, a user needs to:

(1) copy the new compiled E+MIT-CFD.exe and input.cfd and grid.dat to the root directory of EnergyPlus, where the EnergyPlus software was installed;
(2) replace the name of the executable file (E+MIT-CFD.exe) to EnergyPlus.exe;
(3) choose case.idf and weather.epw (if required) from appropriate file locations in the EP-Launch interface,
(4) click "Simulate..." button that will start running the simulation automatically.

E+MIT-CFD provides a number of simulation options a user may be able to choose, based on the case characteristics and design purpose. All available selection options have been presented in Figure A.4 – A.7.

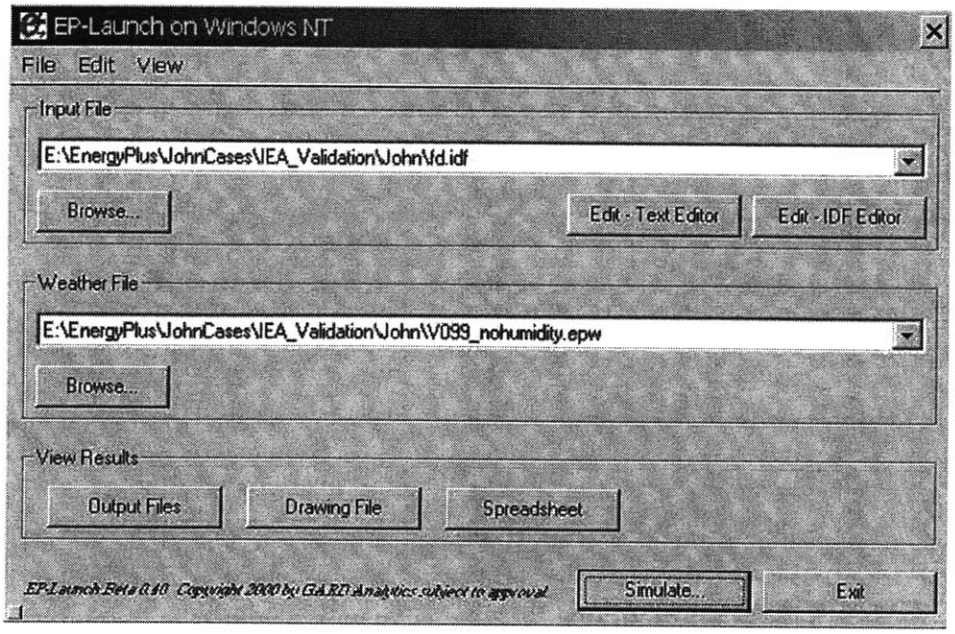

Figure A.3 EP-Launch interface for EnergyPlus

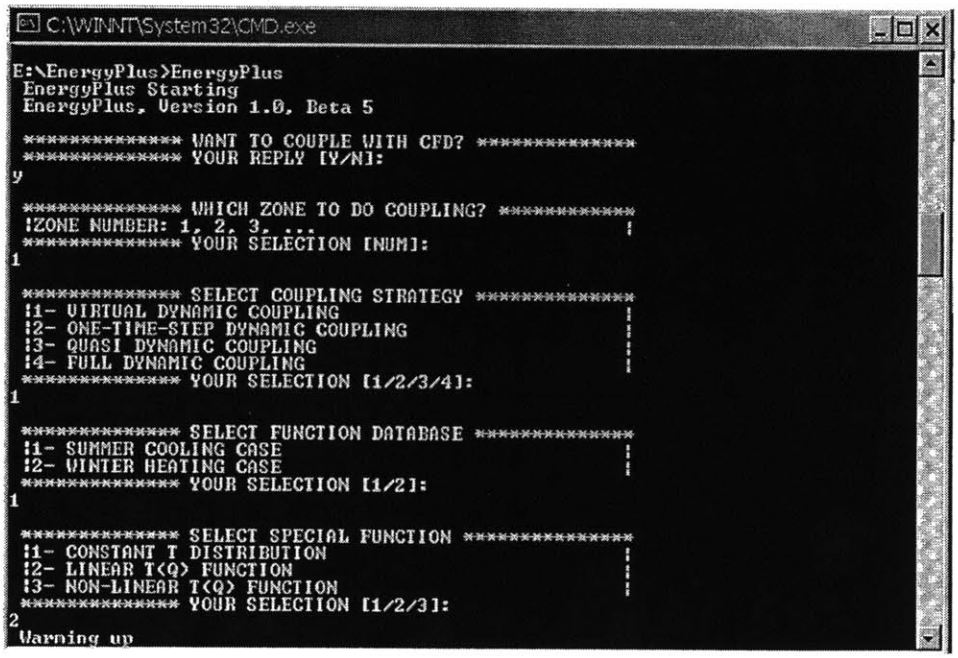

Figure A.4 Selections of static bin coupling in E+MIT-CFD

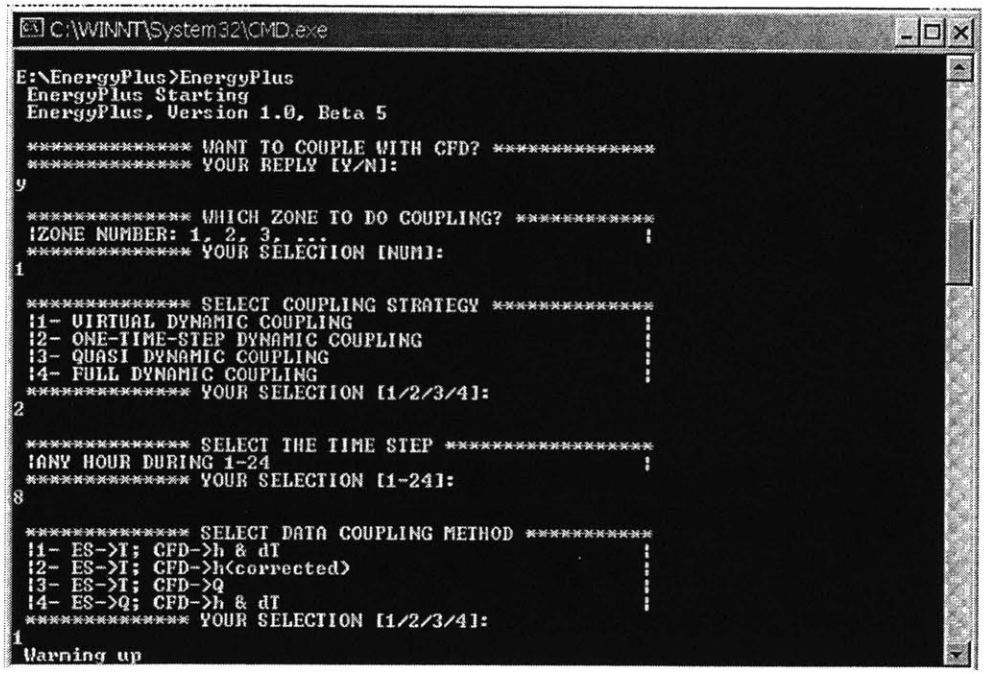

Figure A.5 Selections of one-time-step dynamic coupling in E+MIT-CFD

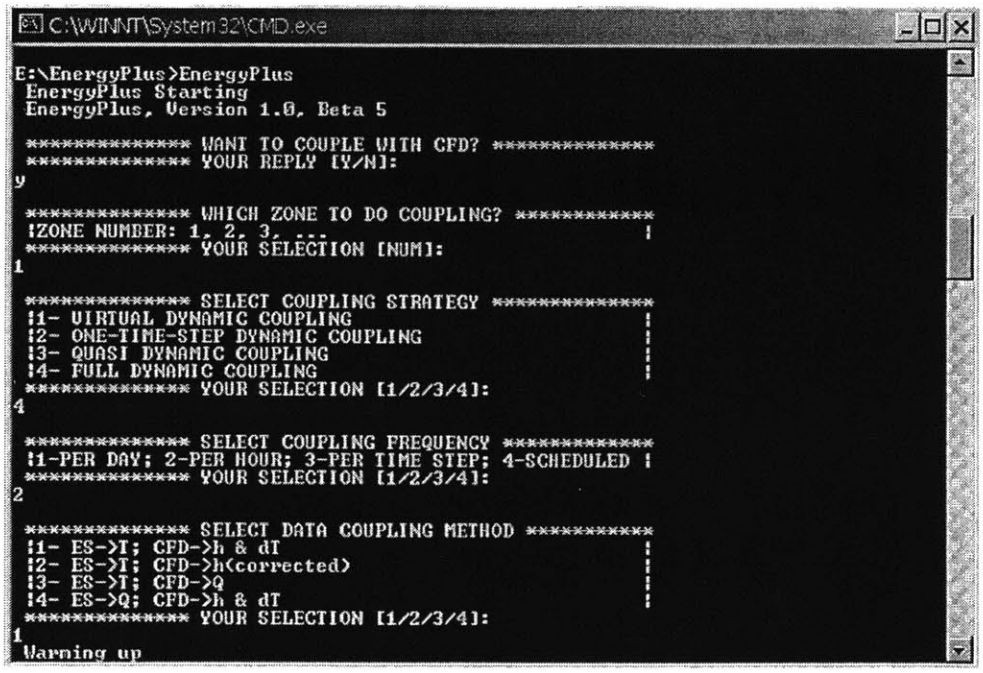

Figure A.6 Selections of full dynamic coupling in E+MIT-CFD

Figure A.7 Selections of full dynamic coupling in E+MIT-CFD with scheduled coupling frequency

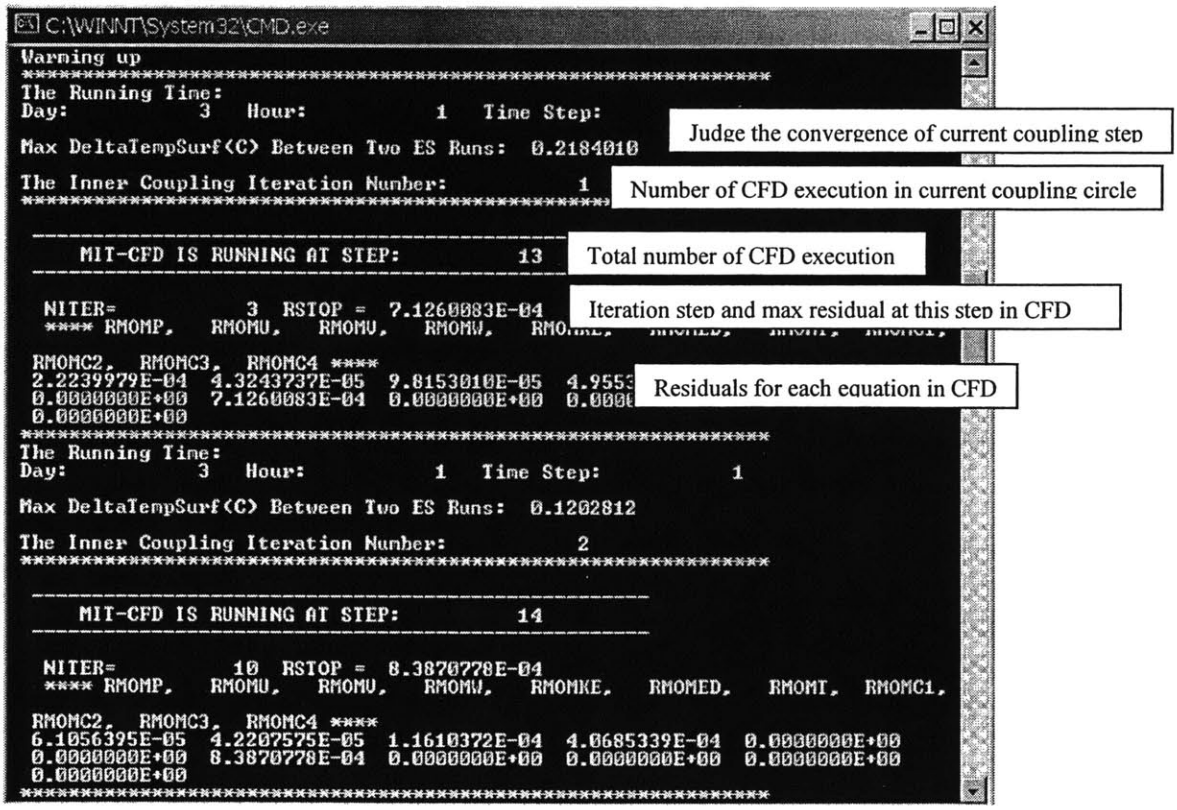

Figure A.8 Screen output during E+MIT-CFD calculation

Figure A.8 shows the screen output of the relevant information during the E+MIT-CFD calculation. The screen output is also saved to a data file, which can be viewed later on after the calculation.

A.5.3 View the results

E+CFD simulation produces several output files, which can be viewed and handled using different software, such as, MS Excel, Notepad, and Techplot. The contents of most output files can be customized by E+MIT-CFD input files and codes.

Typically, EnergyPlus creates the following files:

Audit.out	Echo of input
Eplusout.err	Error file
Eplusout.eso	Standard output file
Eplusout.eio	One time output file
Eplusout.rdd	Report variable data dictionary
Eplusout.dxf	DXF (from Report,Surfaces,DXF;)
Eplusout.end	A one line summary of success or failure

Eplusout.dxf shows the geometry of the building simulated. Eplusout.eso can be easily turned into a form that is read into commonly used spreadsheet programs where it can be further analyzed, graphed, etc. In EP-Launch, a user can configure and employ the preferred tools to handle the outputs.

MIT-CFD generates three output files:

Screen.dat	Screen display record
Tech.dat	Standard result output file for Techplot Software
Summary.cfd	Output of inter-coupled data

Tech.dat can be imported to Tecplot, a popular flow visualization tool, to show the pressure, flow, temperature and concentration distributions. Summary.cfd can be turned into a form that is readable by commonly used spreadsheet programs where it can be further analyzed, graphed, etc.

A.6 Practice of CFD Solver Switch

In practice, other CFD solvers, rather than the MIT-CFD program, may be chose to simulate the indoor airflows due to different capability emphases of CFD solvers and users' preferences. The modular structure of the present coupling program allows easy switch of CFD solver without substantial changes of the EnergyPlus source codes and interface modules developed. This section will introduce how to practically incorporate

an arbitrary CFD solver with the interface modules and the EnergyPlus to establish an integrated and ready-to-use building simulation tool.

Step One: change an independent CFD program into a group of modules that can be integrated with the ES modules and the interface modules to form an integrated simulation program. As indicated in Section A.1, in order to generate a single executable file and automate the coupling in the simulation, individual ES and CFD programs should be assembled into one body. Since ES programs simulate the whole building performance for a long period of time while CFD programs focus on the "snap-shot" of the flow and heat transfer in a single space, embedding a CFD program into an ES program is a reasonable assemble strategy. An independent CFD program can be easily modified from a separate solver to the interior modules of a comprehensive program by changing the main "Program" of the CFD program into a "Subroutine" of the CFD program and creating a new module that contains this subroutine, for instance,

```
Program  Flow3D  ------------>  Module CFDSolver
                                    Subroutine Flow3D
                                    End Subroutine
End Program                     End Module
```

Step Two: change the CFD solver name called by the interface module – CFDSimulation to the corresponding one. For example, using the CFD module created in the above instance, the change in module **CFDSimulation** is

```
Module CFDSimulation
    Subroutine CFDSimulator
        ......
        Call Flow3D
        ......
    End Subroutine
End Module
```

Step Three: create the first function subroutine – UpdateBoundary Conditions and place it at the beginning of each CFD calculation. The function of this subroutine is to update the relevant boundary conditions based on the last ES calculation. The subroutine is not included in the interface modules although it is related to the data exchange between ES and CFD. It is because the operations in this subroutine are heavily tied to the CFD own data structure. Otherwise, the interface modules may have to frequently call the private data of the CFD modules.

According to the coupling strategy selected and based on the recent ES results, the **UpdateBoundaryConditions** need to update the following boundary conditions before starting the CFD iteration loop:

- surface temperatures based on the interface variable array **TempWall**;

- surface heat fluxes based on the interface variable array **QSurface**;

- inlet conditions:
  - For a constant-air-volume (CAV) system, air supply airflow rate V is fixed and the supply air temperature T_{supply} is determined by T_{supply} = **QEnergyDemand**/($\rho C_p AV$) + T_{outlet}, where **QEnergyDemand** is the interface variable obtained from ES calculation;
  - For a variable-air-volume (VAV) system, T_{supply} is constant and the V is determined by V = **QEnergyDemand**/($\rho C_p A$) (T_{supply}-T_{outlet})

- dynamic outdoor air temperature for openings with natural ventilation based on the variable **OutDryBulbTemp** of ES;

- heat flux for dynamic internal thermal objects (e.g. high temperature radiator) based on the interface variable **DynamicHeat,** which is the total heat flux (watt) from the thermal objects obtained in ES.

Note that the surface sequence of the surface variable arrays is the same as the input sequence in ES. For example, if the sequence of envelope surfaces input into ES is west, south, east, north, bottom, and top, then TempWall(1)=TempWall(west) and TempWall(2)=TempWall(south) and so on.

Step Four: create the second function subroutine – UpdateOutputs and place it at the end of each CFD calculation. The function of this subroutine is to calculate and update the inter-coupled information that may be used in the next ES calculation. The information to be updated includes:

- mean convective heat transfer coefficient at each surface, which will be saved in the interface variable array **CFDHConvIn**;

$$h_{conv} = \sum A_i C_p \frac{\mu_{eff,i}}{Pr} \frac{1}{\Delta x} \Big/ \sum A_i \qquad (A.8)$$

where A_i is surface area of each cell, C_p is air specific heat, $\mu_{eff,i}$ is local effective kinetic viscosity, Pr is Prandtl number, and Δx is normal distance from a point near a surface to the surface.

- mean air temperature gradient between the air temperature close to a surface and the mean indoor air temperature (unconditioned) or the air temperature at the controlled point (conditioned):

$$\Delta T_{air} = T_{air} - T_{room} \qquad (A.9)$$

which will be saved in the interface variable array **DeltaTair**;

- mean surface temperature of each surface:

$$T_s = \sum A_i T_{s,i} / \sum A_i \tag{A.10}$$

which will be saved in the interface variable **TWallCFD**;

- mean surface heat flux through each surface:

$$Q_s = h_{conv}(T_s - T_{air}) \tag{A.11}$$

which will be saved in the interface variable **QSurface**;

- mean exhaust air temperature, which will be saved in the interface variable **TCFDOutlet;**

- volume-weighted mean air temperature:

$$T_{room} = \sum V_i T_{air,i} / \sum V_i \tag{A.12}$$

where V_i is the volume of each cell and T_{room} will be saved in the interface variable **TRoomCFD**;

- cooling capacity of natural ventilation:

$$Q_{natural-ventilation} = \sum \dot{m}_{opening} C_p T_{opening} \tag{A.13}$$

which will be saved in the interface variable **QNV**;,

These saved results will then be used in the interface modules and EenrgyPlus modules for the new ES calculation.

The above four steps are essential to couple an independent CFD solver into the coupling program. The specific codes developed to export, import, calculate, and update those interface variables may vary with CFD programs because of different data and program structures and different implementation methods of various boundary conditions. Some other modifications may also apply based on the special situations of individual CFD codes, such as dynamic saving methods of CFD results during a coupled simulation.